UNIVERSIDADE DE LISBOA

INSTITUTO SUPERIOR TÉCNICO

Towards the development of potency assays and 3D inflammation models to evaluate the regenerative potential of Mesenchymal Stem/Stromal Cell (MSC) and MSC-derived products

Raquel Medina dos Santos Cunha

Supervisor: Doctor Cláudia Alexandra Martins Lobato da Silva

Co-supervisors: Doctor António José Calhabrês Fiarresga

Doctor Jeffrey Michael Karp

Thesis approved in public session to obtain the PhD Degree in Bioengineering

Jury final classification: Pass with distinction

2018

TÉCNICO LISBOA

UNIVERSIDADE DE LISBOA
INSTITUTO SUPERIOR TÉCNICO

Towards the development of potency assays and 3D inflammation models to evaluate the regenerative potential of Mesenchymal Stem/Stromal Cell (MSC) and MSC-derived products

Raquel Medina dos Santos Cunha

Supervisor: Doctor Cláudia Alexandra Martins Lobato da Silva

Co-supervisors: Doctor António José Calhabrês Fiarresga

Doctor Jeffrey Michael Karp

Thesis approved in public session to obtain the PhD Degree in Bioengineering

Jury final classification: Pass with distinction

Jury

Chairperson: Doctor Joaquim Manuel Sampaio Cabral, Instituto Superior Técnico, Universidade de Lisboa

Members of the Committee:

Doctor Joaquim Manuel Sampaio Cabral, Instituto Superior Técnico, Universidade de Lisboa

Doctor Catarina Rodrigues de Almeida, Universidade de Aveiro

Doctor Cláudia Alexandra Martins Lobato da Silva, Instituto Superior Técnico, Universidade de Lisboa

Doctor Maria Margarida Fonseca Rodrigues Diogo, Instituto Superior Técnico, Universidade de Lisboa

Doctor Hugo Agostinho Machado Fernandes, Faculdade de Medicina, Universidade de Coimbra

Funding Institution - Fundação para a Ciência e a Tecnologia

2018

Desenvolvimento de ensaios de potência e modelos 3D de inflamação para avaliar o potencial regenerativo de células mesenquimais estaminais/estromais e seus produtos derivados

Raquel Medina dos Santos Cunha

Doutoramento em Bioengenharia

Orientador: Doctor Cláudia Alexandra Martins Lobato da Silva
Co-orientadores: Doctor António José Calhabrês Fiarresga
Doctor Jeffrey Michael Karp

Resumo

Terapia de células mesenquimais estaminais/estromais (CME) é uma alternativa promissora no tratamento de doenças relacionadas com inflamação, como doenças cardiovasculares e pulmonares. Algumas destas doenças não têm tratamento, à excepção do transplante do órgão, que é limitado em termos de disponibilidade e risco de infecção e rejeição. O interesse em terapias com CMEs deve-se à possibilidade do seu uso como terapia alogénica, terem propriedades imuno-modulatórias recrutando células imunitárias para locais de lesão promovendo regeneração e também inibindo as células imunitárias para resolução da inflamação, terem capacidade de suporte e de produção de factores de sobrevivência, anti-apoptóticos, angiogénicos e anti-fibróticos, promovendo regeneração por contacto entre células e por via parácrina. Contudo, os benefícios terapêuticos são limitados, os mecanismos de acção não são completamente conhecidos e não há uniformização nos ensaios de potência para avaliar o potencial regenerativo das CMEs e seus produtos, meio conditionado (MC) e vesículas extracelulares (VE). Também não há consenso em relação à fonte celular com melhores propriedades regenerativas para cada aplicação e a gama óptima de dose de CMEs, MC de CMEs (CME-MC) e VEs de CMEs (CME-VEs).

CMEs foram isolados da medula óssea (MO), tecido adiposo (TA) e matriz do cordão umbilical (MCU) e todos os dadores (3 dadores por fonte celular) apresentaram potencial de diferenciação, imuno-fenótipo e morfologia esperada para CMEs. CMEs do TA e MCU apresentaram uma taxa de proliferação maior que CMEs da MO, contudo não houve comparação directa entre fontes celulares do mesmo dador. Ensaios de potência angiogénicos em Matrigel e de "cicatrização de feridas" *in vitro* foram desenvolvidos para avaliar a capacidade de CMEs da MO em providenciar suporte a células endoteliais e do MC promover migração e angiogénesis. Os resultados indicaram que CME-MC promove migração e proliferação de células endoteliais. Um ensaio de potência de stress oxidativo usando H_2O_2 foi desenvolvido para células aderentes e em suspensão para avaliar a resistência de CMEs de MO, TA e MCU, relevante num cenário de transplantação em que as células estão sujeitas a ambiente oxidativo, isquémico, tóxico e inflamatório. A variabilidade entre dadores teve maior impacto que a variabilidade entre fontes, sendo a variabilidade entre dadores de CMEs esperada especialmente quando o número de dadores é pequeno. Para avaliar o efeito immuno-modulatório de CMEs e produtos derivados, foram desenvolvidos ensaios de potência 2D usando células endoteliais e monócitos e modelos 3D de inflamação. Os ensaios de potência com células endoteliais e monócitos permitiram identificar dadores de CME-VEs de MO pro- e anti-inflamatórios. As propriedades inflamatórias de CMEs, CME-MC, CME-VEs dos dadores selecionados usando os ensaios de potência foram testados num modelo de inflamação em transwell e as CME-VEs foram testadas num dispositivo de microfluídica de órgão-em-chip modelando inflamação dos alvéolos pulmonares. Os resultados indicaram que CMEs (em maior extensão) e CME-VEs reduziram parcialmente a inflamação (diminuido expressão de moléculas de adesão endoteliais e a produção de citocina inflamatória) e o edema (promovendo recuperação da função de barreira celular). Mais investigação é necessária para perceber os mecanismos de acção e melhorar o potencial regenerativo das CMEs e seus produtos derivados.

Palavras-chave: Células mesenquimais estaminais/estromais, acção parácrina, vesículas extracelulares, ensaios de potência, modelos 3D de inflamação

Towards the development of potency assays and 3D inflammation models to evaluate the regenerative potential of Mesenchymal Stem/Stromal Cell (MSC) and MSC-derived products

Abstract

Mesenchymal stem/stromal cell (MSC) therapy is a promising cell-based therapy for inflammation-related diseases as cardiovascular and lung diseases. Several of these diseases do not have much treatment options rather than organ transplantation, which has limited availability and is associated with risk of infections and rejection. There is great interest on MSC therapies because MSCs are immune-privileged enabling their use as allogeneic therapy; have immunomodulatory properties, recruiting immune cells to the injury site to promote repair and suppressing immune cells to resolve inflammation; have supportive function and ability to secrete pro-survival, anti-apoptotic, angiogenic, anti-fibrotic and anti-scarring factors, thus, by cell contact and paracrine action MSCs promote regeneration of injured tissues. Nevertheless, clinical benefits are limited, the mechanisms of action are not fully understood and there is no standardization of the potency assays used to assess the regenerative properties of MSCs and MSC-derived products, conditioned medium (CM) and extracellular vesicles (EVs). Moreover, there is still no consensus on which cell source would have enhanced regenerative properties for specific applications and what would be the optimal dose range of MSCs, MSC-CM or MSC-EVs.

MSCs were isolated from bone marrow (BM), adipose tissue (AT) and umbilical cord matrix (UCM) and all donors (3 per cell source) had differentiation potential, immunophenotype and morphology in accordance with what is expected for MSCs. AT and UCM MSCs had higher proliferative rate than BM MSCs, however, there was no match between cell sources from the same donors. Angiogenic potency assays in Matrigel and a wound healing assay by mechanical scratch were developed to evaluate BM MSC supportive function and BM MSC-CM ability to promote migration, proliferation and angiogenesis. Results indicate that BM MSC-CM can enhance migration and proliferation of endothelial cells. An oxidative stress potency assay using H_2O_2, as oxidant agent, were developed for adherent cells and in suspension to evaluate BM, AT and UCM MSC donors ability to resist to oxidative stress, an important feature as cells would be subjected to a harsh oxidant, ischemic, cytotoxic and inflammatory environment upon administration into injury sites. The impact of donor variability was higher than the impact of cell source, moreover, the impact of donor variability is expected for MSCs especially when a low number of donors is used. To evaluate the immunomodulatory properties of MSCs and MSC-derived products, 2D potency assays with endothelial and monocytic cells and 3D models of inflammation were developed. The endothelial and the monocytic potency assays were used to screen pro- and anti-inflammatory BM MSC-EV donors. The immunomodulatory properties, namely the anti-inflammatory properties of MSCs, MSC-CM and MSC-EVs from the donors selected based on the endothelial and monocytic potency assays were then tested on a transwell inflammation model and MSC-EVs were tested on a lung alveolus-on-a-chip inflammation model. Results showed that MSCs and MSC-EVs have the ability to partially reduce inflammation and edema by reducing the expression of endothelial adhesion molecules and the release of an inflammatory chemokine and promoting barrier function recovery by reducing vascular leakage. Moreover, the effect of MSCs on the recovery from inflammation was higher than MSC-derived products. More research is needed to understand the mechanisms of action and to control and boost the regenerative potential and therapeutic efficacy of MSC and MSC-derived products.

Key-words: Mesenchymal stem/stromal cells, paracrine action, extracellular vesicles, potency assays, 3D inflammation models

Desenvolvimento de ensaios de potência e modelos 3D de inflamação para avaliar o potencial regenerativo de células mesenquimais estaminais/estromais e seus produtos derivados

Resumo alargado em Português

O potencial regenerativo de células mesenquimais estaminais/estromais (CMEs) e dos seus produtos derivados, meio condicionado (MC) e vesículas extracelulares (VEs) têm sido estudados extensivamente *in vitro* e *in vivo*. Adicionalmente, tem sido descrito que CMEs possuem função de suporte a outros tipos celulares, previnem apoptose, estimulam a proliferação e migração, produzem factores anti-fibróticos e anti-cicatriz e têm propriedades imunomodulatórias. CMEs e seus produtos derivados têm sido testados em ensaios pré-clínicos e clínicos para diversas doenças, contudo, as expectativas do uso de CMEs como terapia ainda não foram atingidos. Principalmente devido a factores como capacidade de sobrevivência e "homing" após transplante celular mantendo as suas propriedades regenerativas, escolha da via de administração, dose e número de doses e quando realizar a administração de acordo com o estado da doença, escolha de métodos de avaliação do efeito regenerativo, escolha da fonte celular de CMEs, variabilidade entre dadores, falta de métodos robustos e padronizados de isolamento, de condições de cultura e de caracterização das suas propriedades fenotípicas e funcionais bem como falta de conhecimento sobre os mecanismos de acção.

Esta tese pretendeu responder a diversas destas questões pelo estabelecimento de uma plataforma de ensaios de potência de forma a caracterizar as propriedades de CMEs, CME-MC e CME-VEs. Para avaliar o potencial de suporte de CMEs por contacto celular, um ensaio angiogénico de incorporação de tubos foi desenvolvido; para avaliar a capacidade de CMEs para sobreviver após transplantação, um ensaio de stress oxidativo foi desenvolvido; para avaliar a capacidade de CMEs para promover proliferação e migração por acção parácrina, um ensaio de "cicatrização de feridas" *in vitro* foi optimizado; para avaliar as propriedade imunomodulatórias de CMEs, CME-MC e CME-VEs, foram desenvolvidos ensaios de potência 2D usando células endoteliais e monócitos e modelos 3D de inflamação dos alvéolos pulmonares usando transwells e dispositivos de microfluídica. Estes ensaios foram desenvolvidos e usados para avaliar a variabilidade entre dadores da mesma fonte celular e de diferentes fontes celulares bem como a dose de CME-VEs e regimes de administração.

CMEs foram isoladas de medula óssea, tecido adiposo e matrix do cordão umbilical e caracterizadas de acordo com as directrizes da Sociedade Internacional de Terapias Celulares. A proliferação celular de 3 dadores por fonte celular foi determinada. Para os dadores usados, CMEs de tecido adiposo apresentaram maior proliferação, contudo comparação directa entre fontes celulares do mesmo dador não foi realizada.

A resitência e capacidade de sobrervivência de CMEs foi testada desenvolvendo ensaios de stress oxidativo em aderência e suspensão. O ensaio em aderência demonstrou elevada variabilidade entre dadores de CME da mesma fonte, factor com maior predominância comparado com a diferença entre fontes celulares. O ensaio em suspensão foi desenvolvido para maior robustez, reduzindo o tempo e a variabilidade experimental e para maior semelhança à situação de infusão celular.

Apesar de ser necessário optimização, o ensaio de incorporação de tubos por co-cultura entre CMEs e HUVEC indicou que CMEs não possuiam forte capacidade de suporte e angiogénese por contacto celular. O ensaio de disrupção de tubos em Matrigel usando 10-15% DMSO e principalmente o ensaio de formação de tubos permitem a avaliação do potencial angiogénico de CME-MC e CME-VEs, sendo o efeito parácrino determinado pela aceleração da remodelação dos tubos ou pela aceleração da formação de tubos e conecções e sua estabilidade, respectivamente.

Um ensaio de "cicatrização de feridas" *in vitro* por disrupção mecânica da camada confluente de HUVEC foi optimizado para avaliar o potencial do CME-MC em promover a migração de HUVEC de forma a fechar a "ferida". Os resultados mostraram que o CME-MC tem a capacidade de promover a migração de HUVEC, sendo o efeito de um dos dadores semelhante ao controlo positivo constituído por meio de cultura contendo vários factores que promovem proliferação, migração e angiogénese. Contudo, o potential de CME-MC em promover migração de HUVEC é dependente do dador, indicando que a variabilidade das células de origem é replicada no seu MC. Este ensaio pode também ser usado para testar o potencial de CME-VEs.

O potencial imunomodulatório de CME-VEs de diferentes dadores de medula óssea foi testado através de ensaios de potência usando células endoteliais e monócitos, tendo por base o típico processo inflamatório. Para tal, inicialmente foram estabelecidos o método de isolamento de VEs do CME-CM por ultracentrifugação diferencial e os métodos de caracterização das populações de VEs. Os resultados indicaram que se estabelceu um processo de isolamento robusto e consistente originando populações de VEs relativamente puras entre vários dadores e com tamanho entre 91 e 201 nm, na gama de exosomas e pequenas microvesículas, determinado por "Nanoparticle Tracking Analysis", "MicroBCA" e "Cryo-TEM". Nesta tese, é proposto o uso generalizado do quociente PPR como medida da pureza das populações de VEs. Os ensaios de potência usando monócitos THP-1 e células endoteliais HUVEC permitiram identificar CME-VEs com potencial pro- e anti-inflamatório, indicando que variabilidade entre dadores também é replicado no potencial de CME-VEs. O ensaio de potência usando HUVEC também indicou que a dose mais elevada de CME-VEs de dadores não pro-inflammatório resulta num maior grau de redução da inflamação, contudo as VEs foram apenas moderadamente anti-inflamatórias indicando que não só a dose mas também o potencial anti-inflamatório deverá ser melhorado por estratégias de bioengenharia.

Para superar as limitações do uso de modelos animais para prever respostas humanas, a limitada disponibilidade de órgãos *ex vivo*, bem como o uso de modelos 2D simplistas que não recapitulam as funções dos órgãos, foram desenvolvidos modelos 3D de inflamação usando transwells e dispositivos de microfluídica, os quais incluem as interacções entre tecidos endotelial e epitelial e interface ar-líquido mimetizando o alvéolo pulmonar. O modelo de alvéolo pulmonar usando dispositivos de microfluídica também estava sujeito a forças mecânicas de tensão que simulavam a respiração e de tensão de corte nas células endoteliais pelo fluxo contínuo de meio de cultura que simulavam o fluxo sanguíneo nos vasos sanguíneos.

Os modelos 3D de inflamação indicaram que CMEs e CME-VEs têm o potencial de reduzir inflamação e promover a recuperação da função de barreira endotelial-epitelial, contudo o efeito foi moderado, indicando que para uma resolução completa da inflamação será necessário não só

optimizar doses, a sua frequência e regime de administração bem como desenvolver estratégias de bioengenharia que melhorem a eficácia e o potencial terapêutico.

Os modelos 3D desenvolvidos conferem vantagens relativamente aos modelos 2D *in vitro* permitindo o estudo de respostas fisiopatológicas humanas mais aproximadas ao que acontece *in vivo*, contudo, estes modelos podem ainda ser optimizados no que respeita ao uso de células primárias humanas específicas do órgão, aos estímulos mecânicos, à complexidade do sistema incorporando outros tipos de células e também à inflamação causada e tratamento com CMEs e respectivos produtos secretados. Prevê-se que no futuro após optimização e automatização, estes dispositivos de microfluídica poderão ser um requisito das agências regulatórias como modelo complementar aos estudos 2D *in vitro* para melhor prever o efeito em humanos e permitindo a redução do número de animais usados em investigação.

Estratégias de bioengenharia por pre-condicionamento de CMEs para melhorar a eficácia de CME-VEs foram preliminarmente avaliadas e os resultados indicaram que alguns compostos parecem melhorar o potencial anti-inflamatório de CME-VEs. Mais estudos serão necessários para confirmar os resultados, bem como avaliar o seu potencial nos modelos 3D e modelos animais e determinar os mecanismos de acção, vias de sinalização, factores de transcrição ou microRNAs envolvidos.

De realçar que o desenvolvimento de terapias de CME-VEs está dependente do desenvolvimento de métodos de armazenamento optimizados que mantenham não só as propriedades das VEs bem como a sua funcionalidade.

Conclui-se que é necessário o estabelecimento na área de métodos robustos e padronizados para avaliação da qualidade, potência e eficácia de CMEs e seus produtos derivados através de ensaios de potência 2D e modelos 3D avaliando as várias propriedades destes produtos. Conclui-se também que o potencial CMEs e seus produtos derivados é grandemente afectado pela variabilidade entre dadores, o que pode explicar os resultados contraditórios na área, e que o efeito de CMEs e seus produtos derivados é limitado sendo essencial o estabelecimento de estratégias de bioengenharia que permitam aumentar a sua eficácia e potencial terapêutico.

Acknowledgments

First of all, I would like to express my gratitude to Professor Joaquim Cabral and Professor Cláudia Lobato da Silva for accepting me as a PhD student of the MIT Portugal Program. I would like to greatly thank all the supervisors involved in this work, namely Professor Cláudia Lobato da Silva, PhD Ana Fernandes-Platzgummer, MD António Fiarresga, Professor Jeffrey Karp, Professor Donald Ingber, PhD Oren Levy and PhD Rachelle Prantil-Baun for the opportunity of working under their supervision, for their guidance, help and support and for always providing me motivation, inspiration and enthusiasm.

I would like to thank Diogo Pinto, Márcia Mata, Francisco Pinheiro, Joana Carmelo, Marta Costa, Francisco Moreira, Joana Serra, Sara Rosa and António Soure for the company and help at work, teaching me MSC-related techniques, warm friendship and laughs and for sharing with me the joy of working in SCERG-RM team.

I would also like to thank Heidi Kuang, Helena Lan, Alisa Ugodnikov and Thomas Kuncewicz from the Karp Laboratory for teaching me EV-related techniques, for helping with EV isolations and for your inspirational dedication to science.

Also a warm thank you to Amy Wen, Amir Bein, Bryan Hassell, Ratnakar Potla, Sasan Jalili, Bret Nestor, Carlos Ng, Nathan Sabaté del Río, Pawan Jolly and Andres Sanz Garcia from the Wyss Institute for the warm friendship, support, help, brainstorming, motivation and smiles.

I would like to thank MIT Portugal, Fundação para a Ciência e Tecnologia, Karp Laboratory and Wyss Institute for funding.

Last but not less important, I would like to dedicate this thesis to my parents Manuela and Mário and to my brother Bernardo for their unconditional love, support, advices, inspiration and motivation and to thank all my friends and Tiago for always being next to me no matter how much distance was between us, for some time (Por fim e não menos importante, gostaria de dedicar esta tese aos meus pais Manuela e Mário e ao meu irmão Bernardo pelo seu amor incondicional, apoio, conselhos, inspiração e motivação e agradecer a todos os meus amigos e ao Tiago por estarem sempre presentes independentemente da distância que por tempos nos separava).

Contents

List of Figures

List of Tables

Nomenclature

Latin Letters and Measurement units

°C	Degree Celsius
CO_2	Carbon dioxide
fg	Femtogram
g	Gram
h	Hour
H_2O	Water
H_2O_2	Hydrogen peroxide
Hz	Hertz
kPa	Kilopascal
l	Litre
min	Minute
mg	Miligram
ml	Millilitre
mm	Millimetre
mM	Minimolar
N	Normality unit
ng	Nanogram
nm	Nanometre
RCF	Relative centrifugal force
sec	Second
U	Enzymatic unit
µg	Microgram
µl	Microlitre
µm	Micrometre
µM	Micromolar
%	Percentage
3D	Three-dimensional

Greek Letters

α	Alpha
β	Beta
γ	Gamma
µ	Micro

Abbreviations

AMI	Acute myocardial infarction
AT	Adipose tissue
ATP	Adenosine triphosphate
a.u.	Arbitrary units
BSA	Bovine serum albumin
BM	Bone marrow
bFGF	Basic fibroblast growth factor
CAM	Chick chorioallantoic membrane
CD40L	CD40 ligand
CM	Conditioned medium
COPD	Chronic obstructive pulmonary disease
DF	Degrees of freedom
Dil	Diluted
DMSO	Dimethyl sulfoxide
DNA	Deoxyribonucleic acid
EDTA	Ethylenediamine tetraacetic acid
EGF	Epidermal growth factor
ELISA	Enzyme-linked immunosorbent assay
EM	Expansion medium
EMA	European Medicines Agency
ESCRT	Endosomal sorting complex required for transport
EV	Extracellular vesicle
FBS	Fetal bovine serum
FDA	Food and Drug Administration
FGF	Fibroblast growth factor
FM	Flow medium
F value	Fisher's statistic test
G-CSF	Granulocyte-colony-stimulating factor
GM-CSF	Granulocyte/macrophage-colony-stimulating factor
GVHD	Graft-versus-host disease
HGF	Hepatocyte growth factor
HLA	Human leukocyte antigen
HUVEC	Human umbilical vein endothelial cells
hTERT	Human telomerase reverse transcriptase
ICAM-1	Intercellular adhesion molecule-1 or CD54
IDO	Indoleamine 2,3-dioxygenase
IFN	Interferon
Ig	Immunoglobulin

IGF	Insulin-like growth factor
IL	Interleukin
ISEV	International Society for Extracellular Vesicles
JAK	Janus kinase
KGF	Keratinocyte growth factor
KLH	Keyhole-limpet hemocyanin
LDH	Lactate dehydrogenase
LDL	Low-density lipoproteins
LPS	Lipopolysaccharide
MAPK	Mitogen-activated protein kinases
MCP-1	Monocyte chemoattractant protein-1
M-CSF	Macrophage-colony-stimulating factor
MHC	Major histocompatibility complex
MI	Myocardial infarction
miR	microRNA
MM	Maintenance medium
MMP	Matrix metalloproteinases
MS	Mean sum of squares
MSC	Mesenchymal stem/stromal cell
n.a.	Not availiable
NF-ĸB	Nuclear factor-ĸB
NK	Natural killer
NO	Nitric oxide
P	Passage
PBMC	Peripheral blood mononuclear cell
PBS	Phosphate buffered saline
PDGF	Platelet-derived growth factor
PCR	Polymerase chain reaction
PDMS	Poly(dimethylsiloxane)
Pen/Strep	Penicillin-Streptomycin
PFA	Paraformaldehyde
PGE2	Prostaglandin E2
PI	Propidium iodide
PMA	Phorbol-12-myristate-13-acetate
PPR	Protein to particle ratio
P value	Probability value
ROS	Reactive oxygen species
SCF	Stem cell factor
SDF-1	Stromal cell-derived factor-1
SS	Sum of squares

TGF-β	Transforming growth factor-β
TLR	Toll-like receptors
TNF-α	Tumor necrosis factor-α
TSA	Trichostatin A
TSG101	Tumor susceptibility gene 101 protein
UC	Ultracentrifugation
UCB	Umbilical cord blood
UCM	Umbilical cord matrix
VCAM-1	Vascular cell adhesion molecule-1 or CD106
VEGF	Vascular endothelial growth factor
WP	Well plate
ZO-1	Zonula occludens-1

1 Introduction

World population is ageing leading to changes in global public health, thus, it is important to conduct epidemiologic studies to understand how disease incidence, prevalence and mortality change every decade. These studies allow designing better health care systems, predicting and managing governmental budgets to support the burden of increasing health care costs, designing health initiatives for population awareness towards disease prevention and change to healthier habits and life style and also to direct funding for research to better understand disease mechanisms and to develop improved therapies either with drugs or cell-based therapies.

The increase in life expectancy is a consequence of urbanization and better health and sanitary systems resulting in a decrease of communicable diseases such as infectious diseases, however, ageing and incorrect life styles resulted in an increase of chronic non-communicable diseases such as cardiovascular and neurologic diseases and cancer (Beaglehole and Bonita, 2008; GBD 2015 Disease and Injury Incidence and Prevalence Collaborators, 2016). It is predicted that by 2030, the chronic non-communicable diseases will account for about 75% mortality worldwide, as shown in Figure 1.1 (Beaglehole and Bonita, 2008).

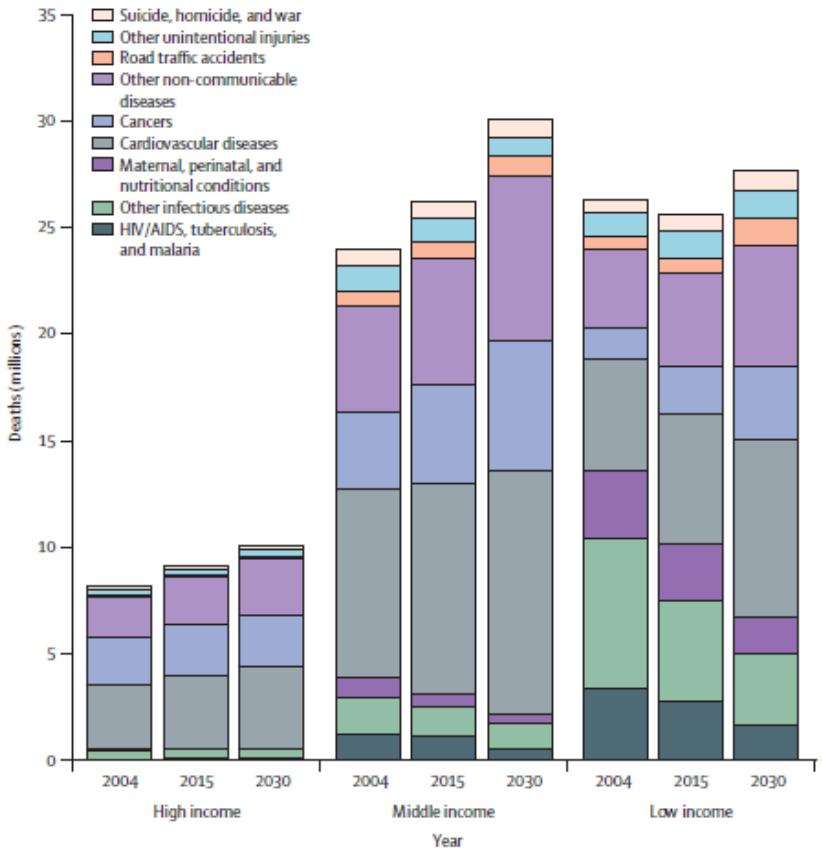

Figure 1.1 – Projected number of deaths (in millions) per cause in 2004, 2015 and prediction for 2030 indicate that non-communicable diseases (cardiovascular diseases, cancer and others) are and will continue to be the major causes of death worldwide (Beaglehole and Bonita, 2008).

Cardiovascular diseases such as ischemic heart and cerebrovascular diseases were the two leading causes of death and are predicted to still cause the highest mortality in 2030 (Figure 1.2). Infectious diseases with exception of human immunodeficiency virus (HIV) tend to decrease by 2030. While chronic diseases such as chronic obstructive pulmonary disease (COPD), diabetes, hypertensive heart disease and cancer will tend to increase in 2030 (Mathers and Loncar, 2006).

Category	Disease or Injury	2002 Rank	2030 Ranks	Change in Rank
Within top 15	Ischaemic heart disease	1	1	0
	Cerebrovascular disease	2	2	0
	Lower respiratory infections	3	5	−2
	HIV/AIDS	4	3	+1
	COPD	5	4	+1
	Perinatal conditions	6	9	−3
	Diarrhoeal diseases	7	16	−9
	Tuberculosis	8	23	−15
	Trachea, bronchus, lung cancers	9	6	+3
	Road traffic accidents	10	8	+2
	Diabetes mellitus	11	7	+4
	Malaria	12	22	−10
	Hypertensive heart disease	13	11	+2
	Self-inflicted injuries	14	12	+2
	Stomach cancer	15	10	+5
Outside top 15	Nephritis and nephrosis	17	13	+4
	Colon and rectum cancers	18	15	+3
	Liver cancers	19	14	+5

Figure 1.2 – Projected ranking of the 15 leading causes of death in 2002 and prediction for 2030 indicating that mortality due to non-communicable diseases (cardiovascular diseases, cancer) and the infectious disease HIV will increase (Mathers and Loncar, 2006).

Inflammation is common to many non-communicable diseases including cardiovascular diseases such as myocardial infarction (MI) and stroke; auto-immune diseases for example diabetes mellitus type I, rheumatoid arthritis, Crohn's inflammatory bowel disease; lung diseases for instance asthma, COPD, pulmonary fibrosis; neurodegenerative diseases such as Parkinson; wound injuries; cancer and infectious diseases.

The focus of this work was the development of therapies directed for cardiovascular and lung diseases, therefore, further detail of these diseases will be described next.

1.1 Cardiovascular diseases

The heart pumps blood through the circulatory system (including arteries, veins, coronary vessels) supplying all organs with oxygen, nutrients, immune cells and other molecules and also allowing removal of cellular waste. Cardiovascular diseases are a group of disorders of the heart and circulation (Labarthe, 2011). Cardiovascular diseases can be divided into several groups of disorders, namely coronary heart diseases, cerebrovascular diseases, peripheral arterial diseases, rheumatic heart diseases, congenital heart diseases and deep vein thrombosis and pulmonary embolism (Labarthe, 2011). Coronary heart diseases are related to diseased blood vessels supplying the heart

muscle, the myocardium, including angina, acute coronary syndrome and acute myocardial infarction (AMI) (Hanson *et al.*, 2013). Cerebrovascular diseases are diseases of the blood vessels that supply the brain, within which stroke is the disorder with higher incidence and also the second cause of mortality worldwide (Labarthe, 2011). Peripheral arterial diseases are related to disorders of the arteries supplying arms and legs (Ouriel, 2001). Rheumatic heart diseases are caused by bacterial infections which injure the myocardium and the heart valves (Marijon *et al.*, 2012). Congenital heart diseases are malformations of the heart or intrathoracic great vessels that occur at birth, being the ventricular septal defect the most common (Hoffman and Kaplan, 2002). Deep vein thrombosis and pulmonary embolism are related to the occlusion of blow flow specially in the legs and pelvic veins forming blood clots that can dislodge to the lungs through the venous circulation (Labarthe, 2011).

Inflammation has important roles in the initiation and progression of atherosclerosis, the process of lipid deposition in the blood vessels and consequent decrease of blood flow which leads to the development of several cardiovascular diseases (Willerson and Ridker, 2004; Hansson, 2005; Libby, 2006; Golia *et al.*, 2014).

1.1.1 Atherosclerosis process

Initialization of the atherosclerosis process

At normal physiological conditions, endothelial cells from the blood vessels are not activated which blocks adhesion of leukocyte immune cells. Moreover, shear stress of the blood flow prevents platelet accumulation and induces the expression of the anti-oxidant enzymes nitric oxide (NO) synthase and superoxide dismutase that protect from oxidative stress (Libby, 2006). Fat diets, reduced physical exercise, obesity, smoking, hypertension, hyperglycemia and insulin resistance cause the deposition of fat and cholesterol in the blood vessels (Libby, 2006). The lipid deposits (atheroma) have the ability to activate endothelial cells resulting in the up-regulation of adhesion molecules such as vascular cell adhesion molecule-1 (VCAM-1), intercellular adhesion molecule-1 (ICAM-1) and selectins (Libby, 2006; Golia *et al.*, 2014). Low-density lipoproteins (LDL) will accumulate in the sub-endothelial space and perturb blood flow resulting in the lack of shear stress signal on endothelial cells to produce anti-oxidant enzymes, which in turn leads to an increase of reactive oxygen species (ROS) that will oxidize the LDL (Libby, 2006; Golia *et al.*, 2014). Oxidized LDL as well as the pro-inflammatory cytokines interleukin (IL)-1β and tumor necrosis factor-α (TNF-α) induce further up-regulation of endothelial cell adhesion molecules (Libby, 2006). Under physiological conditions, NO blocks nuclear factor-ΚB (NF-ΚB), on the other hand oxidized LDL, IL-1β and TNF-α activate NF-ΚB signaling cascade mediating the expression of endothelial cell adhesion molecules. Monocytes and T lymphocytes are two types of leukocytes flowing in the blood which can bind to activated endothelial cells forming early atherosclerotic plaques (Libby, 2006).

Development of the fatty streak and exacerbation to a complex plaque

Activated endothelial cells secrete chemokines such as IL-8 and monocyte chemoattractant protein-1 (MCP-1) which drive the monocyte migration towards the activated endothelium. Recruited monocytes will bind to endothelial cell adhesion molecules and transmigrate to the inner layer of the

vessel, the intima, by diapedesis (Figure 1.3) (Libby, 2006; Soehnlein and Lindbom, 2010; Golia *et al.*, 2014). In the intima monocytes differentiate into macrophages which phagocyte the oxidized LDL and then mature into lipoprotein-loaded macrophages, the foam cells. Macrophages secrete several growth factors, cytokines and chemokines such as IL-1, IL-8, IL-18, TNF-α and also macrophage-colony-stimulating factor (M-CSF), which by a feedback loop induce proliferation of macrophages exacerbating inflammation in the fatty streak, the initial lesion of atherosclerosis (Libby, 2006; Golia *et al.*, 2014). The atherosclerotic plaque secrete other chemokines such as eotaxin which interacts with the receptor CXCR3 overexpressed in macrophages, T lymphocytes and mast cells indicating that these cells also play an important role in the atherosclerosis process (Libby, 2006).

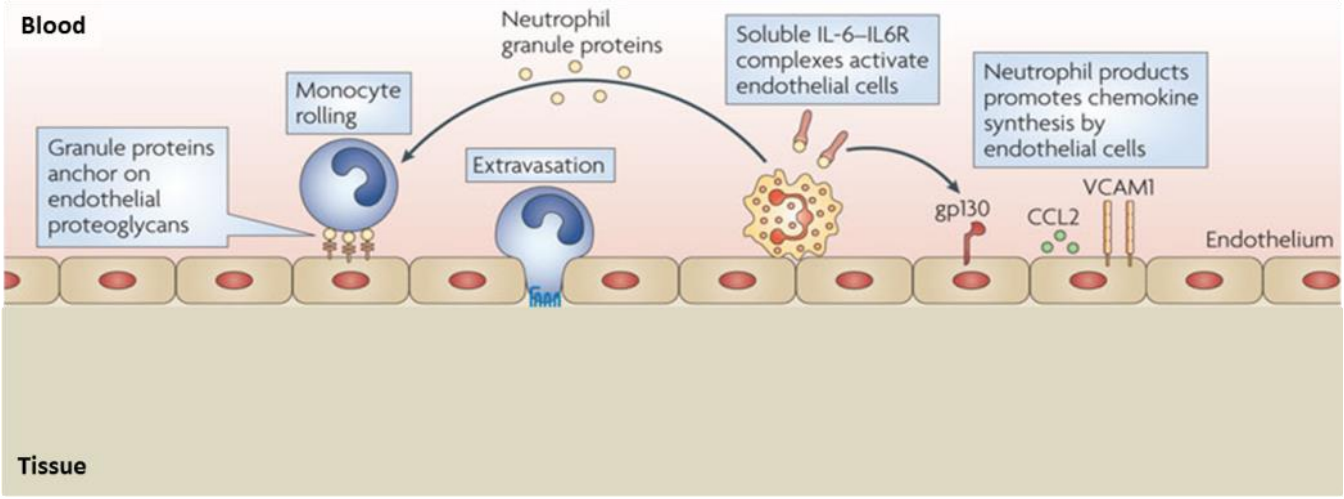

Figure 1.3 – General inflammatory process. Activated neutrophils secrete granule proteins and cytokines such as IL-6 that interact with endothelial cells and monocytes. Monocytes flowing in the blood vessel will roll along the blood vessel towards the chemoattractant CCL2 produced by activated endothelial cells through gp130. Then, monocytes will bind to activated endothelium expressing VCAM-1 adhesion molecules and transmigrate into the tissue. Adapted from (Soehnlein and Lindbom, 2010)

Plaque rupture

There are mechanisms to avoid exacerbation of the atherosclerosis process, for instance, the enlargement of the arteries, however, when the plaque occupies more than 40% of the internal elastic lamina area there will be a narrowing of the arteries, entitled stenosis (Glagov *et al.*, 1987). Vascular smooth muscle cells proliferate in the plaque area producing extracellular matrix proteins such as collagen when stimulated by transforming growth factor-β (TGF-β) and platelet-derived growth factor (PDGF), resulting in a strong and stable fibrous cap over the lesion (Libby, 2006; Golia *et al.*, 2014). However, inflammation progressively destroys the fibrous cap 1) by degrading the existing collagen by matrix metalloproteinases (MMP) produced by macrophages that are activated by monocytes secreting IL-1 and CD40 ligand (CD40L) and 2) by blocking new collagen production by smooth muscle cells through the inhibitory action of interferon (IFN)-γ produced by T lymphocytes (Libby, 2006; Golia *et al.*, 2014). Moreover, the mast cells that are present in the plaque may also secrete TNF-α which also induces MMP production by macrophages. The thinner fibrous cap becomes unstable and plaque rupture occurs exposing the lipid core. Furthermore, CD40L up-regulates tissue

factor in macrophages and in turn the tissue factor will interact with factor VII in the blood triggering the coagulation cascade and formation of thrombus. Thrombus expansion may consequently lead to endothelial damage and complete occlusion of the artery (Libby, 2006; Golia *et al.*, 2014). When occlusion happens in a coronary artery, the supply of oxygen and nutrients is compromised creating an ischemic area in the myocardium. Severe and prolonged ischemia results in the cell death of cardiomyocytes, the cardiac muscle cells, and may originate angina, AMI and sudden cardiac death (White and Chew, 2008; Thygesen *et al.*, 2012). Moreover upon MI, cardiomyocyte hypertrophy and apoptosis occurs as well as collagen replacement and ventricle enlargement (Colucci, 1997).

1.1.2 Other mechanisms involved in myocardial injury

Under physiological conditions adenosine triphosphate (ATP) is mainly produced by oxidative phosphorylation in the mitochondria and high-energy phosphates are not degraded and transformed into purines (de Zwaan, Daemen and Hermens, 2001). However, upon thrombus formation, the cellular supply of oxygen and nutrients is blocked and the high-energy phosphates have to be used as energy source resulting in cellular and subcellular changes in cardiomyocytes and may also result in the loss of cardiomyocyte function and fibrosis (de Zwaan, Daemen and Hermens, 2001). Prolonged ischemia triggers lysosomes that cleave the cell membrane and increase permeability, resulting in the entrance of cations that increase osmotic cell stress and water accumulation in the cells (de Zwaan, Daemen and Hermens, 2001). Intracellular acidification activates pH-dependent ion transport systems followed by increased cation influx, impairment of oxidative phosphorylation, permanent damage of cell membrane and consequently cell necrosis (de Zwaan, Daemen and Hermens, 2001). Cell death might occur not only through necrosis but also by apoptosis when the anti-apoptotic proteins (Bcl-2 and Bcl-x_L) are decreased compared to pro-apoptotic proteins (Bax, Bak and Bid) (de Zwaan, Daemen and Hermens, 2001; Choi *et al.*, 2009). Apoptosis is also triggered by pro-inflammatory cytokines such as TNF-α and by oxidative stress (de Zwaan, Daemen and Hermens, 2001). Oxidative stress results from the accumulation of ROS and free radicals which can lead to lipid peroxidation and cell membrane damage and also stimulate platelet aggregation that typically occurs during the atherosclerosis process (de Zwaan, Daemen and Hermens, 2001). Moreover, ROS and intracellular proteins from dead cells activate toll-like receptors (TLR), recognition patterns for immune cells, which in turn stimulate NF-ΚB inflammatory cascade involved in the atherosclerosis process (Frantz, Bauersachs and Ertl, 2009).

1.1.3 Cardiac remodeling

Initially it was thought that the heart had no regenerative potential. It is now accepted that the heart has repair mechanisms, however, it has low regenerative potential (Torella *et al.*, 2007), thus repair of infarcted myocardium and repopulation of cardiomyocytes does not happen in a fast and effective way, as a result a fibrotic process occurs prior to cardiac remodeling. During the fibrotic process, atherosclerosis and ischemia result not only in cell death but also triggers immune cells (such as Ly-6C(hi) monocytes) that scavenge and clear matrix debris and dead cells (Frantz, Bauersachs

and Ertl, 2009; Chen and Frangogiannis, 2013). Immune cells also activate cardiac fibroblasts, promoting fibroblast expansion and consequent secretion of collagen to form a scar (Chen and Frangogiannis, 2013).

Degradation of matrix debris and removal of dead cells leads to a decrease in the inflammatory response. Macrophages engulf neutrophils that turn into apoptotic cells, apoptosis but not necrosis results in the release by lymphocytes and macrophages of anti-inflammatory cytokines IL-10 and TGF-β suppressing pro-inflammatory molecules, enhancing wound healing and results in the recruitment of monocytes with reparative action (Ly-6C(lo) monocytes) into the infarcted area (Frantz, Bauersachs and Ertl, 2009; Chen and Frangogiannis, 2013). TGF-β also decreases leukocyte adhesion (Frantz, Bauersachs and Ertl, 2009). Suppression of inflammation promotes activation and expansion of fibroblasts and endothelial cells. Angiotensin II and TGF-β1 stimulate cardiac fibroblasts differentiation into myofibroblasts (Krenning, Zeisberg and Kalluri, 2010; Chen and Frangogiannis, 2013) which express contractile proteins and secret matrix proteins such as collagen, maintaining structural integrity and enabling contraction of the infarcted area (Chen and Frangogiannis, 2013). Angiotensin II is thought to be mediated by TGF-β, fibroblast growth factor (FGF) and PDGF (Chen and Frangogiannis, 2013). Endothelial cells promote vascularization of the infarcted area to increase the supply of oxygen and nutrients. After matrix deposition and clearance of dead cells, there is a decrease in the secretion of growth factors and cell expansion is blocked, fibroblasts become quiescent and apoptotic and newly formed blood vessels either gain a muscular coat or regress, forming a dense collagen-based scar (Chen and Frangogiannis, 2013). This dense collagen-based scar may protect fibroblasts from mechanical stress which also contributes to their deactivation (Chen and Frangogiannis, 2013).

Cardiac remodeling is defined as a process involving molecular, cellular and interstitial changes in the infarcted area but also in the non-infarcted area which change the ventricular size and shape and the heart function (Chen and Frangogiannis, 2013). The cardiac remodeling is an orchestrated process involving cardiomyocytes, interstitium, fibroblasts, coronary vasculature and collagen degradation and is influenced by blood flow and mechanical strain, neuroendocrine activation and cytokine secretion (Cohn, Ferrari and Sharpe, 2000; Kehat and Molkentin, 2010). These external stimuli causes changes in chromatin and consequently in cardiac gene and protein expression, alterations in cellular metabolism and contraction ability (Kehat and Molkentin, 2010). The heart develops a compensatory hypertrophy which together with the significant loss of cardiomyocytes after MI leads to changes in the cardiomyocyte length and width, rearrangement of the ventricular wall, increased ventricular volume and, as a result, enlargement of the heart affecting its function (Cohn, Ferrari and Sharpe, 2000; Kehat and Molkentin, 2010). During the remodeling process, the geometry of the heart changes from elliptical to a more spherical shape (Cohn, Ferrari and Sharpe, 2000; Kehat and Molkentin, 2010). Several factors are involved is remodeling such as the neuroendocrine activation, renin angiotensin system, endothelin, TNF-α, interleukins, NO and ROS, in a well-orchestrated process promoting collagen-matrix degradation and cardiomyocyte repopulation (Cohn, Ferrari and Sharpe, 2000; Frantz, Bauersachs and Ertl, 2009).

However, there is a possibility that prolonged hypertrophy of cardiomyocytes and maintenance of activated fibroblasts in the surrounding scared area can result in increased production of matrix proteins, thus, increasing wall stress, changing gene and protein expression, altering the energetic and metabolic state, producing excessive ROS and neuroendocrine molecules (Kehat and Molkentin, 2010). Moreover, the increased stiffness resultant from excessive matrix alters the mechanic-electric coupling of cardiomyocytes, causes cardiomyocyte death and increases the risk of arrhythmias and cardiac failure (Spach and Boineau, 1997; Krenning, Zeisberg and Kalluri, 2010).

1.1.4 Treatment of cardiovascular diseases

Conventional therapies for acute and chronic cardiovascular diseases include oxygen supply, administration of aspirin, clopidogrel, prasugrel or glycoprotein IIb/IIIa inhibitors to block platelet aggregation, anti-thrombotic (unfractionated heparin, enoxaparin, low molecular weight heparin, factor X inhibitor) or thrombin inhibitors (bivalirudin) to reduce thrombus formation or block thrombin activity, fibrinolytic agents (streptokinase, urokinase, tissue plasminogen activator, tenecteplase tissue plasminogen activator, reteplase plasminogen activator) to prevent thrombus expansion and tear down the thrombus already formed, β-blockers to decrease blood pressure, nitrates for smooth muscle relaxation, coronary vasodilatation and reduction of ischemia, morphine as pain control, angiotensin-converting enzyme inhibitors or angiotensin receptor blockers for vasodilatation and to decrease left ventricular afterload, calcium channel blockers to inhibit slow calcium channels and for vasodilatation and statins to decrease lipid levels (White and Chew, 2008; Hanson *et al.*, 2013).

Surgical procedures might be necessary for more severe cases when drugs have no efficacy and for the cases for which there is not pharmacotherapy available. Surgical options include balloon angioplasty, stents, coronary artery bypass, valve repair and replacement, heart transplantation, artificial heart transplantation, pacemaker, prosthetic valves and patches (Choi *et al.*, 2009; Hanson *et al.*, 2013). All these surgical options with exception of heart transplantation do not repair the cardiomyocyte cell loss. Heart transplantation may result in higher survival than pharmacotherapy alone, however, it is limited to donor heart availability, immunosuppressive therapy is needed and there is a risk of graft failure, heart failure, infections and malignancies (Fraund *et al.*, 1999).

Non-conventional therapies have been under development to potentially improve patients outcome and to overcome limitations and drawbacks of conventional therapies and surgical procedures including polymeric hydrogels for delivery of therapeutic proteins and gene, protein and cell therapy (Choi *et al.*, 2009). Although promising, these therapies are still under research and there is a need for further proof of its potential and to boost its efficacy as some of the therapies have only a partial effect. Combination of several therapeutic strategies should also be investigated for potential enhanced results (Choi *et al.*, 2009).

Polymeric hydrogels for delivery of therapeutic proteins such as basic FGF (bFGF), vascular endothelial growth factor (VEGF), keratinocyte growth factor (KGF) and PDGF-BB have been tested to promote vascularization and recovery from ischemia by a controlled and prolonged release of functional proteins. Hydrogels are three-dimensional (3D) structures mainly composed of water with a network of hydrophilic polymer, which can be natural (gelatin, fibrin, hyaluronic acid, alginate,

chitosan) or synthetic (poly(ethylene glycol), polyacrylamide, poly(aspartic acid), poly(γ-glutamic acid)) (Choi *et al.*, 2009).

With regards to protein therapy, the delivery of heat shock proteins, angiogenic and anti-apoptotic proteins have been tested. Within heat shock protein family, the heat shock protein-27 is a chaperone that protects other proteins and promotes the degradation of damaged proteins, moreover, it blocks the caspase cascade protecting heart cells from apoptosis (Choi *et al.*, 2009). Angiogenic proteins such as FGF, VEGF and hepatocyte growth factor (HGF) have been used to promote revascularization of the injured myocardium. Anti-apoptotic proteins have cytoprotective ability, suppressing apoptosis and reducing the ischemic zone. Thus, FNK a derivative of Bcl-x_L anti-apoptotic protein and BH4 domain from Bcl-2 anti-apoptotic protein have been explored (Choi *et al.*, 2009).

Gene therapy delivering VEGF and FGF angiogenic growth factors have been shown to boost heart responses by improving vascularization and reducing infarcted area using viral (for instance adenovirus) and non-viral (for example plasmids) therapies (Choi *et al.*, 2009).

Cell therapy has been explored for the regeneration of lost cardiac cells, namely cardiomyocytes, smooth muscle cells and endothelial cells through differentiation of administered cells or activation of endogenous stem cell populations (Templin *et al.*, 2008; Choi *et al.*, 2009). Although cell therapy is promising, further research is needed to answer several open questions and elucidate mechanisms of action which will clarify the conflicting results observed so far in pre-clinical and clinical trials (White and Chew, 2008; Choi *et al.*, 2009). Hematopoietic progenitor cells, endothelial progenitor cells, skeletal myoblasts, embryonic stem cells, induced pluripotent stem cells, cardiac stem cells and mesenchymal stem/stromal cells (MSCs) have been tested (Beeres *et al.*, 2008; H. Yu *et al.*, 2017). MSC regenerative potential will be further described (in chapter 1.3) as these cells were the focus of the work developed.

1.2 Lung diseases

The main function of the lung is gas exchange by transferring the oxygen from the air into the bloodstream to supply all organs with oxygen and in the opposite direction it removes from the bloodstream the carbon dioxide resultant from cell metabolism (West, 2012). The lung is considered to be a blood reservoir and it is also an immunologic active site with barrier function protecting from infectious agents and other toxic particles and filters undesirable materials from the circulatory system (West, 2012; Chuquimia *et al.*, 2013).

Breathing consists of inspiration and expiration of air through nose and mouth to the lungs associated with an increase and decrease of the thoracic cavity, respectively. The airways are composed of several types of tubes that branch into narrower and shorter tubes but in higher number. Initially the air goes through the trachea which is divided into two main bronchi that in turn branch into lobar and segmental bronchi until the terminal and respiratory bronchioles (Figure 1.4). The bronchioles terminate in air sacs or alveoli. The gas exchange occurs in the alveoli which are small (1/3 mm) and in a high number (about 500 million) in the human lung resulting in a high surface area

for gas exchange. Moreover, the alveoli are in close contact with small capillaries allowing gas exchange by diffusion (West, 2012).

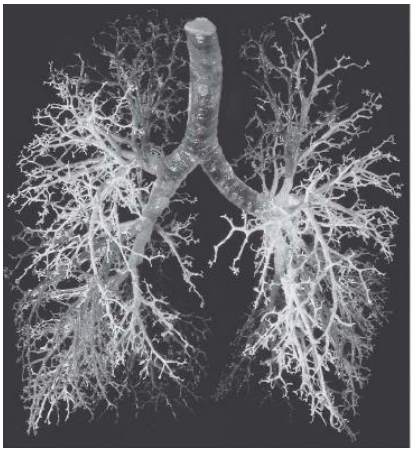

Figure 1.4 – Representation of the human lung airways showing the trachea and bronchioles after alveoli removal (West, 2012).

The lung alveolus is composed of an epithelial and an endothelial cell barrier at an air-liquid interface (Figure 1.5). The epithelium is a mixture of alveolar epithelial cells type I and type II (West, 2012; Chuquimia *et al.*, 2013; Sapru *et al.*, 2015). Alveolar epithelial cells type I are in higher number maintaining lung architecture and are mainly responsible for gas exchange but are also involved on inflammatory responses to microbial agents. Alveolar epithelial cells type II are responsible for healing upon injury, ion transport and removal of excess alveolar fluid as well as surfactant production which is important for clearance of pathogens and lung defense but also for reducing the surface tension during gas exchange avoiding alveoli collapse due to elevated pressures and surface tension while keeping a thin layer of liquid to avoid cell drying, therefore, stabilizing the alveoli structures (West, 2012; Chuquimia *et al.*, 2013; Sapru *et al.*, 2015). The endothelial cell barrier has an important role on gas, fluid and solute exchange (Kelly *et al.*, 1998).

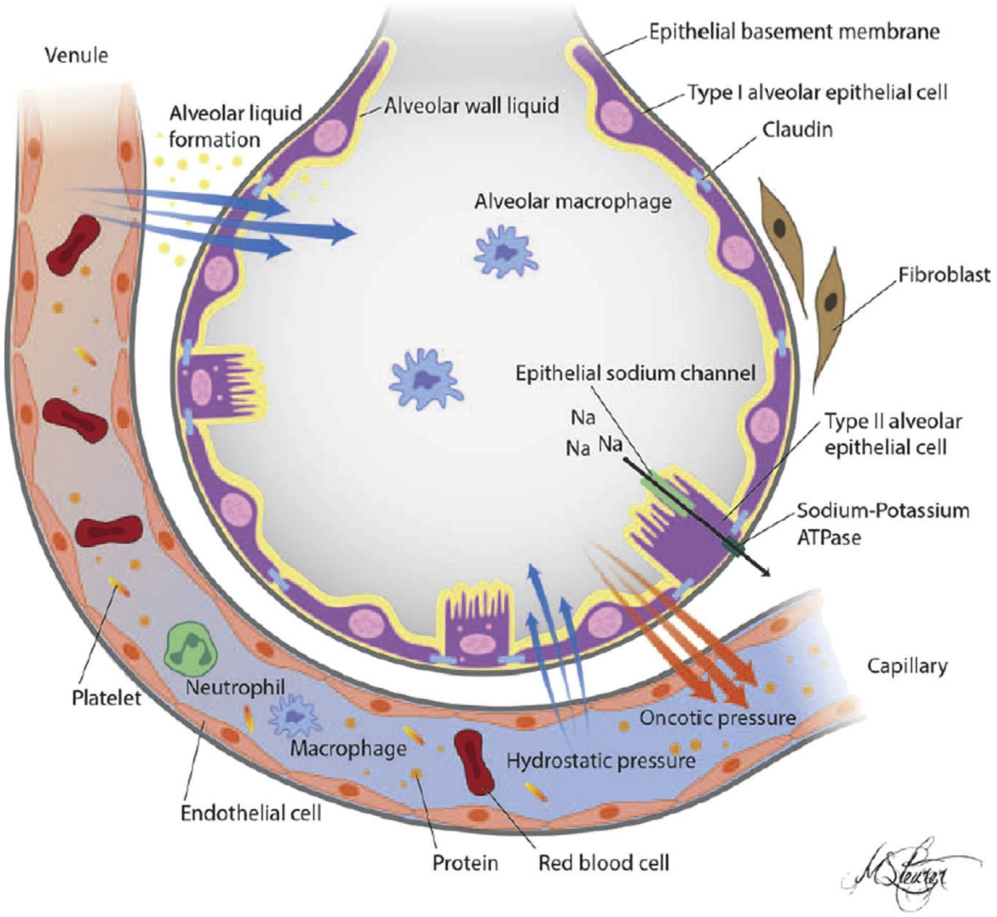

Figure 1.5 – Representation of lung alveoli under physiological conditions. Air-liquid interface is established between the capillary endothelium surrounding the alveolar epithelium maintaining a close contact that facilitates gas exchange. The thin barrier between epithelium and endothelium also allows alveolar macrophages and other immune cells to transmigrate from the blood vessel into to the epithelial chamber, which is a key host defense mechanism. Alveolar epithelial cells type II regulate surfactant production and the removal of excess alveolar fluid through sodium-potassium ATPase channels (Sapru *et al.*, 2015).

According to the world health organization, chronic respiratory diseases are diseases of the airways and pulmonary structures and the major preventable chronic respiratory diseases include asthma and respiratory allergies, COPD, occupational lung diseases, sleep apnea syndrome and pulmonary hypertension. Other common chronic diseases include bronchitis, emphysema, hypersensitivity pneumonitis, lung cancer, lung fibrosis, chronic rhinosinusitis and sarcoidosis (WHO, 2007).

COPD was the 5th leading cause of death worldwide in 2002 and it is predicted to surpass the number of deaths from HIV infectious disease and be the 4th leading cause of death worldwide (Mathers and Loncar, 2006). Asthma causes about 250,000 annual deaths worldwide (WHO, 2007). COPD prevalence in the year 2000 was about 210 million persons, while asthma was estimated in 300 million persons by 2004 and allergic rhinitis in 400 million between in the years 1996-2006 (WHO, 2007).

These diseases significantly reduce life quality of patients and are associated with a growing economic burden not only in terms of medical care but also in terms of working days lost. Among the risk factors of chronic respiratory diseases are tobacco smoke, air pollution, allergens, occupational agents, high altitude and diseases such as schistosomiasis or sickle cell disease (WHO, 2007).

Inflammatory lung diseases

Inflammation is a common state to several lung diseases, for instance, asthma (Barnes, 2008), COPD (Barnes, 2008), pulmonary hypertension (Price *et al.*, 2012), pneumonia (Dallaire *et al.*, 2001), sarcoidosis (Patterson and Chen, 2017), acute respiratory distress syndrome (Sapru *et al.*, 2015), pulmonary fibrosis and edema (Scadding and Hinson, 1967; Phan, 2002; Sapru *et al.*, 2015).

Asthma is a chronic inflammatory lung airway disease characterized by increased sensitivity which results in exacerbated responses when inflammation increases and consequent obstruction of the air flow. Frequently, asthma has significant impact on patient health and life quality especially with co-morbidities such as rhinitis which is the nasal mucosa inflammation. It is possible to reverse exacerbated responses and breathing obstruction with appropriate treatment (Barnes, Shapiro and Pauwels, 2003; WHO, 2007). Asthma acute events are controlled mostly by inhaled corticosteroids and asthma is frequently responsive to corticosteroid therapy with resistance only in severe asthma patients (Barnes, 2008).

COPD is a chronic inflammatory lung airway disease and is characterized by a progressive breathing obstruction and by exacerbated inflammatory response when harmed with tobacco smoke and other toxic agents. Prolonged breathing obstruction is triggered by a mixture of conditions as small airway obstructive bronchiolitis disease and destruction of the parenchyma, or emphysema (WHO, 2007; Barnes, 2008). COPD is usually not responsive to corticosteroid therapy (Barnes, 2008), other alternatives such as bronchodilators and oxygen therapy have been used (Celli *et al.*, 2004). In severe cases surgery (lung volume reduction surgery, bullectomy and lung transplantation) might be needed (Celli *et al.*, 2004).

New therapies to suppress T cells and treat inflammation are under development for asthma and COPD such as immunotherapy including deoxyribonucleic acid (DNA) vaccines, T cell peptides and sublingual therapy as well as therapies targeting specific transcription factors as NF-ĸB and small molecule inhibitors for certain chemokines (Barnes, 2008).

Pulmonary hypertension is characterized by high mean pulmonary artery pressure (above 25 mmHg) and is associated to several diseases as COPD, pulmonary fibrosis, sickle cell disease and schistosomiasis as well as systemic sclerosis, congenital heart diseases and HIV infection. Pulmonary hypertension results in a bad prognosis if not treated (WHO, 2007; Price *et al.*, 2012). During the onset of pulmonary hypertension disease, thickening of the pulmonary arteries occurs as well as thrombosis and fibrosis, typical of inflammatory and atherosclerosis processes (Price *et al.*, 2012). Elevated artery pressure results in chronic raise of pulmonary vascular resistance, right ventricular failure and potentially death. About 80% of patients with pulmonary hypertension have a genetic mutation in the gene bone morphogenetic protein receptor type 2 (Price *et al.*, 2012). Pulmonary

hypertension treatment may include vasodilators, endothelin receptor antagonists, calcium channel blockers (similarly to cardiovascular disease treatment) as well as anti-coagulants, digoxin, diuretics, oxygen, phosphodiesterase type 5 inhibitors and guanylate cyclase stimulators, rostacyclin analogues and prostacyclin receptor agonists (Galiè *et al.*, 2015). For severe cases surgery (atrial septostomy and heart and/or lung transplantation) may be necessary (Galiè *et al.*, 2015).

Pneumonia is a common lung alveoli infectious disease caused by bacteria, virus or other infectious agents and its treatment is based on potent antibiotics and intensive health care support (Dallaire *et al.*, 2001).

Sarcoidosis is a systemic inflammation disease characterized by the presence of granulomas (microscopic inflammatory lumps), which when inflammation is not cleared, can progress to pulmonary fibrosis compromising breathing. Corticosteroids can be used to reduce inflammation and granuloma formation and immunotherapy is under investigation, however, there is no treatment for lung fibrosis (Patterson and Chen, 2017).

Acute respiratory distress syndrome is a non-cardiogenic lung disease characterized by fluid accumulation in the alveoli and low oxygen in the blood, moreover, hypoxia leads to worsen prognosis and death. Treatment options to control the disease onset are very limiting and include lung protective ventilation and oxygen supply (Sapru *et al.*, 2015; Heidemann *et al.*, 2017), although alternatives are being tested such as fluid management, surfactant administration, inhalation of NO, prone positioning, sedation and neuromuscular blockade (Heidemann *et al.*, 2017).

Pulmonary fibrosis and edema are conditions that affect the alveoli and are associated with other lung diseases, infections or toxic agents. Pulmonary fibrosis is characterized by an inflammatory process and thickening of the alveolar walls resulting in increasing stiffness affecting breathing. Tissue damage, similarly to what was described for cardiac remodeling (1.1.3), activates fibroblasts that become myofibroblasts secreting extracellular matrix to form a fibrotic scar tissue (Scadding and Hinson, 1967; Phan, 2002). There is no treatment available for pulmonary fibrosis other than lung transplantation, which has limited availability. Pulmonary edema is the accumulation of alveolar fluid in the alveoli resultant from prolonged inflammation which dysregulates surfactant production and the ion transport channels involved in fluid removal and weakens the endothelium-epithelium cell barrier (Sapru *et al.*, 2015; Heidemann *et al.*, 2017). Pulmonary edema is a condition associated to several lung diseases but can also be caused by side effects of chemotherapeutic drugs such as IL-2 (Conant, Fox and Miller, 1989; Baluna and Vitetta, 1997). Fluid management and surfactant administration are potential therapies to control disease conditions.

Thus, inflammation is a key condition in many lung diseases although there are different and complex mechanisms and pathways involved in each disease. Moreover, there is no cure for lung inflammatory diseases and for some of the disorders no treatment is available. Many drugs and immunotherapies are under development and testing. Cellular therapies are also a great promise and the use of hematopoietic cells, MSCs and lung progenitor cells is under investigation not only for transplantation and repopulation of the lung but also to stimulate resident cell populations (Garcia *et al.*, 2012).

1.2.1 Lung defense mechanisms and inflammatory response

The lungs are an immunological active site that is continuously subjected to harmful air agents and toxic molecules circulating in the vasculature (Yu, 2008; Chuquimia *et al.*, 2013). Upon an inflammatory stimuli, lung alveoli epithelial cells produce surfactant, ROS, cytokines (such as TNF-α, IL-1β, granulocyte/macrophage-colony-stimulating factor (GM-CSF)) and platelet-activating factor which recruit immune cells from the vasculature (Adler *et al.*, 1994). Surfactants A and D besides decreasing surface tension, are also involved in defense mechanisms through binding with the pathogen and mediating leukocyte activity towards removal of the harmful agent (Kuroki, Takahashi and Nishitani, 2007; Yu, 2008).

Different types of immune cells are involved in lung inflammation. Dendritic cells and macrophages are sentinels of the immune system that first act on the phagocytosis of pathogens, particulates and apoptotic cells (Yu, 2008). Macrophages and epithelial cells secrete cytokines and chemokines that recruit neutrophils to the site of inflammation and activate endothelial cells that express adhesion molecules (VCAM-1 and ICAM-1) that allow transmigration of the neutrophils from the vasculature to the epithelial chamber. Neutrophils engulf the pathogens and destroy them with ROS, anti-microbial proteins and enzymes (Yu, 2008; Soehnlein and Lindbom, 2010). Lymphocytes are also recruited to the inflammation site. Th1 $CD4^+$ T lymphocytes secrete pro-inflammatory cytokines, such as IFN and TNF-α, to neutralize virus, parasites and cancer cells (Yu, 2008). Th2 $CD4^+$ T lymphocytes secrete IL-4, IL-5, IL-9, and IL-13 cytokines that trigger B cells (Yazdanbakhsh, Kremsner and Van Ree, 2002; Yu, 2008). Immune response comprises a balance between Th1 and Th2 (Yazdanbakhsh, Kremsner and Van Ree, 2002; Yu, 2008). Cytotoxic $CD8^+$ T lymphocytes and natural killer (NK) cells also act on destroying pathogenic agents and cancer cells (Yu, 2008). B cells, produce immunoglobulin (Ig) A which protects the epithelium cell barrier from microbial and viral infections causing pathogen phagocytosis, on the other hand, IgE exacerbates immune responses (Yu, 2008). Mast cells are activated by IgE releasing pro-inflammatory mediators as histamine, leukotrienes, proteases, cytokines and chemokines which, besides host defense, contributing to chronic airway inflammation (Stone, Prussin and Metcalfe, 2010). Eosinophils are also activated by IgE and are responsible for secretion of inflammatory-related mediators and the secretion of mast cell stem cell factor that regulates mast cell proliferation and degranulation (Kariyawasam and Robinson, 2007; Yu, 2008). Eosinophil infiltration is associated with increased vascularity and VEGF up-regulation which, besides being involved in inflammation, angiogenesis and tissue remodeling, also promotes antigen presentation and Th2 cell inflammation (Kariyawasam and Robinson, 2007; Yu, 2008).

As the defense mechanisms take action and inflammation decreases, macrophages increase the production of anti-inflammatory cytokines including: IL-10 which blocks the production of pro-inflammatory cytokines by T cells, NK cells, and monocytes; TGF-β that enhances wound healing and scar formation and IL-1 receptor antagonist that also reduces inflammation (Moore *et al.*, 1992; Yu, 2008). Resolution of inflammation is dependent not only on the suppression of inflammatory mediators but also on the removal of apoptotic cells and remodeling of the tissue (Fadok *et al.*, 1998). The remodeling of the tissue involves cellular matrix deposition, fibroblasts, smooth muscle cells,

endothelial cells and leukocytes (Jeffery, 2001; Yu, 2008). Different lung diseases have different remodeling processes with (for example, COPD) or without (for example, asthma) fibrosis (Jeffery, 2001).

The lung inflammatory process is similar between different lung diseases although specific mechanisms and immune cells are primarily used for each disease. In the case of chronic lung diseases there is a decrease in apoptosis and dysregulation of the immune system leading to continuous infiltration of immune cells into the alveoli releasing pro-inflammatory mediators and maintaining the inflammatory mechanism active (Yu, 2008).

In asthma, there is a dysregulation in the balance between Th1 and Th2 lymphocytes (Yazdanbakhsh, Kremsner and Van Ree, 2002; Yu, 2008). In COPD, cytotoxic $CD8^+$ T lymphocytes are predominant, moreover, oxidative stress further increases the production of inflammatory cytokines and growth factor mediators such as IFN-γ, TNF-α, IL-1β, IL-6 and GM-CSF resulting in chronic inflammation, constriction of the airway and emphysema (Barnes, Shapiro and Pauwels, 2003; Sutherland and Martin, 2003; Sarir *et al.*, 2008). In acute respiratory distress syndrome, the anti-inflammatory cytokine IL-10 is reduced and is not able to decrease the secretion of the pro-inflammatory cytokines TNF-α and IL-1β maintaining the NF-ΚB inflammatory cascade active and leading to exacerbation of inflammation, increased vascular permeability and edema (Suter *et al.*, 1992; Armstrong and Millar, 1997; Yu, 2008). In bacterial infections, bacteria are recognized by TLR that activates NF-ΚB inflammatory cascade and the production of pro-inflammatory cytokines and chemokines (TNF-α and IL-8) which trigger neutrophils and T and B cells, which in turn activate macrophages for phagocytosis (Khair *et al.*, 1994; Shaw *et al.*, 2008; Yu, 2008). When the host defense mechanisms are not able to clear the bacteria, the inflammatory state is maintained leading to chronic inflammation (Yu, 2008). In pulmonary fibrosis, Th2 cells are primarily involved and IL-1α and IL-1β production stimulates fibroblast proliferation and collagen-matrix deposition leading to the formation of a fibrotic scar tissue (Yu, 2008). In sarcoidosis, Th1 lymphocytes and macrophages are firstly activated leading to the secretion of cytokines, chemokines and growth factors (IFN-γ, TNF-α, TGF- β, IL-1β, IL-2, IL-6, IL-12, IL-15, IL-16, IL-18, CCL2, CCL3, CCL5, CCL20, CXCL8, CXCL10, CXCL16, GM-CSF) and inflammatory mediators (angiotensin-converting enzyme) which recruit immune cells to the granuloma formation sites (Gerke and Hunninghake, 2008).

Increased oxidative stress burden is observed in several inflammatory lung diseases (MacNee, 2001). Eosinophils, alveolar macrophages, and neutrophils from patients with asthma and COPD were reported to generate more ROS than the ones from healthy persons (MacNee, 2001). ROS are used as a defense mechanism neutralizing pathogen and stimulating pro-inflammatory mechanisms through NF-ΚB signaling cascade but when dysregulated promote histamine release from mast cells, mucous production from airway epithelial cells, increase permeability of the endothelial and epithelial cell barriers, promote neutrophil transmigration as well as affect gene expression and oxidize proteins and lipids (MacNee, 2001).

1.3 MSC

1.3.1 Defining MSC populations

Stem cells are defined by the ability to self-renew (or self-maintenance) under undifferentiated state by mitotic cell division (clonogenicity) and the potential to differentiate into several lineages (Potten and Loeffler, 1990), which can be used for regenerative medicine. Stem cells are classified according to their developmental potential in: totipotent (capacity to give rise to all embryonic and extra-embryonic cell types), pluripotent (potential to give rise to all cell types of the embryo), multipotent (ability to give rise to limited number of cell types) and unipotent (specialized to only one cell type) (Wagers and Weissman, 2004).

Adult stem/stromal cells are multipotent cells that are found in almost all tissues and organs such as bone marrow (BM), heart, brain, adipose tissue (AT), muscle, skin, eyes, kidney, liver, gut, pancreas and others. These cells can differentiate into tissue specialized cells to repopulate the tissue, to maintain homeostasis or to repair and regenerate an injured tissue (Mimeault, Hauke and Batra, 2007).

MSCs are multipotent cells with ability to expand *ex vivo* and with regenerative potential and its use as cell therapy has been under investigation for a broad range of diseases (Dominici *et al.*, 2006; Pountos *et al.*, 2007). Aiming standardization in the MSC field, the International Society for Cellular Therapy defined the minimal criteria for human MSCs as plastic adherent cells under standard culture conditions, immunophenotype positive (≥95%) for CD73, CD90, CD105 and negative (≤2%) for CD14 (or CD11b), CD34, CD45, CD19 (or CD79α), HLA-DR and ability for *in vitro* differentiation at least into 3 lineages (osteoblasts, adipocytes and chondroblasts) under standard differentiation conditions (Dominici *et al.*, 2006).

Regarding MSC positive markers, CD73 is an ecto 5' nucleotidase, CD90 is also named Thy-1, CD105 is an endoglin. As for the negative markers, CD14 excludes monocyte and macrophage populations, CD34 excludes hematopoietic progenitors and endothelial cells, CD45 excludes leukocytes, CD19 excludes B cells, HLA-DR is the human leukocyte antigen-DR which is present in antigen presenting cells and is only present in MSCs when its immune response is stimulated, for instance, by IFN-γ (Dominici *et al.*, 2006).

Concerning MSC differentiation potential, osteoblast differentiation is analyzed by alizarin red or von Kossa staining, adipocyte differentiation is verified with oil-red-o staining and chondroblast differentiation is validated by alcian blue staining or immunohistochemical staining for collagen type II (Dominici *et al.*, 2006).

MSC have the ability to expand *ex vivo* for several passages, therefore, it is also recommended to perform a karyotype analysis for cells at higher passages to evaluate the presence of possible chromosome abnormalities and transforming events (Dominici *et al.*, 2006). However, this analysis does not need to be routinely performed for MSC characterization (Dominici *et al.*, 2006).

MSCs may have different morphology according to culture conditions, however, using standard culture conditions MSCs typically have a spindle-shaped, triangular shaped and fibroblastic like morphology (Liu *et al.*, 2016).

MSC isolation methods can be divided into plastic adherence methods (including direct plating of tissue explants; density centrifugation using a high density with low viscosity and low osmotic pressure reagent, typically Ficoll, to isolate the mononucleated fraction which contains MSCs that are then isolation by plastic adherence; enzymatic digestion followed by isolation by plastic adherence) or by more sophisticated methods such as magnetic bead sorting technique and fluorescence-activated cell sorting (Pountos *et al.*, 2007).

1.3.2 MSC sources

Friedenstein initially reported the isolation of a BM subpopulation with osteogenic potential in the 1960s and 1970s, which was later denominated MSC by Caplan in 1991 (Bianco, Robey and Simmons, 2008). BM was considered the preferable source of MSCs, however, MSC low frequency, of only 0.001-0.01% of nucleated cells, led to the search of other potential MSC sources (Kern *et al.*, 2006; Peng *et al.*, 2008). Moreover, MSC frequency and potential for differentiation was found to decrease with age (Kern *et al.*, 2006; Peng *et al.*, 2008).

Indeed, MSCs can be found in several tissues, including BM (Caplan, 1991), AT (Zuk *et al.*, 2002), umbilical cord matrix (UCM) (Wang *et al.*, 2004), umbilical cord blood (UCB) (Bieback *et al.*, 2004), lungs (Lama *et al.*, 2007), scalp tissue (Shih *et al.*, 2005), placenta (in 't Anker *et al.*, 2004), brain (Kang *et al.*, 2010) and liver (Najimi *et al.*, 2007). Although respecting the minimal criteria to define MSCs, MSCs form different cell sources may have different potential and regenerative properties (Q. Wang *et al.*, 2016).

As previously described, BM has been the main cell source for MSC isolation and BM MSCs have been widely characterized. BM MSC frequency is low and cell number decreases with age. BM harvesting is an invasive and painful procedure by puncturing the posterior iliac crest (Kern *et al.*, 2006). Alternatively, BM MSCs can be mobilized to the peripheral blood by granulocyte-colony-stimulating factor (G-CSF) which is not a painful procedure and leads to faster recovery (Lund, Tolar and Orchard, 2008). However, lower BM MSC frequency is achieved (0.0002%) (Lund, Tolar and Orchard, 2008).

AT and UCM could be alternative MSC sources. AT MSCs can be isolated from lipoaspirates which are usually discarded as waste from cosmetic liposuctions (Kern *et al.*, 2006). It is a less invasive and painful procedure when compared to BM harvesting by puncturing the posterior iliac crest and larger quantities can be obtained per procedure as well as higher number of MSCs that grow fast when cultured under standard conditions (Kern *et al.*, 2006; Peng *et al.*, 2008). UCM MSCs can be isolated from umbilical cord units that are usually discarded as medical waste. Umbilical cord collection is a standard procedure upon birth and it is not invasive or painful for the mother neither the infant (Kern *et al.*, 2006; Q. Wang *et al.*, 2016). UCM MSCs are a more primitive cell source with lower immunogenicity and higher safety, however, cell number is limited (Q. Wang *et al.*, 2016).

There are conflicting results regarding which cell source would be more appropriate for a certain application. Several studies compared MSCs from different cell sources concerning plastic adherence, immunophenotype, differentiation potential, proliferation potential, angiogenic potential and resistance to oxidative stress (Kern *et al.*, 2006; Karahuseyinoglu *et al.*, 2007; Peng *et al.*, 2008;

Li *et al.*, 2015; Q. Wang *et al.*, 2016; Burrow, Hoyland and Richardson, 2017). However, most of the studies do not directly compare the different MSC sources isolating cells from the same donor, therefore, it is not adequate to conclude which cell source has higher regenerative potential when there is not donor matching even when ages are similar (Burrow, Hoyland and Richardson, 2017). This is also a consequence of lack of availability of sample donations from different tissues and it is also not feasible to have a donor matching comparison when comparing to umbilical cord cell source.

Optimal range of cell dose is not establish for MSC therapy, nevertheless, several millions of cells per kg of body weight have been tested in pre-clinical and clinical trials (Elnakish *et al.*, 2012). The low frequency of MSCs isolated from different cell sources does not yield enough cell number to reach the doses typically used, therefore, to achieve a clinically significant cell number, an *ex vivo* expansion of MSCs is required.

1.3.3 MSC expansion

Ex vivo expansion of MSCs is required to obtain clinically relevant cell numbers, however, this process is time consuming and expensive with associated risks of cell contamination and cell loss (Zuk *et al.*, 2001). Therefore, several methods of cell expansion have been under development.

Ex vivo expansion can be affected by the MSC donor characteristics or the technique. MSC donor characteristics include donor age and sex, cell source, healthy donor or diseased patient and the presence of trauma or systemic diseases (Pountos *et al.*, 2007). Technique dependency includes passage number, culture medium, culture conditions and methods of isolation and culture (Pountos *et al.*, 2007).

Concerning age of the donor, it has been reported a decrease in the number of stem cells and its potential with ageing (Stenderup *et al.*, 2003; Kern *et al.*, 2006; Peng *et al.*, 2008). In regard to cell passage, it has been reported in several studies that increasing cell passage leads to growth arrest and senescence which can result in apoptosis (Pountos *et al.*, 2007). A MSC cell line has been established by a stable retroviral transduction of human telomerase reverse transcriptase (hTERT) which leads to increased telomere length and ability of the cells to undergo up to 260 population doublings (Simonsen *et al.*, 2002).

Regarding culture medium, typically the basal medium contains glucose, amino acids and ions and is supplemented with animal serum (10-20%) and antibiotics (EAGLE, 1955). The type of basal medium and the type of plastic culture surface also affect cell adherence and growth (Sotiropoulou, Perez, Salagianni, *et al.*, 2006). Typically MSCs are grown in 2D standard tissue culture flasks using culture medium containing fetal bovine serum (FBS), however, the use of serum is related to batch to batch variability, lower proliferative capacity compared to human serum and to safety issues due to immune reactions and xenogeneic contaminants (prions, viral, and zoonotic agents) (Spees *et al.*, 2004; Pountos *et al.*, 2007; Panchalingam *et al.*, 2015). To avoid safety concerns of animal serum, MSC culture medium can be supplemented human platelet lysate or replaced by serum-free culture medium. Culture medium supplemented with human platelet lysate or serum-free StemPro MSC SFM Xeno-Free were reported to increase proliferation of BM and AT MSCs when compared to culture medium supplemented with FBS (Oikonomopoulos *et al.*, 2015). Moreover, differentiation potential of

BM and AT MSC was higher for medium supplemented human platelet lysate, while immunosuppressive potential was improved for serum-free StemPro MSC SFM Xeno-Free (Oikonomopoulos *et al.*, 2015). UCM MSCs were reported to grow more rapidly when cultured in medium supplemented human platelet lysate compared to serum-free StemPro MSC SFM Xeno-Free (de Soure *et al.*, 2017).

To increase the proliferative potential of MSCs, the addition of growth factors has been tested, including PDGF-BB and epidermal growth factor (EGF) (Gronthos and Simmons, 1995), however, attention should be taken regarding alterations of MSC immunophenotype, differentiation potential and regenerative potential (Pountos *et al.*, 2007).

MSCs are typically cultured in a humidified atmosphere at 37ºC and 5% CO_2 and atmospheric oxygen (Pountos *et al.*, 2007). It has been reported that MSCs have lower proliferative rate at normoxia (21% oxygen tension) than hypoxia (1-5% oxygen tension), which closer resembles physiological oxygen tension (Dos Santos *et al.*, 2010; Widowati *et al.*, 2014; Ejtehadifar *et al.*, 2015). Moreover, culture of MSCs under hypoxia reduces oxidative stress, DNA damage, telomere shortening and chromosomal abnormalities (Estrada *et al.*, 2012) and increases secretion of growth factors such as VEGF and HGF (C.-P. Chang *et al.*, 2013).

MSCs can be cultured as adherent or in spheroids. MSC culture as spheroids was reported to enhance MSC anti-inflammatory and anti-apoptotic potential as well as immunomodulatory potential suppressing inflammation on macrophages (Bartosh *et al.*, 2010; Zimmermann and Mcdevitt, 2014). As adherent cultures, MSC can be expanded under 2D or 3D culture systems. 2D culture systems include tissue culture flasks with one layer or multilayer, well plates and Petri dishes. These 2D culture systems are simple to handle and promote gas exchange through a high volume headspace, but are labor intensive when higher number of flasks are needed for scale-up increasing the risk of contamination (Panchalingam *et al.*, 2015). Moreover, there may be variability between flasks or between layers of a multiflask, productivity is limited and culture parameters are not monitored (Panchalingam *et al.*, 2015). 3D systems include but are not limited to roller bottle, rotary bioreactors, spinner vessel and stirred tank bioreactor, perfusion bioreactor, biomaterials and scaffolds (Pountos *et al.*, 2007; Panchalingam *et al.*, 2015). Unlike 2D culture systems, bioreactors enable a full control of the environment, namely pH, temperature, dissolved oxygen, gas flow, agitation, shear stress. Moreover, bioreactors are scalable, reproducible and allow culture homogeneity, straightforward operation and easier sampling (Cabrita *et al.*, 2003). It was also reported that UCM (de Soure *et al.*, 2017), BM and AT (Dos Santos *et al.*, 2014; Carmelo *et al.*, 2015) MSCs cultured in xeno-free conditions in spinner vessels and stirred tank bioreactors using microcarrier technology (for cell adherence and increased surface area-to-volume ratio) increased proliferation while maintaining immunophenotype and differentiation potential.

The use of scaffolds and biomaterials has also been developed and their use to encapsulate cells envision mimicking native properties, providing mechanical cues and promoting angiogenesis and regeneration (Pountos *et al.*, 2007).

1.3.4 Autologous or allogeneic MSC therapy

In the case of an autologous cell therapy, the cells are originated from the recipient involving cell harvesting from the recipient, *ex vivo* expansion and cell administration. While in the case of allogeneic cell therapy, cells are harvested from a healthy matched related or unrelated donor, *ex vivo* expanded and administered into the recipient.

MSCs are considered to be immune-privileged and to have immunomodulatory properties, which enables these cells to survive when transplanted in an allogeneic setting by immunosuppression of host immune system (Le Blanc *et al.*, 2003; Nauta and Fibbe, 2007). The mechanisms of immune-tolerance have been attributed to MSC hypoimmunogenic characteristics, T cell modulation and immunosuppression of the local environment by the secretion of specific factors (Nicola *et al.*, 2002; Ryan *et al.*, 2005; Atoui, Shum-Tim and Chiu, 2008). MSC immune-privilege and immunomodulatory potential allows the use of these cells as a ready-to-use and off-the-shelf product for an allogeneic setting, in which MSCs would be harvested from healthy and young donors, expanded and stored until further use (Richardson *et al.*, 2013). Nevertheless, further studies should be performed to ensure the benefits of MSC therapy and limit immune rejection or other complications to the patients (Patel *et al.*, 2008). Besides minimizing the risk of immune rejection that is the advantage of autologous therapy, allogeneic therapy also overcomes the disadvantages of autologous therapy namely economical and time constrains of cell harvesting from patient own cells and expansion to achieve the cell number necessary and the constrains of cell harvesting from elderly patients frequently with comorbidities whose cells may have lower regenerative potential and genetic abnormalities (Zhuo *et al.*, 2010; Nayan *et al.*, 2011; Atoui and Chiu, 2012; Shin and Peterson, 2012). The use of MSCs as an off-the-shelf product requires cryopreservation and cell banking, which raises important concerns related to not only cell viability but also MSC functionality after thawing (Mendicino *et al.*, 2014). The use of MSCs directly from culture would be preferable, however, it would be associated to logistic limitations.

Donor-to-donor variability has been reported and variability is reflected on their protein content and secreted factors as well as in their function, therefore, careful screening of MSC donors and its characterization should be performed when considering an allogeneic therapy (Mindaye *et al.*, 2013; Mendicino *et al.*, 2014). Further insight on the paracrine action and immunomodulatory properties of MSCs will be given next.

1.3.5 MSC regenerative properties

Regeneration of injured tissues upon MSC transplantation was initially attributed to transdifferentiation and cell fusion events, however, it has been shown that these mechanisms are inefficient and would occur at low frequency (Kopen, Prockop and Phinney, 1999; Morigi *et al.*, 2004; Noiseux *et al.*, 2006; Uccelli, Moretta and Pistoia, 2008; Loffredo *et al.*, 2011; Gnecchi *et al.*, 2016). Moreover, low engraftment rate of cells upon transplantation was observed in several studies as a consequence of the low survival in a harsh environment described to be inflammatory, ischemic, with cytotoxic cytokines and oxidative stress and potentially with a matrix that does not promote cell

adhesion (Song, Cha, *et al.*, 2010; Song, Song, *et al.*, 2010; Gnecchi *et al.*, 2016). Together, these factors and several following studies indicated that MSCs act mainly through the secretion of soluble factors, which is denominated paracrine action (Gnecchi *et al.*, 2016). Focus was then given to the identification of the factors contained in the MSC-conditioned medium (CM) which are responsible for MSC regenerative properties, in order to develop stem cell-based but cell-free therapies (Gnecchi *et al.*, 2016). MSCs possess several characteristics that make them suitable for cell therapy applications, including the ability to prevent apoptosis, to promote proliferation, migration and angiogenesis, capacity to suppress fibrosis and scar formation, supportive function and immunomodulatory properties (Figure 1.6) (Lin *et al.*, 2011; Gnecchi *et al.*, 2016).

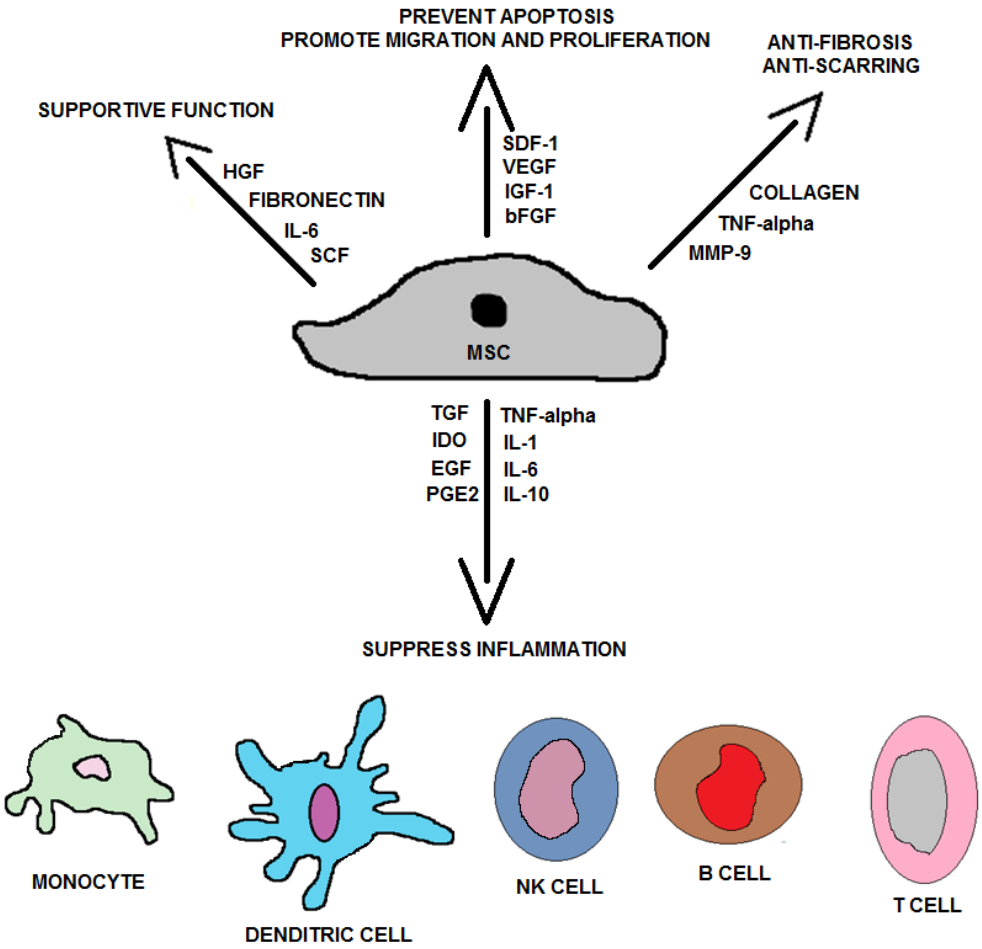

Figure 1.6 – MSCs have regenerative potential by paracrine action. MSCs secrete several growth factors and cytokines that act on other cell types providing supportive function, preventing apoptosis, promoting migration and proliferation, suppressing inflammation (on monocytes/macrophages, dendritic cells, NK cells, T and B cells) and suppressing fibrosis and scar formation. HGF – hepatocyte growth factor, IL – interleukin, SCF – stem cell factor, SDF-1 – stromal cell-derived factor-1, VEGF – vascular endothelial growth factor, IGF-1 – insulin-like growth factor, bFGF – basic fibroblast growth factor, TNF-α – tumor necrosis factor-alpha, MMP-9 – matrix metalloproteinase-9, TGF – transforming growth factor, IDO – Indoleamine 2,3-dioxygenase, EGF – epidermal growth factor, PGE2 – prostaglandin E2. Based on (Lin *et al.*, 2011)

MSCs prevent apoptosis by secreting anti-apoptotic cytokines such as stromal cell-derived factor (SDF)-1 and VEGF (Lin *et al.*, 2011). SDF-1 interacts with the chemokine receptor CXCR4 activating the pro-survival Akt and Erk pathways and promotes the production of anti-apoptotic proteins as Bcl-2 and angiogenic cytokines as bFGF and VEGF leading to increased survival, proliferation and migration (Liu *et al.*, 2011). Insulin-like growth factor (IGF) was reported to promote proliferation, migration and reduce apoptosis (Hu *et al.*, 2008; Guo *et al.*, 2014) also acting on MSC receptor CXCR4 (Guo *et al.*, 2014) and Erk pathway (Hu *et al.*, 2008) and preventing the expression of the pro-inflammatory cytokines TNF-α, IL-1β and IL-6 (Guo *et al.*, 2014). MSCs overexpressing Akt-1 gene were also reported to have cytoprotective ability, to reduce apoptosis of cardiomyocytes and decrease infarct size (Gnecchi *et al.*, 2005). MSC administration improved renal function in an ischemia/reperfusion injury, decreased the expression of pro-inflammatory factors (TNF-α, IL-1β and IFN-γ and NO) and increased pro-survival, anti-inflammatory and anti-apoptotic factors (IL-10, bFGF, TGF-α and Bcl-2) (Tögel *et al.*, 2005). In a model of focal cerebral ischemia, administration of MSCs promoted functional recovery by up-regulation of IGF, VEGF, EGF and bFGF (Wakabayashi *et al.*, 2010).

The secretion of growth factors by MSCs also promotes angiogenesis. MSC-CM from amniotic tissue increased vascular density in a cardiac model of ischemia/reperfusion injury containing VEGF, VEGF-D, bFGF, IGF-1, thrombopoietin, PDGF-BB and angiogenin in its CM (Danieli *et al.*, 2015). In another study, the angiogenic factors VEGF, HGF and IGF-1 were detected in MSC-CM promoting endothelial cell growth and survival and also showed renoprotective activity in a model of acute kidney injury upon MSC administration (Tögel *et al.*, 2007). Likewise, AT MSCs were reported to secrete VEGF, HGF, TGF-β and bFGF and the release of VEGF and bFGF was further increased by hypoxia enhancing endothelial cell proliferation, protecting from apoptosis and ameliorating perfusion in a hindlimb ischemia model (Kinnaird *et al.*, 2004; Rehman *et al.*, 2004). In a wound healing model, BM MSCs secreted VEGF and angiopoietin-1 accelerating wound closure, re-epithelialization and angiogenesis (Wu *et al.*, 2007).

MSC ability to prevent apoptosis can also be tested by a resistance to oxidative stress potency assay *in vitro*, while ability to promote proliferation, migration and angiogenesis can be assessed by angiogenic potency assays using Matrigel and wound healing potency assays *in vitro*, reducing the use of animal models.

MSCs are considered to be anti-fibrotic and anti-scaring, being able to decrease fibrosis upon transplantation in the heart (Nagaya *et al.*, 2005), liver (Oyagi *et al.*, 2006), kidney (Ninichuk *et al.*, 2006) and lung (Ortiz *et al.*, 2003). MSCs inhibited collagen and TGF-β1 secretion leading to decreased fibrosis in an animal model of liver fibrosis (Higashiyama *et al.*, 2007; Tsai *et al.*, 2009). MSCs down-regulated the expression of collagen type I, collagen type III, tissue inhibitor of MMP-1 and TGF-β1 in a MI model, resulting in the inhibition of left ventricular remodeling and enhancing cardiac function compared to control (Xu *et al.*, 2005). Paracrine action of MSC-CM was found to decrease cardiac fibroblast expansion and expression of collagen type I and III *in vitro* (Ohnishi *et al.*, 2007). It was also reported that MSCs ameliorated heart function in a MI model, decreased collagen

deposition and MMP-2 and MMP-9 activation and also promoted myogenesis and angiogenesis through the secretion of angiogenic, anti-apoptotic and mitotic factors (VEGF, HGF, IGF-1, adrenomedullin) (Ohnishi *et al.*, 2007). In a bleomycin-induced lung fibrosis model, MSC administration decreased inflammation, collagen deposition and MMP-2 and MMP-9 activation, thus promoting lung regeneration and survival (Ortiz *et al.*, 2003). The decrease in inflammation was related to the expression of IL-1 receptor antagonist which blocked the secretion of pro-inflammatory cytokines as TNF-α and IL-1.

MSCs also have supportive function for other cell types such as hematopoietic stem cells. MSCs secrete extracellular matrix proteins as fibronectin and collagen which are important for hematopoietic stem cell homing and differentiation (Nilsson *et al.*, 1998; Chen *et al.*, 2007; Wagner, Saffrich and Ho, 2008). BM and AT MSC supportive function for hematopoiesis was also related to the secretion of the cytokines G-CSF, M-CSF, GM-CSF, IL-6, IL-7, IL-12, stem cell factor (SCF) and FMS-like tyrosine kinase 3 ligand (Kilroy *et al.*, 2007). MSCs secrete HGF which enhances hematopoietic cell growth besides its roles on inhibiting T cell expansion and cytotoxicity, promoting angiogenesis and recruiting progenitor cells (Mizuno *et al.*, 1993; Baraniak and McDevitt, 2010). MSC supportive function together with immunosuppressive ability suggested the co-transplantation of MSCs with hematopoietic stem cells which is a promising therapy for hematological cancers to promote recovery of immune competence and blood production after chemotherapy in cancer patients (Baraniak and McDevitt, 2010) and for the treatment of graft-versus-host disease (GVHD) (Ringdén *et al.*, 2006; Le Blanc *et al.*, 2008).

Additionally, MSC secreted factors are able to recruit progenitor cells leading to endogenous regeneration. As previously described, in a wound healing model, BM MSCs recruited endothelial and epithelial cells promoting angiogenesis, re-epithelialization, thus accelerating wound closure, (Wu *et al.*, 2007). Moreover, MSCs were reported to activate cardiac progenitors cells when administered in MI models (Hatzistergos *et al.*, 2010; Karantalis and Hare, 2015), possibility through the secretion of HGF and IGF-1 which were reported to induce cardiac progenitors cell migration, proliferation and differentiation (Linke *et al.*, 2005).

Increased importance is giving to MSC immunomodulatory properties. MSC immunosuppressive action is activated by IFN-γ in co-stimulation with TNF-α and/or IL-1β leading to the secretion of chemokines, which recruit immune cells into close proximity with MSCs, and inducible NO, which locally inhibits T cell proliferation (Ren *et al.*, 2008). NO is unstable and has a fast diffusion, thus, NO secretion by MSCs only exerts its function on recruited macrophages and T cells (Ren *et al.*, 2008). However, more recently, administration MSC-CM without cell infusion also showed ability to modulate and suppress the activity of different types of immune cells (van Buul *et al.*, 2012; Watanabe *et al.*, 2014; Kay *et al.*, 2017) indicating that other growth factors, cytokines, chemokines, microRNAs (miRs) and extracellular vesicles (EVs) are also involved in its immunosuppressive activity (Lin and Du, 2017). Further details on EV properties and biogenesis will be given in chapter 1.4. MSC action on different types of immune cells, namely macrophages, dendritic cells, neutrophils, NK cells, T cells, and B cells is described next.

Macrophages

Macrophages are a type of leukocyte (or white blood cell) of the immune system that can reside in a tissue or be recruited from monocytes flowing in the blood that differentiate into macrophages, whose main functions include phagocytosis, antigen presentation, immune regulation and tissue repair (Unanue, 1984; Shi and Pamer, 2011; Davies *et al.*, 2013; Wynn, Chawla and Pollard, 2013). MSC secreted molecules can affect migration, maturation, polarization and function of macrophages (Lin and Du, 2017).

MSCs were able to secrete EGF, VEGF-α, IGF-1, KGF, angiopoietin-1, SCF-1, erythropoietin, macrophage inflammatory protein-1α and macrophage inflammatory protein-1β which recruited and promoted migration of macrophages, endothelial cells and keratinocytes into a wound injury leading to wound healing (Chen *et al.*, 2008). Tumor associated MSCs secreted chemokines as CCL-2, CCL-7, CCL-12 that recruited CCR2 expressing monocytes into the tumor, which proliferated and differentiated into macrophages leading to tumor growth (Ren *et al.*, 2012). BM MSC-EVs were also reported to contain CCR2 which blocked the effect of CCL2 on macrophage recruitment and activation (Shen *et al.*, 2016). Suppression of CCL2 resulted in improved recovery from renal ischemia/reperfusion injury (Shen *et al.*, 2016).

MSCs modulate macrophage polarization towards M2 phenotype instead of M1, increasing macrophage secretion of molecules such as IL-10 , IL-4, CD206 and arginase-1 and decreasing inducible NO, IL-6, IL-1β, TNF-α, MCP-1 (Cho *et al.*, 2014; Geng *et al.*, 2014). MSCs activated by TNF-α or LPS also produced prostaglandin E2 (PGE2) which polarizes macrophages towards M2 phenotype (Vasandan *et al.*, 2016) and promoted the expression of the anti-inflammatory cytokines IL-10 (Németh *et al.*, 2009) and TGF- β (Németh *et al.*, 2009; Chiossone *et al.*, 2016). In turn, these anti-inflammatory macrophages blocked T cell and NK cell activity. MSCs also expressed IL-1 receptor antagonist which polarizes macrophages towards M2 phenotype secreting IL-10 (Lee *et al.*, 2015; Luz-Crawford *et al.*, 2016) which has the ability to inhibit T cell activity (Luz-Crawford *et al.*, 2016). It was also reported that miR-223 was enriched in MSC-CM and in MSC-EVs and is in part responsible for decreased release of IL-6, IL-1β and TNF-α from macrophages (X. Wang *et al.*, 2015). MSC pre-conditioned with LPS secreted EVs enriched in let-7b which is also associated to the ability to polarize macrophages towards M2 phenotype, reducing inflammation and promoting wound healing (Ti *et al.*, 2015). Moreover, let-7b was reported to act on TLR4 modulating NF-ΚB, STAT3 and Akt signaling pathways (Ti *et al.*, 2015).

Dendritic cells

Dendritic cells are BM derived cells with potent action as antigen presenting cells. Dendritic cells are immune sentinels positioned at places of potential entrance of pathogens, undergoing maturation if activated by a pathogen stimuli and migrate to the lymph nodes to present the antigen to lymphocytes (Stockwin *et al.*, 2000).

MSCs are able to immune regulate monocyte-derived dendritic cells by suppressing CD40, CD80 and CD86 and HLA-DR during dendritic cell differentiation and CD40, CD86 and CD83 during maturation, by blocking dendritic cell endocytosis and by decreasing IL-12 release and T cell

activation by dendritic cells (Zhang *et al.*, 2004). MSC-CM showed partial suppression of dendritic cell differentiation, with IL-6 being one of the cytokines involved (Djouad *et al.*, 2007). MSCs also produced TSG-6 which hinders BM derived dendritic cell maturation, decreasing the expression of CD80, CD86 and major histocompatibility complex (MHC) class II, and inhibiting dendritic cell functions, namely IL-12 secretion and T cell activation (Liu *et al.*, 2014). Furthermore, TSG-6 inhibited the activation of mitogen-activated protein kinases (MAPKs) and NF-ΚB signaling pathways of LPS-stimulated dendritic cells (Liu *et al.*, 2014). In another study, MSC and MSC-derived EVs hindered dendritic cell maturation and promoted dendritic cell secretion of IL-10 and IL-6 (Favaro *et al.*, 2016).

Neutrophils

Neutrophils are originated from the BM and are usually the first type of leukocytes recruited during acute inflammation (Kolaczkowska and Kubes, 2013). Neutrophils eliminate pathogens by phagocytosis, degranulation and neutrophil extracellular traps (Kolaczkowska and Kubes, 2013). Phagocytosis consists of engulfment of the pathogens forming phagosomes which are then destroyed by ROS and anti-bacterial proteins compartmentalized in granules (Kolaczkowska and Kubes, 2013). Neutrophil extracellular traps are a net of secreted DNA, histones, proteins and enzymes which immobilize pathogens and helps on its phagocytosis (Kolaczkowska and Kubes, 2013). After resolving inflammation neutrophils undergo apoptosis and are cleared by macrophages and dendritic cells (Kolaczkowska and Kubes, 2013).

MSC are able to recruit neutrophils to the site of inflammation, promote neutrophil survival and then block neutrophil action to resolve inflammation avoiding further damages of the tissue. MSCs were reported to constitutively secrete IL-6, IL-8, macrophage migration inhibitor factor, G-CSF, TGF-β, SDF-1α, TNF-α and IFN-γ and LPS-stimulated MSCs secreted even higher amounts of IL-6, IL-8 and G-CSF (Brandau *et al.*, 2010). IL-8 and macrophage migration inhibitor factor were found to be important for neutrophil recruitment. Moreover, LPS-stimulated MSCs were able to promote longer neutrophil survival (Brandau *et al.*, 2010) and to increase anti-microbial neutrophil activity by accelerating pathogen phagocytosis and destruction by ROS (Brandau *et al.*, 2014). MSCs pre-conditioned with TNF-α secreted higher amount of CCL5, CCL2, CCL7, CCL8, CXCL1, CXCL 2 and CXCL5, from which CXCL1, CXCL 2 and CXCL5 were found to bind to recruited $CXCR2^{+}$ neutrophils into the tumor (P. F. Yu *et al.*, 2017). In another study, as low ratios as 1 MSC to 500 neutrophils could improve neutrophil survival and the chemokine IL-6 was identified for being involved in preventing neutrophil apoptosis, moreover, MSCs could hinder ROS production by neutrophils without affecting their phagocytosis and chemotaxis functions, indicating that MSCs activate ROS-mediated protection to fight pathogens and then hinder ROS production to avoid tissue damage from permanent neutrophil activation (Raffaghello *et al.*, 2008).

NK cells

NK cells are effector lymphocytes of the innate immune system that have cytotoxicity and cytokine-producing activity (Vivier *et al.*, 2008).

MSCs can regulate NK cell activity, although the mechanisms are not fully understood and both suppression and stimulation of NK cells by MSCs has been reported. At low NK cell to MSC ratios (1:1 to 1:10), MSCs were able to suppress IL-15-stimulated NK cell expansion, decrease cytokine release (TNF-α, IFN-γ and IL-10) and decrease cytotoxicity against different HLA class I expressing cells (Sotiropoulou, Perez, Gritzapis, *et al.*, 2006). MSC action on NK cells was mediated by cell contact and by paracrine action through TGF-β and PGE2 (Sotiropoulou, Perez, Gritzapis, *et al.*, 2006). Through the release of indoleamine 2,3-dioxygenase (IDO) and PGE2, MSCs were able to suppress NK cell activity by decreasing IFN-γ secretion of NK cells and down-regulating its surface markers (Spaggiari *et al.*, 2008). On the other hand, studies showed MSC ability to increase NK cell function possibly to boost immune system defense, although it can compromise tissue regeneration. Increasing number of MSCs in co-culture with NK cells were shown to promote increased release of IFN-γ from IL-12/IL-18-stimulated NK cells acting by both cell contact and paracrine action (Thomas *et al.*, 2014).

T cells

T cells are lymphocytes originated from the thymus, which are involved in the adaptive immune response (Alberts *et al.*, 2002).

MSCs are able to modulate T cell proliferation and differentiation. MSCs activated by pro-inflammatory cytokines (IFN-γ together with TNF-α, IL-1α or IL-1β) were able to modulate T cells (Ren *et al.*, 2008). Activated murine MSCs secreted chemokines such as CXCL9 and CXCL-10 which recruited T cells and also secreted inducible NO which suppressed T cell activity, preventing GVHD in mice (Ren *et al.*, 2008). In human MSCs, the immunosuppressive effect on T cell is mediated by IDO instead of inducible NO in mice, indicating different specie immune responses (Ren *et al.*, 2009). Moreover, different mechanisms of immunosuppressive function of MSCs were reported, being mediated through paracrine action by IDO, HLA-G and LIF and by cell contact through IL-10 and TGF-β (Nasef *et al.*, 2007). In another study, MSCs secreted monocyte chemotactic protein-1 and FasL, monocyte chemotactic protein-1 acted on recruiting T cells and then T cells suffered apoptosis by as FasL-mediated mechanism (Akiyama *et al.*, 2012). Release of TGF-β (Patel *et al.*, 2010), PGE2 (Duffy *et al.*, 2011), Notch1 (Del Papa *et al.*, 2013) and IL-10 (Qu *et al.*, 2012) by MSCs was also reported to promote regulatory T cell differentiation (Patel *et al.*, 2010; Qu *et al.*, 2012) and inhibit T-helper 17 differentiation (Duffy *et al.*, 2011; Qu *et al.*, 2012).

B cells

B cells are lymphocytes originated from the BM in adults, which are involved in the adaptive immune response (Alberts *et al.*, 2002). When activated, B cells produce antibodies, denominated, immunoglobulins, which flow in the blood vessels and when they reach the antigen, the antibodies bind and block the receptors of the antigen and signalize them for phagocytosis (Alberts *et al.*, 2002).

Both direct and indirect co-culture of umbilical cord MSCs with B cells (stimulated by CpG 2395, sCD40L, anti-IgM, and IL-4) blocked the expansion of B cells by cell cycle arrest at G_0/G_1 phase and not by apoptosis as well as B cell differentiation which was observed by a decrease in IgG, IgM

and IgA antibodies (Corcione *et al.*, 2006; Che *et al.*, 2012). MSC immunosuppressive action on B cells was mediated by Akt and p38 signaling pathways (Che *et al.*, 2012). On the other hand, it has been reported that treatment with umbilical cord MSCs on stimulated-B cells resulted in B cell proliferation and differentiation and antibodies production in a process mediated by PGE2 (Ji *et al.*, 2012).

Deeper understanding of the role of MSC immune regulation on homeostasis and disease is needed to clarify conflicting results as well as to decipher mechanisms of action. The development of standardized and robust potency assays to evaluate the immunomodulatory properties of MSCs and MSC-derived products can potentially overcome problems related to conflicting results enabling direct comparisons between works.

Boosting MSC regenerative properties

MSC regenerative properties can potentially be improved. To boost MSC potency several strategies have been tested namely by physiological, protein and pharmacological pre-conditioning, genetic manipulation and cellular interactions and physical cues (Ranganath *et al*., 2012).

Physiological pre-conditioning includes MSC exposure to hypoxia and anoxia conditions to promote survival and angiogenic potential. MSCs were reported to secrete increased amounts of angiogenic growth factors such as VEGF and bFGF when exposed to hypoxia (Kinnaird *et al*., 2004; C.-P. Chang *et al.*, 2013). Different groups have used different values of oxygen tension and exposure time to hypoxia and their impact on signaling pathways and MSC secreted factors is still not known, thus further optimization is needed (Ranganath *et al.*, 2012).

Protein pre-conditioning through incubation with cytokines, chemokines and growth factors typically present at injury sites provides signals that stimulate MSC regenerative properties. MSC have been pre-conditioned with TNF-α (Croitoru-Lamoury *et al.*, 2007; Wang *et al.*, 2007; Lee *et al.*, 2010), SDF-1 (Pasha *et al.*, 2008), IFN-β/LPS (Yao *et al.*, 2009) and TGF-α/TNF-α (Herrmann *et al.*, 2010). The pre-conditioning with these proteins has been reported to increase the secretion of the angiogenic cytokine VEGF and the chemokines MCP-1, IL-6, IL-8 and CXCL6 (Croitoru-Lamoury *et al.*, 2007; Wang *et al.*, 2007; Pasha *et al.*, 2008; Yao *et al.*, 2009; Herrmann *et al.*, 2010; Lee *et al.*, 2010). Similarly, different groups have used different concentrations and incubations time and different combinations of proteins, thus optimization is necessary to define better pre-conditioning strategy to boost the activation of MSC signaling pathways, ameliorate inflammation and promote repair at the injury sites (Ranganath *et al.*, 2012).

Pharmacological pre-conditioning through incubation with small molecules have the advantages of being easy to produce, less costly and more specifically target signaling pathways when compared to proteins. MSC pre-conditioning with melatonin was reported to increase secretion of bFGF and HGF and the expression of the anti-oxidant enzymes catalase and superoxide dismutase-1, thus promoting angiogenesis, proliferation, survival and resistance to oxidative stress in a ischemic kidney animal model (Mias *et al.*, 2008). MSC pre-conditioning with trimetazidine was reported to protect cells from oxidative stress by increasing the expression of the anti-apoptotic Bcl-2 protein, thus ameliorating myocardial function in a MI animal model (Wisel *et al.*, 2009). MSC pre-

conditioning with diazoxide targeted NF-KB signaling pathway, enhanced cell survival and angiomyogenesis, resulting in ameliorated heart function in a MI animal model (Afzal *et al.*, 2010). Further optimization of the incubation time and concentration of small molecules as well as identification small molecules highly specific towards their target is needed and it is necessary to ensure that after incubation minimal amounts of small molecules remain in culture and would be transplanted to avoid adverse effects (Ranganath *et al.*, 2012).

Cellular interactions and physical cues such as culture with other cell types (Block *et al.*, 2009), 3D spheroid culture (Potapova *et al.*, 2007), shear stress (Bassaneze *et al.*, 2010) and stiffness (Seib *et al.*, 2009) of the biomaterial have been reported to increase the secretion of cytokines such as VEGF. Nevertheless, additional elucidation of the mechanisms of action and signaling pathways activated by cellular interactions and physical cues is needed as well as ways to fully control them (Ranganath *et al.*, 2012).

Genetic manipulation (typically of one transgene) is used for overexpression of a protein that boosts MSC angiogenic potential and survival, for instance, by overexpressing Akt-1 (Gnecchi *et al.*, 2006), VEGF (F. Yang *et al.*, 2010), IGF-1 (Haider *et al.*, 2008) and SDF-1 (J. Tang *et al.*, 2010). Drawbacks of genetic manipulation are related to safety concerns, limited control of protein release and it is frequently limited to one target gene while MSC action is mediated by many genes and proteins (Ranganath *et al.*, 2012).

Despite promising, more research is needed to develop better pre-conditioning strategies, possibly by combining several strategies, and also to understand the mechanisms of action.

1.3.6 MSC and clinical trials

The US Food and Drug Administration (FDA) and the European Medicines Agency (EMA) regulate not only drugs but also cell and gene therapies. General criteria for therapeutic products include identity, purity, potency, safety and efficacy (Jung, Bauer and Nolta, 2012; Mendicino *et al.*, 2014). Cellular products should also be sterile with high viability and endotoxin free. Stem cell products should follow stricter criteria including characterization of *in vitro* and *in vivo* potency, absence of undesired cell types and teratoma formation, absence of immunogenicity and rejection (GVHD), characterization of interactions with other tissues, drugs and devices, biodistribution and homing and for genetically modified cells the potential of uncontrolled biological activity of the transgene and other mutations should be evaluated (Jung, Bauer and Nolta, 2012).

MSCs have been widely tested and increasing number of clinical trials have been registered at *clinicaltrials.gov* over the years and most of the trials are in phase I and II (Mendicino *et al.*, 2014; Squillaro, Peluso and Galderisi, 2016). Due to the immunomodulatory, homing, angiogenic, anti-apoptotic and regenerative properties, MSCs have been tested for a broad range of diseases in clinical trials including bone and cartilage injuries (19.1%), neurological diseases (17.8%), cardiovascular diseases (14.8%), GVHD (7.2%), liver diseases (6.3%), diabetes (5.5%), hematological diseases (5.1%), lung diseases (4.8%), Crohn's disease (2.6%) and others (Figure 1.7) (Squillaro, Peluso and Galderisi, 2016).

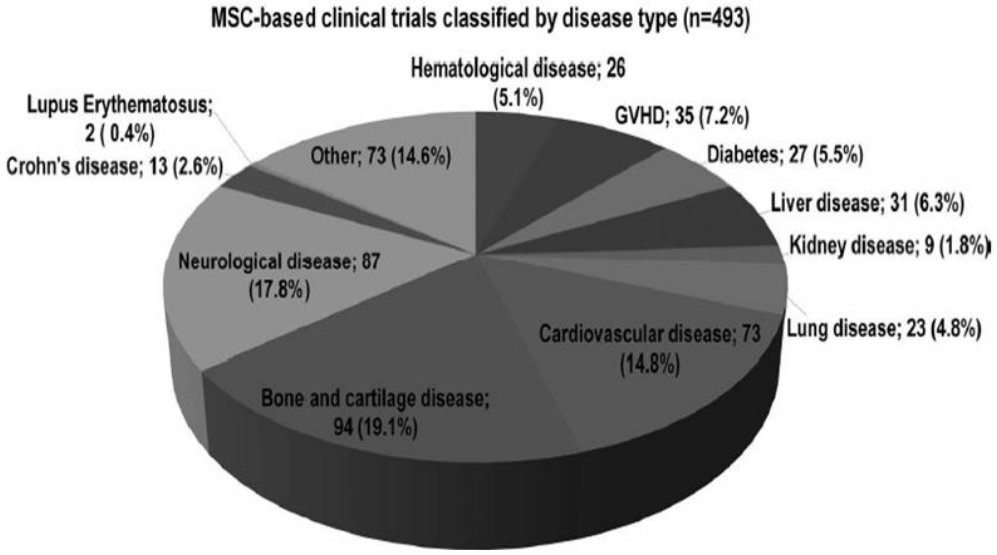

Figure 1.7 – Representation of the number and percentage of MSC-based clinical trials classified by disease type with a total of 493 clinical trials registered at *clinicaltrials.gov* by June 2015 (Squillaro, Peluso and Galderisi, 2016).

There is a much higher number of clinical trials using MSCs to treat cardiovascular diseases than lung diseases and the number of clinical trials completed and with results is also higher for cardiovascular diseases than lung diseases with only 4 trials with published results (Squillaro, Peluso and Galderisi, 2016). The results of the clinical trials for cardiovascular diseases generally showed safety and feasibility of MSC administration into patients and some trials showed potential functional improvements (Table 1.1). The results for lung diseases tend to show safety and feasibility, however, only the bronchopulmonary dysplasia showed potential clinical benefits (Table 1.1). As previously stated, clinical trials with MSCs covers broad range of diseases, however, in this work the focus was on cardiovascular and lung diseases.

Table 1.1 – Examples of clinical trials completed and with published results using MSCs for cardiovascular and lung diseases showing safety of MSC administration.

Disease	Patient profile	MSC Source	Dose ($\times 10^6$)	Administration	Outcome	Ref
AMI	N=27	Autologous BM MSC	50 (n = 6), 700 (n = 21)	Intracoronary (FINCELL II clinical trial)	Dose did not affect outcome. Marked improvement in left ventricle ejection fraction in patients with low pCO_2 and HCO_3	(Miettinen *et al.*, 2012)
AMI	N=53 (MSC n=39, control n=21)	Autologous BM MSC	0.5, 1.6 and 5 per kg	Intravenous (Prochymal clinical trial)	Global symptom score and ejection fraction were significantly better (p = 0.027) in MSC group than control. Safety and provisional efficacy of MSC therapy	(Hare *et al.*, 2009)
AMI	AMI with percutaneous coronary implant (n=16)	Autologous BM MSC	12.2 ± 1.77 GroupI, 13.2 ± 1.76 GroupII	Left anterior descending branch artery GroupI (n=8), Right coronary artery GroupII (n=8)	No adverse events after 6 months. Improved cardiac function and myocardial perfusion. Safety and provisional efficacy of MSC therapy	(Z. Yang *et al.*, 2010)
AMI	AMI with percutaneous coronary implant (MSC n=35, control n=35)	Autologous BM MSC	8×10^3 - 1×10^4/mL	Intracoronary	Significant improvement (p<0.05) in cardiac function in MSC group than in control at 3 and 6 months. Safety and provisional efficacy of MSC therapy	(Chen *et al.*, 2004)
MI (old)	N=16 (MSC n=8, control n=8)	Autologous BM MSC	5.55 (2.1-9.1)	Injected at the coronary artery bypass graft or percutaneous coronary implant	Significant improvement in New York Heart Association class, single-photon emission computed tomography and left ventricle ejection fraction (<0.05) in MSC group compared to control. No serious adverse effects	(Mohyeddin-Bonab *et al.*, 2007)
MI (old and recent)	N=22 (MSC n=11, control n=11)	Autologous BM MSC and endothelial progenitor cells	1-2	Intracoronary	MSC therapy is feasible, safe, and ameliorates local regeneration of the myocardium early or late following MI	(Katritsis *et al.*, 2005)
MI	N=60 (MSC n=30, control n=30)	Autologous BM cells	2460 ± 940	Intracoronary (BOOST clinical trial)	Increased mean global left ventricular ejection fraction at 6 months compared to control and enhanced left ventricular systolic function. No improvment at 18 and 60 months	(Wollert *et al.*, 2004; Meyer *et al.*, 2009)
MI	N=58 (MSC n=30, control n=28)	Autologous BM MSC	72 ± 9	Intracoronary	Modest increase in left ventricular ejection fraction at 6 months compared to control	(J.-W. Lee *et al.*, 2014)
MI	N=204 (MSC n=101, control n=103)	Autologous BM progenitors cells	315 ± 43	Intracoronary (REPAIR-AMI clinical trial)	Increase in left ventricular ejection fraction	(Erbs *et al.*, 2007; Assmus *et al.*, 2010)
MI	N=10	Autologous BM MSC	61.5	Intramyocardial (MESAMI clinical trial)	Safe administration and potential improvements in cardiac performance and left ventricule remodeling	(D. *et al.*, 2013)
Refractory angina	N=31	Autologous BM MSC	21.5 (3-62)	Intramyocardial	Significant improvement (p < 0.001) in left ventricle ejection fraction, exercise tolerance and symptoms. Safety and provisional efficacy of MSC therapy	(Friis *et al.*, 2011)
Ischemic cardiomyopathy	Left ventricular dysfunction with remote MI (n=8)	Autologous BM MSC (n=4) and BM mononucleated cells (n=4)	100, 200	Transendocardial injection (TAC-HFT clinical trial)	Improvement of regional contractility of chronic myocardial scar and subsequently reverse remodeling by mononucleated cells and MSCs. Decrease in end diastolic volume and infarct size and improvement of regional left ventricle function more likely with treatment. No serious adverse effects	(Williams *et al.*, 2011)
Ischemic cardiomyopathy	N=30	Autologous (n=15) or Allogeneic (n=15) BM MSC	20 (n=5), 100 (n=5) or 20 (n=5) per cell type	Transendocardial injection (POSEIDON clinical trial)	MSC therapy positively affected patient functional capacity and ventricular remodeling relative to baseline. Lower MSC dose resulted in greater reduction in left ventricle volume and increased ejection fraction. Low rates of serious adverse events including immunologic reactions	(Hare *et al.*, 2012)
Chronic ischemic left ventricular dysfunction secondary to MI	N=6	Autologous BM MSC	20 (n=2) or 200 (n=4)	Intracoronary injection (PROMETHEUS clinical trial)	Improvement in left ventricle ejection fraction and decrease in scar mass relative to baseline	(Karantalis *et al.*, 2014)
Idiopathic pulmonary fibrosis	N=14	Autologous AT MSC-stromal vascular fraction	0.5 per kg	Intra-endobronchial	No serious adverse effects. Acceptable safety profile of endobronchially administered MSCs	(Tzouvelekis *et al.*, 2011)
Idiopathic pulmonary fibrosis	N=8	Allogeneic placenta derived-MSC	1 (n=4) or 2 (n=4) per kg	Intravenous	Feasible MSC administration and minor and transient acute adverse effects. No worsening of fibrosis neither improvement	(Chambers *et al.*, 2014)
Bronchopulmonary dysplasia	N=9	Allogeneic UCB MSC	1 (n=3) or 2 (n=6) per kg	Intratracheal	Significant decrease in inflammatory cytokines (IL-6, IL-8, MMP-9, TNF-α, TGF-β1) in lung aspirates after 3 days compared to baseline. Decrease in bronchopulmonary dysplasia severity. No difference in adverse effects between groups	(Chang *et al.*, 2014)
Acute respiratory distress syndrome	N=9	Allogeneic BM MSC	1 (n=3), 5 (n=3) or 10 (n=3) per kg	Intravenous (START clinical trial)	Serious adverse events in 3 out of 9 patients, although they were not believed to be related to cell infusion. Tolerance of MSC infusion on phase I and proceeded to phase II	(Wilson *et al.*, 2015)

1.3.7 MSC commercialized products

The promise of using MSC and MSC-derived products as therapies has been widely reported, however, the approval and translation of MSC products into the market has not been as fast as expected and by 2014 there was no FDA-approved biologics license applications for MSC-based products (Mendicino *et al.*, 2014). There are concerns regarding the conflicting results related to the function and potency of these cells and the mechanisms of action are not fully understood. Moreover, there is a lack of standardization in terms of cell harvesting, cell source and culture methods as well as standardized and robust product characterization platforms including *in vitro* potency assays and *in vivo* testing (Mendicino *et al.*, 2014). It was reported that less than half of the MSC-based products submitted to FDA as Investigational New Drug evaluated MSC product bioactivity (Mendicino *et al.*, 2014).

Nevertheless, MSCs and MSC-derived products have been tested in several pre-clinical and clinical trials and the regulatory agencies of some countries already approved MSC products for commercialization in their own countries. One example is Korea with several companies with MSC products commercialized for therapeutic and cosmetic purposes, which were approved by the Korean regulatory agency (Table 1.2).

Table 1.2 – Examples of MSC cell therapy products approved and under commercialization in Korea as well as products under development (S. Lee *et al.*, 2014).

Company	Product	Cell type	Indication	Classification	Company's website
Anterogen	Cupistem	Human autologous AT MSC	Crohn's fistula	Ethical drug, orphan drug	http://anterogen.com/main/en/sub02_01.html?type=1
	Queencell	Human autologous stromal vascular fraction containing MSCs	Regeneration of subcutaneous adipose tissue	Ethical drug	
	SCM2 and SCM2 - Black	Human AT MSC-CM	Skin and hair loss	Cosmetics, passed toxicity tests requested by Korean-FDA	
FCB-Pharmicell	Cellgram-AMI (Heartcellgram-AMI)	Human autologous BM MSC	AMI	Stem cell drug approved by the Ministry of Foods and Drug Safety of Korea	http://www.pharmicell.com/eng/index.html
	Celgram_IS, Celgram_SCI, Celgram_Lung, Celgram_LC, Celgram_ED, Celgram_CLI, Celgram_DC	Human autologous BM MSC	Brain/nerve disorders, pulmonary fibrosis, hepatic insufficiency, GVHD, cancer and others	Under development at different stages	
Medipost	Cartistem	Human allogeneic UCB-derived MSC	Cartilage regeneration in osteoarthritis	Stem cell drug approved by the Ministry of Foods and Drug Safety of Korea	http://www.medi-post.com/
	Pneumostem	Human allogeneic UCB-derived MSC	Bronchopulmonary Dysplasia for premature infants	Phase 2 clinical trial in Korea, phase 1/2 clinical trial in the USA. Orphan Drug	
	Neurostem	Human allogeneic UCB-derived MSC	Alzheimer's disease	Phase 1/2a clinical trial Ministry of Foods and Drug Safety of Korea, in preparation for clinical trials in USA.	

In other countries, several MSC products are under clinical trials and have been commercialized for several applications (examples in Table 1.3). MSC products have been produced and commercialized by different companies, some of which in partnership with pharmaceutical companies.

Table 1.3 – Examples of under development and commercialized MSC products and respective companies (S. Lee *et al.*, 2014).

Company	Product name	Product type	Indication
Allosource distributed by NuVasive	Osteocel	Autologous bone graft containing MSCs and osteoprogenitors cells	Skeletal defects
Allosource distributed by Activize	AlloStem	Allogeneic bone graft with AT MSCs	Bone repair and regeneration
NuTech distributed by Organogenesis	NuCel, ReNu	Amniotic suspension allograft derived from human amnion and amniotic fluid cells, containing growth factors, extracellular matrix and cells such as stromal cells	Wound healing, soft tissue defects, skeletal defects
Organogenesis	Affinity	Amniotic membrane containing growth factors, extracellular matrix and cells such as stromal cells	Wound healing
Orthofix	Trinity Evolution	Allogeneic bone graft containing MSCs and osteoprogenitor cells	Musculoskeletal defects
Osiris Therapeutics	Grafix	Placental membrane containing extracellular matrix, growth factors, fibroblasts, MSCs and epithelial cells	Acute and chronic wounds
	Stravix	Umbilical amnion and Wharton's jelly containing extracellular matrix, growth factors, epithelial cells, fibroblasts and MSCs	Surgical covering for tendon, cartilage, ligaments and foot amputations
	BIO4	Bone matrix containing MSCs, osteoprogenitor cells, osteoblasts, osteoinductive and angiogenic growth factors	Bone repair and regeneration
Osiris Therapeutics and Genzyme, Mesoblast	Prochymal	Allogeneic BM MSCs	GVHD and Crohn's disease
Osiris Therapeutics and Genzyme	Chondrogen	Allogeneic BM MSCs	Knee osteoarthritis
Reliance Life Science	CardioRel	Autologous BM MSCs	MI

Although worldwide approval of MSC and MSC-derived products is still a promise and not reality, the world stem cell market, evaluated in 2.7 billion dollars in 2010, was estimated to be 11.4 billion in 2021, indicating that interest and expectations on stem cell products will keep increasing (S. Lee *et al.*, 2014).

1.4 EV

Cell to cell communication is required for coordination between different cells and tissues and that is performed through direct cell contact, soluble factors as well as EVs (Camussi *et al.*, 2010; EL Andaloussi *et al.*, 2013). There is a fast growing interest on EVs as mediators of cell communication since its relevance was first reported and, nowadays, EVs have been isolated from several body fluids and cell types and their role on physiological processes has been described, for example, stem cell

maintenance (Ratajczak *et al.*, 2006), tissue repair (Gatti *et al.*, 2011), immune surveillance (Raposo, 1996) and blood coagulation (Del Conde *et al.*, 2005), as well as on pathological processes, for instance, cancer (Hong *et al.*, 2009), neurological diseases (Chivet *et al.*, 2012) and HIV-1 infection (Mack *et al.*, 2000).

EVs can be classified according to their biogenesis into exosomes, microvesicles and apoptotic bodies (EL Andaloussi *et al.*, 2013). There has been a focus on exosomes and microvesicles due to its potential therapeutic use.

Exosomes are originated from the endolysosomal pathway by intraluminal budding of multivesicular bodies and fusion of multivesicular bodies with the cell membrane for exosome release (Figure 1.8) (EL Andaloussi *et al.*, 2013). Cargo sorting is mediated by endosomal sorting complex required for transport (ESCRT), programmed cell death 6 interacting protein (or ALIX) and tumor susceptibility gene 101 protein (TSG101). ESCRT sorts ubiquitylated proteins while sorting of proteins that do not require ubiquitination and other cargo might be mediated by lipids such as ceramides and lysobisphosphatidic acid and tetraspanins such as CD9 and CD63 (Bobrie *et al.*, 2011; EL Andaloussi *et al.*, 2013). The exosome release by fusion with the cell membrane is mediated by GTPases of the RAB family such as RAB11 (Savina *et al.*, 2005), RAB35 (Hsu *et al.*, 2010), RAB27A and RAB27B (Ostrowski *et al.*, 2010). SNARE proteins also mediate EV release, namely the release WNT-bound exosomes (Bobrie *et al.*, 2011; Gross *et al.*, 2012). Exosome size range is between 40 to 120 nm and can be identified by the following markers: tetraspanins (CD9 or TSPAN29, CD63 or TSPAN30, CD81 or TSPAN28), ESCRT components, ALIX, TSG101, flotillin and milk fat globule-EGF factor 8 protein (EL Andaloussi *et al.*, 2013; Lötvall *et al.*, 2014). Exosomes may contain and deliver mRNA, microRNA, non-coding RNA, cytoplasmic and membrane proteins including receptors and MHC molecules (EL Andaloussi *et al.*, 2013).

Microvesicles are originated by the outward budding of the cell membrane (Figure 1.8) through the formation of small cytoplasmic protrusions followed by detachment from the cell membrane, which is dependent on calcium influx, calpain and cytoskeleton reorganization (Camussi *et al.*, 2010; EL Andaloussi *et al.*, 2013). Microvesicles closer resemble the membrane composition of the cell of origin and their markers include integrins, selectins and CD40L (EL Andaloussi *et al.*, 2013). The outward budding of the cell membrane to form microvesicles is mediated by membrane lipid microdomains and regulatory proteins as ADP-ribosylation factor 6 (Muralidharan-Chari *et al.*, 2009; EL Andaloussi *et al.*, 2013). Microvesicles have a size range between 100 to 1,000 nm and their content include mRNA, microRNA, non-coding RNA, cytoplasmic and membrane proteins including receptors (Lee *et al.*, 2012; EL Andaloussi *et al.*, 2013).

Apoptotic bodies are formed by the outward blebbing of apoptotic cell membranes and have a size range between 500 and 2,000 nm. Apoptotic bodies are characterized by high amounts of phosphatidylserine and contain nuclear fractions and cell organelles (EL Andaloussi *et al.*, 2013).

Although the exact mechanisms regulating EV biogenesis and deliver to the target cells are not fully understood, it is thought that EVs directly stimulate target cells by antigen presentation, interaction with cell receptors and MHC molecules and cell signaling leading to the activation of downstream regulatory cascades or can deliver their cargo by cell membrane fusion or enter the target

cell through the endocytic pathway including pinocytosis, phagocytosis, clathrin-dependent endocytosis, caveolin-dependent endocytosis and lipid raft-mediated internalization (Camussi *et al.*, 2010; EL Andaloussi *et al.*, 2013; Mulcahy, Pink and Carter, 2014).

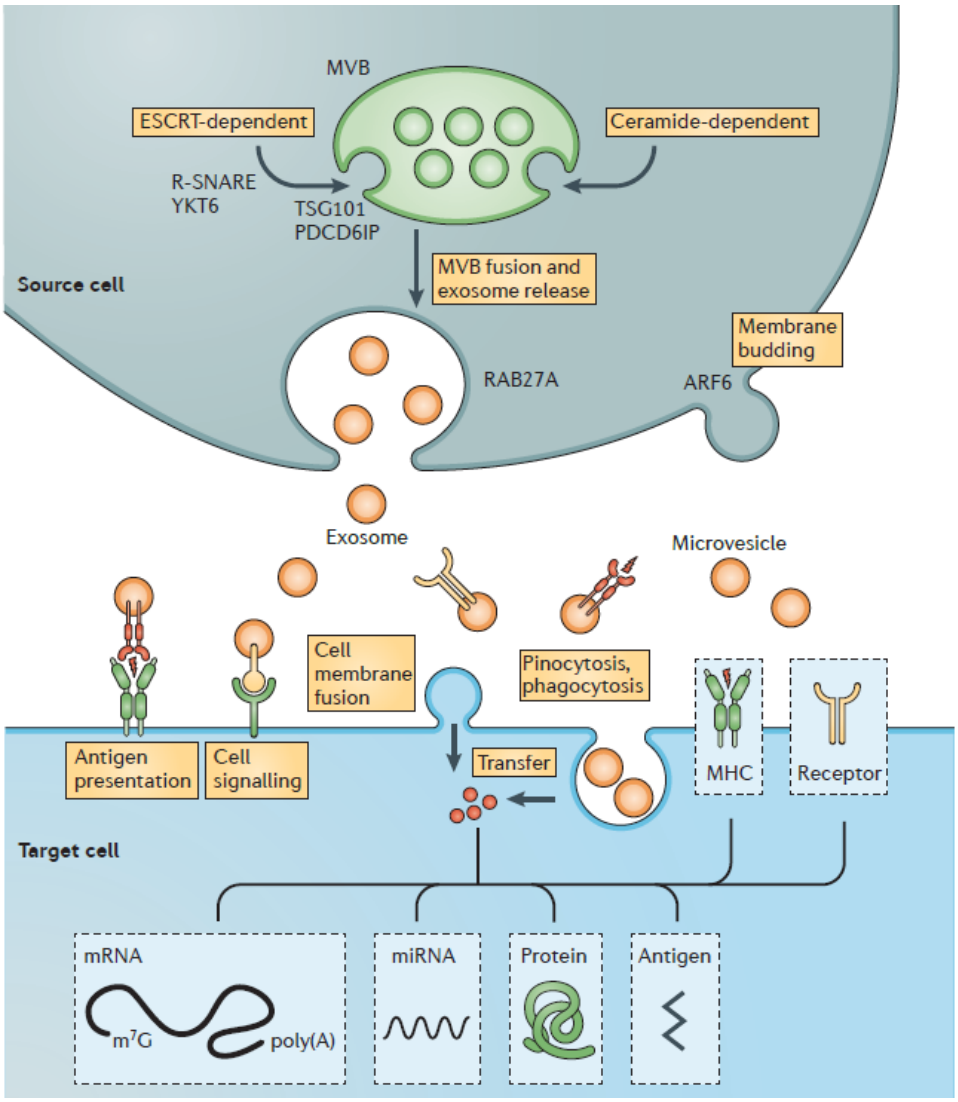

Figure 1.8 – Biogenesis of EVs and their interactions with recipient cells. Exossomes are formed by the inward budding of the multivesicular body (MVB) membrane and cargo sorting is mediated by endosomal sorting complex required for transport (ESCRT), programmed cell death 6 interacting protein (PDCD6IP or ALIX), tumor susceptibility gene 101 protein (TSG101) and by lipids such as ceramides. The release of exosomes by fusion with the cell membrane is mediated by RAB protein family. The SNARE complex is also involved in exosome secretion. Microvesicles are originated by the outward budding and fission of the cell membrane, which is mediated by membrane lipid microdomains and regulatory proteins such as ADP-ribosylation factor 6 (ARF6). EVs can mediate immune regulation by antigen presentation and transfer of major histocompatibility complex (MHC) molecules to target cells. EVs can activate cell surface receptors and transfer transcription factors, mRNA, microRNA, non-coding RNA and proteins or other bioactive lipid ligands to the target cell (EL Andaloussi *et al.*, 2013).

There is increasing evidence of the role of genetic material in EV action since mRNA and microRNA were first identified in EVs and that mRNA could be translated into protein in a target cell (Bobrie *et al.*, 2011). Moreover, it seems that RNA molecules are not randomly incorporated into EVs during biogenesis and that there are mechanisms that specifically select the RNA molecules encapsulated within EVs (Bobrie *et al.*, 2011). However, these mechanisms are largely unknown and it would be important to understand if RNA molecules are in fact sorted and how these mechanisms work possibility to be able to modulate the production of EVs with set of RNA molecules of interest specific to the treatment of each pathological condition (Bobrie *et al.*, 2011).

1.4.1 EV production

As described in chapter 1.3.3, different culture media have been used to culture MSCs, which include culture medium containing animal serum, culture medium supplemented with human platelet lysate and serum-free culture medium. The type of culture medium has impact on the cell culture and the regenerative properties of the cells, moreover, that impact can also be reflected on the secreted EVs (Bobis-Wozowicz *et al.*, 2017). EVs are isolated from MSC-CM, therefore, the type of the culture medium is an important parameter as it could be a source of contaminant EVs. Serum constitutes a source of contaminants EVs as it contains EVs with overlapping size to the EV population of interest, thus FBS-derived EVs will be co-isolated and any subsequent analysis will be biased (Szatanek *et al.*, 2015). To circumvent this problem, filtration and long ultracentrifugation (UC) processes have been used to remove EVs from serum-containing media (Szatanek *et al.*, 2015).

It has been demonstrated that FBS-derived EVs were able to promote migration of a lung carcinoma epithelial cell line (A549) and that FBS-derived EVs contained RNA molecules. It was also shown that a short UC process did not result in high removal of FBS-derived EVs and it is recommended at least 18 h of UC at 100,000 relative centrifugal force (RCF) to remove approximately 95% of RNA-containing FBS-derived EVs (Shelke *et al.*, 2014). There is already EV-free FBS for purchase, however, it increases the costs of the cell culture process (Szatanek *et al.*, 2015). It was also suggested the use of culture medium supplemented with 1% Bovine Serum Albumin (BSA) for the collection of CM for EV isolation (Théry *et al.*, 2006).

Alternatively, serum-free culture media such as StemPro MSC SFM Xeno-Free medium can be used, which besides avoiding EV contamination also avoids batch to batch variability and xenogeneic contaminants as previously stated in chapter 1.3.3. EVs isolated from umbilical cord MSCs cultured in StemPro MSC serum-free medium were reported to enhance to a higher extent the proliferation and cardiac differentiation of human cardiac cells, to promote to a higher extent the formation of tube structures by endothelial cells and inhibit mitogen-stimulated peripheral blood mononuclear cell (PBMC) proliferation when compared to other serum-free culture media and FBS-supplemented medium (Bobis-Wozowicz *et al.*, 2017).

Even serum-free culture medium and freshly open medium bottles contain trace particles on the EV size range and the number of particles increases with storage time and temperature, which lead to an increase in the background when analyzing EV samples by nanoparticle tracking analysis or nano-flow cytometry (Szatanek *et al.*, 2015).

1.4.2 EV isolation methods

EVs can be isolated using different methods. The gold standard technique has been UC, however, chromatographic, filtration and precipitation techniques have also been developed for EV isolation. A combination of two techniques can be performed to increase purity.

Although UC technique is widely used, the duration and speed of UC varies between studies and it has been reported that optimal EV isolation conditions might vary with cell type of origin (Jeppesen et al., 2014). There are mainly two types of UC, differential and density gradient UC.

Differential UC consists of centrifugation steps at increasing speed. Usually it comprises one step of centrifugation at low speed (2,000 RCF) to remove cells and cell debris, another centrifugation at higher speed (5,000-10,000 RCF) to remove larger EVs, EV and protein aggregates, usually followed by two UC steps at ≥100,000 RCF for 1-3 h at 4ºC and the EV pellet containing protein is resuspended in cold phosphate buffered saline (PBS) (Kotmakçı, 2017). Disadvantages of this method include aggregation of particles due to high centrifugal forces, variable yield even when performed by the same user, volume limitation per UC step and is a time-consuming method (Kotmakçı, 2017). Purity can be increased by combination with other types of EV isolation methods.

Density gradient UC includes the initial steps of the differential centrifugation and a first step of UC or CM concentration by centrifugal filters, followed by a discontinuous sucrose or iodixanol gradient added to UC tubes, then EV samples are loaded and long UC is performed to discriminate EV populations by density (Kotmakçı, 2017). The disadvantages of this method are the lack of standardization regarding volume and viscosity of reagents, time-consuming and an extra step the sucrose or iodixanol reagent is needed (Kotmakçı, 2017).

Size exclusion chromatography (or gel filtration chromatography) is a simple single-step method that separates biological molecules by size. EV samples are loaded to a column with a stationary phase such as Sepharose and Sephacryl, then a mobile phase (PBS) is loaded into the column resulting in the elution first of larger particles and protein aggregates and later of smaller vesicles and proteins (Szatanek *et al.*, 2015; Kotmakçı, 2017). Size exclusion chromatography results is higher purity, less variability and shorter processing time when compared to UC (Böing *et al.*, 2014). Disadvantages include the risk of contamination when aseptic conditions are not ensured, the need of optimization to determine which elution fractions are of interest and consequent time consuming process to evaluate all elution fractions and it is not appropriate for large volumes of CM (Kotmakçı, 2017).

Tangential flow filtration also relies on the separation of biological molecules by size using membrane filters (Kotmakçı, 2017). Tangential flow filtration enables to separate different EV populations and to obtain higher purity when compared to UC and it enables to process large volumes of CM and there is no need to add extra reagents. Disadvantages comprise the inability to process small volumes, the possible occlusion of the membranes and the membranes need to be regenerated or discarded after use (Kotmakçı, 2017).

Precipitation is a simple and fast isolation method that consists of incubation of the EV sample with a precipitating agent (as polyethylene glycol, sodium acetate, protamine sulfate) resulting in EV

precipitation and collection by low speed centrifugation (Kotmakçı, 2017). Purification of EV samples is followed by a salting-out step in which acetate ions cause precipitation of EVs by releasing them from the precipitating agent, resulting in high EV yield (Kotmakçı, 2017). However, it is a multi-step process and extra purification methods might be necessary (Szatanek *et al.*, 2015; Kotmakçı, 2017).

Affinity precipitation method is based on the isolation of particles that interact with specific antibodies typically present in the EV populations using magnetic beads or microfluidic devices Szatanek *et al.*, 2015; Kotmakçı, 2017). The success of the isolation is dependent on the binding efficiency of the antibodies used. Drawbacks include the possible loss of function after detachment from the antibodies, the need of efficient antibodies and it is not suitable for large volumes of CM (Szatanek *et al.*, 2015; Kotmakçı, 2017).

There are several EV isolation kits commercially available claiming higher purity and efficiency with reduced operating times that are based on immunocapture and magnetic separation (ExoCap exosome isolation kit from JRS Life Sciences GmbH, Exosome-Human CD81/CD63/CD9/EpCAM isolation kits from Life Technologies), sedimentation and column filtration (Exo-spin exosome purification kit from Cell Guidance Systems), size exclusion chromatography (qEV Size Exclusion Column from iZON) and sedimentation (Invitrogen total exosome isolation kit from Life Technologies, ExoQuick and ExoQuick-TC exosome isolation kits from System Biosciences, ME exosome isolation kit from New England Peptide, miRCURY exosome isolation kit from Exiquon) (Kotmakçı, 2017). Each commercial kit is designed to obtain certain EV population for specific applications, thus, the EV populations isolated from each kit are different and also different from UC isolated EVs (Kotmakçı, 2017).

When considering the use of EVs for therapeutic purposes, large amounts of EVs are necessary, thus the choice should be for EV isolation methods that allow scale-up such as tangential flow filtration.

Following EV isolation, EV samples can be immediately used or stored. Optimal EV storage conditions were not determined yet. However, it is now generally accepted that EVs should be used fresh and the sooner the better to maintain physical properties and functionality (Szatanek *et al.*, 2015). EV size is affected by temperature and storage time (Sokolova *et al.*, 2011). Storage at -80ºC has been frequently used when the use of fresh EVs has logistical constrains, however, loss of EV function has been observed even when cycles of freeze and thawing are avoided by aliquoting EV samples and when EV size and number is similar (Lőrincz *et al.*, 2014; Szatanek *et al.*, 2015). Thus, for functional studies the use of fresh EVs is recommended, while for other characterization studies such as EV size and number and RNA content storage at -80ºC for about one week is acceptable (Lőrincz *et al.*, 2014).

1.4.3 EV characterization methods

The International Society for Extracellular Vesicles (ISEV) established the minimal biochemical and biophysical criteria as well as guidelines for the use of controls for functional studies to be able to attribute the outcome observed to a specific cargo or function of EVs (Lötvall *et al.*, 2014). Thus, the

minimal criteria include one semi-quantitative technique of the EV components and two different techniques for the characterization of single vesicles (Lötvall *et al*., 2014).

For the semi-quantitative technique of the EV markers, Western Blot, high resolution nano-flow cytometry or global proteomic analysis using mass spectrometry techniques could be used. Controls for this semi-quantitative analysis should include isotype controls and comparison to the expression of the cells of origin, the CM, the CM EV-depleted and/or culture medium incubated and processed as for EV production and isolation but without cells to determine the specific presence and enrichment of the EV components (Lötvall *et al*., 2014). The semi-quantitative technique should evaluate 3 or more EV markers including markers expected to be present in the EV population such as transmembrane and cytosolic proteins with membrane binding capacity (group 1 an 2 from Table 1.4) and markers expected to be absent in EV populations such as intracellular proteins (group 3 from Table 1.4). At least one marker of group 1, 2 and 3 from Table 1.4 should be evaluated. It is also recommended that the evaluation of non-specific EV markers (group 4 from Table 1.4) should be limited to cases where no other quantitative measurements can be used with a clear justification for its use (Lötvall *et al*., 2014).

Table 1.4 – Different groups of expected markers to be present (group 1 and 2) and absent (group 3) in EV samples and examples of protein markers for each group. At least one protein of each group 1, 2 and 3 should be evaluated. The use of protein markers from group 4 should be avoided due to variability and lack of specificity (Lötvall *et al*., 2014).

1. Transmembrane or lipid-bound extracellular proteins	2. Cytosolic proteins	3. Intracellular proteins	4. Extracellular proteins
Argues presence of a membrane in the isolate	With membrane- or receptor-binding capacity	Associated with compartments other than plasma membranes or endosomes	Binding specifically or non-specifically to membranes, co-isolating with EVs
Present or enriched in EVs	Present or enriched in EVs	Absent or under-represented in EVs/exosomes, but present in other types of EVs	Variable association with EVs
Examples: Tetraspanins (CD9, CD63, CD81) Integrins or cell adhesion molecules Growth factor receptors Heterotrimeric G proteins Phosphatidylserine-binding MFGE8/lactadherin	Examples: Endosome or membrane-binding proteins (TSG101, annexins, RAB proteins) Signal transduction or scaffolding proteins (syntenin)	Examples: Endoplasmic reticulum (Grp94, calnexin) Golgi (GM130) Mitochondria (cytochrome C) Nucleus (histones) Argonaute/RISC complex	Examples: Acetylcholinesterase Serum albumin Extracellular matrix (fibronectin, collagen) Soluble secreted proteins (cytokines, growth factors, metalloproteinases)

Regarding the two different techniques that should be used for characterization of single vesicles, several methods are available to determine the heterogeneity of EV samples such as imaging techniques and techniques to determine size distribution. Regarding the imaging techniques, transmission electron microscopy or atomic force microscopy can be performed and it is recommended a wide field of multiple vesicles and a close-up of single vesicles. To determine the EV size distribution, nanoparticle tracking analysis, dynamic light scattering or resistive pulse sensing can be used. Nanoparticle tracking analysis also allows the determination of particle concentration. Size distribution techniques should be complemented with the imaging technique to confirm size range and to distinguish EVs from possible co-isolated non-membranous particles of similar size (Lötvall *et al*., 2014).

Although not specified in the ISEV minimal criteria to define EV populations, protein concentration of the EV samples is very relevant and typically determined by MicroBCA, BCA and Bradford protein assay. It has been used to indirectly quantify the amount of EVs in the samples and to describe the quantity of EVs used for *in vitro* and *in vivo* studies. More importantly, the protein concentration together with the EV concentration determined by nanoparticle tracking analysis allows determining the protein to particle ratio (PPR), a parameter that should also be widely implemented as a measure of purity of the EV samples (Webber and Clayton, 2013).

There are also no guidelines and acceptable criteria regarding the characterization of all EV contents, namely lipids, metabolites and RNA. Protein and lipid EV content can be characterized by omic tools such as liquid chromatography and gas chromatography coupled with mass spectrometry or direct infusion electrospray ionization into the mass spectrometer (Kreimer *et al.*, 2015). High-resolution mass analyzers including Orbitrap, Fourier transform cells and time-of-flight can be used for proteomic and lipidomic analysis. EV lysis and lipid extraction can be performed by liquid-liquid phase extraction using THF and diethyl ether and water partitioning or by Bligh and Dyer liquid−liquid phase extraction using with chloroform and methanol (Kreimer *et al.*, 2015). For EV proteomic analysis, EV samples can be digested and separated by 1D or 2D gel electrophoresis or 2D differential gel electrophoresis prior to mass spectrometry analysis (Kreimer *et al.*, 2015; Rosa-Fernandes *et al.*, 2017). Metabolimic analysis of EV content consists of extraction and measurement of EV metabolites by high-field nuclear magnetic resonance or gas or liquid chromatography coupled with mass spectrometry (Palomo *et al.*, 2014). RNA EV content includes mRNA, microRNA and non-coding RNA and techniques for RNA analysis include microarray analysis or deep sequencing (or next generation sequencing) (Hill *et al.*, 2013). Deep sequencing systems include Illumina HiSeq, Roche 454 pyrosequencing, SOLiD, MiSeq, Ion Torrent Personal Genome Machine and GS Junior. Typically, prior to library preparation for deep sequencing, the size distribution and quantity of RNA for EV samples should be analyzed, for instance, using a Bioanalyzer (Hill *et al.*, 2013).

1.4.4 EVs and pre-clinical and clinical trials

It is important to understand if EVs recapitulate MSC regenerative properties and could be used as a cell-based but cell-free therapy or in co-administration, therefore, the therapeutic potential of MSC-EVs has been tested in several pre-clinical and clinical trials.

Similarly to MSCs, MSC-EVs have been tested in pre-clinical trials for a broad range of diseases and evidence of MSC-EV therapeutic potential has been described for myocardial and reperfusion injury (Lai, Arslan, Lee, *et al.*, 2010; Arslan *et al.*, 2013), lung injury (Lee *et al.*, 2012), acute kidney injury (Bruno *et al.*, 2009, 2012; Gatti *et al.*, 2011), hindlimb ischemia (H.-C. Zhang *et al.*, 2012) and liver injury (T. Li *et al.*, 2013). Due to the scope of this project, examples of pre-clinical trials will the giving for cardiovascular and lung diseases.

In studies evaluating the regenerative potential of MSC-EVs in MI and reperfusion injury, the infarct size is typically assessed and an average of several studies showed about 18% reduction of the infarct size (Akyurekli *et al.*, 2015), which is a modest reduction indicating that, similarly to MSC cell-based therapy, it is necessary to boost clinical benefits possibility by bioengineering strategies.

The therapeutic effect of MSC-EVs on MI models has been attributed to restoration of bioenergetics, decrease of oxidative stress, stimulation of pro-survival signaling, decrease in inflammation (Arslan *et al.*, 2013) and stimulation of angiogenesis (H.-C. Zhang *et al.*, 2012).

EVs from fetal MSCs were reported to be cardio-protective in a mouse model of MI and reperfusion injury and the EVs were cardio-protective at approximately 1/10 of the dose of CM (Lai, Arslan, Tan, *et al.*, 2010).

MSC-EVs intravenously injected on a MI model were reported to reduce infarct size and improve cardiac performance by endocytosis or phagocytosis of EVs at the infarct area leading to the restoration of bioenergetics by replenishing ATP and NADH levels, reduction of oxidative stress, stimulation of pro-survival signaling by increasing the phosphorylation of the survival pathways Akt/GSK3 and decreasing the phosphorylation of the pro-apoptotic pathway c-JNK and reduction of inflammation by a decrease in the neutrophil and macrophage infiltration and decrease in the total white blood cell count (Arslan *et al.*, 2013).

MSC-EVs isolated from BM MSCs cultured under hypoxia conditions were able to promote angiogenesis *in vitro* enhancing human umbilical vein endothelial cells (HUVEC) proliferation, migration and tube formation to similar extent as VEGF and *in vivo,* in a rat model of MI, MSC-EVs intramyocardialy injected enhanced angiogenesis, cardiac function and decreased infarct size to similar extent as the administration of the cells (Bian *et al.*, 2014). In another study, human umbilical cord MSCs pre-conditioned by hypoxia were reported to secrete EVs with angiogenic potential *in vitro* by promoting endothelial cell proliferation and tube formation and *in vivo* in a rat hindlimb ischemia model by enhancing blood flow recovery (H.-C. Zhang *et al.*, 2012).

MSC-EVs isolated from BM MSCs pre-conditioned by ischemia were enriched in miR-22 which had an anti-apoptotic effect *in vitro* by targeting methyl CpG binding protein 2 and reduced cardiac fibrosis *in vivo* in a MI mice model (Feng *et al.*, 2014). Cardioprotective effect was not fully inhibited when blocking miR-22, which indicated that other microRNAs such as miR-21, miR-199a-3p and miR-210 could also be involved (Feng *et al.*, 2014). A list of microRNAs identified in MSC-EVs and that have been related to MSC-EV regenerative properties is later enumerated in Table 1.6.

In hypoxia-induced pulmonary hypertension mice model, it was described that intravenous administration of human umbilical cord MSC-EVs protected from oxygen deprivation and suppressed vascular remodeling through the inhibition of the hyperproliferative STAT3 signaling pathway, the down-regulation of the pro-proliferative miR-17 superfamily and the up-regulation of miR-204, which is often decreased in pulmonary hypertension models (Lee *et al.*, 2012). Moreover, MSC-EVs reduced macrophage infiltration and reduced the secretion of pro-inflammatory and pro-proliferative cytokines as MCP-1 and hypoxia-inducible mitogenic factor (Lee *et al.*, 2012).

In an *Escherichia coli* endotoxin-induced acute lung injury mice model, human BM MSC-EVs intratracheal administered were able to promote recovery by reducing edema and inflammation through a 43% reduction in fluid accumulation in the lung alveoli and 35% reduction in the protein permeability as well as 73% reduction in neutrophil infiltration and 49% decrease in the release of macrophage inflammatory protein-2 (Zhu *et al.*, 2014). Moreover, the therapeutic potential of MSC-EVs was partially mediated by KGF mRNA (Zhu *et al.*, 2014).

In an *Escherichia coli* pneumonia mice model, intravenous administration of human BM MSC-EVs improved mice survival in a process mediated by KGF, decreased bacteria load and decreased inflammation (Monsel *et al*., 2015). Reduction in inflammation was a consequence of increased monocyte phagocytosis of bacteria and decreased inflammatory cell infiltration (40% of white blood cells and 53% of neutrophils), protein permeability (22%) and pro-inflammatory cytokines TNF-α and macrophage inflammatory protein-2. Phagocytosis of bacteria could be further boosted by the pre-conditioning of MSCs with TLR3 agonist. MSC pre-conditioning with TLR3 agonist also increased the anti-inflammatory cytokine IL-10 and the enzyme COX-2 which mediates PGE2 production that in turn is involved in the differentiation of macrophages towards the anti-inflammatory M2 phenotype. MSC-EVs also restored bioenergetics of epithelial cells by increasing ATP levels. Additionally, EV uptake by monocytes and epithelial cells was mediated by CD44 receptors (Monsel *et al*., 2015).

In an *aspergillus hyphal* extract allergic airway inflammation mice model mimicking asthma, CM and EVs from human and murine BM MSCs reduced airway hyperreactivity and the antigen-specific $CD4^+$ T cell Th2 and Th17 phenotype, together with an increase in IFN-γ indicating that a Th2/Th17 inflammatory shift towards anti-inflammatory Th1 phenotype, consequently reducing inflammation (Cruz *et al.*, 2015). CM and EVs from human MSCs produced enhanced results compared to murine MSC-derived CM and EVs, indicating that xenogeneic use is acceptable but also that they act through different mechanisms of action (Cruz *et al.*, 2015).

In a silica-induced inflammation and fibrosis lung mice model, BM MSC-EVs reduced intracellular oxidative stress by directing depolarized mitochondria to the cell membrane in a process mediated by arrestin domain-containing protein 1 and ameliorated bioenergetics by promoting the engulfment of EV-containing mitochondria by macrophages which re-used those mitochondria (Phinney *et al.*, 2015). Moreover, MSC-EVs contained microRNAs such as miR-451 that reduced macrophage activation and white blood cell infiltration in response to silica, by blocking TLR signaling, thus decreasing the cytokines TNF-α and macrophage migration inhibitory factor and also reduced fibrosis by decreasing the anti-inflammatory and pro-fibrotic cytokines IL-10 and TGF-β (Phinney *et al.*, 2015). A few more examples of pre-clinical trials using MSC-EVs are indicated in Table 1.5.

Table 1.5 – Examples of pre-clinical trials using MSC-EVs as therapeutics for lung diseases.

Animal model	Treatment	Therapeutic effect	Reference
Ovalbumin-induced asthma	Human AT MSC-EVs	EVs reduced lung elastance, inflammation, collagen deposition, through reduction in IL-4, IL- 5, eotaxin, TGF-β, eosinophils and T lymphocytes	(de Castro *et al.*, 2017)
LPS-induced acute respiratory distress syndrome	Human BM MSC-EVs	EVs transferred mitochondria, suppressed cytokine production, increased M2 macrophage phenotype markers and promoted phagocytosis, partially mediated by CD44-EVs	(Morrison *et al.*, 2017)
Elastase-induced COPD	Human AT MSC nanovesicles mimic	Artificial nanovesicles increased regeneration mediating FGF2 signaling	(Kim *et al.*, 2017)
Silica-induced idiopathic pulmonary fibrosis	Human BM MSC-EVs	EVs reduced collagen deposition and the number of inflammatory cells in the lungs	(Choi, Ban and Rhim, 2014)
Monocrotaline-induced pulmonary hypertension	Murine compact bone MSC-EVs	Exosomes enriched in anti-inflammatory and anti-proliferative miR-34a, miR-122, miR-124, miR-127 reduced pulmonary hypertension	(Aliotta *et al.*, 2016)

Results from pre-clinical trials for cardiovascular and lung diseases seem to be promising, however, more insight into the mechanisms of action and functional characterization are needed to develop and translate MSC-EV therapeutics to humans. To the extent of my knowledge there is no clinical trial with MSC-EVs for cardiovascular and lung diseases that is completed or terminated with published results (by May 2018).

Clinical trials involving MSC-EVs have been performed for other disease settings, namely GVHD. Increasing doses of BM MSC-EVs were reported to be safe and to improve GVHD symptoms in grade IV GVHD patients (Kordelas et al., 2014). Pro-inflammatory cytokines IL-1β, TNF-α, IFN-γ were reduced and anti-inflammatory cytokines IL-10, TGF-β and HLA-G were increased. The highest EV dose consisted of 4 units of 1.3-3.5 x 10^{10} EV/unit or 0.5-1.6 mg/unit isolated from the CM of 4 x 10^{7} MSCs (Kordelas et al., 2014).

Regarding clinical trials with EVs isolated from other cell types, EV-based cancer vaccines were already tested in Phase I clinical trials using autologous dendritic cell-EVs isolated from advanced metastatic melanoma patients and non-small lung cancer patients resulting tolerated administration with minor inflammatory responses (Escudier *et al.*, 2005; Morse *et al.*, 2005). Repeated administrations of EVs from autologous ascites fluid of colorectal cancer patients co-administered with GM-CSF resulted in no major toxicity with only mild inflammation at the site of vaccination (Dai *et al.*, 2008). EV vaccine efficacy was not shown yet, but it potentially arrested disease progression (Morse *et al.*, 2005; Dai *et al.*, 2008) and phase II clinical trials should follow together with deeper research to understand the mechanisms of action.

More research is also needed regarding biodistribution and bioavailability of EVs for different routes of administration to evaluate which administration route would be more efficient allowing retention of EVs at the injury site to promote repair without causing cytotoxic effects (Gimona *et al*., 2017). Determination of the EV dose range that has therapeutic effect is also very important.

MSC-EV action has been attributed in part to the effect of microRNAs encapsulated in the EVs. Several microRNAs and their action on regeneration have been identified. Some of the studies that identified sets of microRNAs present in MSC-EVs and their role on regeneration are present in the next Table 1.6. MicroRNAs such as miR-10, miR-16, miR-21, miR-22, miR-23, miR-24, miR-34a, miR-122, miR-125, miR-133, miR-143, miR-145, miR146, miR-148a, miR-181c, miR-191, miR-210, miR-302b, miR-451 and let-7 family were identified in more than one study.

Table 1.6 – Examples of studies which identified microRNAs enriched in MSC-EVs and their role on regeneration.

miRNA	Action	Application	Reference
miR-22 (and potentially miR-21, miR-199a-3p, miR-210)	Mouse BM MSC-EVs from ischemia pre-conditioned MSCs had anti-apoptotic effect and improved cardiac fibrosis	Cardio-protection	(Feng *et al*., 2014)
miR-29, miR-24 (and potentially miR-16, miR-23, miR-31a, miR-103)	Rat BM MSC-EVs are enriched in microRNAs that regulate fibrosis, apoptosis, inflammation (and angiogenesis, proliferation, necrosis)	Vascular and cardiac disorders	(Shao *et al*., 2017) ((Bang, Fiedler and Thum, 2012; J. X. Wang *et al*., 2015))
miR-147, let-7i, miR-503, miR-362 (and potentially miR-181c)	Rat BM MSC-EVs stimulated proliferation, migration, angiogenesis and survival and reduced cardiac fibrosis	Cardio-protection and repair, Myocardial infarction	(Zhang *et al*., 2016)
miR-19a, miR-451, miR-221	EVs from rat BM MSCs overexpressing GATA4 had increased anti-apoptotic and pro-survival effect resulting in increased activity of Akt and ERK signaling pathway, and reduced infarct size	Cardio-protection	(Yu *et al*., 2015)
miR-210	EVs from mouse BM MSCs serum-deprived promoted angiogenesis and improved cardiac function	Myocardial infarction, Angiogenesis	(N. Wang *et al*., 2017)
miR-21	Human endometrium-derived MSC-EVs promoted angiogenesis and survival, restored cardiac function and decreased infarct size through PTEN/Akt pathway	Myocardial infarction, Angiogenesis, Survival	(K. Wang *et al*., 2017)
miR-451 (and potentially miR-1202, miR-630, miR-638)	Human BM MSC-EVs reduced macrophage activation and white blood cell infiltration and decreased anti-inflammatory and pro-fibrotic cytokines	Immunomodulatory, Silica-induced pulmonary fibrosis and inflammation	(Phinney *et al.,* 2015)
miR-486, miR-10a, miR-10b miR-191, miR222, miR-21, miR-22, miR143, let-7a, let-7f, miR-146a, miR-146b	Human BM and AT MSC-EVs are enriched in several microRNAs involved in replicative senescence, cell cycle progression and proliferation, migration, MSC differentiation, angiogenesis, anti-apoptosis, immunomodulatory	Immunomodulatory, Proliferation, Survival, Angiogenesis	(Baglio *et al.*, 2015)
miR-16, miR-21, let-7b	Human umbilical cord MSC-EVs promoted recovery from hypoxia-induced pulmonary hypertension by suppressing macrophage influx, the secretion of pro-inflammatory trophic factors and vascular remodeling and increased miR-204 levels in the lungs	Immunomodulatory, Lung inflammation and edema, Vascular inflammation	(Lee *et al*., 2012)
miR-34a, miR-122, miR-124, miR-127, miR-101a, miR-193, miR-224, miR-302b	Mouse BM MSC-EVs induced anti-inflammatory, anti-proliferative, apoptotic and senescent effects, reducing pulmonary hypertension	Immunomodulatory, Pulmonary hypertension	(Aliotta *et al.*, 2016)
miR-146a (and potentially miR-21, miR-149)	EVs from umbilical cord MSCs pre-conditioned with IL-1β induced macrophage polarization toward an anti-inflammatory M2 phenotype and increased survival in a sepsis model	Immunomodulatory, Inflammatory diseases as sepsis	(Song *et al*., 2017)
miR-223	Mouse BM MSC-EVs reduced inflammation and cell death and induced cardio-protection in sepsis	Immunomodulatory, Inflammatory diseases as sepsis	(X. Wang *et al.*, 2015)
miR-181c	Human umbilical cord MSC-EVs decreased TNF-α, IL-1β and increased IL-10 levels, reducing NF-ΚB/p65 activation attenuating burn-induced excessive inflammation	Immunomodulatory, Burns	(Li *et al*., 2016)
Let-7b (and potentially miR-1180, miR-183, miR-550b, miR-133a)	EVs from LPS pre-conditioned human umbilical cord MSCs up-regulated anti-inflammatory cytokines and promoted M2 macrophage activation, through TLR4/NF-KB/STAT3/AKT signaling pathway	Immunomodulatory, Wound healing	(Ti *et al*., 2015)
miR-16	Mouse BM MSC-EVs suppressed angiogenesis in breast cancer cells	Angiogenesis	(J.-K. Lee *et al.*, 2013)
miR-100	EVs from human BM MSCs cultured in BSA or serum-free medium for 48h suppressed angiogenesis in breast cancer cells by suppression of vascular endothelial growth factor	Angiogenesis	(Pakravan *et al*., 2017)

miR-30b, miR-30c, miR-424 and let-7f	MSC-EVs promoted proliferation, tube-like structure formation, sprouting and migration of HUVEC	Angiogenesis	(Gong *et al*., 2017)
miR-148a, miR-532, miR-378, let-7f	EVs from porcine AT MSCs serum deprived were enriched in microRNAs involved in angiogenesis, cellular transport, apoptosis and proteolysis	Angiogenesis, survival and adipogenesis	(Eirin *et al*., 2014)
miR-125a	Human AT MSC-EVs stimulated angiogenic genes and supressed the expression of angiogenic inhibitor delta-like 4	Angiogenesis, Wound healing	(Liang *et al*., 2016)
miR-21, miR-23a, miR-125b, and miR-145	Mouse UCM MSC-EVs suppressed myofibroblast formation by inhibiting excess α-smooth muscle actin and collagen deposition acting on transforming growth factor-β/SMAD2 signaling pathway	Wound healing	(S. Fang *et al.*, 2016)
miR-122	Human AT MSC-EVs decreased genes related to proliferation and maturation of collagen, decreasing activation of hepatic stellate cells in liver fibrosis	Liver fibrosis	(Lou *et al*., 2017)
miR-494	EVs from human BM MSCs serum deprived stimulated myogenesis and angiogenesis, and muscle regeneration	Skeletal muscle regeneration	(Nakamura *et al*., 2015)
miR-199b, miR-218, miR-148a, miR-135b, let-7a, miR-203, miR-219, miR-299, miR-302b	EVs from human BM MSCs subjected to osteogenic differentiation showed altered microRNA profile	Osteogenic differentiation	(Xu *et al*., 2014)
Let-7a, miR-21, miR143, miR-145, miR-451a, miR-338, miR-1260, miR-1908	Human AT MSC-EVs from cancer and healthy individuals showed similar microRNA profile under serum conditions	Potential autologous transplantation	(García-Contreras *et al.*, 2014)
miR-23b	Human BM MSC-EVs induced dormant phenotypes through cell cycle arrest, inhibition of proliferation, invasion and migration	Dormancy in metastatic breast cancer cells	(Ono *et al*., 2014)
miR-133b	Rat BM MSC-EVs promoted neurite remodeling, axonal plasticity and functional recovery after stroke in rats	Stroke	(Xin *et al*., 2013)
miR-21, miR-34a, lncRNA 7SK, lncRNA Y1	Human BM MSC-EVs from serum-deprived MSCs had anti-apoptotic effect, promoted survival and proliferation of breast cancer cells	Survival and Proliferation	(Vallabhaneni *et al*., 2015)
miR-196a, miR-27, miR-206	Human BM MSC-EVs stimulated osteoblast activity and differentiation	Bone regeneration	(Qin *et al*., 2016)
miR-483, miR-191, miR-28, miR-423, miR-744, miR-129, miR-24, miR-148a	EVs from mouse BM MSCs serum-deprived (but supplemented with BSA) reversed deregulation of kidney genes after injury, namely genes related to inflammation, matrix-receptor interaction, cell cycle and cell adhesion molecules	Acute kidney injury	(Collino *et al.*, 2015)

1.4.5 EV commercialized products

There are many unanswered questions related to the biogenesis, loading, manufacturing, delivery, function, biodistribution and regulatory issues. Nevertheless, the EV field is growing fast raising the interest of many biotechnology and pharmaceutical companies. Thus, there are already several EV-related products in the market.

The exosome diagnostic market was evaluated in 10 million dollars in 2016 and is expected to grow to 100 million dollars by 2021 and diagnosis through the blood has the highest growth potential and shares in that market (Roy, Hochberg and Jones, 2018). While the exosome therapeutic market was evaluated in 5 million dollars in 2016 and is expected to grow to 10 million dollars and it's slower growth is mainly due to regulatory issues for approval of EV therapeutics (Roy, Hochberg and Jones, 2018).

EV isolation and purification products have been commercialized by Life Sciences GmbH, Life Technologies, Cell Guidance Systems, iZON, System Biosciences, New England Peptide, Exiquon, Qiagen, HansaBioMed and Exosome Diagnostics (György *et al.*, 2015; Kotmakçı, 2017).

EV diagnostic products have been developed based on the presence of disease biomarkers on secreted EVs, especially for the detection of biomarkers in biofluids as blood to facilitate sampling and to be minimally invasive (György *et al.*, 2015). Companies commercializing EV diagnostic products for cancer include Exosome Diagnostics, Exosomics Siena, Exosome Sciences, for viral infections is Exosome Sciences and for small interfering RNA is Alnylam (György *et al.*, 2015).

Finally other companies are interested on the development of EV therapeutics for cardiovascular, neurologic, orthopedic and autoimmune diseases as well as for skin lesions, aging and other cosmetic applications (Gimona et al., 2017). In Table 1.7 are examples of companies developing and offering MSC-EV products for therapeutic purposes.

Table 1.7 – Examples of companies offering MSC-EV-based services and products and respective therapeutic target (Gimona *et al*., 2017).

Company	Therapeutic target	Product	Company's website
Esperite Group/ The Cell Factory	Various diseases from neurology to orthopedics	MSCs and MSC-derived EVs and exosomes	http://www.esperite.com/?page_id=13 http://www.cell-factory.com/
Kimera Labs	Orthopedic, cosmetic and regenerative medicine applications	MSC-derived exosomes "XoGloTM", amniotic fluid-derived product "Amnio2xTM"	http://kimeralabs.com/
Paracrine Therapeutics	Stroke, MI, osteochondral defect, GVHD	Embryonic stem cell-derived MSC-EVs	http://paracrinetherapeutics.com/
Stemedica Cell Technologies, Inc	Cardiovascular diseases, traumatic brain injury, cutaneous photoaging, Alzheimer's disease	Ischemia-tolerant MSCs and neural stem cells; stem cell factors from MSCs	https://www.stemedica.com/
ZenBio	Skin lesions	Exosomes from pre-adipocytes, placental MSCs and cord blood serum	http://www.zen-bio.com/

The company Aethlon Medical is interested on the development of a therapy based on EV depletion in cancer (György *et al.*, 2015). Increasing interest is also on the use of EVs as vaccines for infectious diseases and cancer as well as vehicles for gene therapy including the strategies of gene replacement, gene editing and small interfering RNA, taking advantage of the immune-privileged potential of the EVs (György et al., 2015).

EVs deliver not only proteins but also nucleic acids and EV therapeutics might be produced from genetically modified cells, thus not only the regulatory agencies FDA and EMA might be involved in the development and approval of these EV therapeutics but also entities such as the National Institutes of Health DNA Recombinant Advisory Committee in order to demonstrate and ensure all the safety requirements (György et al., 2015).

1.5 Predictive potency assays and deciphering the mechanism of action of MSCs and MSC-derived products

To translate MSC, MSC-CM and MSC-EVs to the clinics, the evaluation of the therapeutic potency *in vitro* and *in vivo* is required. Typically a combination of several potency assays is necessary to assess the multiplicity of effects of MSCs and MSC-derived products and potentially determine the mechanisms of action. Moreover, to submit MSCs and MSC-derived products for testing in pre-clinical trials, it is necessary to propose a mechanism of action even if not fully uncovered. If successful the pre-clinical trials will provide a proof of concept, which can then be used to submit the therapy for clinical trials.

As previously described in chapter 1.3 and 1.4, the therapeutic properties of MSC, MSC-CM and MSC-EV include but are not limited to prevention of apoptosis, enhancement of proliferation, migration and angiogenesis and immunomodulatory function. These properties have been assessed using *in vitro* potency assays including simpler 2D assays and more complex 3D systems such as transwell and organ-on-a-chip models and using *in vivo* animal models. Nevertheless, there is a lack of standardized and robust platforms to characterize the potency of MSCs and MSC-derived products, thus there are no much comprehensive studies characterizing and assessing the multiplicity of MSC therapeutic properties and the lack of standardization also hinders the comparison of results between different groups.

Oxidative stress

When considering the administration of MSCs into an injury site, MSCs have to be able to survive to a harsh oxidant, ischemic and inflammatory environment (Song, Cha, *et al.*, 2010; Song, Song, *et al.*, 2010; Gnecchi *et al.*, 2016). The harsh oxidant environment can hinder MSC regenerative properties and cause their apoptosis (Denu and Hematti, 2016). However, MSCs have been reported to be resistant to oxidative stress (Brandl *et al.*, 2011) and if the transplanted cells are able to survive, they can exert their protective action and prevent apoptosis of the host cells by direct contact and by paracrine action mediated by soluble factors and EVs. Therefore, there is a need to develop robust and standardized potency assays to screen MSC donors, cell sources, culture conditions and bioengineering strategies and to select MSCs with enhanced resistance to oxidative stress and that release pro-survival and anti-apoptotic factors that promote host cell survival.

Oxidative stress is a perturbation in the balance between the production of ROS and the anti-oxidant defense mechanisms, which can result in tissue damage (Betteridge, 2000). ROS can be produced as a consequence of aerobic respiration, oxidation of catecholamines and activation of the arachidonic acid cascade, nitric oxide production by stromal cells and electromagnetic radiation. ROS are unstable molecules which react with biological molecules causing lipid peroxidation, protein and DNA damage, which can result in apoptosis (Betteridge, 2000). Oxidative stress has a relevant role on inflammatory-related diseases such as cardiovascular and lung diseases, for instance, on the atherosclerosis process as described in chapters 1.1.1 and 1.1.2 but also as defense mechanism by neutrophils to neutralize pathogens during phagocytosis.

Cellular anti-oxidant defense mechanisms include but are not limited to dismutase, peroxidase and catalase enzymes, metal binding proteins (transferrin, lactoferrin, ceruloplasmin, haptoglobins, hemopexin and albumin) and low-molecular-weight molecules (bilirubin, vitamin C, vitamin E and urate) (Betteridge, 2000).

It is not possible to directly measure ROS, thus oxidative stress is typically measured by their reaction products of oxidative damage as lipid peroxidation and DNA and protein oxidation, by depletion anti-oxidants as vitamin C and E and thiol groups as well as by their consequent effect on cellular viability, senescence, apoptosis or necrosis (Betteridge, 2000).

Cellular senescence is a process characterized by permanent growth arrest in response to different stress stimuli which typically occurs with aging, age-related diseases and as anti-cancer response mechanism (Childs et al., 2015). Apoptosis is an ATP-dependent cell death process which does not typically induce inflammation and that is characterized by cell shrinkage, maintenance of plasma membrane integrity, chromatin condensation, nuclear fragmentation, activation of caspases family, while necrosis is an ATP-independent process which typically causes inflammation and that is characterized by cell and organelle swelling, pyknosis, loss of ion gradient, loss of cell membrane integrity and consequent release of intracellular content (Cummings, Wills and Schnellmann, 2004).

Methods to evaluate lipid peroxidation include thiobarbituric acid-reactive substances assays, conjugated dienes, hydroperoxides, F2 isoprostanes and nitroxides detection (Betteridge, 2000). For instance, F2 isoprostanes are detected by gas chromatography-mass spectrometry, while malondialdehyde can be detected spectrophotometrically by thiobarbituric acid-reactive substance assay or by enzyme-linked immunosorbent assay (ELISA) (Ho *et al.*, 2013). Methods to evaluate DNA and protein damage include molecular strategies (polymerase chain reaction (PCR) methods and agarose gel electrophoresis, evaluation of DNA repair proteins Ku protein, phosphorylated histone 2AX protein, X-ray repair cross complementing-1 protein), fluorescence strategies (Annexin V/propidium iodide (PI) labeling analyzed by flow cytometry, comet assay, alkaline single-cell gel electrophoresis, neutral single-cell gel electrophoresis, detection of lesion-specific enzymes, bromodeoxyuridine-labelled DNA-comet fluorescence *in situ* hybridization, halo assay, TUNEL assay, DNA breakage detection-fluorescence *in situ* hybridization, radioimmunoassay), chemiluminescence strategies (ELISA, immunohistochemical assay, immunological assay) and analytical strategies (high performance liquid chromatography-electrospray tandem mass spectrometry, gas chromatography-mass spectrometry, electrochemical methods) (Figueroa-González and Pérez-Plasencia, 2017).

Cell survival and viability can be assessed by cell count or indirectly by the metabolic activity and mitochondrial function using MTT, Alamar or Presto Blue (Yedjou and Tchounwou, 2012).

Apoptosis is frequently measured using the marker caspase-3 and measured by western blot, immunohistochemistry or flow cytometry (Yedjou and Tchounwou, 2012). Simultaneous detection and quantification of apoptosis and necrosis by flow cytometry is possible using Annexin V to measure apoptosis and PI to measure necrosis (Yedjou and Tchounwou, 2012; Kusuma *et al.*, 2017). Frequently, the release of intracellular contents is evaluated by lactate dehydrogenase (LDH) colorimetric method, however, it is a less sensitive method when compared to Annexin V/PI analysis.

Alternative methods or a combination of more than one method to assess apoptosis and necrosis can also be used (more examples of markers and biological events related to apoptosis and necrosis are present in Table 1.8).

Table 1.8 – Methods and markers to assess different morphological and biochemical events of apotosis and necrosis. Adapted from (Cummings, Wills and Schnellmann, 2004).

Morphological or biochemical event	Marker	Reference
Phosphatidylserine externalization	Annexin V binding	(Schutte *et al.*, 1998; Cummings and Schnellmann, 2002)
Caspases activation	Fluorometric substrate cleavage Expression of specific caspases Cytochrome c translocation	(Liu *et al.*, 1996; Thornberry *et al.*, 1997; Saraste and Pulkki, 2000)
Plasma and lysosomal membrane integrity	PI staining Neutral red	(Ferlini *et al.*, 1996; Singh, 2000)
Cellular volume	Cell size	(Bortner and Cidlowski, 2007)
Intracellular content release	LDH	(Mertens *et al.*, 1995; Moran and Schnellmann, 1996)
Inflammation	Inflammatory cell infiltration or expression of markers of inflammation	(Jaeschke *et al.*, 1996; Licht *et al.*, 1999)
Formation of cellular buds, fragments, or blebs	Cell morphology	(Lemasters *et al.*, 1987; Zhang *et al.*, 1999)
Chromatin condensation	DAPI or Hoechst staining	(Lieberthal, Triaca and Levine, 1996)
ATP level	HPLC analysis	(S. Li *et al.*, 2013)
DNA fragmentation	DAPI or Hoechst staining Agarose gel electrophoresis DNA hypoploidy	(Singh, 2000; Cummings and Schnellmann, 2002)
Ca^{2+} gradients	FURA-2	(Lemasters *et al.*, 1999)
Mitochondrial function and integrity	MTT JC-1 tetramethylrhodamine	(Reers *et al.*, 1995; Lemasters *et al.*, 1999; Cummings and Schnellmann, 2002)

To cause oxidative stress and ROS production *in vitro* hydrogen peroxide (H_2O_2) (Nakajima *et al.*, 1999; Peng *et al.*, 2008; Ertaş *et al.*, 2012), high glucose and hypoxia (Tsubokawa *et al.*, 2010; Ishizuka, Hinata and Watanabe, 2011; Castilho *et al.*, 2012; Chang, Hsu and Wu, 2015) or serum deprivation (Peng *et al.*, 2008; Ertaş *et al.*, 2012) have been used. To cause oxidative stress and ROS production *in vivo* the compounds paraquat, diquat, heavy metals, tert-butyl-hydroperoxide, buthionine sulfoximine, ionizing radiation or oxidized dietary lipids have been used as well as knock-down of anti-oxidant gene expression by interference RNA (Koch and Hill, 2017).

Several kits to measure cell survival, apoptosis, necrosis and ROS production are commercially available. Examples of studies using commercially available kits to evaluate MSCs resistance to oxidative stress and induction of resistance by anti-oxidant molecules are described next.

Canine MSCs subjected to the toxin thioacetamide were reported to reduce LDH release, promote survival and decrease ROS (using Cell Rox assay kit) *in vitro* (Quintanilha *et al.*, 2014). Moreover, *in vivo* in a liver injury mice model, canine MSCs were also reported to reduce the total oxidant activity (measured by ELISA) and lipid peroxidation (measured by malondialdehyde assay kit) (Quintanilha *et al.*, 2014).

Rat BM MSCs transiently overexpressing heme oxygenase-1 showed increased resistance to apoptosis and oxidative stress *in vitro* when challenged by H_2O_2 or serum deprivation/hypoxia compared to normal MSCs, which was also observed *in vivo* in a myocardial ischemia model enhancing myocardium regeneration by promoting cell survival and VEGF secretion through a PI 3-kinase/Akt pathway (Tsubokawa *et al.*, 2010). Viability was assessed by MTS assay and apoptosis by Annexin V detection kit for flow cytometry (Tsubokawa *et al.*, 2010).

In another study, rat BM MSCs administered to an *in vivo* animal stroke model resulted in decreased oxidative stress, apoptosis and hippocampal damage, by increasing the expression of the anti-apoptotic Bcl-2 gene and by reducing superoxide and lipid peroxidation (Calió *et al.*, 2014). Cell survival and viability was assessed by MTT assay, the expression of pro-apoptotic Bax and anti-apoptotic Bcl-2 genes was assessed by reverse transcription PCR, superoxide was evaluated by the oxidative fluorescent probe dihydroethidium, lipid peroxidation was detected by thiobarbituric acid-reactive substances assay and apoptosis was evaluated by TUNEL assay (Calió *et al.*, 2014).

Proliferation, migration and angiogenesis

The ability of MSCs and MSC-derived products to promote proliferation, migration and angiogenesis on other cell types such as endothelial cells has been evaluated using angiogenic potency assays *in vitro* and *in vivo*. Different types of *in vitro* and *in vivo* angiogenic assays are summarized in Table 1.9 and respective advantages and disadvantages are described.

In vitro potency assays are typically designed to be fast, quantifiable, reproducible and potentially in a high throughput manner, however, these assays do not mimic neither evaluate all the complexity of physiological conditions in which more than one cell type interact dynamically.

Variability of the potency assays *in vitro* is a consequence but no limited to the specific type of assay used, MSC isolation and culture protocols, passage number, characteristics of donors, quantity of MSCs and MSC-derived products added to the assay and also of the type of endothelial cells used. Endothelial cells have different phenotypes according to the organ of origin, the blood vessel type and will also differ from the cell lines, thus different responses to stimuli might occur and more than one endothelial cell source and angiogenic assay should be performed to minimize the impact of this factor (Staton *et al.*, 2004; Aird, 2012).

Proliferation assays are mainly divided into two types, one type of assay evaluates cell number by direct cell count or indirectly by the metabolic activity (as previously described for oxidative stress) and the other type of assay evaluates cell-cycle kinetics by measuring DNA synthesis using tritiated thymidine or BrdU complemented with cell necrosis analysis using PI (Staton *et al.*, 2004). MSC ability to promote proliferation can be assessed by indirect co-culture or by the addition of MSC-CM and MSC-EVs to the endothelial cell culture medium.

Table 1.9 – Most commonly used *in vitro* and *in vivo* angiogenic potency assays and respective advantages and disadvantages. Adapted from Staton *et al.*, 2004.

Type of assay	Specific assay	Advantages	Disadvantages
Proliferation	MTT	Measures cell number	Cells not necessarily proliferating Does not measure drug toxicity
Proliferation	Tritiated thymidine	Measures DNA replication	Uses radiation Does not measure drug toxicity
Proliferation	BrdU	Measures DNA replication No radiation	Does not measure drug toxicity
Proliferation	Cell-cycle analysis	Measures apoptosis and drug toxicity Measures DNA replication Measures percentage of proliferating cells	Cells have to be in suspension for analysis
Migration	Boyden chamber	Measures migration in response to a gradient Very sensitive to small changes in concentration Automated imaging software can be used for cell counting	Technically difficult to set up Problems in maintaining trans-filter gradients Difficult to obtain accurate cell counts Time consuming to analyze
Migration	Phagokinetic track	Measures total cell movement Measures directional effects of drugs	Low number of cells analyzed Unnatural substrate for cells to migrate on
Migration	Wound healing	Measures endothelial cell migration rate	Quantification is somewhat arbitrary Technical problems in achieving identical conditions of confluence
Differentiation	Matrix assays	Endothelial cells pushed down the differentiation pathway Formation of tube-like structures Quick	Lumen formation is under debate Non-endothelial cells also form tubes Homogeneous pattern of tubule lengths
Differentiation	3D gel	More closely mimics the *in vivo* situation 3D Tubules formation	Long time period Difficult to quantify the 3D structures
Differentiation	Co-culture	Tubules form lumen More heterogeneous pattern of tubule lengths Closer to *in vivo* situation	Long time period Undefined interactions between endothelial and other cell types
Organ Culture	All	Mimic the *in vivo* environment Includes surrounding cells and matrix Endothelial cells are not proliferating at the start of the assay	Difficult to quantify Growth requirements differ between explant and cell outgrowth Time consuming In animal organs, response might be different between species
In vivo	Sponge implant	Inexpensive Technically simple	Non-specific immune responses may lead to an angiogenic response Sponge composition varies, making inter experimental comparisons difficult
In vivo	Matrigel plug	Non-artificial, providing a more natural environment for angiogenesis	Expensive Analysis is time consuming
In vivo	Chick chorioallantoic membrane (CAM) assay	Technically simple Inexpensive Suitable for large-scale screening	Very sensitive to oxygen tension Pre-existing vascular network may difficult visualization of new capillaries Immune response can mask new vasculature
In vivo	Corneal angiogenesis assay	Reliable	Expensive Technically difficult Ethically concerns
In vivo	Dorsal air sac model	Technically simple Natural environment to study blood vessels	Invasive Pre-existing vascular network may difficult visualization of new capillaries
In vivo	Chamber assays	Ability to follow 3D vessel growth over a relatively long period Minimizes number of mice used	Invasive Technically difficult Expensive (in rabbits) Can get surgery associated angiogenesis
In vivo	Tumor models	Ability to follow pharmacokinetics of drug as well as anti-angiogenic effects Long-term studies possible	Tumor environment depends on tumor growth site (orthotopic versus subcutaneous) Real-time studies not possible
In vivo	Angiomouse	Visualization is non-invasive Allows for real-time imaging of angiogenesis	Sensitivity can be limited by quenching of the surrounding tissue, especially skin Hypoxia can decrease green fluorescent protein expression and fluorescence
In vivo	Zebrafish	Relatively fast assay (6–12 h) Fully quantitative Disruption of vasculature does not damage embryo	Does not indicate specifically which step of the angiogenic cascade was disrupted Expensive to maintain in breeding condition Does not distinguish between cytotoxic effects and genuine inhibition

Migration assays, including Boyden chamber, phagokinetic track and wound healing assays, are used to evaluate endothelial cell migration mediated by angiogenic cytokines and chemokines, denominated chemotaxis (Staton *et al.*, 2004). Modified Boyden chamber or transwell migration assay consists of seeding of endothelial cells on top of a filter and the migration of endothelial cells across the filter is evaluated in response to MSC, MSC-CM or MSC-EVs in the bottom chamber (Staton *et al.*, 2004). Cell motility can be evaluated using a phagokinetic track assay using a colloidal gold-plated coverslip or in high throughput manner with a 96 well plate with beads attached to the bottom, in which cell movements, direction and area changes are measured (Staton *et al.*, 2004). Wound healing assay consists of the seeding of endothelial cells and growth until confluence, followed by a scratch to clear part of the cell monolayer and the angiogenic effect of MSC-CM and MSC-EVs are evaluated by the rate of endothelial cell migration to close the scratch (Staton *et al.*, 2004).

Differentiation assays using matrix assays, 3D gels and co-culture systems can also be performed to evaluate capillary-like tube formation. In matrix assays, tissue culture surfaces are coated with fibrin, collagen or Matrigel and the endothelial cells seeded on top of the coating attach, migrate into the coating layer and differentiate to form capillary-like tubes (Staton *et al.*, 2004). The angiogenic potential of MSC-CM and MSC-EV can be assessed by the effect of their addition to the culture medium of endothelial cells in the matrix measuring the improvement of tube formation in terms of the number of tubes and connections and tube length and thickness. Non-endothelial cell types such as MSCs have been proposed to transdifferentiate towards the endothelial lineage and to be able to form capillary-like tubes (Nagaya *et al.*, 2004; Silva *et al.*, 2005; Janeczek Portalska *et al.*, 2012). High throughput systems coupled with automated imaging softwares can be used to screen 96, 384 and 1536 well plates and to determine the number of connections, number of connected and unconnected tubes and tube length and thickness (Staton *et al.*, 2004). In 3D gel systems, endothelial cells are sandwiched between layers of matrix (fibrin clots or Matrigel) and allowed to form a 3D network of tubules over an extended period of time and the vessel density, length and the largest diameter of each vessel-like structure are quantified. In the co-culture systems, endothelial cells are co-cultured with stromal cells as MSCs with or without matrix and allowed to form tube structures, evaluating MSC ability to support and promote angiogenesis, similarly by evaluating the number of tubes and connections and their length and thickness (Staton *et al.*, 2004).

Organ culture assays assess angiogenesis in the whole or partial organ culture, for example, rat aortic ring, chick aortic arch, porcine carotid artery, placental vein disk and fetal mouse bone explant, by explanting the biological material in a matrix to an animal model and evaluating the outgrowth of cells and microvessels over a long period of time (Staton *et al.*, 2004).

Other *in vivo* angiogenic assays include sponge implant, Matrigel plug, CAM assay, corneal angiogenesis assay, chamber assays, tumor models and Angiomouse and Zebrafish animal models (Staton *et al.*, 2004). In the case of sponge implant, a sponge or polymer containing cells or angiogenic factors is implanted *in vivo* and neovascularization of the sponge is evaluated. CAM assay consists of the implantation of the cells or angiogenic factors through a window cut in the eggshell and the number of blood vessels is quantified. In the corneal angiogenesis assay, a pocket is created in the corneal stroma of an animal model, a polymer containing the angiogenic factors is implanted and

the vascularization of the cornea is imaged and quantified. Dorsal air sac model is used to assess the angiogenic response of cancer cells to drugs. In chamber assays, partial skin or skull is removed and a chamber such as rabbit ear chamber, dorsal skinfold chamber and cranial window chamber is placed on the surface and covered by glass, then the gel containing cells or angiogenic factors is added and vascularization is evaluated over time. Tumor models have been implanted *in vivo* and the effect of anti-cancer and anti-angiogenic drugs on vascularization is measured. Angiomouse allows imaging tumor angiogenesis by the detection of green fluorescent protein in tumor cells and metastasis while the new blood vessels formed by angiogenesis are not fluorescent. Zebrafish embryos develop outside the progenitor and are transparent enabling the easy and direct observation of blood vessel formation and development and can be used to test angiogenic inhibitors or enhancers (Staton *et al.*, 2004).

Immunomodulatory potential

The immunomodulatory properties of MSCs and MSC-derived products can also be assessed by *in vitro* and *in vivo* potency assays. *In vitro*, the immunomodulatory properties of MSCs can be evaluated by direct co-culture of MSCs with immune cells in a tissue culture surface of by culturing MSCs as feeder layer prior to co-culture with immune cells or by indirect co-culture using Boyden chambers or transwells and microfluidic devices. *In vitro*, the immunomodulatory properties of MSC-CM and MSC-EVs can also be tested by their addition to the culture medium of immune cells cultured in tissue culture surfaces, transwells or microfluidic devices. *In vivo*, the immunomodulatory potential can be evaluated by the administration of MSCs, MSC-CM and MSC-EVs to animal models of inflammation, for instance, cardiovascular, lung and auto-immune disease models. Typically, immunosuppression ability of MSC and MSC-derived products on whole blood, PBMCs, monocytes, macrophages, dendritic cells, neutrophils, T cells, B cells or NK cells is evaluated by the presence and proliferation of immune cells, secretion of pro- and anti-inflammatory cytokines and chemokines, phenotypic analysis and by the evaluation of specific functions of each immune cell type.

Proliferation of immune cells such as monocytes and T cells can be evaluated by the detection of tritiated thymidine incorporation into the DNA as a measure of DNA replication, however, the use of radiation has safety concerns (Hsu *et al.*, 2015). Alternatively, the fluorescent dye carboxyfluorescein succinimidyl ester does not have safety concerns related to radiation and can be used to evaluate cell proliferation by flow cytometry (Hsu *et al.*, 2015). Moreover, it can be coupled with other antibodies to identify specific cell populations within a mixed culture or to identify phenotypic changes within one immune cell type (Hsu *et al.*, 2015). This fluorescent dye can also be used to determine the number of cell divisions by the decrease in fluorescence with cell replication and for *in vivo* cell tracking up to several months (Quah, Warren and Parish, 2007; Hsu *et al.*, 2015). Based on the reactivity against certain antibodies, magnetic beads can also be used to select specific cell type populations by magnetic-activated cell sorting, for instance, CD4 is often used for T helper lymphocytes and CD14 for monocytes (Hsu *et al.*, 2015). Proliferation can also be evaluated by flow cytometry using the CytoTell green indicator of proliferation which will be diluted over time with cell division (Bertolo *et al.*, 2017). An

alternative to measure cell proliferation is the cell cycle analysis of the immune cells (Corcione *et al.*, 2006).

The secretion of pro- and anti-inflammatory cytokines and chemokines can be performed by ELISA, real time reverse transcription PCR, flow cytometry and global proteomic analysis using mass spectrometry techniques (Hartung and Corsini, 2013; Hsu *et al.*, 2015).

Phenotypic analysis can be performed by staining with antibodies specific to certain surface markers and then analyzed by flow cytometry (Hartung and Corsini, 2013).

PBMCs can be stimulated by IL-2, IL-10, IL-21, CpG2429 and pokeweed mitogen (Bertolo *et al.*, 2017). The immunomodulatory potential of MSCs and MSC-derived products on stimulated and non-stimulated PBMCs can be evaluated by PBMC proliferation, antibody production and cytokine secretion (Bertolo *et al.*, 2017). MSCs were able to suppress PBMC proliferation and modulate PBMCs to reduce TNF-α and IL-10 and increase IL-6, G-CSF and MCP-1 (Bertolo *et al.*, 2017). Proliferation can be assessed as previously described. Moreover, PBMC proliferation can also be assessed by mixed lymphocyte reaction assay which consists of co-culture of labelled PBMCs in tissue culture plates containing HLA-mismatched and irradiated PBMCs and MSCs, followed by evaluation of proliferation and surface marker expression by flow cytometry (Gieseke *et al.*, 2010). Cytokines can be analyzed by ELISA or Bio-Plex Pro Cytokine, Chemokine and Growth Factor Assay (Bertolo *et al.*, 2017). Antibody production is a B cell function and its quantification method will be described next.

Monocytes such as THP-1 cells can be activated by LPS to secrete pro-inflammatory cytokines (as TNF-α and IL-1β) and MSC and MSC-derived products have the ability to modulate monocytic cytokine production by reducing the secretion of pro-inflammatory cytokines measured by ELISA and real time PCR (Shu *et al.*, 2015). Moreover, MSC immunomodulatory effect was mediated by the inhibition of NF-ĸB activation and ERK and JNK phosphorylation (Shu *et al.*, 2015).

Macrophages can be differentiated from monocytes by phorbol-12-myristate-13-acetate (PMA), 1α, 25-dihydroxyvitamin D3 or M-CSF (Chanput, Mes and Wichers, 2014). MSCs were reported to modulate macrophage phagocytic activity, inducing IL-6 and IL-10 anti-inflammatory cytokines and decreasing IL-12 and TNF-α pro-inflammatory cytokines (Kim and Hematti, 2009). An alternative to ELISA which measures released cytokines is the staining of intracellular cytokines, for that after macrophage activation, the cytokine secretion is blocked by Brefeldin A or Monensin, the cells are stained with respective antibodies and measured by flow cytometry. The phagocytic assay consists of measuring macrophage phagocytic activity of labelled *Escherichia coli* bacteria and consequent analysis by flow cytometry (Kim and Hematti, 2009).

Monocytes can be differentiated into dendritic cells by GM-CSF and IL-4 treatment and the immunomodulatory potential of MSCs and MSC-derived products on monocytes-derived dendritic cells can be evaluated by inhibition of differentiation, activation and antigen presentation (Nauta and Fibbe, 2007; Ramasamy *et al.*, 2007; Gao *et al.*, 2016). The suppression of monocyte differentiation to dendritic cells and inhibition of dendritic cell activation and function by MSCs and MSC-derived products can be assessed by surface marker expression and cell cycle analysis (Ramasamy *et al.*, 2007). MSCs, in part by the secretion of IL-6 and M-CSF, were able to modulate monocyte

differentiation to dendritic cells leading to decreased expression of surface markers CD83, CD1a, HLA-DR, the co-stimulatory molecules CD80 and CD86 and the secretion of IL-12, while increasing the expression of the monocytic cell surface marker CD14 (Jiang *et al.*, 2005). MSCs also suppressed dendritic cell function as antigen-presenting cell by shifting dendritic cell phenotype towards monocytes/macrophages, which can be evaluated by the expression of their surface markers and co-stimulatory molecules by flow cytometry and cytokine and chemokine release by ELISA (Jiang *et al.*, 2005). Moreover, MSCs partially reversed differentiation of mature dendritic cells and suppressed endocytosis (Jiang *et al.*, 2005). Endocytosis can be assessed by incubation with fluorescent dyes, as FITC-dextran, and uptake can be quantified by flow cytometry (Jiang *et al.*, 2005). Another functional assay is to evaluate dendritic cell ability for antigen presentation and for induction of T cell activity using a Keyhole-limpet hemocyanin (KLH) assay by loading dendritic cells with KLH and co-culturing them with T cells and evaluating T cell proliferation and the release of pro-inflammatory cytokines IL-12 and IFN-γ and anti-inflammatory cytokine IL-10 (Jiang *et al.*, 2005).

MSCs secrete IL-6, IL-8 and macrophage migration inhibitor factor which recruit neutrophils and prevent neutrophil apoptosis, thus the immunomodulatory properties of MSC and MSC-derived products on neutrophils can be evaluated by chemotaxis, anti-microbial and phagocytic activity, ROS production and prevention of apoptosis (Raffaghello *et al.*, 2008; Brandau *et al.*, 2010, 2014). Neutrophil chemotaxis assay consists of seeding of neutrophils on a transwell insert and neutrophil migration is measured in response to MSCs and MSC-derived products or in alternative by MSC and MSC-derived product pre-conditioning of neutrophils followed by chemotactic stimuli, for instance, with IL-8, C5a or f-MLP (Raffaghello *et al.*, 2008; Brandau *et al.*, 2010, 2014). Activation of polymorphonuclear neutrophil granulocytes by MSC-derived products can be evaluated by the release of the pro-inflammatory cytokines and chemokines such as CCL4 measured by ELISA (Brandau *et al.*, 2010, 2014). Phagocytic activity of neutrophils can be assessed with a phagocytosis assays in which neutrophils are pre-conditioned by MSCs or MSC-derived products, then seeded into a cover slip and phagocytosis of *Escherichia coli* bacteria is visualized using Pappenheim's staining (Brandau *et al.*, 2014) or MSC ability to promote neutrophil phagocytic activity can be determined by the release of superoxide anion when challenged with opsonized Zymosan A from *Saccharomyces cerevisiae* (Raffaghello *et al.*, 2008). Release of ROS during phagocytosis can also be measured by a respiratory burst assay which consists of measuring the oxidation of dihydrorhodamine-123 by flow cytometry after *Escherichia coli* insult of polymorphonuclear neutrophil granulocytes pre-conditioned by MSCs or MSC-derived products (Brandau *et al.*, 2014). MSC ability to prevent neutrophil apoptosis can be assessed by neutrophil pre-conditioning with MSCs or MSC-derived products, followed by staining, for instance with Annexin V and 7-AAD or PI, and quantification of apoptotic and necrotic cells is performed by flow cytometry (Raffaghello *et al.*, 2008; Brandau *et al.*, 2010). The presence of the pro-apoptotic Bax protein and anti-apoptotic MCL-1 protein can also be evaluated by immunocytochemistry and by morphological changes such as cell shrinking, nuclear condensation and fragmentation, plasma membrane ruffling and blebbing, by imaging of cells fixed and stained with May-Grunwald-Giemsa (Raffaghello *et al.*, 2008).

For T cells, the immunosuppressive activity of MSC-derived products is evaluated by the suppression of the proliferation of activated T cells, by the secretion of pro- and anti-inflammatory cytokines (TNF-α, IFN-γ, IDO, HLA-G, LIF, IL-10, TGF-β) and by the expression of surface markers (CD4, CD8, CD25, CD44, CD62L) (Nasef *et al.*, 2007; Yu, 2008; Qu *et al.*, 2012; Hartung and Corsini, 2013). T regulatory cells can also be modulated by MSCs in direct co-culture and that interaction can be evaluated by the expression of cell adhesion molecules (CD274, VCAM-1, galectin-1) by flow cytometry or immunohistochemistry analysis, and by the number of adherent T cells quantified by an adhesion assay (Selmani *et al.*, 2008; Gieseke *et al.*, 2010; Ren *et al.*, 2010; Najar *et al.*, 2012; Gao *et al.*, 2016)

B cells can be stimulated by anti-immunoglobulins, anti-CD40L, CpG 2395, cytokines (IL-4) or KLH and the immunomodulatory potential of MSCs and MSC-derived products on B cells can be evaluated by B cell proliferation, chemokine receptors (CXCR4, CXCR5 and CCR7) by ELISA and antibody production (IgM, IgG and IgA) by ELISA or by enzyme-linked immunospot assay (Corcione *et al.*, 2006; Che *et al.*, 2012; Hartung and Corsini, 2013).

NK cells are typically stimulated by IL-2 or IL-15 and the effect of MSCs and MSC-derived products on the suppression of NK cell proliferation, cytotoxicity and cytokine secretion (IFN-γ, TNF-α) can be assessed (Sotiropoulou, Perez, Gritzapis, *et al.*, 2006; Selmani *et al.*, 2008). Cytotoxicity can be evaluated by NK cell degranulation by measuring the expression of the surface marker CD107b by flow cytometry (Selmani *et al.*, 2008), by sodium chromate assay (Sotiropoulou, Perez, Gritzapis, *et al.*, 2006) or by measuring apoptosis of K562 target cells by co-culture with NK cells pre-cultured with MSCs and MSC-derived products (Krampera *et al.*, 2006).

In vivo immunomodulatory and anti-inflammatory properties of MSCs and MSC-derived products have been tested and many pre-clinical animal models (examples in Table 1.10) showed promising results, which have the advantage of representing the complexity of the interaction between different cell types and tissues under dynamic conditions with appropriate mechanical stimuli, however, mechanisms of action and cellular responses are often different between species.

Table 1.10 – MSC immunomodulatory action ameliorates inflammation in different *in vivo* diseased animal models.

Disease model	Animal model	MSC source	Effect	Reference
MI	Sprague-Dawley	Sprague-Dawley BM MSCs	Anti-inflammatory and cardioprotecive effect of MSCs. Decreased inflammatory cytokines TNF-α, IL-1β and IL-6. Suppression of collagen deposition, MMP-1 and TIMP-1 proteins. Attenuated left ventricle cavitary dilation and transmural infarct thinning. Improved hemodynamic measurements	(Guo *et al.*, 2007)
Asthma	Balb/c mice and C57BL/6 mice	C57BL/6 mice BM MSCs	MSC administration inhibited airways hyper-reactivity and lung inflammation partly by IFN-γ dependent mechanism. MSC induce a Th1 phenotype in CD4 T lymphocytes, inhibiting Th2-mediated allergic airway inflammation	(Goodwin *et al.*, 2011)
Rheumatoid arthritis	DBA/1 mice	Human umbilical cord MSCs	MSCs attenuated the development of collagen-induced arthritis, induced T regulatory cells and a shift in Th1/Th2 phenotype and promoted the secretion of anti-inflammatory cytokines (IL-10, IDO, TGF-β)	(Liu *et al.*, 2010)
GVHD	DBA/2(H-2K^{d}) mice	Human umbilical cord MSCs	MSCs attenuated acute GVHD symptoms and prolonged survival after allogeneic bone marrow transplantation potentially by IDO and TGF-β	(Guo *et al.*, 2011)

Both the *in vitro* potency assays and *in vivo* models used to evaluate several features of MSC regenerative properties (as prevention of apoptosis, enhancement of proliferation, migration and angiogenesis and immunomodulatory function) have limitations and disadvantages. Namely, 2D *in vitro* models often do not evaluate the effect and interaction of different cell types and are not able to mimic tissue-specific functions, thus do not accurately predict the effect of a therapy in the phenotype, metabolism and function of the cells, tissues and organs (Bhatia and Ingber, 2014). 3D *in vitro* models have been under development to allow interaction between cell types and to provide spatial, chemical and mechanical cues, for instance, using hydrogels, synthetic polymers and scaffolds or by self-assembly in spheroids and organoids (Bhatia and Ingber, 2014). These 3D models provide further insight on the effect of a therapy on tissue functions and signaling pathways compared to 2D models, however, spheroids and organoids tend to have variable size and shape, may have limitations on the nutrients and oxygen transport into the core causing necrosis and it is difficult to sample the luminal contents and to harvest the cells from the several cell layers for biochemical and genetic analysis (Bhatia and Ingber, 2014). Microfluidic devices such as organ-on-a-chip overcome some limitations of these 3D models such as the lack of tissue-tissue interfaces, for example the interfaces with vascular endothelium which play an important role in many organs, and the limited mechanical cues provided, for instance, fluid shear stress (typical of the vascular system), tension and compression which affect organ function under physiological and pathological conditions (Ingber, 2003; Mammoto, Mammoto and Ingber, 2013).

Frequently, animal models are used to study the safety and efficacy of therapies and drugs, enabling to study their effect in multiple organs. The drawbacks of using animal models include differences in mechanisms and cellular responses between species, often are not suitable to predict toxicity of drugs and therapies in humans and have ethical concerns related to the sacrifice of the animals. To overcome some of these limitations, human organ-on-a-chip microfluidic devices can be used eliminating the problem of species-related differences by using human cells and by allowing the screening of different conditions, thus enabling to reduce the number of animals sacrificed for research. It is predictable that organ-on-a-chip microfluidic devices will reduce animal testing and will be a required step by the regulatory agencies as improved human organ-on-a-chip microfluidic devices are developed, however, the regulatory agencies will probably still require pre-clinical trials for proof of concept prior to clinical trials in humans.

Organ-on-a-chip microfluidic devices

Organ-on-a-chip microfluidic devices consist of micrometer-sized chambers in which cells are cultured and continuously perfused to model not the whole living organ but the minimal physiological functions of a tissue or organ (Bhatia and Ingber, 2014). It can be as simple as one chamber containing only one cell type continuously perfused (for example, endothelial cells lining in a blood vessel-like structure) or with increased complexity with two or more chambers connected by a porous membrane with different cell types lined in each side of the membrane emulating the interface between tissues (for instance, lung alveoli epithelial-endothelial interface) (Bhatia and Ingber, 2014). Body-on-a-chip could also be mimicked by fluidically linking the main organs-on-a-chip in different

microfluidic devices (Bhatia and Ingber, 2014). Organ-on-a-chip microfluidic devices can integrate mechanical forces including physiological relevant fluid shear stress (as the shear stress in the blood vessels), cyclic strain (as the breathing motion of the lung, peristalsis of the gastrointestinal tract and cardiovascular cycling), tension and compression, which condition the normal cellular responses but also have impact on pathological responses to drugs, toxins, infections or other pathogens (Bhatia and Ingber, 2014). To emulate cyclic mechanical strain to which cells are typically subjected *in vivo*, flexible side chambers in the microfluidic device can be created and the membrane and lateral wall can be rhythmically stretched and relaxed by applying cyclic vacuum suction (Figure 1.9) (Huh *et al.*, 2010, 2012; H. J. Kim *et al.*, 2012; Kim and Ingber, 2013).

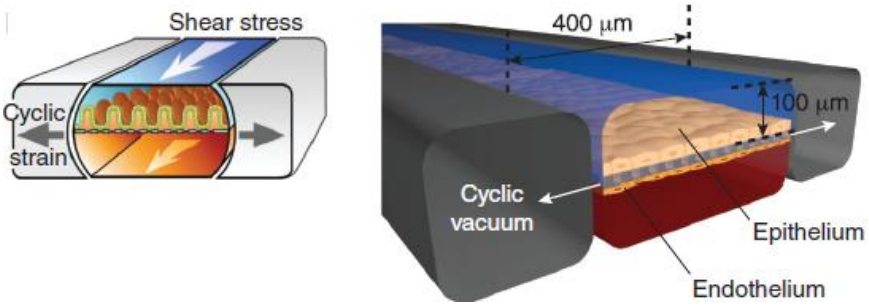

Figure 1.9 – Schematic examples of gut-on-a-chip (image on the left) and lung-on-a-chip (image on the right). In the gut-on-a-chip, human intestinal epithelial cells are cultured on top of a porous poly(dimethylsiloxane) (PDMS) membrane coated with an extracellular matrix and are subjected to fluid shear stress caused by the flow of culture medium and cyclic strain applied to the side chambers to mimic peristalsis and promote the formation of villi-like structures. In the lung alveolus-on-a-chip, human alveolar epithelial cells are cultured on top of a porous PDMS membrane coated with an extracellular matrix and human capillary endothelial cells on the bottom. Endothelial cells are subjected to fluid shear stress and epithelial cells are exposed to air to mimic the air-liquid interface of the alveoli and the breathing motion is mimicked by the rhythmic cyclic strain on the side chambers (Bhatia and Ingber, 2014).

These devices also allow studying the dynamic interaction between cells from different tissues with the immune system and their recruitment under pathological conditions by perfusion of whole blood or selected types of immune cells through the blood-like vessel in the endothelial chamber (Bhatia and Ingber, 2014). Microfluidic devices have also the advantages of enabling to control fluid shear stress, for instance, by adjusting flow rate and channel design (Carraro *et al.*, 2008; Griep *et al.*, 2013) and by controlling cell patterning (Bhatia and Ingber, 2014).

Microfluidic devices are frequently manufactured by soft lithography with biocompatible and flexible materials such as poly(dimethylsiloxane) (PDMS) forming chambers with inlets and outlets from which it is possible to coat with extracellular matrix, to infuse cells that attach to the matrix and to perfuse culture medium (Folch *et al.*, 1999; Kane *et al.*, 1999; Bhatia and Ingber, 2014). PDMS has the advantages of been easy to use, biocompatible, gas permeable and optically clear, allowing real-time high-resolution imaging of the cells to monitor their responses upon stimuli, however, PDMS has the capacity to absorb compounds such as drugs, thus, it should be taken into account when

performing drug studies (Bhatia and Ingber, 2014). Other types of materials such as polyurethanes, silicon, plastic, glass and silk and other manufacturing techniques as micromolding, microetching, laser etching, injection molding, photopolymerization, solid object printing can also be used, however, more research is needed to optimize manufacturing and the properties of the materials used to minimize compound absorption while being biocompatible and allowing extracellular matrix and cell attachment and culture (Bhatia and Ingber, 2014). Similar to bioreactors in which culture conditions can be monitored and controlled, organ-on-a-chip also have the potential to incorporate microsensors to measure tissue barrier integrity (Douville *et al.*, 2010), cell migration (Nguyen *et al.*, 2013), fluid pressure (Liu *et al.*, 2013) and important culture parameters as glucose, lactate, oxygen and pH (Eklund *et al.*, 2009).

Several tissues and organs have been emulated using organ-on-a-chip microfluidic devices such as lung (Huh *et al.*, 2010, 2012; Tavana *et al.*, 2011; Kambez H Benam *et al.*, 2016; Kambez H. Benam *et al.*, 2016), heart (Cheng *et al.*, 2006; Grosberg *et al.*, 2011; Khanal *et al.*, 2011; Agarwal *et al.*, 2013), liver (Kane *et al.*, 2006; Lee, Hung and Lee, 2007; Carraro *et al.*, 2008), kidney (Jang and Suh, 2010; Jang *et al.*, 2013; Musah *et al.*, 2017), intestine (Esch *et al.*, 2012; H. J. Kim *et al.*, 2012; Kim and Ingber, 2013; Jalili-Firoozinezhad *et al.*, 2018), smooth and striated muscle (Grosberg *et al.*, 2012), fat (Viravaidya and Shuler, 2004), bone (Zhang *et al.*, 2011; Park *et al.*, 2012), marrow (Torisawa *et al.*, 2014; W. Zhang *et al.*, 2014), cornea (Puleo *et al.*, 2009), skin (O'Neill, Monteiro-Riviere and Walker, 2008), blood vessels (Shin *et al.*, 2004; van der Meer *et al.*, 2013; Kim *et al.*, 2016), blood-brain barrier (Shayan *et al.*, 2011; Booth and Kim, 2012; Griep *et al.*, 2013) and nerves (Shi *et al.*, 2013; Tsantoulas *et al.*, 2013). These systems can be used to study the development and physiological responses but also acute pathological responses such as inflammation (Huh *et al.*, 2010; Kambez H Benam *et al.*, 2016), edema (Huh *et al.*, 2012), oxidative stress and apoptosis (Jalili-Firoozinezhad *et al.*, 2018) and cancer (Hassell *et al.*, 2017).

There is also increasing interest from the pharmaceutical industry on using organ-on-a-chip microfluidic devices for drug testing to decrease to time and expenses of the drug development process reducing the number of animals sacrificed (Bhatia and Ingber, 2014). Thus, these microfluidic devices being composed of several cell types mimicking organ-level functions and also linking different organs enable assessing adsorption, distribution, metabolism, elimination and toxicity of drugs, chemicals, toxins and therapeutics as well as to perform pharmacokinetic and pharmacodynamics studies and to evaluate doses and efficacy of drugs and therapies (Bhatia and Ingber, 2014). For example, the effect of the toxic silica nanoparticles, bacterial infection and the inflammatory cytokine TNF-α have been shown to cause inflammation and vascular leakage in a human lung alveolus-on-a-chip model and to activate immune response of neutrophils engulfing the pathogen, which recapitulated *in vivo* responses with breathing motions (Huh *et al.*, 2010). The importance of breathing motions was also shown in another study with human lung alveolus-on-a-chip model in which the side effect of the human anti-cancer drug IL-2 was assessed and pulmonary edema was observed similar to what was seen in cancer patients (Huh *et al.*, 2012).

In a rat heart-on-a-chip, the inotropic effects of the beta-adrenergic agonist isoproterenol were tested and similar results were obtained compared to *in vivo* results, additionally the higher throughput

of the system could be coupled with high-resolution imaging of the cellular structures and function, being a useful tool to evaluate the toxicity effect of drugs on diastolic and systolic stresses (Agarwal *et al.*, 2013).

In a human kidney-proximal-tubule-on-a-chip, the anti-cancer drug cisplatin showed toxicity similarly to what happens in cancer patients, however, toxicity was not detectable under static cultures neither in animal models due to specie differences in membrane transporters that mediate drug accumulation and production of ROS (Jang *et al.*, 2013).

Together, these studies indicate that organ-on-a-chip microfluidic devices have the potential to be useful tools for basic research to recapitulate biological processes, decipher mechanisms of action and identify biomarkers as well as for drug and therapy development and to test safety and efficacy, thus, filling the gap between the *in vitro* potency assays and *in vivo* animal models and the human clinical trials (Bhatia and Ingber, 2014).

Besides studying drug toxicity, inflammatory and infectious diseases and cancer, these microfluidic devices also have the potential to be used for personalized medicine using patient-derived cells for the screening of therapies and dosing studies towards tailored and improved therapies (Konar *et al.*, 2016).

Cell lines, primary cells and differentiated cells derived from induced pluripotent stem cells can be used in microfluidic devices. It has been shown that endothelial cells from different organ and vessel types are phenotypically and functionally different which is also valid for other cell types, thus, although more challenging it is preferable to use organ-specific and primary cells rather than cell lines (Bhatia and Ingber, 2014; Jain *et al.*, 2018). The microfluidic devices can be used to study the interaction of different organs with circulating cells such as immune cells by flowing whole blood or a purified immune cell type, tumor cells or bacteria (Bhatia and Ingber, 2014; Jain *et al.*, 2018).

The use of organ-on-a-chip devices is coupled to the development of tools to monitor and analyze cellular responses and functions such as fluorescence confocal microscopy, microfluorimetry, transmonolayer electrical resistance measurements, macromolecular transport of fluorescent dyes, multiple electrode arrays and nanoscale sensors as well as multiplexed microscopes and robotic systems to enable scale-up, commercialization and its use by pharmaceutic companies (Bhatia and Ingber, 2014).

Although organ-on-a-chip devices are promising tools, they are still under development and have limitations. Namely, lower cell number for certain analytical assays as mass spectrometry, cannot mimic macroscale architecture and cannot mimic the whole organ and organ functions, bubbles may injure cells, extracellular matrix does not fully mimic *in vivo* composition and degrades and contracts with long culture period, difficulty in defining a culture medium that supports growth but does not promote overgrowth and that is compatible with different cell types, variability between microfluidic devices, risk of contamination, lack of knowledge on how to fully control cell and matrix interactions and tissue functions and the need of engineering capabilities and expertise or the development of automated control systems.

Organ-on-a-chip microfluidic devices emulating pathological conditions can be used to evaluate the regenerative potential MSCs such as the ability of MSCs and derived products to

promote survival, resistance to oxidative stress, reduction of inflammation and edema, for instance, by evaluating cell death and ROS production by flow cytometry or immunohistochemistry and LDH release sampling the outlet fluid of the device, by evaluating the expression of endothelial cell surface markers typically up-regulated during inflammation such as VCAM-1 and ICAM-1 by flow cytometry or immunohistochemistry, by the release of pro- and anti-inflammatory cytokines sampling the outlet fluid of the device which can be measured by ELISA and by assessing barrier integrity or vascular permeability measuring the transmonolayer electrical resistance or the macromolecular transport of fluorescent dyes. Therefore, these devices are useful tools to complement the *in vitro* 2D potency assays while reducing the number of animal models used for research.

1.6 Objectives of the project and thesis layout

The objectives of this PhD thesis include the isolation and production of MSCs and MSC-derived products (CM and EVs), the evaluation of the regenerative potential of three MSC sources, namely BM, AT and UCM, and the development of a robust platform for the characterization of MSCs and MSC-derived products by developing *in vitro* potency assays and 3D inflammation models (transwell and microfluidic device) to evaluate MSC regenerative properties.

Regarding the layout of the thesis, it is divided in two main parts. Part A comprises MSC isolation from BM, AT and UCM cell sources and their characterization following established guidelines in the field as well as the optimization of *in vitro* potency assays to evaluate MSC and MSC-CM regenerative properties (angiogenesis, proliferation, migration, resistance to oxidative stress, supportive function). Part B comprises the establishment of a platform for MSC-EV production and isolation and the development of *in vitro* potency assays to evaluate MSC, MSC-CM and MSC-EV immunomodulatory properties, including the optimization of an endothelial and monocytic 2D potency assays to evaluate MSC-EV immunomodulatory potential and development of lung alveolus inflammation models on transwell and organ-on-a-chip microfluidic device to assess the potency of MSC and MSC-derived products. Each part is divided into the chapters material and methods, results and discussion, conclusions and future work. Part A and B are followed by general conclusions and considerations.

Moreover, Part A of this work was performed at SCERG, iBB from Instituto Superior Técnico, Universidade de Lisboa, in Portugal, under the supervision of Professor Cláudia Lobato da Silva, PhD Ana Fernandes-Platzgummer and also by MD António Fiarresga from Hospital Santa Marta, and Part B was performed at Karp laboratory, Brigham and Women's Hospital under the supervision of Professor Jeffrey Karp and at Wyss Institute for biologically inspired engineering, Harvard University under the supervision of Professor Donald Ingber and PhD Oren Levy both in Boston, USA.

Part A

2 Materials and Methods

2.1 Materials

Cell handling was performed using aseptic conditions and sterile materials.

BM aspirates were obtained from healthy donors and provided by Instituto Português de Oncologia Francisco Gentil. AT aspirates were obtained from donors subjected to lipoaspiration and were provided by Clínica de Todos os Santos. UCM was provided by Hospital São Francisco Xavier. All samples were provided upon informed consent and in accordance with the Declaration of Helsinki. When appropriate donor information regarding age and sex was asked (Table 2.1). MSCs were isolated from each source and cryopreserved in the liquid nitrogen tank until further use.

Table 2.1 – MSC donor information regarding cell source (BM-bone marrow, AT-adipose tissue, UCM-umbilical cord matrix), year of sample collection, and donor age and gender. N.a. stands for not available.

Cell source	Donor	Year of harvesting	Donor age	Donor gender
BM	M67A07	2007	40	Male
BM	M72A07	2007	35	Male
BM	M79A15	2015	36	Male
BM	M83A15	2015	32	Male
AT	L090403	2009	n.a.	n.a.
AT	L090602	2009	n.a.	n.a.
AT	L090724	2009	n.a.	n.a.
UCM	2	2010	-	-
UCM	38	2014	-	-
UCM	78	2015	-	-

MSCs were cultured in medium containing FBS. The culture medium containing FBS was composed 9 g Dulbecco's modified Eagle's medium (DMEM) low glucose (Thermo Fisher Scientific), 3.33 g sodium bicarbonate (Sigma-Aldrich), 10% FBS MSC grade (Thermo Fisher Scientific) and 1% antibiotic-antimycotic 100X (Thermo Fisher Scientific) in MiliQ water up to 1 l. Medium was filtered using a 0.22 µm vacuum filter unit (Merck Milipore) and stored at 4ºC.

HUVEC were purchased from BD Biosciences and expanded in EGM-2 MV culture medium composed of EBM-2 basal medium (Lonza) and full EGM-2 MV SingleQuot kit supplement & growth factors (Lonza) including FBS at a final concentration of 5%. Culture media was filtered with 0.22 µm vacuum filter unit and stored at 4ºC.

Mouse connective tissue fibroblast L929 cell line were acquired from DSMZ, Germany, and expanded in the same medium used for MSC (DMEM low glucose with 10% FBS and 1% antibiotic-antimycotic 100X).

2.1.1 MSC culture

Cells were partially thawed inside the cryovials (Thermo Fisher Scientific) in a 37°C water bath and transferred to a falcon tube (Corning) containing pre-warmed culture medium. Cells were centrifuged at 349 RCF for 7 min (ScanSpeed 1580 MGR Centrifuge) and resuspended in pre-warmed cultured medium. Cell number and viability were assessed with the dye trypan blue 0.1% (Thermo Fisher Scientific) and a haemocytometer.

Cell suspension was further diluted according to viability and desired cell seeding density (about 3 x 10^3 cell/cm^2) and incubated in a humidified atmosphere at 37°C and 5% CO_2. Medium change was performed every 3 to 4 days.

Cell passaging was performed when cells reached about 70-80% confluency. Cells were washed with PBS and detached by incubation with 0.05% trypsin-ethylenediamine tetraacetic acid (EDTA) (Thermo Fisher Scientific) or accutase (Sigma-Aldrich) for a maximum of 7 min. The detachment agents were quenched by adding culture medium in 2x the volume of detachment agent in the case of trypsin or 1x in the case of accutase. Cells were centrifuged at 349 RCF for 7 min and resuspended in pre-warmed medium. After cell counting, cells were re-seeded at the desired cell seeding density and incubated at 37°C and 5% CO_2.

Proliferation potential was evaluated by cell counting using 0.1% trypan blue and a haemocytometer enabling to calculate cellular fold increase, population doubling and cumulative population doubling. Fold increase is the ratio between the number of viable cells at the end of a passage *i* and number of viable cells at seeding of passage *i* (Equation 1). Population doubling is ratio between the logarithm base 10 of the fold increase of passage *i* and the logarithm base 10 of 2 (Equation 2). Cumulative population doubling is the sum of the *n* population doublings of each consecutive passage *i* (Equation 3).

$$Fold\ increase_{at\ passage\ i} = \frac{Number\ of\ viable\ cells\ at\ the\ end\ of\ passage\ i}{Number\ of\ viable\ cells\ at\ seeding\ of\ passage\ i}$$

Equation 1 – Fold increase at a giving passage *i*.

$$Population\ doubling_{at\ passage\ i} = \frac{log_{10}(Fold\ increase_{at\ passage\ i})}{log_{10}(2)}$$

Equation 2 – Population doubling at cell passage *i*.

$$Cumulative\ population\ doubling = \sum_{i=1}^{n} Population\ doubling_{at\ passage\ i}$$

Equation 3 – Cumulative population doubling is the sum of *n* population doublings of consecutive passages *i*.

For freezing, cells were centrifuged and resuspended in the appropriate volume of freezing media on ice. The freezing medium was composed of 90% FBS or culture medium and 10% dimethyl sulfoxide (DMSO, Sigma-Aldrich). Cryovials were stored in freezing containers at -80°C freezer overnight to avoid crystal formation by freezing at a rate of 1ºC per minute and then transferred to the liquid nitrogen tank.

2.1.2 MSC isolation from bone marrow

BM mononuclear cells were isolated by plastic adherence after a ficoll density gradient. BM aspirates were dil 1:2 in PBS with 2 mM EDTA (Thermo Fisher Scientific) and solution was added to the top of a Ficoll-paque premium (GE Healthcare) layer. Samples were centrifuged at 503 RCF for 30 min with slow break. The buffy coat containing the mononucleated cells was collected, diluted in PBS with 2 mM EDTA and centrifuged at 685 RCF for 10 min. The supernatant was discarded, the cells were resuspended in DMEM containing 1% antibiotic-antimycotic 100X and the cell number was quantified using Turk's solution (Merck Milipore) and a haemocytometer. MSC isolation was then performed by plastic adherence and mononucleated cells were plated at 200,000 cell/cm^2 in culture medium containing serum.

2.1.3 MSC isolation from umbilical cord matrix

Umbilical cord units were washed with PBS with 1% antibiotic-antimycotic 100X and then cut into smaller pieces. Each umbilical cord unit contains two arteries and one vein, which were discarded to avoid contamination with other cell types such as endothelial cells, and the tissue surrounding them was collected and minced.

The enzymatic digestion method comprised the incubation of minced umbilical cord tissue with 0.1% collagenase type II (Sigma-Aldrich) in DMEM containing 1% antibiotic-antimycotic 100X at 37ºC for 4 h with agitation using a Thermomixer comfort (Eppendorf AG). The solution was filtered with Steriflip-GP 0.22 µm (Merck Milipore) and centrifuged at 503 RCF for 10 min. The supernatant was discarded, the pellet resuspended in DMEM containing 1% antibiotic-antimycotic 100X and centrifuged again at 349 RCF for 7 min. The pellet was resuspended in culture medium and the cell number determined using Turk's solution and a haemocytometer. MSC were isolated by plastic adherence plating the mononucleated cells at 10,000 cell/cm^2 and incubating at 37°C and 5% CO_2 or immediately frozen.

2.1.4 MSC isolation from adipose tissue

AT aspirate was mixed 1:1 with PBS containing 1% antibiotic-antimycotic 100X. After mixing, the solution was allowed to sit and separate in two phases according to density. The aqueous infranatant was discarded and the washing was repeated two or three times. The AT aspirate was then digested with 0.1% collagenase type II at 37ºC for 30 min with agitation (500 rpm) using a

Thermomixer. The solution was filtered with 0.22 µm filters and centrifuged at 349 RCF for 7 min. The supernatant was removed and the cell pellet resuspended in FBS containing medium. The cell number was determined using Turk's solution and a haemocytometer. The mononucleated cells were plated at high density and incubated at 37ºC and 5% CO_2 or immediately frozen.

2.1.5 MSC characterization by flow cytometry and differentiation potential

To assess identity and purity of isolation methods, after expansion as a plastic adherent culture, MSCs were characterized by flow cytometry and differentiation potential.

Flow cytometry was used to evaluate the expression of the surface markers CD14 (PE anti-human IgG1, clone HCD14), CD19 (FITC anti-human IgG1, clone HIB19), CD31 (PE anti-human IgG1, clone WM59), CD34 (FITC anti-human IgG1, clone 581), CD45 (FITC anti-human IgG1, clone HI30), CD73 (PE anti-human IgG1, clone AD2), CD80 (PE anti-human IgG1, clone 2D10), CD90 (FITC anti-human IgG1, clone 5E10), CD105 (PE anti-human IgG1, clone SN6) and HLA-DR (PE anti-human IgG2a, clone L243). IgG1 κ PE/ IgG1 κ FITC and IgG2a κ PE were used as isotype controls. All antibodies for flow cytometry were acquired from Biolegend with exception of IgG1 κ PE/ IgG1 κ FITC that was purchased from BD Biosciences and CD105 that was acquired from Invitrogen.

Per antibody reaction about 30-100 x 10^3 cell was used. The cells were centrifuged at 349 RCF for 7 min. The cell pellet was resuspended in PBS and incubated for 15 min at room temperature with antibodies dil 1:20, light protected. After incubation, PBS was added and cell suspension was centrifuged at 224 RCF for 5 min. The supernatant was discarded and the cells were resuspended in 1% paraformaldehyde (PFA, Sigma-Aldrich). The cells were stored at 4ºC, light protected, up to one week. The samples were analyzed in the flow cytometer FACSCalibur with CellQuest software from Becton Dickinson. Data analysis was performed with FlowJo software, version 10.

To evaluate the differentiation potential of MSCs, the cells were plated in a 24 well plate (WP, Corning) at 6-20 x10^3 cell/cm^2 and allow to grow until confluence before addition of adipogenic and osteogenic differentiation media. For chondrogenic differentiation, the cells were centrifuged and cell pellets were plated in 24 well ultra-low attachment plates (Corning). The cell pellets were allowed to dry at 37ºC and 5% CO_2 for up to 1 h and then chondrogenic differentiation medium was added. Adipogenic differentiation medium was composed of 10% adipogenesis supplement (Thermo Fisher Scientific) and 1% antibiotic-antimycotic 100X in StemPro adipogenesis differentiation basal medium (Thermo Fisher Scientific). Osteogenic differentiation medium was composed of 10% osteogenesis supplement (Thermo Fisher Scientific) and 1% antibiotic-antimycotic 100X in StemPro osteo/chondrogenesis differentiation basal medium (Thermo Fisher Scientific). Chondrogenic differentiation medium was composed of 10% chondrogenesis supplement (Thermo Fisher Scientific) and 1% antibiotic-antimycotic 100X in StemPro osteo/chondrogenesis differentiation basal medium. Differentiation lasted for 14 days with media changes 3X per week. After 14 days, cells were washed with PBS, fixed with 4% PFA incubated for 20 min and washed again before staining. Adipogenesis staining was performed by incubating cells with 0.3% oil-red-o (Sigma-Aldrich) in 60% isopropanol (Sigma-Aldrich) for 1 h. Osteogenesis staining was performed by incubating with 0.1 mg/ml naphthol AS-MX phosphate (Sigma-Aldrich) and 0.6 mg/ml red violet LB salt (Sigma-Aldrich) for 40 min.

Chondrogenesis staining was performed by incubating cells with 1% w/v alcian blue (Sigma-Aldrich) in 0.1 N hydrochloric acid (Sigma-Aldrich) for 30 min. After staining, a washing with distilled water was performed. For adipogenic and chondrogenic differentiation, PBS was added and cells were imaged. For osteogenic differentiation, cells were incubated with 2.5% w/v silver nitrate solution (Sigma-Aldrich) for 30 min, washed with distilled water and then PBS was added for imaging. Imaging was performed using Leica DMI3000 B fluorescent microscope and the software Nikon ACT-1 2.70.

2.1.6 HUVEC culture

Cells were partially thawed inside the cryovials in a 37°C water bath and transferred to a falcon tube containing pre-warmed culture medium. Cells were centrifuged at 349 RCF for 7 min and resuspended in pre-warmed EGM-2 MV medium. Cell number and viability were assessed with 0.1% trypan blue dye and a haemocytometer.

Cell suspension was further diluted according to viability and desired cell seeding density (about 5,000 cell/cm^2) and incubated in a humidified atmosphere at 37°C and 5% CO_2.

Medium change was performed every 3 days. HUVEC were passaged when reaching about 90% confluency by aspirating medium, washing with PBS and detaching cells by incubation with 0.05% trypsin-EDTA or accutase for 7 min at 37°C and 5% CO_2. Cell suspension was centrifuged, resuspended in culture medium, cell number was determined and cells were re-plated.

For freezing, HUVEC were resuspended in freezing solution composed of 10% DMSO in culture medium. The cryovials were stored in freezing containers at -80ºC overnight and then transferred to liquid nitrogen tanks.

2.1.7 Fibroblast L929 culture

Cells were partially thawed inside the cryovials in the 37°C water bath and transferred to a falcon tube containing pre-warmed culture medium. Cells were centrifuged at 349 RCF for 7 min and resuspended in pre-warmed cultured medium. Cell number and viability were assessed with the 0.1% trypan blue dye and a haemocytometer. Cell suspension was further diluted according to viability and desired cell seeding density (about 1-3 x 10^3 cell/cm^2) and incubated in a humidified atmosphere at 37°C and 5% CO_2.

Medium change was performed every 3 to 4 days. Cell passaging was performed when cells reached about 80-90% confluency. Cells were washed with PBS and detached by incubation with 0.05% trypsin-EDTA. The detachment agent was quenched by adding culture medium in 2x the volume of detachment agent. Cells were centrifuged at 349 RCF for 7 min and resuspended in pre-warmed medium. After cell counting, cells were re-seeded at the desired cell seeding density and incubated at 37°C and 5% CO_2.

For freezing, cells were resuspended in the appropriate volume of freezing media. The freezing medium was composed of 90% culture medium and 10% DMSO. Cryovials were stored in freezing containers at -80°C freezer overnight and then transferred to the liquid nitrogen tank.

2.1.8 Oxidative stress

To evaluate the ability of MSCs to resist to oxidative stress, MSCs were challenged with H_2O_2. To develop a robust potency assay to assess the resistance to oxidative stress, the influence of several factors such as cell density, H_2O_2 incubation time, H_2O_2 concentration and number of moles, cell confluence and cell passage were explored.

Design of Experiments as well as ANOVA and Fisher's statistical analysis was performed using the software Statistica, version 10, StatSoft.

Cells at different cell seeding densities were plated and incubated at 37ºC and 5% CO_2 on 12 WP (Corning) or maintained in suspension using 24 well ultra-low attachment plates for different periods of time. Extra wells were included to be used as unstained and stained untreated controls for flow cytometry. H_2O_2 (Sigma-Aldrich) was diluted in PBS and on the day of the assay further diluted in MSC culture medium containing FBS and cells were challenged with H_2O_2 at several concentrations and incubation time.

The effect of H_2O_2 was evaluated with two methods, metabolic activity by alamar blue (Invitrogen) and cellular apoptosis and necrosis by FITC Annexin V apoptosis detection kit (BD Biosciences). For the metabolic activity protocol, alamar blue was diluted 1:10 in MSC culture medium containing FBS and incubated for 3 h. After incubation, the supernatant was transferred to a 96 black WP (Corning) in triplicates and the fluorescence was measured at 560 nm excitation and 590 nm emission wavelength using the fluorescent plate reader TECAN infinite M200Pro.

For apoptosis and necrosis assessment, the cells were washed with PBS and incubated with accutase solution for 7 min at 37ºC. The detachment agent was quenched with culture medium and cell suspension was collected to FACS tubes. Cell number was estimated and cells were centrifuged at 349 RCF for 7 min and the cell pellets (10^4 -10^5 cell) were stained with FITC Annexin V according to manufacturer's guidelines. Briefly, the cell pellets were resuspended in 1X binding buffer, then FITC Annexin V dil 1:40 and PI dil 1:20 were added and incubated for 15 min, light protected. Untreated control unstained was incubated with 1X binding buffer only. After incubation, 1X binding buffer was added and samples were immediately analyzed by flow cytometry.

2.1.9 Angiogenic assays

Tube formation, incorporation and remodeling assays were developed to test MSC angiogenic potential.

For the tube formation assay, Matrigel matrix basement membrane (Corning) was thawed overnight at 4ºC on ice and 96 black WP with clear bottom (BD Biosciences) and pipette tips were pre-cooled. The wells of the 96 black WP with clear bottom were coated with Matrigel (10 mg/ml) and incubated for 1 h at 37ºC and 5% CO_2. Cell seeding density and incubation time of HUVEC (at passage 11 or less) and MSCs (at passage 8 or less) were under optimization. After tube formation, the cells were imaged by contrast phase microscopy or stained with calcein AM fluorescent dye (BD Biosciences) dil 1:62.5 in PBS for 30 min at 37ºC and 5% CO_2, washed and imaged using the fluorescent microscope.

For the tube incorporation assay, MSCs were seeded at a ratio of 1:4 to HUVEC on Matrigel coated 96 WP and incubated at 37ºC and 5% CO_2 for 8 h before imaging.

For tube remodeling, HUVEC were seeded on Matrigel coated plates and allowed to form tubes using the tube formation protocol described. Disruption of tubes was performed with DMSO testing different concentrations and incubation time and by mechanical scratch.

2.1.10 Wound healing assay by mechanical scratch

The paracrine action of MSC-CM on HUVEC was assessed by the migration rate of HUVEC on a wound assay upon mechanical scratch.

MSC-CM from passage 3 and 4 cells at 80% confluence was collected and centrifuged at 503 RCF for 10 min. The supernatant was collected, filtered with 0.22 µm filter low protein binding (Merck Milipore) and stored at -80ºC until further use.

HUVEC were seeded at about 125,000 cell/cm^2 in 96 WP to obtain a confluent monolayer after overnight incubation at 37ºC and 5% CO_2. A scratch was made using a pipette tip vertically to the cell culture surface in a single movement across the well. Only wounds with width in the range of 120 to 280 µm were used to test the effect of MSC-CM for consistent results as cell migration rate will be affected by the width of the scratch. Dead cells were removed with 2 washes with EGM-2 MV and then MSC-CM was added and incubated at 37ºC and 5% CO_2 until wound closer. EGM-2 MV or MSC culture medium containing serum were used as controls. Wound remodeling was imaged every hour and cell migration rate was determined after 75-200 measurements of the scratch width per condition per time point using the software ImageJ, version 1.51u.

2.1.11 Statistical analysis

Statistical analysis was performed by One-way or Two-way ANOVA using Tukey correction for multiple comparisons as indicated in the legend of each figure. A P value lower than 0.05 was considered statistically significant, which upon correcting for multiple comparisons is denoted as *GP=0.0332, **GP=0.0021, ***GP=0.0002, ****GP<0.0001. For the statistical analysis the software GraphPad Prism 7, version 7.03 from GraphPad Software was used.

3 Results and Discussion

In this chapter, it will be described the MSC characterization results in terms of morphology, immunophenotype, differentiation potential as well as MSC proliferation potential. It will also be described the development of potency assays to evaluate MSC and MSC-CM regenerative potential, namely angiogenic, wound healing and oxidative stress assays.

3.1.1 MSC characterization

MSCs are characterized by their plastic adherence, surface marker expression and differentiation potential according to The International Society for Cellular Therapy (Dominici *et al.*, 2006).

MSCs isolated from different cell sources, namely BM (Figure 3.1 A), AT (Figure 3.1 B) and UCM (Figure 3.1 C), cultured under standard 2D culture flasks using medium containing serum (FBS) have similar morphology. MSCs have a spindle-shaped, triangular shaped and fibroblastic like morphology, according to what is expected for MSCs (Liu *et al.*, 2016).

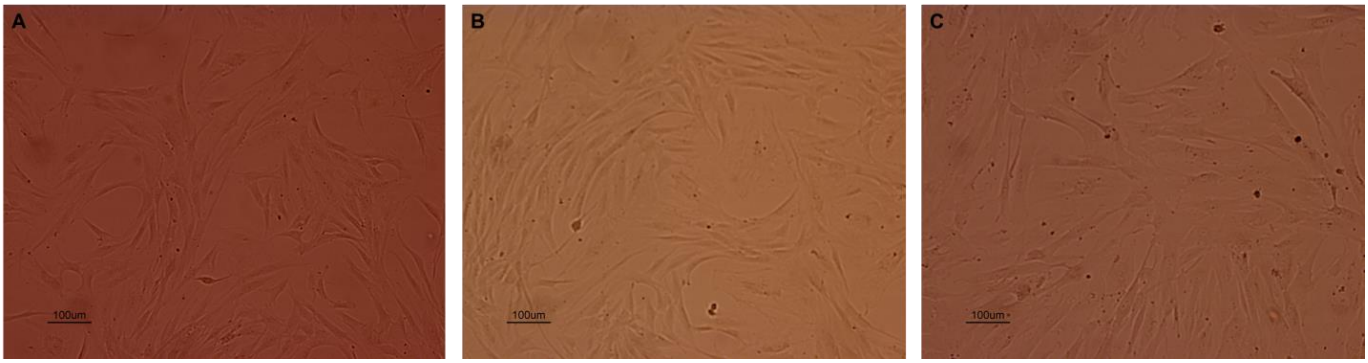

Figure 3.1 – MSCs from different cell sources cultured in 2D standard culture flasks with culture medium containing serum had similar spindle-shaped and fibroblastic like morphology. Representative images of MSCs from bone marrow (A), adipose tissue (B) and umbilical cord matrix (C) obtained by contrast phase microscopy. Scale bar 100 µm.

Three MSC donors per cell source (BM, AT and UCM) were selected and immunophenotypically characterized by flow cytometry. MSCs are characterized by high expression (≥95%) of CD73, CD90 and CD105 and by lack of expression (≤2%) of CD14, CD19, CD34, CD45, HLA-DR, according to The International Society for Cellular Therapy (Dominici *et al.*, 2006). Additionally to the markers defined by The International Society for Cellular Therapy, CD31 (endothelial cell marker (Pountos *et al.*, 2007)) and CD80 (T cell marker (Vasilevko *et al.*, 2002)) were also evaluated and are expected to be negative (≤2%) for MSCs. The expression of the surface markers from the different donors selected was in line with that expected for MSCs, negative expression for the hematopoietic lineage markers CD14, CD19, CD34, CD45, CD80 and HLA-DR and endothelial lineage marker CD31 and highly positive for CD73, CD90 and CD105 with exception of UCM donor 2 that had 91% of positive cells and UCM donor 78 with only 57% of positive cells for the

surface marker CD105 (Table 3.1). All MSC donors were at passage 4 with exception of BM M79A15 that was at passage 5.

CD105 or endoglin is a membrane glycoprotein and a receptor integrating the TGF-β receptor complex. CD105 is potentially involved in osteogenic and chondrogenic differentiation through TGF-β signaling (Barry *et al.*, 1999; Jin *et al.*, 2009) and is also involved in migration, angiogenesis and vascular remodeling (Conley *et al.*, 2004; Mark *et al.*, 2013). In another work the accentuated decrease in CD105 in UCB MSC was hypothesized to be related to differentiation towards an adipogenic phenotype (Jin *et al.*, 2009). It was also reported that CD105 expression might be affected by culture conditions such as culture medium and hypoxia (Mark *et al.*, 2013) as well as the enzymatic agents and respective incubation time (Tsuji *et al.*, 2017). Synovial MSCs were incubated for 5, 30 and 60 min with different detachment agents and longer incubation time with trypsin greatly reduced CD105 expression while CD73 and CD90 expression were maintained (Tsuji *et al.*, 2017). Similarly, longer incubation time with the detachment agent also reduces CD105 expression in HUVEC (Brown *et al.*, 2007). Therefore, it is hypothesized that the decrease in CD105 expression observed for UCM MSCs might be due to trypsin exposure (as there seems to be no increase in adipogenic differentiation for UCM MSCs compared to other cell sources Figure 3.2 and expression increased when lower incubation time with trypsin was used later, data not shown for other passages).

Table 3.1 – MSCs from different donors and cell sources showed the typical immunophenotype expected for MSCs. Passage 4 and 5 MSCs from three donors per cell source BM (bone marrow), AT (adipose tissue) and UCM (umbilical cord matrix) were cultured in 2D standard culture flasks using serum containing medium, detached, stained with antibodies and the cell population positive for the different surface markers (in %) was measured by flow cytometry. N = 1. Green shading indicates compliance with reference, while yellow indicates deviation from the reference.

% Of positive cell population	Reference value	BM			AT			UCM		
		M72A07	M79A15	M83A15	L090403	L090602	L090724	2	38	78
CD14	≤2%	1.7	0	0	0	0	0	0.1	0.7	0
CD19	≤2%	0.3	0	0	0	0	0	0	0	0
CD31	≤2%	1	0	0.1	0	0	0	0	0	0
CD34	≤2%	0.3	0	0	1.7	1.2	0	0	0	0
CD45	≤2%	0.6	0	0	0	0	0	0	0	0
CD80	≤2%	0.2	0	0	0	0.1	0	0	0	0
HLA-DR	≤2%	0	0	0	0	0	0	0	0	0
CD73	≥95%	99.1	98.2	99.0	98.9	99.5	97.1	98.5	98	99.2
CD90	≥95%	98.7	98.6	95.7	99.0	98.1	97.0	98.1	97.9	97.4
CD105	≥95%	99.1	98.6	99.2	99.2	99.0	97.3	91.2	96	56.9

All MSC donors from BM (M72A07, M79A15, M83A15), AT (L090403, L090602, L090724) and UCM (2, 38, 78) retained their multilineage differentiation potential, being able to undergo adipogenic, osteogenic and chondrogenic differentiation although to a still immature state. Representative images of one MSC donor for each cell source showed: 1) visible lipid vacuoles in the cell cytoplasm stained by oil-red-o indicative of adipogenic differentiation, which were more mature for BM and AT (Figure 3.2 A and D, respectively) compared to the smaller and less frequent lipid vacuoles for UCM MSCs (Figure 3.2 G), which is in line with published work (Karahuseyinoglu *et al.*, 2007); 2) alcian blue staining of proteoglycans in the extracellular matrix of cell aggregates representative of chondrogenic differentiation (Figure 3.2 B, E, H); 3) the presence of calcium deposits and ALP activity demonstrating osteogenic differentiation (Figure 3.2 C, F, I).

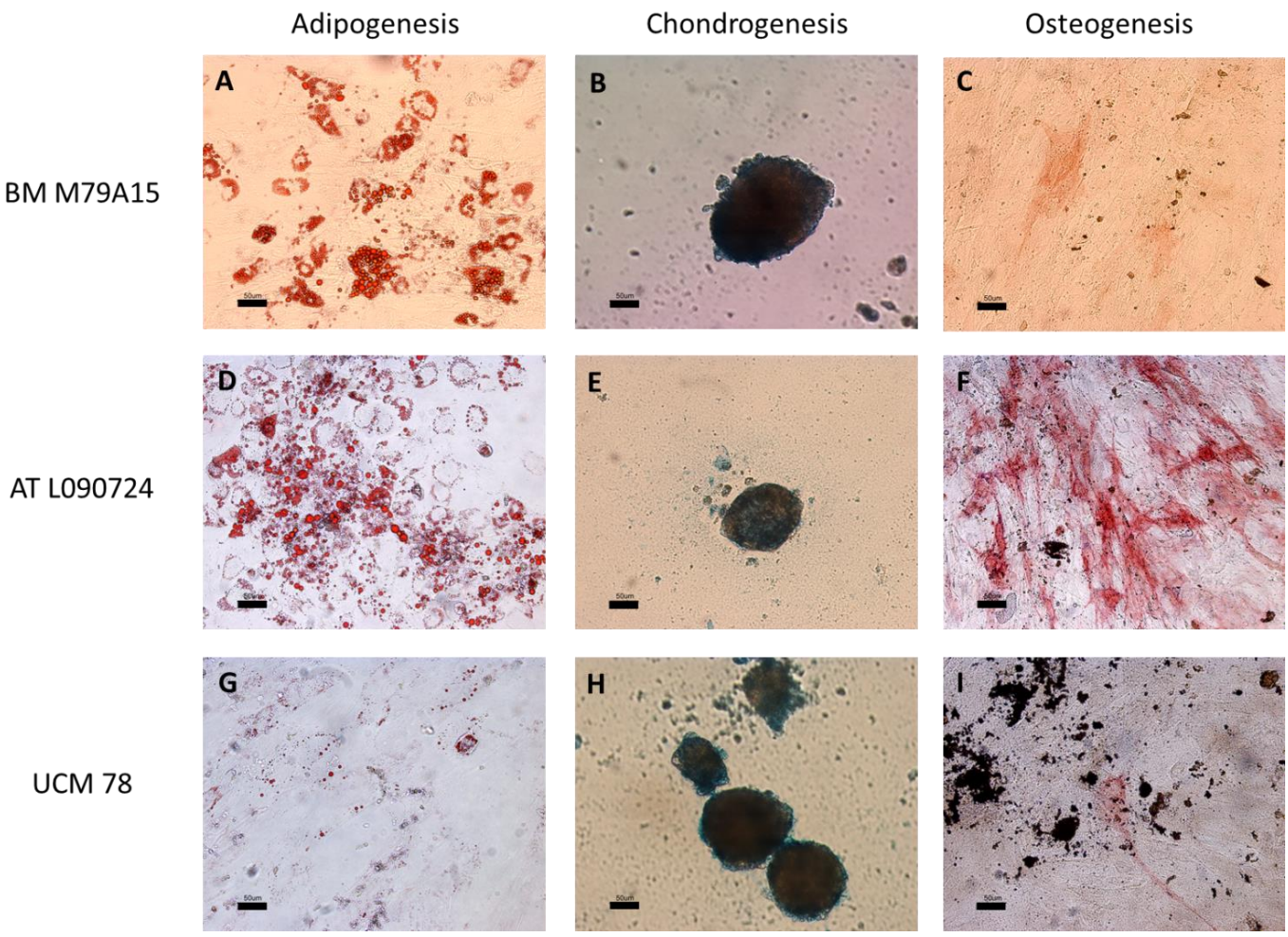

Figure 3.2 – MSC donors from different cell sources exhibited multilineage differentiation potential, being able to differentiate into immature adipocytes (A, D, G), chondroblasts (B, E, H) and osteoblasts (C, F, I) after 14 days of differentiation. MSC donors from BM (bone marrow), AT (adipose tissue) and UCM (umbilical cord matrix) were at passage number 4 to 6. Scale bar 50 µm.

The proliferative potential of all donors of each MSC source was also evaluated by cell counting at each cell passage considering cells from passage 2 to 9 grown in 2D standard culture

flasks in medium containing FBS. The fold increase, population doubling and cumulative population doubling were calculated based on Equation 1, Equation 2 and Equation 3, respectively. AT and UCM MSCs seem to have higher proliferation and to reach higher cumulative population doubling than BM MSCs (Figure 3.3 A and B) for the set of donors tested. The cumulative population doubling rate was 1.6 for BM MSCs, 2.2 for UCM MSCs while for AT MSCs it was 2.4.

Conflicting results have been published on the classification of the most proliferative MSC cell source, which is a consequence of donor dependent differences as age, technique dependent differences as isolation process and also a consequence of comparing cell sources using MSCs isolated from different donors.

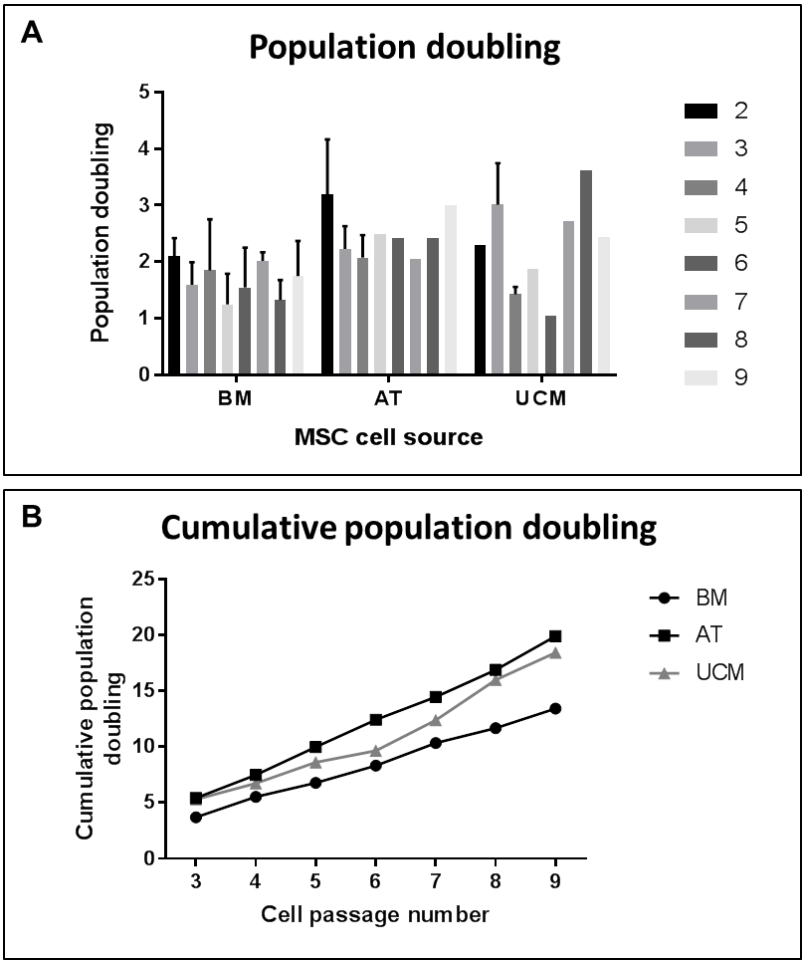

Figure 3.3 – Proliferative potential of the MSC donors from AT (adipose tissue, n = 1-3) and UCM (umbilical cord matrix, n = 1-5) seem to be higher than the set of BM (bone marrow, n = 2-7) MSC donors tested. A – Population doubling of AT MSCs tended to be higher throughout passage number compared to BM and UCM MSCs. Population doubling was calculated based on the fold increase at the end of each passage (passage 2 to 9), for each cell source (Equation 2). B – Cumulative population doubling of AT and UCM MSCs tended to be higher than of BM MSCs. Cumulative population doubling is the sum of each consecutive population doubling (Equation 3). Error bars represent the standard error of the mean.

It was reported that donor age significantly affects proliferation of BM MSCs with MSCs isolated from older donors having much lower proliferative capacity than MSCs isolated from younger

donors (Stenderup *et al.*, 2003). While for UCM MSCs, it was found that there are two cell populations with different proliferative potential according to the region from which the cells are isolated in the UCM unit (Karahuseyinoglu *et al.*, 2007). In a study comparing different MSC sources, fetal BM MSCs and Wharton's Jelly (UCM) derived MSCs had higher proliferation potential than AT MSCs, however, there is no match between donors neither donor age (Q. Wang *et al.*, 2016). Therefore, to effectively assess which MSC source is more proliferative, a direct comparison of human MSC proliferation rate between cell sources using the same donors should be performed, however, it is quite difficult due to sample availability. In one study a comparison between BM and AT MSC sources using matched donors resulted in higher proliferative capacity of AT MSCs than BM MSCs when cultured in culture medium containing serum (Burrow, Hoyland and Richardson, 2017), which is in accordance with the tendency obtained herein (although there was no donor matching between different cell sources). To overcome the difficulty of isolating human MSCs from different cell sources from the same donor, several authors used animal models, for instance, Peng and co-workers isolated rat BM and AT MSCs from the same animals and AT MSCs showed higher proliferative potential than BM MSCs (Peng *et al.*, 2008).

In summary, MSCs isolated from different cell sources have similar morphology and immunophenotype and all have multilineage differentiation potential. AT and UCM MSCs seem to be more proliferative than BM MSCs for the set of donors tested, however, this conclusion cannot be extended for all cases without a direct comparison of cell sources isolated from the same donor and without performing statistical analysis with a higher number of donors.

3.1.2 Oxidative stress assay

For a successful MSC therapy upon transplantation to an injured site, MSCs have to be able to survive to a harsh environment at higher oxidative stress while maintaining their regenerative properties to enhance healing. However, there is no standardized and widely used potency assay to evaluate MSC resistance to apoptosis by oxidative stress. Moreover, it is still under debate which MSC cell source and culture conditions would lead to enhanced resistance to oxidative stress and, therefore, higher chance of a successful regeneration at the injured site.

Oxidative stress results from a perturbation in the pro- and anti-oxidant cellular balance and it can be induced, for instance, by γ-irradiation, hyperoxia, extracellular $O_2^{-\cdot}$, H_2O_2, free radical-generating drugs or by inhibition of cellular anti-oxidant defenses (Gille and Joenje, 1992).

The aim was to develop a simple, quick and sensitive oxidative stress assay and, to develop the assay, the influence of several parameters on the cellular response to oxidative stress were evaluated. The oxidative stress agent H_2O_2 was selected for the development of an oxidative stress potency assay. It is known that H_2O_2 can induce lipid peroxidation, DNA damage (Gille and Joenje, 1992) and consequently cell senescence and death.

A preliminary screening was performed using alamar blue, a fluorescent and colorimetric indicator of the metabolic activity of the cells, which can be used to predict cell viability (Rampersad, 2012). Two BM MSC donors M72A07 and M79A15 were seeded onto 96 WP and the parameters H_2O_2 concentration and incubation time as well as cell seeding density per cultured area were tested.

The preliminary results allowed narrowing the initial range of the variables to: H_2O_2 concentration between 3 to 10 mM, incubation time of 1 h and number of cells seeded between 5,000 and 37,500 cell/cm^2, for a loss of cell viability between 50 and 100%. Of note, this assay is intended to evaluate cell death (apoptosis and necrosis) and not cell senescence, which takes longer time.

The selection of shorter H_2O_2 incubation time of 1 h is in accordance with Gille and Joenje guidelines (Gille and Joenje, 1992), who described that shorter incubation time of 30-45 min are preferable to several hours and overnight incubation due to H_2O_2 half-life and effective cell exposure time, also it allows the replacement of serum containing medium or even the culture medium by PBS supplemented with glucose and glutamine and finally when the analysis is performed after a longer H_2O_2 incubation, the cells could be already adapting to or recovering from the oxidative stress.

The impact of cell passage, confluence, H_2O_2 concentration and also the effect of the number of H_2O_2 moles per cell were tested. For higher sensitivity, Annexin V/PI staining was used to be able to distinguish live cells from apoptotic and necrotic cells by flow cytometry.

Regarding cell passage, 3 BM MSC donors M67A07, M72A07 and M79A15 were tested from cell passage (P) 3 to 7. For each H_2O_2 concentration, there was no statistical difference in total cell death between cell passages 3 through 7 (Figure 3.4 A). There was a significant increase in total cell death of BM MSCs between P4 through P7 at 3 mM H_2O_2 and P4 through P7 at 10 mM H_2O_2, which is in accordance with the expected higher cell death with higher H_2O_2 concentration. It was expected to observe higher cell death with increasing passage number, however, no statistical difference between passages was observed and high standard error of the mean were obtained. It is hypothesized that the effect of cell passage number would be observed when cells reach senescence, at higher cell passages than P7, and the effect of cell passage would result in higher sensitivity of MSCs to oxidative stress. During cell division, DNA is replicated and chromosomes get shortened at the telomeres. Oxidative stress accelerates the telomere shortening (Von Zglinicki, 2002). Moreover, aged MSCs have lower anti-oxidant power and protection against ROS which will cause molecular damage and consequently cell death and tissue loss of function (Kasper *et al.*, 2009).

It was reported that MSC differentiation potential and number of colony forming units is significantly reduced even in early passages (Schellenberg *et al.*, 2011). Additionally, it was observed that higher passage number in human AT MSC resulted in significantly higher doubling time and senescence when comparing P1 to P13 (Gruber *et al.*, 2012). And in another work, AT MSC senescence was maintained low until P10, which then significantly increased at P15 (Zuk *et al.*, 2001). These reports can explain the lack of effect of cell passage on MSC resistance to oxidative stress as no more than P7 was tested.

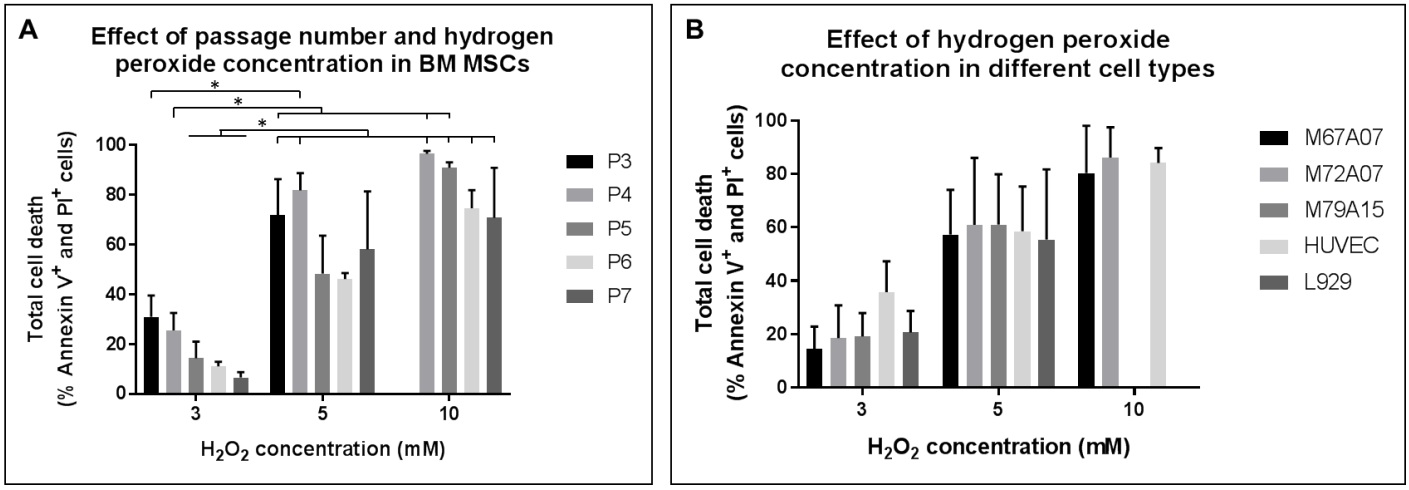

Figure 3.4 – Resistance to oxidative stress decreases with increased hydrogen peroxide concentration (H_2O_2 in mM), however, no trend is observed between passage number 3 to 7 for bone marrow MSCs (BM MSC). A – Passage number (P) between 3 to 7 did not affect the total number of dead cells (% of total Annexin V and PI positive cells) measured by flow cytometry, while cell death increased with H_2O_2 concentration for 3 BM MSC donors M67A07, M72A07 and M79A15 (n = 2-3). B – No difference on resistance to oxidative stress was observed between BM MSC donors (P3 to P8) and the endothelial cell line HUVEC (P7 to P11) and fibroblast cell line L929 (P10 to P16). N = 4-9. *P value < 0.05, Two-way ANOVA with Tukey correction. Error bars represent the standard error of the mean.

On the other hand, it was stated that DNA repair proteins such as SIRT1 are up-regulated to a higher extent in old MSCs than in young MSCs resulting in reduced p53 activity, which could increase cellular tolerance and survival while preventing growth arrest and apoptosis in older cells compared to younger cells (Brandl *et al.*, 2011). This indicates that there is still lack of understanding on the oxidative stress and senescence mechanisms besides experimental differences leading to the published conflicting results.

Cell death increased with H_2O_2 concentration as expected, however, there was no significant difference on cell death between the different cell types BM MSC, HUVEC and L929 (Figure 3.4 B). The results indicate that the BM MSC donors tested did not show improved mechanisms of resistance to oxidative stress compared to HUVEC and L929 at the H_2O_2 concentrations used or that the protocol is not robust and optimized yet as there are high standard errors of the mean per condition.

BM MSCs were reported to be more resistant to oxidative stress than somatic cells such as fibroblasts as a consequence of a fast decrease in p21 expression to normal values for somatic cells while for MSCs the up-regulation of p21 expression is maintained for longer time resulting in lower DNA damage (Brandl *et al.*, 2011). In another study which analyzed cell senescence, it was observed that BM MSCs had higher senescence than AT MSCs and both had higher senescence than human foreskin fibroblasts (De Luca *et al.*, 2013). However, comparison between works should be done carefully as differences in culture conditions and cell sources could lead to opposite results, namely BM and AT MSCs were grown in culture medium containing human platelet lysate, which leads to higher proliferation rate and population doubling than FBS, and also human foreskin fibroblasts were used and had undefined passage number instead of known passage number of mouse connective tissue fibroblasts used herein. Michiels and colleagues showed that HUVEC are more sensitive to high oxygen tensions and H_2O_2 than lung fibroblasts due to lower amounts of several anti-oxidant

enzymes, although in HUVEC glutathione is present in higher amount it only partially compensated the lack of other anti-oxidant enzymes (Michiels, Toussaint and Remacle, 1990).

The importance of the parameters number of moles of H_2O_2 per cell and cell confluence was described in Gille and Joenje review (Gille and Joenje, 1992), who observed that the volume of H_2O_2 solution (and therefore the number of H_2O_2 moles) affects oxidative stress results and also that cells at higher confluence seem to be less sensitive to H_2O_2 than cells at lower cell densities as a consequence of decreased H_2O_2 effective exposure per cell and its metabolism. Another study also described that cells at lower confluence levels are more sensitive while confluent cultures are more resistant to oxidative stress (Burova *et al.*, 2013), which could also be explained by the higher cell surface exposure for H_2O_2 diffusion into the cell which is responsible for increased cell death. The effect of number of moles of H_2O_2 per cell and cell confluence was also tested herein and preliminary results indicated that the number of H_2O_2 moles per cell seems to be the parameter to select instead of H_2O_2 concentration (which is in accordance with Gille and Joenje work) and that cells at lower confluency seem to be more sensitive to oxidative stress (which is in accordance with Gille and Joenje work as well as Burova and co-workers study), thus number of cells seeded should also be another parameter to select for further protocol optimization studies.

Consequently, it was decided to optimize the oxidative stress protocol using Design of Experiments methodology based on three parameters: the number of cells seeded (cell/cm^2), passage number and the number of moles of H_2O_2 per cell. The Design of Experiments software allows the determination of a model that describes the oxidative stress effect on cells based on the variation of the parameters/variables selected and on the cell death values obtained experimentally. The model is fitted into a polynomial equation which can be used for prediction of other scenarios as long as the variable values are within the range tested. This optimization method has the advantages of allowing to test several variables simultaneously and determine the significance of the interaction between variables, while reducing the number of experiments to the minimal relevant ones with savings in terms of time and expenses (Bezerra *et al.*, 2008). Furthermore, statistical analysis of the model can also be performed using this software.

A central composite face centered star point design was used to optimize the number of cells seeded x_1 (in cell/cm^2), passage number x_2 and the number of moles of H_2O_2 per cell x_3, each having a center point, a low and a high level (Table 3.2). To build the model BM MSC donor M79A15 was selected. Cells were seeded in 12 WP and incubated at 37ºC and 5% CO_2 for 17 h. Extra wells were seeded to determine the exact cell number on the plates for each set of initial cell seeding densities immediately before H_2O_2 incubation for 1 h in order to determine the exact number of moles of H_2O_2 to add per cell.

The central composite design analysis was selected because this model does not make any assumptions about the structure of the data, it can analyze any set of continuous values of the variables and also it reduces the number of experimental runs when compared to a complete three-level factorial design when three or more variables are tested. The model of standard design was select with 3 variables, 1 block, 16 center points and 7 replications originating a total of 128 experimental runs that were consequently performed.

Table 3.2 – Design of experiment variables and respective values at three levels. The 3 variables selected were initial cell density (x_1 in cell/cm^2), passage number (x_2) and number of moles of H_2O_2 per cell (x_3 in mol H_2O_2/cell).

Variable	Low level	Center point	High level
Cell/cm^2 x_1	5,800	10,500	17,900
Passage x_2	4	7	10
Mol H_2O_2/cell (x10^{-11}) x_3	2.2	3.7	5.1

After obtaining the experimental data, the statistical analysis of the model was performed using ANOVA and Fisher's statistical test (F-test) to determine which variables significantly affect cell death. The effect estimates and respective significance for each variable and all the linear and quadratic interactions between the variables were determined. The effect estimate represents its contribution to the outcome, in this case, the total cell death. Effects with P value higher than 0.05 (or significance lower than 95%), were discarded and pooled into the residual error. The linear interaction between variables x_1 and x_2 as well as linear interaction between variables x_2 and x_3 were discarded from the analysis because their P value was higher than 0.05, as it can be observed in the Pareto chart of the standardized effect estimates that their effects are to the left of the P value threshold red line (Figure 3.5). After discarding the effect of the linear interaction between cell seeding density and passage number and of the linear interaction between passage number and the number of H_2O_2 moles per cell and pooling them into the residual error, the statistical analysis was re-done for the reduced model.

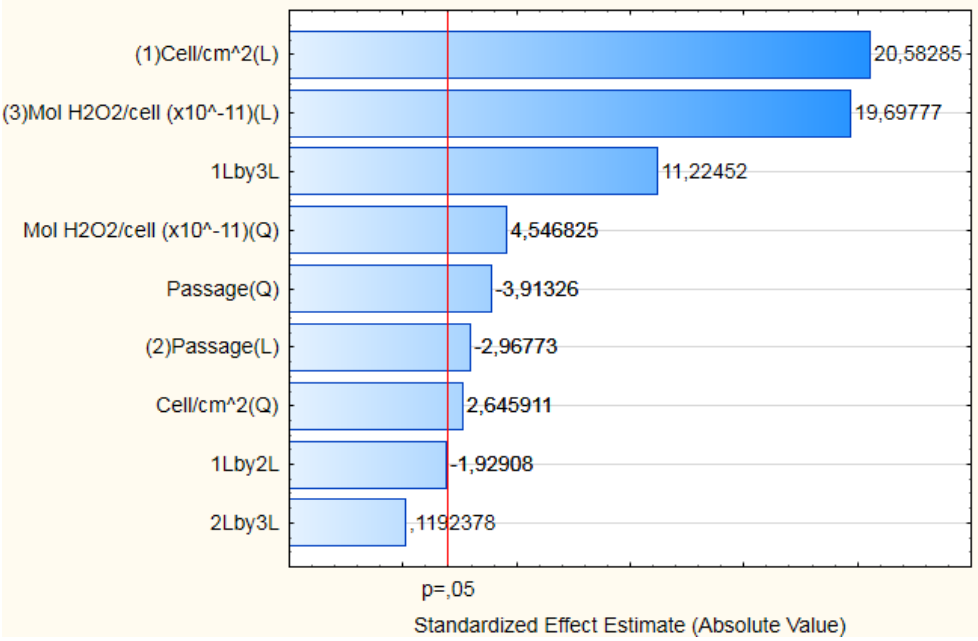

Figure 3.5 – Pareto chart of the standardized effect estimates of cell death by oxidative stress manipulating the variables number of cells seeded (variable 1 - Cell/cm^2), cell passage number (variable 2) and moles of hydrogen peroxide per cell (variable 3 – mol H_2O_2/cell). Linear (L), quadratic (Q) and interaction between linear variables were considered significant when P value was lower than 0.05 (to the right of the red line), thus 1L by 2L and 2L by 3L were not statistically significant.

The pure error accounts for the variability of the measurements and random errors inherent to the system and the lack-of-fit describes how well the data is represented by the model accounting for the effect estimates discarded. The statistical analysis of the reduced model was used to determine the sum of squares (SS) and the degrees of freedom (DF), from which the mean sum of squares (MS), and the statistic F value and the P value were determined (Table 3.3). MS is given by the ratio between SS and DF. F value of the model is the ratio between the MS of the model and the MS of the pure error and the F value of the lack-of-fit is given by the ratio between the MS of the lack-of-fit and the MS of the pure error. P value is calculated in the software based on each F value and DF. The model is well fitted to the experimental data if the P value of the model is lower than 0.05 and the P value of the lack-of-fit higher than 0.05 and also when F value of the model is higher than the F critical and the F value of the lack-of-fit lower than the F critical (Bezerra *et al.*, 2008).

The SS of the lack-of-fit was lower than the pure error. Additionally, the F value of the model (141.3) was higher than the F critical of 1.98 (determined using the software) and the F value of the lack-of-fit (1.92) was lower than the F critical. Furthermore, the P value of the model is much lower than 0.05 and the P value of the lack-of-fit (0.073) is higher than 0.05. Altogether, the comparison of SS, MS, F value and P value indicate that the mathematical model is statistically significant and that the lack-of-fit is not statistically significant, consequently the reduced model is well fitted to the experimental data and, therefore, the equation describing the model (Equation 4) can be accepted.

Table 3.3 – Design of experiment statistical analysis of the reduced model describing the oxidative stress of bone marrow MSC donor M79A15 was statistically significant. The model described the total cell death (in %) by varying the 3 independent variables, number of cells seeded, passage number and moles of H_2O_2 per cell. ANOVA and F-test were used to determine the sum of squares (SS), degrees of freedom (DF), mean sum of squares (MS), Fisher's statistic value (F value) and the probability value (P value) of the reduced model.

Variable	Source	SS	DF	MS	F value	P value
% Death	Model	72524.9	7	10360.7	141.3	<<0.05
	Error	9272.0	120	77.3		
	Lack-of-fit	984.7	7	140.7	1.92	0.073
	Pure error	8287.3	113	73.3		
	Total	82052.0	127			

$$Y = -(0.005 \pm 0.001)x_1 + (10 \pm 3)\,x_2 - (33 \pm 7)\,x_3 + (0.00000014 \pm 0.00000005)\,x_1^2 - (0.8 \pm 0.2)\,x_2^2 + (4.0 \pm 0.9)\,x_3^2 + (0.0014 \pm 0.0001)\,x_1\,x_3 + (35 \pm 12)$$

Equation 4 – Mathematical equation describing the oxidative stress model of BM MSC M79A15. Y is the total cell death (in %), x_1 is the number of cells seeded, x_2 is the cell passage number and x_3 is the number of moles of H_2O_2 per cell multiplied by a factor of 10^{-11}.

The residuals should also be analyzed for model verification. Residuals correspond to the difference between predicted and experimental results for a certain set of conditions (Bezerra *et al.*, 2008). In a good fit between the experimental data and the mathematical model, the distribution of the residuals in the residual plot should be random, the residuals in the normal residual plot should fall into the diagonal and the residuals in the histogram of the residuals should be fitted into a Gaussian distribution. The residuals analysis indicates a good fit of the data because the residuals are distributed randomly and do not show a specific tendency (Figure 3.6 A), the residuals are normally distributed as most of the values are in the diagonal (Figure 3.6 B) and the histogram of the residuals shows that the residuals are approximately distributed in a Gaussian shaped curve (Figure 3.6 C).

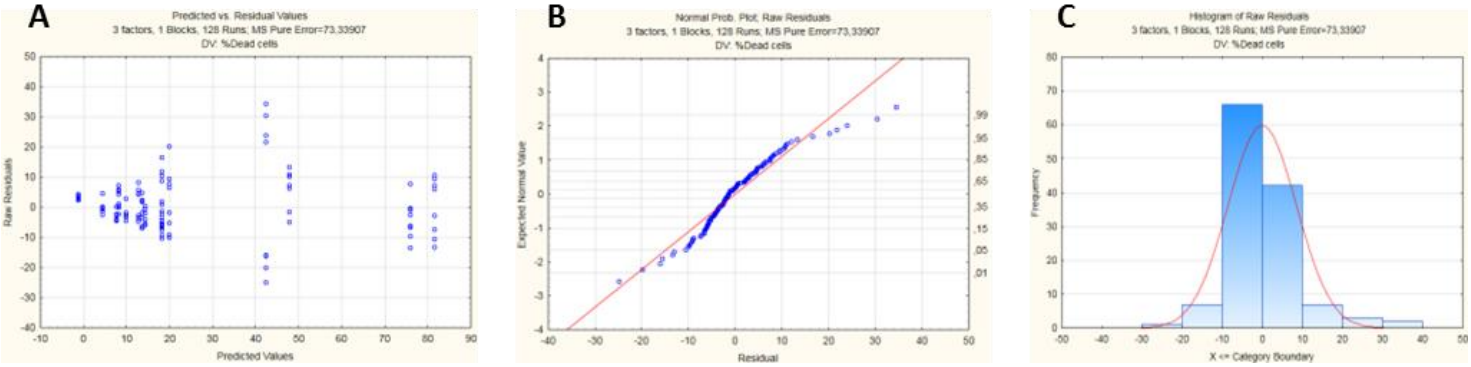

Figure 3.6 – Analysis of the residuals indicated a good fit of the model describing oxidative stress for BM MSC donor M79A15. A – Residuals plot did not show a trend in the distribution of the residuals. B – Normal residual plot showed that the residuals approximately fitted into the diagonal. C – Histogram of the residuals showed a Gaussian like distribution.

The final step of the Design of Experiments was the validation of the model. Three different combinations of the three variables were chosen. The predicted cell death was obtained by the equation of the model (Equation 4) and compared with the experimental data of the total cell death. The experimental values were within the range of the predicted values, considering the experimental and the predicted error (Table 3.4), therefore, the model was considered valid.

Table 3.4 – Oxidative stress model of BM MSC donor M79A15 obtained by design of experiments was validated by testing three different sets of the 3 independent variables, cell seeding density (x_1 in cell/cm^2), passage number (x_2) and number moles of H_2O_2 per cell (x_3 in mol H_2O_2/cell) and experimental (n = 3-8) total cell death (in %) was in the range of the one predicted by the model. Experimental data is represented by the mean and standard deviation.

x_1 (Cell/cm^2)	x_2 (Passage)	x_3 (Moles H_2O_2 per cell x10^{-11})	Predicted Cell death (%)	Experimental Cell death (%)
10500	10	4.4	20±5	22±12
10500	5	5.0	40±7	42±5
10500	5	4.2	25±5	23±5

Design of experiments has not been widely used in the stem cell field (Toms, Deardon and Ungrin, 2017) and to the extent of my knowledge it was never used to optimize an oxidative stress potency assay. The limited number of studies that took advantage of Design of experiments approach used it to optimize stem cell expansion under 2D culture systems screening the effect of cytokines (Audet *et al.*, 2002; Andrade *et al.*, 2010; Marinho, Chailangkarn and Muotri, 2015) and incubation temperature (Audet *et al.*, 2002), and cell seeding density, serum concentration, media volume and culture time (Thomas, Hourd and Williams, 2008), to optimize stem cell expansion under 3D culture systems screening initial cell seeding density and agitation rate for bioreactor suspension cultures (Hunt *et al.*, 2014) and the number of cells per spheroids, oxygen tension and inflammatory stimuli for spheroid cultures (Murphy *et al.*, 2017), to optimize cell passaging screening cell seeding density,

media volume and media exchange time (Ratcliffe *et al.*, 2013), to optimize biomaterial composition (Nih *et al.*, 2017) and degradation (Zhou *et al.*, 2016) and to optimize stem cell differentiation screening time, cell seeding density, matrix substrates and cytokines and growth factors (Jakobsen *et al.*, 2014; Glaser *et al.*, 2016).

Based on the oxidative stress model developed herein, it was decided to choose the parameters cell seeding density of 10,500 cell/cm^2 and $5x10^{-11}$ moles H_2O_2 per cell and passage number of 5. These parameters resulted in a total cell death of about 42% which is an intermediate value and would allow to see differences between MSC donors, MSC cell sources, culture conditions or any other conditions to be tested as opposite to very low or very high cell death which may hinder the sensitive discrimination between conditions.

Three MSC donors per cell source, BM, AT and UCM, at passage 5 were seeded at 10,500 cell/cm^2, incubated for 17 h and then challenged with H_2O_2 for 1 h at 5 x 10^{-11} moles H_2O_2 per cell but also at 10 x 10^{-11} moles H_2O_2 per cell. For all donors except BM MSC M72A07, there was a significant increase in cell death from 5 to 10 x 10^{-11} moles H_2O_2 per cell as expected (Figure 3.7 A). At 5 x 10^{-11} moles H_2O_2 per cell, there were significant differences between donors of the same cell source for BM and AT and there was no statistically significant difference between UCM donors. At 10 x 10^{-11} moles H_2O_2 per cell, there were significant differences between BM M79A15 and the donors M72A07 and M83A15, between AT L090724 and the donors L090403 and L090602, and between UCM 78 and the donors 2 and 38. Therefore, there was considerable MSC donor-to-donor variability within each cell source, especially when a low number of donors is tested (Figure 3.7 A). Although UCM MSCs had the tendency to have higher resistance to oxidative stress (lower cell death), when the total cell death from the 3 donors per cell source was averaged, it resulted in no statistically significant difference between cell sources due to high standard error of the mean as a consequence of donor-to-donor variability (Figure 3.7 B). These results also indicate that the model obtained by Design of Experiments cannot be used to predict cell death of other BM MSC donors neither other cell sources as a consequence of variability between donors and cell sources.

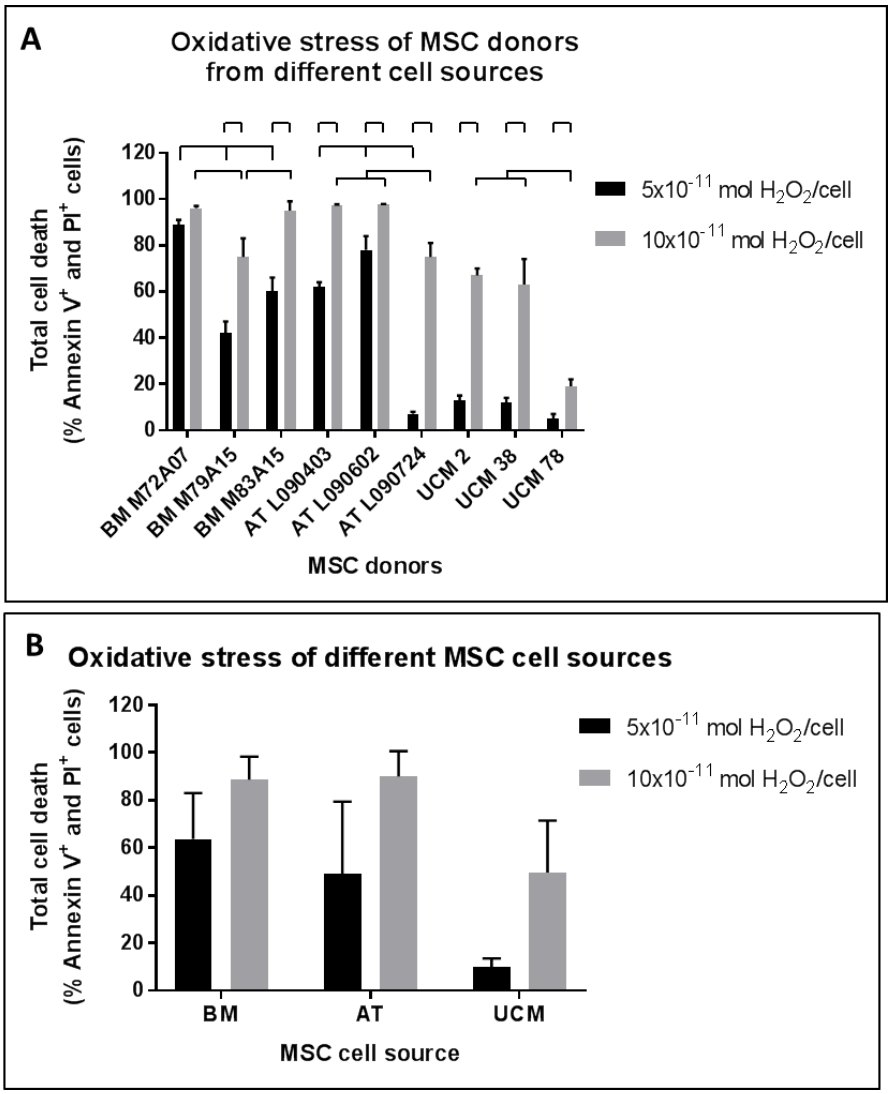

Figure 3.7 – Higher number of moles of hydrogen peroxide per cell (mol H_2O_2 per cell) resulted in higher oxidative stress for all MSC donors from bone marrow (BM), adipose tissue (AT) and umbilical cord matrix (UCM), however, resistance to oxidative stress varied greatly with donor rather than with cell source. MSCs at passage 5 were seeded at 10,500 cell/cm^2 and incubated with 5 and 10 x 10^{-11} mol H_2O_2 per cell for 1 h and the total cell death (%) including Annexin V and PI positive cells was measured by flow cytometry. A – Average total cell death increased with H_2O_2 dose and varied greatly between different donors from the same cell source (n = 3-5, error bars represent the standard deviation). B – No statistical difference between the average total cell death of 3 MSC donors per cell source (n = 3, error bars represent the standard error of the mean). P value < 0.005 (for all comparisons denoted in A), Two-way ANOVA with Tukey correction.

To account for that variability and if the construction of a new model is desired for a broad prediction instead of just protocol optimization, then the Design of Experiments approach could be repeated using a pool of much more than 3 MSC donors per cell source and statistically analyzed for significance.

Conflicting results can be found in the literature regarding the resistance to oxidative stress by H_2O_2 from different MSC cell sources. One study reported that passage 3 rat BM MSCs cultured in serum containing medium are more resistant to oxidative stress than passage 3 rat AT MSCs by

incubation with 2 mM H_2O_2 for 90 min (Peng *et al.*, 2008). In contrast, it was observed that passage 3-4 rat BM MSCs cultured in serum containing medium are less resistant than rat AT MSCs to oxidative stress after two H_2O_2 treatments at 600 µM for 2 h (El-Badawy *et al.*, 2016). Differences may be attributed to donor variability and oxidative stress protocol, moreover, it is not clear if MSCs were isolated from a single or multiple donors to test their resistance to oxidative stress. Additionally, it was observed that passage 3 human BM MSCs cultured in medium containing serum are less resistant than human AT MSCs to apoptosis by oxidative stress after 1 h exposure to 2 mM H_2O_2 (Ertaş *et al.*, 2012), however, MSCs from BM and AT were not harvested from matching donors. Therefore, it still remains to be elucidated if there is a MSC source that has higher resistance to oxidative stress or if the effect of donor variability has more impact than cell source on the resistance to oxidative stress.

The work presented here in not in accordance with the published data as no statistically significant difference was observed between UCM, AT and BM MSCs due to donor-to-donor variability. The difference between works could be a consequence of species related differences, lower variability between laboratory animals compared to human samples from which MSCs were harvested, the number of donors tested as well as differences in MSC isolation methods. Of note that for a direct comparison between MSC sources regarding resistance to oxidative stress, cells from different sources should be harvested from the same donors. Also, when using low number of MSC donors it is possible that higher impact of donor-to-donor variability is observed, therefore, higher number of donors should be tested (instead of the 3-5 donors typically necessary to publish scientific results).

Regarding the resistance to senescence by oxidative stress, AT MSCs were reported to be less sensitive than BM MSCs and that UCB MSCs have higher sensitivity to oxidative stress (Kern *et al.*, 2006). Moreover, UCB MSCs seem to be less resistant to oxidative stress due to reduced activity of anti-oxidant enzymes (Ko *et al.*, 2012). In the work herein, UCM and not UCB MSCs were used and opposite results were observed with UCM MSCs more resistant to oxidative stress than BM and AT MSCs. The reasons of the opposite results might be due the source, donor-to-donor variability, possible errors in cell counting and wrong determination of the number of H_2O_2 molecules per cell, or also because after H_2O_2 incubation the supernatant was discarded and the possible presence of necrotic cells in the supernatant was not taken into account, and, therefore, the lower values cell death obtained for UCM MSCs might be misleading and actually this cell source could be more sensitive to oxidative stress.

To overcome this limitation, one could account for both cells in the supernatant and attached cells for apoptosis and necrosis assessment by flow cytometry or one could perform the oxidative stress assay in suspension. The first option would not change considerably the protocol developed, so the parameters optimized could still be used. For the second option of testing the resistance to oxidative stress in suspension, there was a need to adapt the protocol developed. First, it was important to evaluate if there was significant cell death associated with the cells being in suspension for the incubation time period of 1 h (H_2O_2 incubation time used) and also to take into account that cells might be more sensitive in suspension because of higher exposure to the oxidative stress agent. Preliminary testing of oxidative stress in suspension was performed with AT L090403 at passage 4.

Cells cultured in tissue culture flasks were detached and the cell number determined. Then, 39,900 cells (correspondent to 10,500 cell/cm^2 previously used) were added to ultra-low attachment plates and incubated for 1 h with culture medium with 5 x 10^{-11} moles H_2O_2 per cell or 1 x 10^{-11} moles H_2O_2 per cell (lower number H_2O_2 moles were also tested as cells could be more sensitive in suspension).

The results showed that there was minimal cell death after 1 h incubation with culture medium in ultra-low attachment plates (about 5%), indicating that a suspension assay can be used to assess resistance to oxidative stress (Table 3.5). Suspension cultures incubated with 1 x 10^{-11} mol H_2O_2 per cell also resulted in minimal cell death (about 7%), while incubation with 5 x 10^{-11} mol H_2O_2 per cell resulted in high cell death (about 92%). Comparison of oxidative stress results between suspension and adherent culture protocols showed that cells in suspension were indeed more sensitive to hydrogen peroxide. Therefore, future oxidative stress studies with cells in suspension should not use as high number of H_2O_2 moles per cell as for adherent cultures (recommended to be between 1-5 x 10^{-11} mol H_2O_2 per cell).

Moreover, the oxidative stress in suspension could then be used to evaluate resistance to oxidative stress of individual and pooled donors from each MSC cell source to build a model using Design of Experiments or the developed assay could be used to test the effect of different culture conditions (for instance, normoxia and hypoxia, pre-conditioning with small molecules, transfected cells expressing certain genes of interest) and culture systems (2D and 3D culture systems) on MSC resistance to oxidative stress and also to compare MSCs to other cell types. The oxidative stress in suspension to some extent also mimics the conditions of cell infusion to an oxidative injury site.

Table 3.5 – Adipose tissue (AT) MSCs are more sensitive to oxidative stress in suspension culture than as adherent culture, however, it is a more accurate method and feasible as no significant death was observed for the control. AT MSC L090403 (39,900 cells) at passage 4 and 5 were challenged for 1 h with H_2O_2 at different number of moles per cell in suspension (n = 3, except for control with n = 1) and as adherent culture (n = 5) and the total cell death (in %) given by the total Annexin V and PI positive cells was measured by flow cytometry. Experimental data is represented by the mean and standard deviation.

	Suspension culture of AT L090403 P4			Adherent culture AT L090403 P5	
	Control	1 x 10^{-11} mol H_2O_2/cell	5 x 10^{-11} mol H_2O_2/cell	5 x 10^{-11} mol H_2O_2/cell	10 x 10^{-11} mol H_2O_2/cell
Total cell death (%)	5.3	6.8 $\pm$ 0.1	91.8 $\pm$ 0.1	62 $\pm$ 2	97.4 $\pm$ 0.3
Actual H_2O_2 concentration (mM)	0	0.8	5.0	3.9	7.7

To the extent of my knowledge, the oxidative stress assay in suspension is innovative for stem cell applications and might bring more accuracy and robustness to the assay. Moreover, most published work of the oxidative stress assays by H_2O_2 challenge in suspension is with plant cells and there are no much publications with mammalian cells. Two examples of studies using mammalian cells are with human brain glioblastoma astrocytoma (Wu *et al.*, 2005) and bovine tracheal epithelial cells (Nakajima *et al.*, 1999).

In summary, two oxidative stress protocols were under development. One as adherent cultures, in which cells are seeded at 10,500 cell/cm^2 (39,900 cells) in 12 WP, incubated for 17 h, after that time the cell number of adherent cells is assessed and 5 x 10^{-11} mol H_2O_2 per cell are incubated for 1 h. Then, cells in the supernatant and adherent cells should be pooled and stained with Annexin V and PI to measure total cell death by flow cytometry. The second protocol as suspension culture comprised the detachment of cells from tissue culture flasks and incubation of 39,900 cells for 1 h in 24 WP ultra-low attachment plates with 1-5 x 10^{-11} mol H_2O_2 per cell, followed by staining with Annexin V and PI to measure total cell death by flow cytometry.

In a context of MSC therapy, the development of potency assays that allow to evaluate the resistance of the expanded cells to oxidative stress will be very helpful on selecting the cell source and donors that are more resistant to oxidative stress and, thus, more prone to survive and promote regeneration when transplanted to sites of injury where cells will be exposed to an environment with higher levels of oxidative stress. These assays can be used to compare MSC potential in terms of resistance to oxidative stress to other cell types, for instance, endothelial cells and fibroblasts as controls. Moreover, these assays can be applied to evaluate the pro-survival and anti-apoptotic potential of MSC-CM and MSC-EVs by pre-conditioning or in co-treatment with H_2O_2.

3.1.3 Angiogenic assays

Many studies have been reporting MSC regenerative ability, in particular its angiogenic potential (Miyahara *et al.*, 2006; Gandia *et al.*, 2008; Zhang and Chopp, 2009; Edwards *et al.*, 2014) and possible mechanisms of action are through paracrine action by secretion of angiogenic factors, such as VEGF (Chen *et al.*, 2003; Miyahara *et al.*, 2006; Zacharek *et al.*, 2007), bFGF (Chen *et al.*, 2003), angiopoietin-1 (Zacharek *et al.*, 2007) and HGF (Rehman *et al.*, 2004; Miyahara *et al.*, 2006), cell-to-cell contact and integration into new blood vessels created by endothelial cells (Al-Khaldi *et al.*, 2003; Duffy *et al.*, 2009) or transdifferentiation towards endothelial-like phenotype (Nagaya *et al.*, 2004; Silva *et al.*, 2005).

To build a characterization platform of MSC angiogenic potential, there is a need of simple, quick, quantitative and high throughput assays that can be widely used. First a tube formation and tube incorporation assay were developed to assess MSC angiogenic potential through cell-to-cell contact and integration into new blood vessels and lastly a tube disruption assay and a wound healing assay were developed to allow the assessment of MSC angiogenic potential through paracrine action.

3.1.3.1 Tube formation and tube incorporation assays

The tube formation and tube incorporation angiogenic potency assays were based on published endothelial cell tube formation assays on Matrigel basement membrane. Matrigel basement membrane is composed of many proteins and it is responsible for maintaining tissue integrity, endothelial cell differentiation and tight cell-to-cell contact, filtering nutrients and metabolic waste, storing growth factors and proenzymes, transducing mechanical cues and it is a barrier to cell invasion, separating the endothelial layer and the stroma (Arnaoutova *et al.*, 2009). Additional

advantages of using this type of angiogenic assay is that it recapitulates the steps that occur during angiogenesis, such as cell adhesion and migration, protease activity, alignment and tube formation (Arnaoutova *et al.*, 2009).

For the tube formation assay, initially HUVEC seeding density of 31,250 to 250,000 cell/cm^2 was tested for an incubation time in Matrigel up to 16 h, in 96 WP (surface area 0.32 cm^2). Preliminary results indicate that after 8 h incubation the tubes were already formed and sprouting was maintained at least for 16 h after plating. There was tube formation for all the cell seeding densities tested 31,250, 125,000 and 250,000 cell/cm^2 (Figure 3.8). HUVEC seeded at 125,000 cell/cm^2 (Figure 3.8 C and D) and 250,000 cell/cm^2 (Figure 3.8 E and F) formed a monolayer in the middle of the well and thicker tubes were only established from the cell aggregate towards the periphery of the well, indicating that increasing HUVEC concentration for 125,000 cell/cm^2 or higher does not proportionally result in higher number of tubes. Table 3.6 also seems to indicate that higher total tube length and total number of tubes and connections was obtained for lower cell seeding densities. Therefore, to obtain higher tube length and number of tubes and connections the choice of cell seeding density should be between 31,250 and 125,000 cell/cm^2. It was decided to use an HUVEC seeding density of 78,125 cell/cm^2 and an incubation time in Matrigel of 8 h for tube formation.

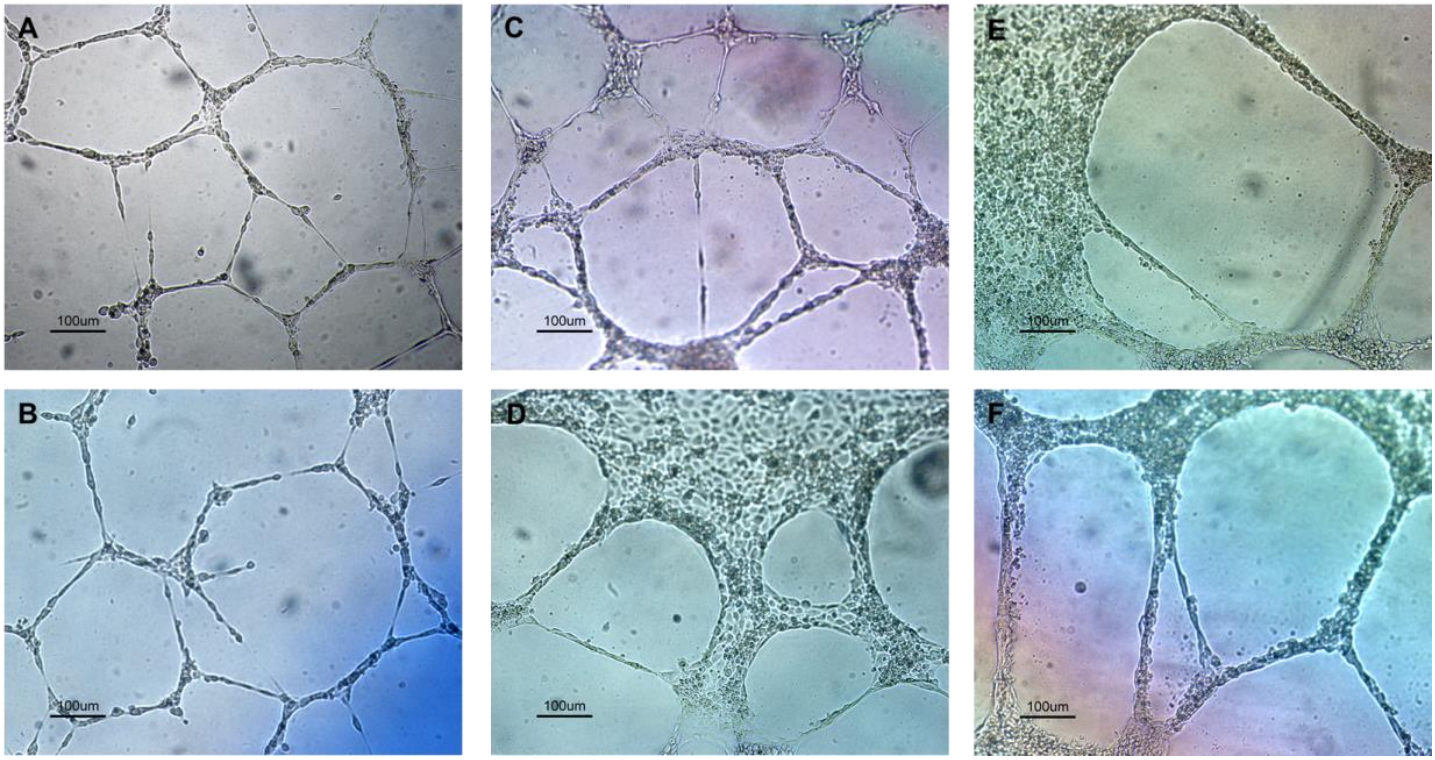

Figure 3.8 – Tube formation of HUVEC plated at several seeding densities in Matrigel after 16 h incubation indicates that optimal cell seeding density should be between 31,250 cell/cm^2 (A and B) and 125,000 cell/cm^2 (C and D), while higher cell seeding density up to 250,000 cell/cm^2 (E and F) resulted in cell monolayer formation. N = 1. Scale bar 100 µm.

Table 3.6 – Effect of cell seeding density (in cell/cm^2) of HUVEC plated in Matrigel after 16 h incubation, indicating that higher cell seeding density results in lower total tube length (in µm), number of tubes and number of connections. To calculate the total tube length and the total number of tubes and branching points, 11 images from 6 wells per condition were used and summed (n=1).

	Cell seeding density (cell/cm^2)		
	31,250	**125,000**	**250,000**
Total tube length (µm)	32,532	26,801	20,837
Total number of tubes	244	180	128
Total number of connections	198	150	124

The importance of cell seeding density was previously reported and high cell seeding density resulted in larger areas of cell monolayers (Arnaoutova *et al.*, 2009), similarly to the results herein observed. Furthermore, the same authors reported that optimal cell seeding density is about 15,000 cell/well in a 96 WP (46,875 cell/cm^2) for an incubation time of 4 to 20 h, and it is recommended to use HUVEC from earlier passages from 2 to 6 (Arnaoutova *et al.*, 2009). The incubation time of 8 h determined herein is within the range reported. The optimal cell seeding density of 46,875 cell/cm^2 is within the range 31,250 and 125,000 cell/cm^2 determined herein. It was decided to use a cell seeding density of 78,125 cell/cm^2 for further experiments, which is about 1.6X higher than the optimal recommended by Arnaoutova and co-workers and the rational for the higher cell seeding density of 78,125 cell/cm^2 was the formation of more tubes and connections of HUVEC at higher passage number (cells at up to P11).

Of note, that a lower magnification objective in the microscope would be required to picture the well in a single image in order to accurately measure all tubes and connections and specially for accurate measurements of the tube length as the length of longer tubes was too long to fit in one image and therefore were discarded in this analysis.

HUVEC seeded at 31,250 cell/cm^2 for 16 h were also stained with calcein (Figure 3.9) and it was possible to observe that the HUVEC tubes formed are not planar and form 3D sprouts embedded in the Matrigel layer as evidenced by the different focal plans of the stained images.

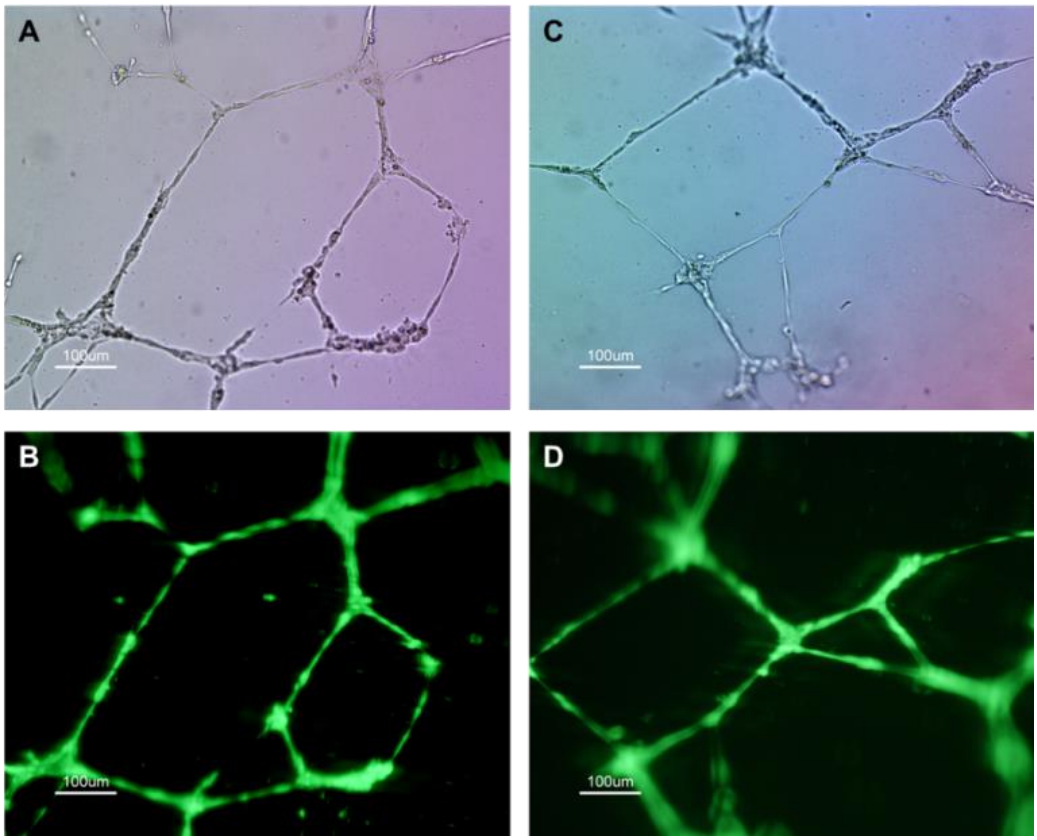

Figure 3.9 – Tube formation of HUVEC plated at 31,250 cell/cm^2 after 16 h incubation by contrast phase microcopy (A and C) and fluorescent microscopy (B and D) after calcein staining (in green) showed non planar tube structures embedded in Matrigel. N = 1. Scale bar 100 µm.

Tube formation was then tested with HUVEC seeded at 78,125 cell/cm^2 and with two BM MSC donors, M72A07 and M79A15, seeded at 31,250 cell/cm^2. Preliminary qualitative analysis indicated that, after 7 to 8 h seeding, BM MSC donor M72A07 was able to form tube-like structures (Figure 3.10 B and D), although in much lower number when compared to HUVEC seeded at 78,125 cell/cm^2 (Figure 3.10 A and B) as well as when HUVEC were seeded at 31,250 cell/cm^2 (Figure 3.8 A and B). BM MSC donor M79A15 formed only a few single-like tube structures and most of the cells were in aggregates (Figure 3.10 E and F). Higher seeding densities of MSCs resulted only in the formation of cell aggregates and not in tube formation (data not shown). Quantification was not performed as different number and not enough number of images were recorded, nevertheless, a clear difference was observed between the high number of tubes formed by HUVEC in all the well and MSCs that only formed lower (MSC M72A07) or much lower and sparse (MSC M79A15) number of tubes in the well.

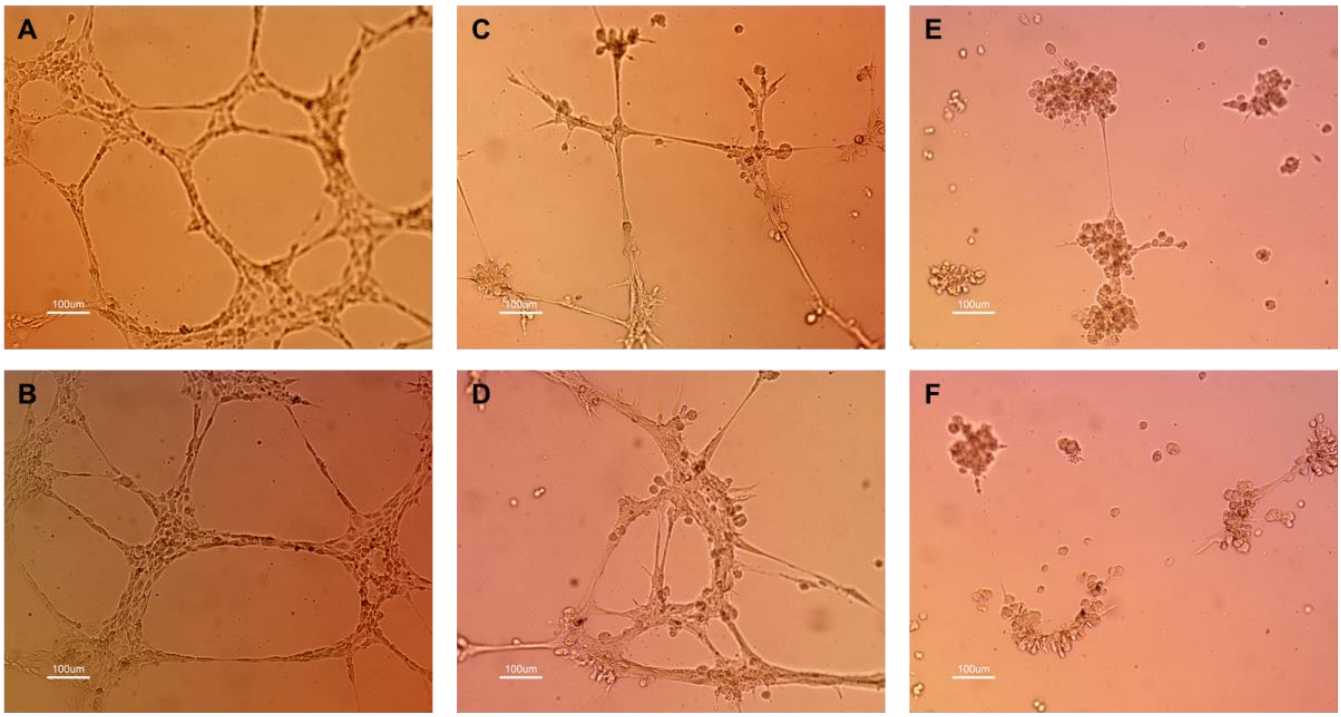

Figure 3.10 – BM MSCs were able to form tube-like structures, although in much lower extent than HUVEC. HUVEC (A and B) were seeded at 78,125 cell/cm^2, while BM MSCs from donor M72A07 (C and D) and BM MSC donor M79A15 (E and F) were plated at 31,250 cell/cm^2 and incubated for 8 h in a Matrigel coated plate. BM MSC donors seem to have different angiogenic potential and both had lower potential when compared to HUVEC. N = 1. Scale bar 100 µm.

Szöke and co-workers observed that AT MSCs alone or in co-culture with AT endothelial cells were not able to sprout, forming only a few single tube-like structures, while AT endothelial cells alone formed a branched network of tubular structures (Szöke *et al.*, 2012), similar to what was observed here for BM MSCs. On the other hand, it was observed that early passage BM MSCs cultured with EGM-2 culture medium, after being under agitation and subjected to endothelial induction in Matrigel, form tubes with similar tube length, area and branching points compared to HUVEC (Portalska *et al.*, 2012). Furthermore, it was observed that tube formation is time dependent and that MSCs expanded in basic medium and then cultured in basic medium or EGM-2 medium in a Matrigel culture formed tube structures after 8 h which were unstable and disrupt to form aggregates after 24 h, while MSCs expanded in EGM-2 medium and then cultured in basic medium or EGM-2 in a Matrigel culture formed tube structures after 24 h which were stable up to 7 days (Portalska *et al.*, 2012). In this work, BM MSCs were not subjected to the endothelial induction as in Portalska and co-workers study, which could explain the lower angiogenic potential as tube formation after 8 h incubation was seen in only one of the two BM MSC donors tested and to much lower extent that in Portalska and co-workers study.

The absence of tube formation of BM MSC donor M79A15, in which cells were mainly in aggregates after 8 h incubation, could indicate less angiogenic potential or that several incubation time points should be evaluated when testing the angiogenic potential of different MSC donors from the

same cell source or from different cell sources. Moreover, it is important to evaluate not only the time necessary for tube formation but also the stability and the total tube size and number and branching points throughout time instead of at the maximum time point of one of the donors due to donor-to-donor variability. Moreover, the use of later passage cells herein could also explain the reduced angiogenic potential observed when compared to Portalska and co-workers published work.

Conflicting results regarding MSC angiogenic potential and ability to differentiate into endothelial cells may be explained by the presence of several cell subtypes within the MSC populations that are all in agreement with International Society for Cellular Therapy guidelines to define MSC. Pacini and Petrini reported that the heterogeneity and morpho-functional variability of MSCs as well as the conflicting results regarding the angiogenic potential of MSCs could be related to a subtype of cells called mesodermal progenitor cells that are $Nestin^{+}$ and $CD31^{+}$ cells having angiogenic potential and the ability to differentiate into MSCs under appropriate conditions (Pacini and Petrini, 2014). Moreover, donor variability, isolation process, cell source and sub-localization of the cells upon harvesting, *ex vivo* culturing (culture medium, cell surface coating type, seeding density, passage number, culture time, detachment agent and incubation time, etc) as well as stochastic events can greatly affect MSC culture selecting for certain cell subtypes (reviewed in Pacini and Petrini, 2014). All these factors may also have contributed to the differences observed between MSC donors M72A07 and M79A15.

To further test MSC angiogenic potential by cell contact, tube incorporation of MSCs and HUVEC was evaluated by seeding BM MSCs from donor M72A07 or M79A15 and HUVEC at a ratio of 1:4 (Figure 3.11). Similarly to what was observed with BM MSC donor M79A15 alone, the co-culture between MSC donor M79A15 and HUVEC resulted in loss of ability from HUVEC to form sprouts (Figure 3.11 E and F). For BM MSC M72A07, sprouting was observed (Figure 3.11 C and D), however, the tubes seem to be thinner when compared to HUVEC alone (Figure 3.11 A and B) even though the HUVEC cell number was equal to the total number of cells plated for the co-culture. Once again, the results indicate variability between MSC donors isolated from the same cell source and also that the protocol needs further optimization evaluating several time points, cellular ratios and earlier passage cells. Moreover, quantification was also not performed due to unequal and not enough number of images recorded.

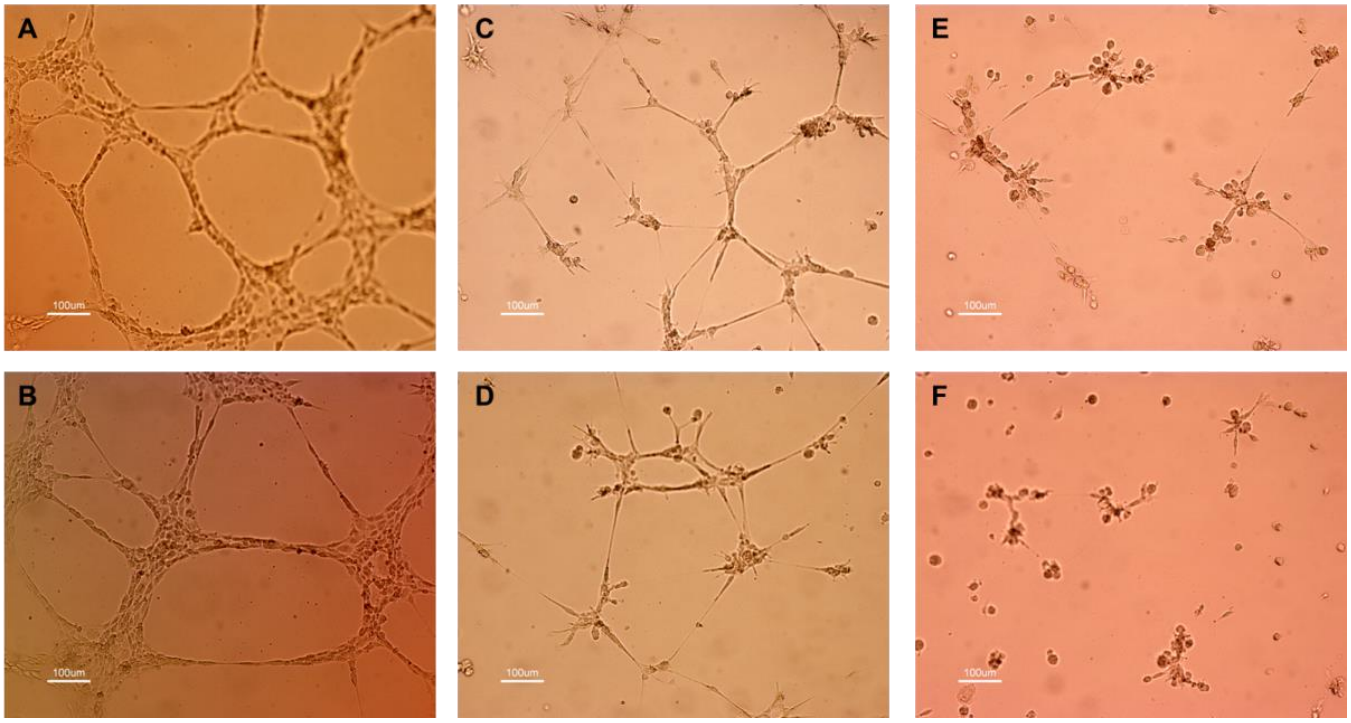

Figure 3.11 – Tube incorporation of HUVEC and BM MSCs plated in a Matrigel coated plate after 8 h incubation indicated that MSC donors have different ability to incorporate tube structures, therefore, there is donor variability regarding angiogenic and supportive potential. HUVEC (A and B) were plated at 78,125 cell/cm^2, BM MSC donor M72A07 (C and D) and donor M79A15 (E and F) were co-cultured with HUVEC at a ratio of 1 MSC: 4 HUVEC. N = 1. Scale bar 100 µm.

Arutyunyan and co-workers reported that UCM MSCs and UCM MSCs co-cultured in 1:1 ratio with endothelial cells started to sprout 1 h after seeding in Matrigel forming unstable networks that disrupted after 3 h while endothelial cells only started to sprout after 3 h seeding (Arutyunyan *et al.*, 2016). Additionally, the tube structures formed by endothelial cells were thinner, shorter and had more branching points than the structures formed by UCM MSCs and UCM MSCs co-cultured with endothelial cells. These observations (Arutyunyan *et al.*, 2016) together with previously reported work of Portalskal and colleagues (Portalska *et al.*, 2012) indicate that earlier and several time points should be evaluated in MSC angiogenic assays.

It was also suggested that MSCs stabilize endothelial cell tube structures in Matrigel in a time dependent manner. BM MSCs, from passage 5, were added to endothelial cells at 0, 12 and 24 h after seeding at a MSC to endothelial cell ratio of 1:10 (Duffy *et al.*, 2009). Addition of MSCs together with endothelial cells resulted in limited tube structures after 24 h incubation, which disrupted after 48 h. When MSCs were added 12 h after endothelial cell seeding, an extensive tubular network was formed after 24 h culture, however, disruption occurred after 48 h. When MSCs were added 24 h after endothelial cell seeding, the tube structures were maintained for 72 h which was longer than for tube structures of endothelial cells alone which was interpreted as the MSC ability to stabilize endothelial cell tubular networks (Duffy *et al.*, 2009). Once again, the relevance of time dependency of this process was shown indicating that the protocol in the work herein needs to be further optimized by testing different seeding conditions, evaluating earlier and more frequent time points as well as to

optimize the time point for MSC addition and understand if it better mimicks the time course of *in vivo* tube formation. Incorporation of imaging equipment with an incubator as well as the use of automated microscopes and imaging analysis software will greatly reduce the time and work involved in this assay towards a high throughput quantitative assay.

Moreover, to ensure that there was MSC integration in the tubes and/or some extent of MSC differentiation towards endothelial cell phenotype, MSC could have been stained with Dil-Ac-LDL. LDL is a protein complex that carries fat molecules, such as cholesterol, maintaining the normal physiological functions. LDL binds to specific membrane receptors to transport cholesterol by endocytosis. Acetylated LDL can be uptaken and metabolized by endothelial cells, then it will accumulate in the lysosomal membranes and can be detected by fluorescence microscopy or flow cytometry when conjugated to the Dil fluorescent probe (Voyta *et al.*, 1984). Dil-Ac-LDL is uptaken by endothelial cells, however, it is not an exclusive marker of endothelial cells and, therefore, can be used to label MSCs prior to co-culture with HUVEC to evaluate their integration in the tube structures.

Although tube formation and tube incorporation assays in Matrigel mimic several steps of angiogenesis, these *in vitro* assays have limitations and both HUVEC and MSCs are missing several cues that allow them to form and maintain tube structures throughout time, thus, due to that lack of knowledge it is possible that at this point *in vivo* animal models or more complex 3D models might provide a better insight on MSC angiogenic potential by incorporation into new blood vessels. Overall, as expected MSCs have lower ability to form tube structures compared to HUVEC and lower number of tube structures were formed in MSC and HUVEC co-culture indicating limitations of the potency assays and a not strong supportive and angiogenic potential through cell-to-cell contact and integration into tube structures. Therefore, the MSC angiogenic potential through paracrine action was subsequently evaluated.

3.1.3.2 Tube disruption assay

MSC paracrine action can be evaluated through the effect of its CM on promoting angiogenesis. Therefore, the feasibility of using a tube remodeling assay was assessed, in which tube disruption in HUVEC tubes would be caused by a chemical or mechanical stress and the potential angiogenic effect of MSC-CM in promoting tube remodeling would be evaluated.

Tube remodeling assay by mechanical scratch caused tube disruption, however, HUVEC were not able to remodel the tubes because the Matrigel layer was damaged. Addition of a new layer of Matrigel did not promote tube remodeling. Therefore, mechanical disruption was not pursued.

Chemical disruption of HUVEC tubes by DMSO was tested and then the tubes were allowed to remodel. First, 0.5% DMSO was incubated for 8 and 24 h after HUVEC tube structures were formed and preliminary results indicated that there was no disruption of the tubes. Then, DMSO was incubated for 90 min at different concentrations (2-100%) after seeding HUVEC at 78,125 cell/cm^2 and allowing for tube formation for 8 h. Tube disruption was imaged after 30 and 90 min DMSO incubation and remodeling was imaged after overnight (16 h) incubation with culture medium.

Preliminary results showed that DMSO at 2% in EGM-2 MV culture medium caused very small tube disruption after 30 min incubation and at the end of 90 min DMSO incubation the disruption did

not increase, in fact, the tubes had already remodeled (Figure 3.12 B and G). DMSO at 5% caused considerable tube disruption after 30 min incubation and after 90 min incubation with DMSO the disruption was still observed although it seemed that the cells were already aligning and remodeling (Figure 3.12 C and H). DMSO at 10% for 30 min caused complete disruption of tubes such that HUVEC were as single cell in the Matrigel layer and the tubes were still disrupted after 90 min DMSO incubation (Figure 3.12 D and I). Higher DMSO concentration than 10% up to 100% for 30 and 90 min caused significant cell death that was clearly observed by single cells in suspension, although some live cells still remained embedded in the Matrigel layer in a sprout shape (Figure 3.12 E and J). All the HUVEC challenged with DMSO at several concentrations were able to remodel after overnight incubation with culture medium (Figure 3.12 L, M, N and O), even the HUVEC subjected to 100% DMSO which formed thinner tubes (compared to the HUVEC control that was not subjected to DMSO, Figure 3.12 K) as much less cells were present due to cell death after DMSO incubation (Figure 3.12 O). Consequently, DMSO concentrations much higher than 10% should be avoided because of cell death; 5% DMSO in medium caused tube disruption, however, remodeling started still in the presence of DMSO; and 10% DMSO in medium caused full tube disruption that was still maintained to similar extent during DMSO incubation time, however, within one hour after DMSO removal the remodeling was already happening which indicates that the time window to observe remodeling might be too short to assess the impact of MSC-CM or MSC-EVs on promoting remodeling.

In one study, 1% DMSO incubated overnight caused 40% disruption in the tube structures formed by human aorta endothelial cells and 3% DMSO totally disrupted the tubes (Koizumi *et al.*, 2003). Herein, higher DMSO concentration was necessary to observe disruption of HUVEC tube structures and remodeling was observed still in the presence of 5% DMSO. This difference could potentially be explained by lower sensitivity of human aorta endothelial cells compared to HUVEC.

Broadwell and colleagues used 10 to 15% DMSO to open the blood-brain barrier of mice to be able to transport horseradish peroxidase to the brain which lasted for 2 h. It was also reported that the opening of the blood-brain barrier was reversible and morphology of endothelial cells or brain parenchyma was not altered (Broadwell *et al.*, 1982). The reversible effect of 10 to 15% DMSO on endothelial permeability after 2 h is to some extent in accordance with the range herein indicated of 10% DMSO for 90 min for tube disruption and remodeling started immediately after.

Therefore, tube disruption potency assays with 10-15% DMSO could be tested to evaluate the angiogenic effect of MSC-CM or MSC-EVs. An alternative to the tube disruption assay is to evaluate the MSC-CM angiogenic potential using the tube formation assay by incubating HUVEC with MSC-CM or MSC-EVs during tube formation in Matrigel. It was published that incubation of HUVEC with BM MSC-CM resulted in increased tube length (Wu *et al.*, 2007) and tube-like structures (Gruber *et al.*, 2005) compared to control medium.

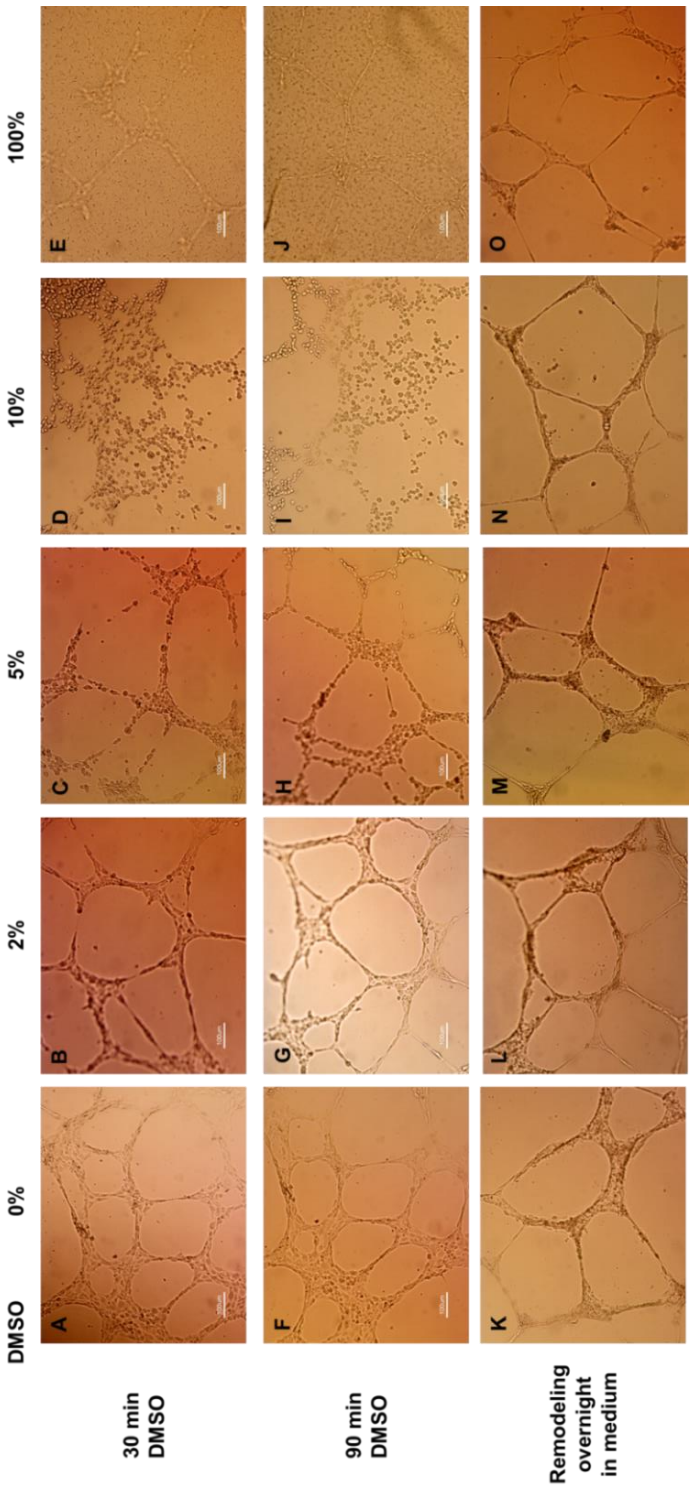

Figure 3.12 – HUVEC were able to remodel tube structures after tube disruption with DMSO, with total tube disruption occurring at 10% or higher DMSO concentration in medium. HUVEC were plated at 78,125 cell/cm^2 and incubated for 8 h in a Matrigel coated plate to allow tube formation, followed by DMSO (in %) challenge at different concentrations and incubated up to 90 min. HUVEC with medium only (0% DMSO) was used as control. After DMSO incubation, fresh medium was added and incubated overnight (for 16 h) to allow tube remodeling. A, B, C, D and E – HUVEC after 30 min incubation with DMSO at 0, 2, 5, 10, 100 % DMSO, respectively. F, G, H, I and J – HUVEC after 90 min incubation with DMSO at 0, 2, 5, 10, 100 % DMSO, respectively. K, L, M , N and O – tube remodeling of DMSO-challenged HUVEC after overnight incubation with HUVEC culture medium. N = 1. Scale bar 100 µm.

An additional potency assay to evaluate the regenerative potential of MSC-CM or MSC-EVs is the wound healing assay by mechanical scratch on a HUVEC monolayer, which will be described next.

3.1.3.3 Wound healing assay by mechanical scratch

The wound healing assay was designed and optimized to be a simple, reliable, reproducible and quantitative assay of the angiogenic response of HUVEC to MSC-CM. The wound healing assay consists of HUVEC seeding in a 96 WP, allowing cells to reach a confluent monolayer, and then a mechanical scratch is performed and the regenerative potential of MSC-CM is evaluated by quantifying HUVEC migration rate to close the wound. A mechanical scratch was preferred to the use of a device that blocks part of the well while seeding and culturing to form a monolayer followed by the removal of the device to evaluate migration, because it is intended to closer resemble the damage and consequent wound healing process and also because different cellular pathways might be activated in response to damage than in the case of migration only.

To optimize the wound assay by mechanical scratch, different sterile scraping tools were tested and the 200 µl pipette tips were selected for resulting in an adequate range of scratch width that was neither too small (in which closer of the scratch was too fast to be able to quantitatively measure HUVEC migration) neither too large (in which very long time would be needed to close the scratch). Consequently, to obtain reproducible and robust results only wounds with a initial width in the range between 120 and 280 µm were considered.

The MSC-CM collected were centrifuged and filtered prior to addition to the HUVEC wounds. Filtration was required to remove cell debris that were negatively affecting HUVEC migration as well as hindering scratch imaging. The downside of the filtration is the loss of biological molecules in the filter, however, low protein binding filters were used to minimize protein loss.

EGM-2 MV culture medium was used as positive control because it contains several growth factors and cytokines that are known to promote angiogenesis and proliferation such as VEGF, FGF, hydrocortisone, EGF, ascorbic acid and IGF. MSC culture medium containing FBS (DMEM+FBS) was used as negative control. The angiogenic potential of BM MSC donors M72A07 and M79A15 was evaluated using the wound assay by mechanical scratch. HUVEC migration rate was higher with statistical significance for EGM-2 MV culture medium and BM MSC-CM from M79A15 compared to MSC culture medium (Figure 3.13 A, Table 3.7). The time necessary for HUVEC to remodel and close the wound was also significantly lower for EGM-2 MV medium and BM MSC-CM M79A15 than for MSC culture medium (Figure 3.13 B, Table 3.7). BM MSC-CM from donor M72A07 tend to perform better in terms of migration rate and time to remodel than MSC culture medium, however, the difference is not statistically significant. The wound assay also shows that there are differences in the angiogenic potential between donors isolated from the same cell source under the same culture conditions, although only two donors were tested. In Figure 3.14 are representative images of the wounds for each condition along time and it is possible to confirm the amount of time needed to close the wound and well as initial width of the scratch present in Table 3.7.

Of note, that the angiogenic assay of tube incorporation indicates that BM MSC donor M72A07 might have higher angiogenic potential, while the wound assay indicates that BM MSC-CM from donor M79A15 had higher angiogenic potential. Due to assay limitation further testing of tube incorporation assay would be needed to confirm results, however, this result could also indicate that some donors might have stronger effect through cell-to-cell contact and others by paracrine action.

Moreover, the optimized wound healing potency assay could be broadly used to screen the angiogenic potential of CM or EVs from donors from the same cell source, but also from different cell sources and culture conditions, for instance, cells grown in 2D and 3D systems or cultured under normoxia and hypoxia. It would also be interesting to analyze the MSC-CM from the two donors, for instance, VEGF and other growth factor's concentration by ELISA, to decipher the mechanisms of action and determine which factors have a relevant role on MSC angiogenic potential.

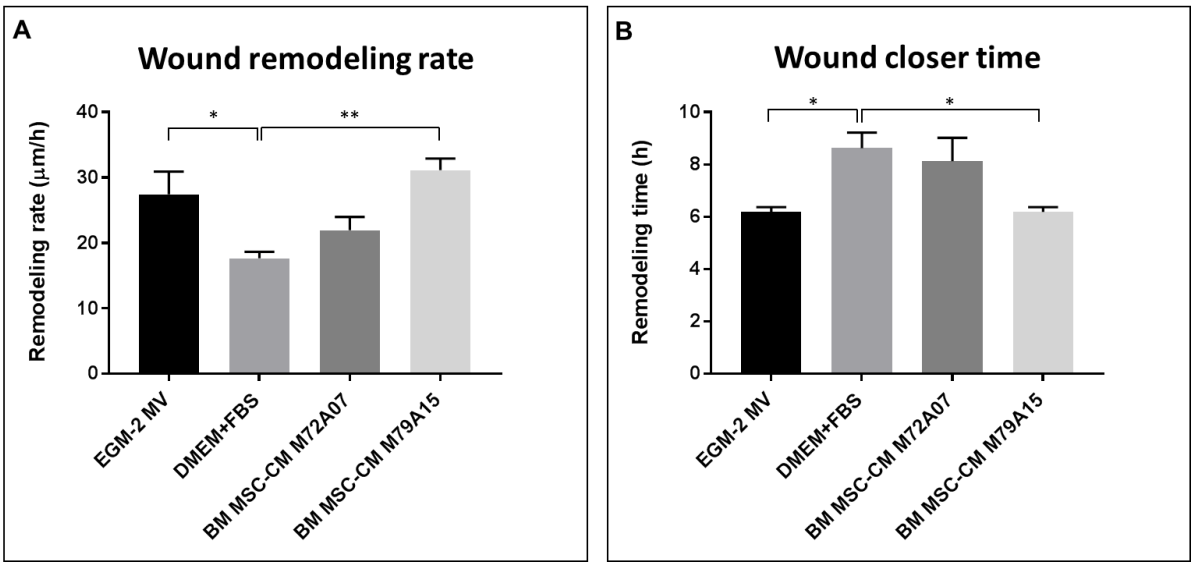

Figure 3.13 – Wound healing assay with HUVEC monolayer disrupted by mechanical scratch showed that bone marrow MSC-conditioned media (BM MSC-CM) have angiogenic potential enhancing remodeling rate and decreasing the time necessary to close the wound, despite of donor variability between BM MSC M72A07 and M79A15. EGM-2 MV culture medium was used as positive control and MSC culture medium supplemented with serum (DMEM+FBS) the negative control. A – Wound remodeling rate (in µm/h) of BM MSC-CM from donor M79A15 was comparable to positive control EGM-2 MV medium and higher than negative control DMEM+FBS. B – Remodeling time (in h) necessary for HUVEC migration and wound closer was lower for BM MSC-CM from donor M79A15 and the positive control EGM-2 MV medium compared to the negative control DMEM+FBS. N = 4, *P value < 0.05, One-way ANOVA with Tukey correction. Error bars represent the standard error of the mean.

Table 3.7 – Bone marrow MSC conditioned medium (BM MSC-CM) from donors M79A15 and M72A07 showed angiogenic potential enhancing HUVEC migration on HUVEC wound healing assay by mechanical scratch. EGM-2 MV culture medium was used as positive control and MSC culture medium supplemented with serum (DMEM+FBS) the negative control. Hourly evaluation of wound widths allowed the determination of the initial width range (in µm), remodeling time (in h) for wound closure and remodeling rate (in µm/h). Data is represented by the mean and standard error of the mean, N = 4.

Medium	Average Initial Width range (µm)	Average Remodeling Time to close wound (h)	Average Remodeling rate (µm/h)
EGM-2 MV	229 $\pm$ 41	6.2 $\pm$ 0.3	27 $\pm$ 6
DMEM + FBS	207 $\pm$ 27	9 $\pm$ 1	18 $\pm$ 2
BM MSC-CM M72A07	202 $\pm$ 49	8 $\pm$ 2	22 $\pm$ 4
BM MSC-CM M79A15	233 $\pm$ 12	6.2 $\pm$ 0.3	31 $\pm$ 3

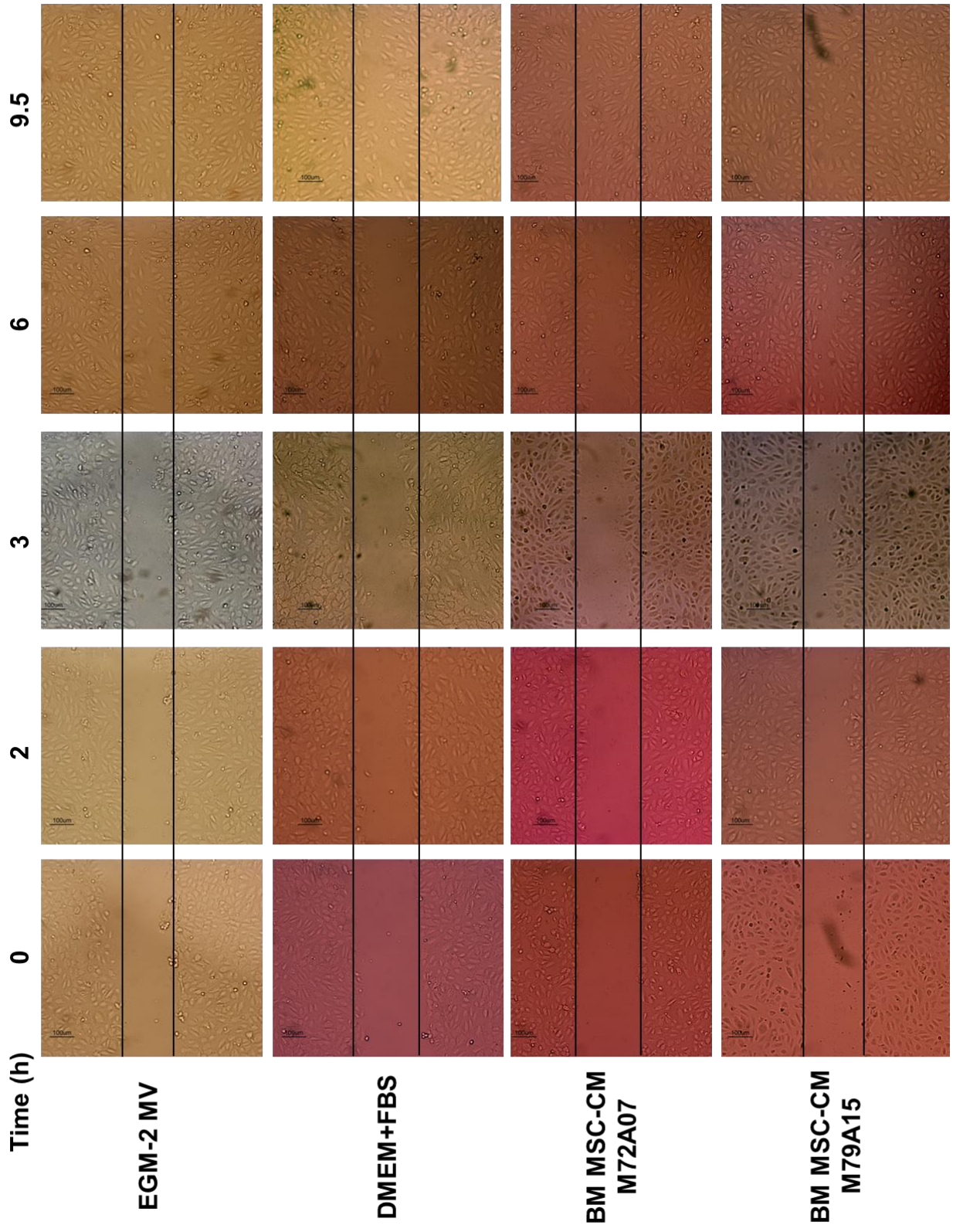

Figure 3.14 – Bone marrow MSC conditioned medium (BM MSC-CM) from donors M79A15 and M72A07 showed angiogenic potential enhancing HUVEC migration on HUVEC wound healing assay by mechanical scratch. Contrast phase microscopy images showed enhanced HUVEC migration throughout time (0-9.5 h, from bottom to top) for BM MSC-CM M79A15 and the positive control EGM-2 MV culture medium compared to the negative control MSC culture medium (DMEM+FBS). Scale bar 100 µm.

It was reported that UCM MSC-CM promoted the migration of the endothelial cells during wound healing after mechanical scratch and closed the wound faster than the control with growth medium (Arutyunyan *et al.*, 2016). Moreover, it was observed that UCM MSC-CM induced higher migration of HUVEC, fibroblasts and UCM MSC in a wound scratch assay compared to DMEM medium (Shen *et al.*, 2015).

Lin and co-workers reported that MSC-CM from UCM, BM, skeletal muscle and myocardium were able to promote proliferation and migration of endothelial colony forming cells as well as to promote tube formation of endothelial colony forming cells when compared to basal medium. Moreover, CM angiogenic properties were similar to the effect of culture medium supplemented with VEGF and bFGF (Lin *et al.*, 2012).

Despite differences in the protocols used, the herein results of increased angiogenic potential of BM MSC-CM are in accordance with published data from Shen (Shen *et al.*, 2015) and Lin (Lin *et al.*, 2012) studies. Setting a standardized and robust wound healing assay is important for direct comparison with other works, however, there are many differences in published work in terms of CM (isolation, purification and concentration, storage and percentage of CM added for wound healing assay), wound healing protocol (coating, cell types used, incubation time to assess migration) and controls used (culture medium controls, growth factors and cytokines, control cell type).

Regarding the cell types, for a more complete analysis of the MSC-CM or MSC-EV angiogenic potential on the wound healing assay by mechanical scratch, besides using HUVEC, the migration rate of the skin cell types dermal fibroblasts and keratinocytes could also be evaluated using the optimized protocol herein. For instance, Walter and colleagues evaluated the effect of BM MSC-CM using the wound healing assay with dermal fibroblasts and keratinocytes and observed increased migration compared to control (Walter *et al.*, 2010).

Besides being used to evaluate MSC-CM and MSC-EV angiogenic potential, this assay can also be used to test different culture conditions, cell sources and bioengineering strategies to boost MSC-CM and MSC-EV regenerative properties.

4 Conclusions and future work

MSCs were successfully isolated from different cell sources. BM, AT and UCM MSCs have similar morphology (spindle-shaped, triangular shaped and fibroblastic like morphology), immunophenotype ($CD73^+$, $CD90^+$, $CD105^+$, $CD14^-$, $CD19^-$, $CD31^-$, $CD34^-$, $CD45^-$, $CD80^-$, $HLA\text{-}DR^-$) and multilineage differentiation potential (adipogenic, osteogenic and chondrogenic differentiation potential) as expected for MSCs and defined by the International Society for Cellular Therapy.

For the set of donors used, AT and UCM MSCs seem to be more proliferative than BM MSCs. This conclusion cannot be extended for all cases without a direct comparison of cell sources isolated from the same donor.

There is lack of robust and standardized platforms to evaluate MSC and MSC-CM regenerative potential which leads to conflicting results of published works. Therefore, angiogenic, wound healing and oxidative stress potency assays were under development.

Two oxidative stress potency assays were under development. One as adherent cultures, in which cells are seeded at 10,500 cell/cm^2 (39,900 cells) in a 12 WP and incubated for 17 h, after that time the cell number of adherent cells is assessed and 5 x 10^{-11} mol H_2O_2 per cell are incubated for 1 h. Then, cells in the supernatant and adherent cells are pooled and stained with Annexin V and PI to measure total cell death by flow cytometry. The second protocol as suspension cultures comprised the detachment of cells from tissue culture flasks and incubation of 39,900 cells for 1 h in ultra-low attachment 24 WP with 1-5 x 10^{-11} mol H_2O_2 per cell, followed by staining with Annexin V and PI to measure total cell death by flow cytometry. Further optimization of the number of moles of H_2O_2 per cell in suspension cultures should be performed by testing it for different MSC donors and cell sources.

MSC angiogenic potential was assessed using several potency assays developed. For the tube formation assay, optimal HUVEC seeding density was 78,125 cell/cm^2 and an incubation time in Matrigel of 8 h and for MSCs a seeding density of 31,250 cell/cm^2 in Matrigel, however, due to donor-to-donor variability it is necessary to evaluate tube formation at several time points throughout time, especially in early time points (1-5 h after seeding). For tube incorporation assay, a ratio of MSC to HUVEC of 1:4 upon seeding on Matrigel was used and several time points throughout time should be evaluated as for MSC tube formation assay due to donor-to-donor variability and lack of stability of the tube-like structures. Instead of seeding MSCs and HUVEC at the same time, MSCs could be added at a later time point and stabilization of tube structures evaluated, however, in this case the potency assay might last several days which is not in accordance with an envisioned quick potency assay. Thus, the observed angiogenic potential of MSCs through cell-to-cell contact and tube integration was not strong.

The tube disruption assay developed consists of seeding HUVEC according to tube formation assay, then tube disruption is caused by 10-15% DMSO during 90 min incubation, followed by washing and addition of MSC-CM to evaluate its effect on the rate of tube remodeling.

The wound healing potency assay by mechanical scratch with a 200 µl pipette tip in a HUVEC monolayer was optimized and the effect of MSC-CM on the rate of cell migration and time to remodel and close the wound was evaluated. MSC-CM was centrifuged and filtered with low protein binding

filters before addition of 100% of MSC-CM to the HUVEC wounds. The wound healing assay allowed the detection of donor-to-donor variability between two BM MSC donors. Moreover, BM MSC-CM from donor M79A15 promoted higher HUVEC migration and resulted in lower time for wound closer when compared to MSC culture medium only and had similar effect to EGM-2 MV culture medium (which contains several growth factors that promote proliferation, migration and vascularization). Therefore, indicating that MSCs can exert a strong angiogenic effect through paracrine action and also that the optimized wound potency assay could be broadly used to screen the angiogenic potential of CM from different donors and cell sources and from cells cultured under different conditions and systems as well as to test MSC-EV angiogenic potential.

In a context of a therapy with MSCs and MSC-derived products, the development of potency assays that allow evaluating the angiogenic potential, wound healing, pro-survival and anti-apoptotic potential as well as the resistance of the expanded cells to oxidative stress will be very helpful to screen MSC donors and select out donors with lower potency and also on selecting the more appropriate cell source, culture conditions and culture system and to test bioengineering strategies to boost efficacy of the treatment (MSC, MSC-CM, MSC-EV) according to the therapeutic application. In the future, the potency assays that were not fully optimized yet, should be optimized as suggested previously, so that it will be possible to build a standardized and robust platform of potency assays to evaluate the different MSC, MSC-CM and MSC-EV regenerative properties for any set of desired conditions to test.

Part B

5 Materials and Methods

5.1 Materials

Cell handling was performed using aseptic conditions and sterile materials.

Human BM MSCs from donors RB55, RB70/RB135 and RB81 were purchased from RoosterBio. MSC donors RB55 and RB81 were isolated from males aged between 18-30 years old. MSC donors RB70 and RB135 were obtained from two isolations from the same female donor aged between 18-30 years old. Human BM MSC donors 305526, 305526 and 318006 were purchased from Lonza. MSC donor 305526 was isolated from a female with 22 years old. MSC donor 494678 was isolated from a male aged 21 years old. And MSC donor 318006 was isolated from a male with 27 years old. Human hTERT immortalized adipose derived MSCs was acquired from ATCC and it was isolated from a female donor.

MSCs were expanded and cultured in Full CTS StemPro MSC Serum-free medium kit (Thermo Fisher Scientific) in T-flasks coated with CTS CELLstart Substrate (Thermo Fisher Scientific). Full StemPro was prepared by combining 75 ml StemPro supplement, 6 ml L-Glutamine 200 mM (Thermo Fisher Scientific), 6 ml Penicillin-Streptomycin (Pen 10,000 U/ml, Strep 10,000 µg/ml, Thermo Fisher Scientific) and 500 ml basal medium. Culture media was filtered with 0.22 µm vacuum filter systems (Corning) and stored at 4ºC. CELLstart was dil 1:100 in 1X PBS +/+ (prepared from UltraPure DNase/RNase-Free Distilled Water from Thermo Fisher Scientific and PBS +/+ (10X) pH 7.4 from Thermo Fisher Scientific). CELLstart was stored at 4ºC and reused a maximum of 5 times.

HUVEC pooled P1017 isolated in EGM-2 medium was purchased from Lonza. HUVEC were expanded in Expansion Medium (EM) and cultured in EM, Flow Medium (FM) or Maintenance Medium (MM) on plate, transwell and on microfluidic systems. EM was composed of EBM-2 basal medium (Lonza) and full EGM-2 SingleQuot Kit Supplement & Growth Factors (Lonza) including FBS at a final concentration of 2%. FM was prepared by adding EGM-2 SingleQuot kit to EBM-2 basal medium, however, FBS final concentration was 0.5%. MM was composed of EBM-2 basal medium with 0.5% FBS. Culture media was filtered with 0.22 µm vacuum filter systems and stored at 4ºC.

The 2D cell culture surfaces for HUVEC culture were coated with 0.1% gelatin. Gelatin solution Type B 2% (Sigma-Aldrich) was diluted in water to 0.1%, filtered with Steriflip-GP 0.22 µm (Merck) and appropriate volume was added to cell culture surfaces and incubated at 37ºC and 5% CO_2 for 30 min.

HUVEC were challenged with TNF-α (Peprotech) and IFN-γ (Peprotech). TNF-α and IFN-γ were centrifuged, reconstituted in deionized water, allowed to sit at room temperature for 2 h, further

diluted with MM and aliquots were stored at -80ºC. After thawing and using the required volume of the cytokines, the aliquots were discarded.

THP-1 human acute monocytic leukemia cell line was purchased from ATCC. THP-1 culture medium was composed of 500 ml RPMI 1640 (Thermo Fisher Scientific) supplemented with 50 ml heat inactivated FBS (Thermo Fisher Scientific), 5 ml Pen/Strep and 2 µl 2-mercaptoethanol (Sigma-Aldrich). Culture media was filtered with 0.22 µm vacuum filter systems and stored at 4ºC.

3D inflammation *in vitro* models mimicking the air-liquid interface in the lung alveolus were developed using a transwell system and a microfluidic device to assess MSC-EV immunomodulatory potential. The vascular side of the alveolus was mimicked by HUVEC and the epithelial side by human lung carcinoma epithelial A549 cell line. The human lung carcinoma epithelial A549 cell line was purchased from ATCC and cultured in DMEM/F-12, HEPES, no phenol red (Thermo Fisher Scientific) with 10% heat inactivated FBS and 1% Pen/Strep. Culture media was filtered with 0.22 µm vacuum filter systems and stored at 4ºC.

5.1.1 MSC culture

Cell culture surfaces were coated with CELLstart and incubated for 1-2 h at 37°C. Cells were partially thawed inside the cryovials (Thermo Fisher Scientific) in the 37°C water bath and transferred to a falcon tube (Corning) containing pre-warmed full StemPro medium. Cells were centrifuged at 300 RCF for 5 min (Eppendorf 5810 R) and resuspended in pre-warmed full StemPro medium. Cell number and viability were assessed with the dye trypan blue 0.1% (Thermo Fisher Scientific) and a haemocytometer.

After coating, CELLstart was removed. Cell suspension was further diluted according to desired cell seeding density (3,000-5,000 cell/cm^2) and viability and incubated at 37°C and 5% CO_2. Medium change was performed one day after to remove dead cells in suspension and then every 3-4 days.

For passaging, cells were washed with PBS -/- (Thermo Fisher Scientific) and incubated with 0.05% trypsin-EDTA (Thermo Fisher Scientific) for 2-3 min at 37ºC and 5% CO_2 to detach cells. Cell suspension was collected to a quenching solution with full StemPro medium or medium diluted in PBS in a 2:1 ratio to trypsin solution. Cells were centrifuged at 300 RCF for 5 min and resuspended in pre-warmed full StemPro medium. After cell counting, cells were re-seeded at 3,000-5,000 cell/cm^2 in CELLstart pre-coated T-flasks and incubated at 37°C and 5% CO_2.

For freezing, cells were centrifuged and resuspended in the appropriate volume of CryoStor Cell Preservation Media CS5 (Thermo Fisher Scientific) on ice. Cryovials were stored in freezing containers at -80°C freezer overnight to avoid crystal formation by freezing at a rate of 1ºC per minute and then transferred to the liquid nitrogen tank.

5.1.2 MSC-EV isolation

MSC-EVs were isolated from MSCs at passage 3 to 6. Per passage, 1 to 3 EV isolations from the CM could be performed, starting when cells reached at least 50% confluency and then collecting every 3 days.

The CM was collected to falcon tubes and centrifuged at 500 RCF for 10 min at 4ºC to pellet cells (Figure 5.1). The supernatant was transferred to new 50 ml tubes and centrifuged at 2,000 RCF for 20 min at 4ºC to pellet dead cells and cell debris. The supernatant was again centrifuged at 2,000 RCF for 20 min at 4ºC to pellet cell debris, apoptotic bodies and larger microvesicles. The supernatant was then transferred to new falcon tubes and EVs were immediately isolated by UC or stored at 4ºC up to one day before UC.

Open-Top Thinwall Polyallomer Tube for Ultracentrifugation of 38.5 ml and 5 ml (Beckman Coulter) were used for the 1st and 2nd UC, respectively. The UC tubes were washed with 70% ethanol and cold 1x RNase-Free PBS. 1x RNase-Free PBS was prepared by diluting 10x RNase-Free PBS (Thermo Fisher Scientific) in Ultrapure Water and stored at 4ºC.

Supernatants were transferred to 38.5 ml UC tubes making sure weight of tubes inside UC buckets across each other are equal or have less than 0.1 g of difference. The first UC (Beckman Coulter Optima XPN-80) was performed at 100,000 RCF, 4ºC for 1 h 10 min using the rotor SW28 or SW32Ti. Supernatant was aspirated at the air-liquid interface with a glass pipette attached to the vacuum leaving just enough media to cover tube bottom. EVs were resuspended in cold 1x RNase-Free PBS, avoiding bubbles, and transferred to the 5 ml UC tubes. Remaining EVs were collected by a second addition of 1x RNase-Free PBS and it was added to the respective 5 ml UC tubes. Samples were centrifuged at 29,000 rotations per minute (about 100,000 RCF), 4ºC for 1 h 10 min using the rotor SW55Ti. Supernatants were aspirated at the air-liquid interface, and EVs were resuspended with cold 1x RNase-Free PBS and transferred to an Eppendorf Protein Lobind Tube 0.5 ml (Eppendorf) previously sterilized by autoclave.

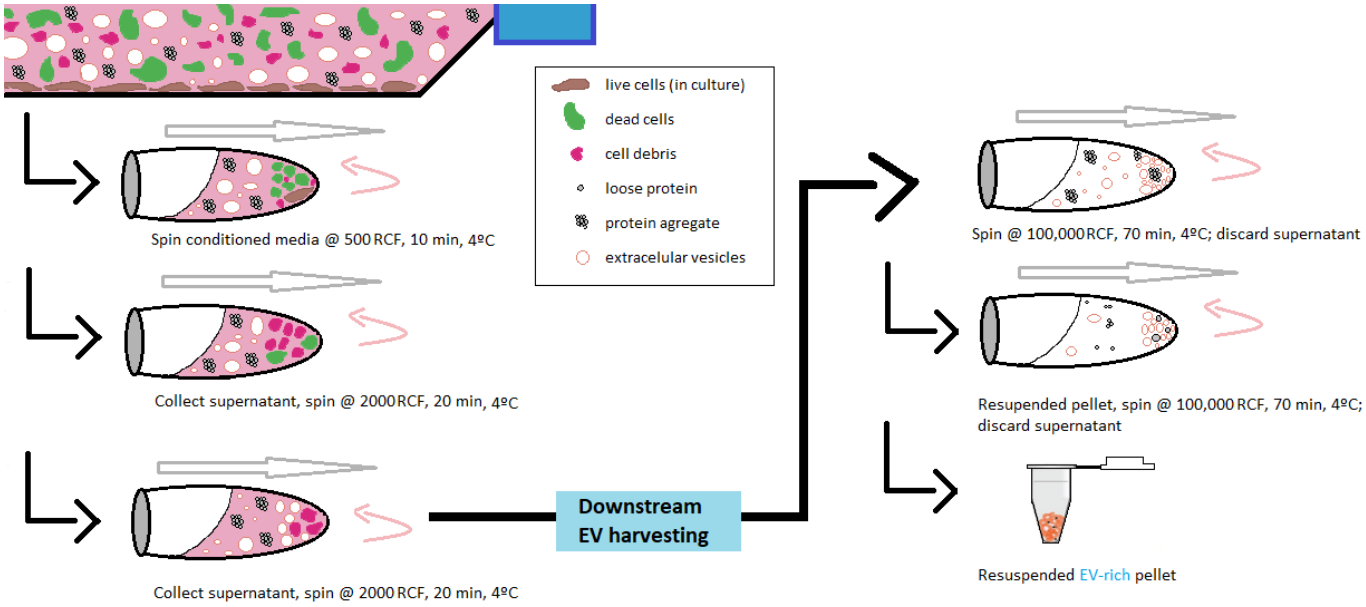

Figure 5.1 – Schematic representation of extracellular vesicle (EV) isolation method by ultracentrifugation.

On ice, samples for EV characterization by nanoparticle tracking analysis and MicroBCA were prepared as well as EV aliquots in Eppendorfs Protein LoBind and all were stored at -80ºC with or without freezing containers. For EV characterization by nanoparticle tracking analysis, EV solution was dil 1:200 in PBS and for EV characterization by MicroBCA, EV solution was dil 1:10 in PBS.

In general, EVs from different isolations of the same donor were pooled by mixing prior to aliquoting and sampling for EV characterization.

5.1.3 MicroBCA

MicroBCA was performed following manufacturer guidelines. Briefly, EV samples were thawed on ice. BSA standards were prepared by diluting the BSA stock at 2 mg/ml provided in the Pierce MicroBCA Protein Assay Kit (Thermo Fisher Scientific) in PBS -/-. Then, samples and standards were added to a 96 flat WP (Corning) and mixed with equal volume of reagent solution. Reagent solution was prepared by combining 50% of A, 48% of B, and 2% of C. The plate was agitated for 30 sec and incubated 2 h at 37ºC. Absorbance was measured at 562 nm in the plate reader (BioTek Synergy NEO, software Gen5 version 2.09).

To calculate protein concentration in EV samples, the absorbance of the blank was subtracted to all the samples and standards, a linear plot of absorbance and concentration of the standards was created and its linear equation was used to calculate the protein concentration of the samples. The actual protein concentration of the EV samples was obtained by multiplying the sample concentration by the dilution factor.

5.1.4 Nanoparticle Tracking Analysis

Nanoparticle tracking analysis was performed using NanoSight NS300 (Malvern Instruments) and the software NanoSight 3.1.

EV samples for NanoSight characterization were thawed on ice or at 4ºC. NanoSight was cleaned with Ultrapure water and 70% ethanol setting camera level to the maximum, before reading the samples.

For sample reading, about 0.6 ml of 1ml sample was injected and the camera level adjusted to appropriate setting (camera level was decreased until dark sign appeared and then increased 2 levels). Camera level was the same for all samples read in the same day and for samples that would be compared.

EV quantification was performed using a Non-Fluorescent Vesicles protocol that captured 3 videos of 60 sec at 20ºC with stable and constant speed of sample infusion. To analyze the videos in the software, the screen gain and detection threshold was set and the same settings were applied to all samples read. The choice of detection threshold should be to reduce the number of false positives and increase the number of true positives. The analysis of the 3 videos by the software allowed determining size distribution and average size as well as particle concentration.

Between samples, NanoSight was cleaned by one injection of Ultrapure water followed by one injection of 70% ethanol and 3 more of Ultrapure water.

To calculate the Protein to Particle Ratio (PPR, in fg of protein per particle number) the Equation 5 was used after obtaining the protein concentration by MicroBCA and the particle concentration determined by nanoparticle tracking analysis.

$$PPR\ (\frac{fg\ of\ protein}{particle}) = \frac{Protein\ concentration\ by\ MicroBCA\ (\frac{g}{ml})}{Particle\ concentration\ by\ NanoSight\ (\frac{particle}{ml})} \times 10^{15} fg/g$$

Equation 5 – Protein to particle ratio (in fg of protein per number of particles) is the ratio between protein concentration (in g/ml) and particle concentration (in particle/ml).

5.1.5 HUVEC culture

Cell culture surfaces were coated with 0.1% gelatin and incubate for 30 min at 37°C. Cells were thawed at 37ºC water bath and transferred into a falcon tube containing pre-warmed EM (5 ml per thawed cryovial). Cells were centrifuged at 200 RCF for 5 min and resuspended in pre-warmed EM. Cell number and viability were assessed using trypan blue 0.1% and a haemocytometer. The coating was aspirated and cell suspension was plated at a cell seeding density of 5,000-10,000 cell/cm^2 and incubated at 37°C and 5% CO_2. Medium was changed every 2 days.

HUVEC were passaged when reaching about 90% confluency by aspirating medium, washing with PBS -/- and detaching cells by incubation with accutase cell detachment solution (Innovative Cell Technologies) for 2 min at 37°C and 5% CO_2. Cell suspension was centrifuged, resuspended in EM, cell number was counted and HUVEC seeded in pre-coated cell culture surfaces. HUVEC were used up to passage 6.

For freezing, HUVEC were resuspended in freezing solution composed of 10% DMSO in EM. The cryovials were stored in freezing containers at -80ºC overnight and then transferred to liquid nitrogen tanks.

5.1.6 HUVEC Potency assay

Coating of 96 flat WP was performed with 0.1% gelatin. HUVEC were detached from T-flasks (Thermo Fisher Scientific), centrifuged, resuspended in EM and the cell number determined. Gelatin was aspirated and HUVEC seeded at 62,500 cell/cm^2 (20,000 cell per well). Triplicates per condition were plated avoiding edges (filled with PBS -/-) and the plate was incubated at 37ºC and 5% CO_2. One day after, the medium was changed to MM and incubated for 24 h. Afterwards, HUVEC were incubated with 10 ng/ml TNF-α and 10^9 EV/ml from desired conditions for 16 h at 37ºC and 5% CO_2. EV solutions were prepared in Eppendorf Protein LoBind tubes, total PBS volume was normalized between samples and it was not higher than 10% of the culture medium. EVs were slowly thawed on ice at 4ºC.

After incubation, the supernatants were collected, centrifuged at 500 RCF for 5 min, transferred to a new 96 flat WP and store at -80ºC. Concentration of the inflammatory cytokine IL-8 in the supernatants was measured by ELISA (see chapter 5.1.11). HUVEC were stained for flow cytometry (see chapter 5.1.7) or used for immunohistochemistry (see chapter 5.1.8).

5.1.7 HUVEC staining for Flow Cytometry

The expression of the surface markers ICAM-1 (APC Mouse Anti-Human CD54, Clone HA58) and VCAM-1 (PE Mouse Anti-Human CD106, Clone 51-10C9) was evaluated by flow cytometry. APC Mouse IgG1 κ Isotype Control, Clone MOPC-21, and PE Mouse IgG1 κ Isotype Control, Clone MOPC-21, were used as isotype controls. All antibodies for flow cytometry were acquired from BD Biosciences.

To analyze HUVEC by flow cytometry, HUVEC were washed, detached with accutase and transferred to 96 round WP (Corning) or flow cytometry tubes (BD Biosciences). Remaining cells were collected with cold staining buffer and transferred to the respective wells in the 96 round WP or tube. Staining buffer was composed of PBS with 0.5% BSA (Sigma-Aldrich) and 2 mM EDTA (Thermo Fisher Scientific). Samples were centrifuged at 500 RCF for 5 min and incubated for 30 min at 4ºC in the dark with antibody master mix, isotype master mix or staining buffer only. The master mixes were composed of Human Fc Blocking reagent (Miltenyi Biotec) dil 1:20, antibodies or isotype controls dil 1:20, mouse serum (Jackson ImmunoResearch) dil 1:20 in staining buffer. The unstained sample was also used as control. After incubation, staining buffer was added and cells were centrifuged and resuspended in 1% PFA (Electron Microscopy Sciences) in PBS to fix cells. Samples were stored at 4°C covered in foil. Within one week, the expression of ICAM-1 and VCAM-1 was measured with a flow cytometer equipment. Prior to analysis, the samples were centrifuged and resuspended in staining buffer. At least 10,000 events per sample were analyzed in the flow cytometer (BD LSRFortessa, software FlowJo Version 10).

5.1.8 HUVEC staining for Immunohistochemistry analysis

For immunohistochemistry, the cells were washed with PBS +/+ (Thermo Fisher Scientific), fixed with 4% PFA for 15 min, followed by 3 washes. Cells were permeabilized with 0.1% Triton X-100 (Sigma-Aldrich) in PBS +/+ for 5 min and washed again 3 times. Blocking with PBDT was performed for 1 h. PBDT was composed of 5% donkey serum (Jackson ImmunoResearch) and 0.01% Triton X-100 in PBS +/+. Primary antibodies mouse monoclonal ICAM-1 My13 (Thermo Fisher Scientific) dil 1:300, rabbit monoclonal VCAM-1 EPR5047 (Abcam) dil 1:200 or mouse monoclonal VE-cadherin (BD Biosciences) dil 1:200 in PBDT were incubated overnight at 4ºC (or 4 h at room temperature) covered in foil. After 3 washes, secondary antibodies Alexa Fluor Donkey Anti-rabbit 647 nm (Thermo Fisher Scientific) dil 1:500 and Alexa Fluor Donkey Anti-mouse 488 nm (Thermo Fisher Scientific) dil 1:500 in PBDT were added and incubated for 1 h at room temperature. Cells were washed 3 times, followed by 10 min incubation at room temperature with Hoechst 33342 (Thermo Fisher Scientific) dil 1:1000 in deionized water. Then, 3 washes were performed and samples stored at 4ºC. One additional washing was performed prior to imaging using the confocal microscope (Zeiss TIRF/ LSM 710 confocal, software Zen Black).

5.1.9 THP-1 culture

THP-1 cells were thawed in a 37ºC water bath and transferred into a falcon tube containing pre-warmed THP-1 culture medium. The cells were centrifuged at 200 RCF for 5 min and resuspended in medium. Cell number and viability were assessed with a haemocytometer and trypan blue 0.1% and cells were seeded at 200,000-500,000 cells/ml. THP-1 cells were incubated in a T-flask cultured at upright position at 37ºC and 5% CO_2.

Every 2 days, cell suspension was mixed gently with a serological pipette before sampling for cell counting. Small medium additions were performed according to cell growth until cells reached a concentration of 800,000 to 1,000,000 cell/ml. When that cell density was reached, cells were passaged by collecting cell suspension, centrifuging at 200 RCF for 5 min, resuspending in medium and incubating cells at 200,000-500,000 cells/ml upright position at 37ºC and 5% CO_2.

For freezing, THP-1 cells were centrifuged and resuspended in appropriate volume of freezing medium (1 ml per cryovial) composed of 5% DMSO in THP-1 culture medium. Cryovials were placed in a freezing container at -80°C overnight and then transfer to a liquid nitrogen tank.

5.1.10 THP-1 Potency Assay

THP-1 cells were collected as previously described (chapter 5.1.9). THP-1 cells were challenged with lipopolysaccharide (LPS) from *Escherichia coli* O111:B4 (Sigma-Aldrich) at a final concentration of 100 ng/ml in THP-1 culture medium. LPS aliquots were discarded after use. Dexamethasone (Sigma-Aldrich) was used as a positive control at final concentration 1 µM in THP-1

culture medium. EVs were thawed slowly on ice at 4ºC and added to the plate at a final concentration of 10^9 EV/ml.

First, 100,000 THP-1 cell per well were seeded in 96 round WP (in half of the total volume per well) in triplicates per condition avoiding edges (filled with PBS). For untreated control, THP-1 culture medium was added. For LPS control, it was added THP-1 culture medium (in a quarter of the total volume of the well) and 4x concentrated LPS solution (in a quarter of the total volume of the well). For EV conditions, it was added 4x concentrated EV solutions (in a quarter of the total volume of the well) and 4x concentrated LPS solution (in a quarter of the total volume of the well). Moreover, the total volume of PBS per EV condition was normalized between different MSC-EV donors and it was not higher than about 10% of the culture medium. For positive control, it was added a 4x concentrated dexamethasone solution (in a quarter of the total volume of the well) and 4x concentrated LPS solution (in a quarter of the total volume of the well). Plates were incubated for 24 h at 37°C and 5% CO_2. After incubation, the plates were centrifuged at 500 RCF for 5 min, the supernatants collected and stored at -80°C. Concentration of the inflammatory cytokine TNF-α in the supernatants was measured by ELISA (see chapter 5.1.11).

5.1.11 ELISA

ELISA protocol was performed following manufacturer's guidelines and using the DuoSet ELISA Ancillary Reagent Kit (R&D systems), Human IL-8/CXCL8 DuoSet ELISA (R&D systems) and Human TNF-α DuoSet ELISA kits (R&D systems). In brief, ELISA plates were coated overnight with Capture Antibody in PBS at 4 ng/ml. The next day, 3 washes with washing buffer dil 1:25 in water were performed. Blocking buffer was incubated for 1 h and it was composed of Reagent Diluent dil 1:10 in water. Blocking was followed by 3 washes and incubation of samples for 2 h. For IL-8 ELISA, samples and standards were diluted in Reagent Diluent dil 1:2 or 1:40 in 0.05% Tween-20 (VWR) TBS (1x, Teknova); for TNF-α ELISA, samples and standards were diluted in Reagent Diluent dil 1:2 in water. Then, 3 washes were performed and Detection antibody was incubated for 2 h at dil 1:60 in Reagent Diluent dil 1:10 in 0.05% Tween-20 TBS (1x) for IL-8 or in Reagent Diluent dil 1:10 in water for TNF-α. The washing steps were repeated and Streptavidin was incubated for 20 min at dil 1:40 in Reagent Diluent dil 1:10 in 0.05% Tween-20 TBS (1x) for IL-8 or in Reagent Diluent dil 1:10 in water for TNF-α. The plates were washed again 3 times, incubated with Substrate solution for 10-20 min (1 Color reagent A: 1 Color reagent B) light protected and reaction was stopped with addiction of Stop solution. The plate was gently taped and absorbance read at 450, 540, 570 nm using the plate reader.

5.1.12 A549 culture

Cryovials with A549 cells were thawed in the 37°C water bath and transferred to a falcon tube containing pre-warmed A549 culture medium. Cells were centrifuged at 250 RCF for 5 min and resuspended in pre-warmed A549 medium. Cell number and viability were determined using trypan blue 0.1% and a haemocytometer and cells were seeded at about 6,000 cell/cm^2 and incubated at 37ºC and 5% CO_2. Medium was changed every 2 days. When reaching about 90% confluency, cells

were washed with PBS -/-, detached with accutase for 3-5 min at 37ºC and 5% CO_2 and centrifuged at 250 RCF for 5 min. After centrifugation, cells were resuspended in A549 medium and seeded in new T-flasks at about 6,000 cell/cm^2.

To freeze cells, after centrifugation, cells were resuspended in 5% DMSO in A549 medium and stored in a freezing container at -80ºC overnight and then transferred to a liquid nitrogen tank.

5.1.13 Lung alveolus inflammation on 3D transwell model

To mimic the air-liquid interface of the lung alveolus, the epithelial cell line A549 was seeded on the top of the insert and the endothelial cell line HUVEC was seeded on the under-membrane of the insert of Polyester Membrane Transwell-Clear Inserts (Corning) with 6.5 mm membrane diameter, 0.4 µm membrane pore size and 0.33 cm^2 growth surface area.

The transwell inserts were coated with 10 µg/ml Fibronectin from bovine plasma (MP Biomedicals) and 10 µg/ml Collagen Type I from rat tail tendon (Corning) in PBS -/- for 45 min in each side of the transwell membrane. HUVEC at passage 4 were detached form T-flasks (as described in chapter 5.1.5), resuspended in EM and seeded at 150,000 cell per insert. The inserts placed upside down in a Petri dish (Corning) were incubated for 1 h at 37ºC and 5% CO_2. After cell adhesion, pre-warmed EM was added to the 24 WP and inserts were transferred to the 24 WP. A549 cells at passage 4 were detached (as described in chapter 5.1.12), 90,000 cell were seeded on top of each insert and plates were incubated 37ºC and 5% CO_2.

The next day, medium change was performed. Then during two days, A549 cells were treated with 1 µM Dexamethasone in A549 medium and FM was added to the HUVEC chamber. To further differentiate epithelial cells, air-liquid interface was established by removing the supernatant on the top of the insert and reducing the height of the FM in the bottom chamber to the membrane level. Air-liquid interface between A549 and HUVEC was then kept for additional 3 days changing the FM on the bottom of insert daily. Cells were starved for 24 h, by addiction of MM to the bottom of the insert, keeping the air-liquid interface. Then, alveolus transwell model was challenged for 24 h with inflammatory molecules such as TNF-α and IFN-γ and co-treated with MSC-EVs, MSC-CM or indirect co-culture with MSCs.

Barrier function (see chapter 5.1.15), cell death (see chapter 5.1.16), IL-8 secretion (see chapter 5.1.11) and VCAM-1 and ICAM-1 expression (see chapter 5.1.7) were evaluated after incubation. To assess cell death and IL-8 secretion, supernatants were centrifuged at 500 RCF for 5 min and then supernatants were stored at 4ºC or -80ºC, respectively, until further analysis.

5.1.14 Lung alveolus-on-a-chip inflammation model

To mimic air-liquid interface and breathing motion of the human lung alveolus, a microfluidic device was used. The patented microfluidic device developed at the Wyss Institute had two stretchable channels with a PDMS membrane between. The epithelial cell line A549 was cultured on the top channel (1 mm high x 1 mm wide) and the endothelial cell line HUVEC was lined in the entire bottom channel (0.2 mm high x 1 mm wide) to mimic a blood vessel. The PDMS membrane was 50

μm thick with 7 μm pore size and pores spaced by 40 μm. The chip had a culture area of 16.7 mm^2 (Huh *et al.*, 2010, 2012; Kambez H Benam *et al.*, 2016; Kambez H. Benam *et al.*, 2016; Hassell *et al.*, 2017; Jain *et al.*, 2018).

The device fabrication method was previously described (Huh *et al.*, 2010, 2012; Kambez H Benam *et al.*, 2016; Kambez H. Benam *et al.*, 2016). Briefly, the molds of the channels were created by stereo-lithography and were used to cast PDMS pre-polymer, followed by curing (10:1 PDMS to curing agent) overnight at 60ºC. The PDMS membrane was manually aligned and bonded to the two channels of the chip.

The chips were plasma treated in the Plasma Etch machine (Diener Electronic Attos) and coated for 1 h with 10 μg/ml Fibronectin and 10 μg/ml Collagen Type I in PBS -/-. Pre-warmed EM was added to both channels. HUVEC at passage 3 to 5 were collected from T-flask (as described in chapter 5.1.5) and 90,000 cells were seeded in the bottom channel in pre-warmed EM. The top channel was filled with EM. The chips were incubated for 30-60 min at 37ºC and 5% CO_2 upside down. To ensure a confluent monolayer in the entire bottom channel, a second HUVEC collection and seeding was performed and cells were seeded at the same concentration. The chips were incubated upside down overnight at 37ºC and 5% CO_2.

Then, A549 cells were collected from T-flasks and 60,000 cells seeded in the top channel in pre-warmed A549 medium. Pre-warmed EM was added to the confluent HUVEC layer in the bottom channel. The chips were incubated upright at 37ºC and 5% CO_2. On the next day, new pre-warmed A549 medium was added to top channel and pre-warmed EM to bottom channel. During the two following days, A549 cells were treated statically with 1 μM Dexamethasone in A549 medium and the vascular bottom channel was under laminar flow at 1.02 – 1.70 μl/min with FM.

As feeding reservoirs, 5 ml Luer-Lok Syringes (BD Biosciences) were used. The plunger was discarded and the syringes were connected to 18 Gauge Luer-lok needles with 0.5 inches length (Jensen Global). The needles were connected to Pharmed BPT Tubing (ID = 0.035 inches, OD = 0.101 inches, Wall = 0.033 inches, from Cole-Parmer) and the tubing was connected to the chip inlets through a 19 Gauge 90º bent pin (Four Slide Products). The chip outlet was connected to Pharmed BPT Tubing through another 19 Gauge 90º bent pin and the tubing was connected through a 19 Gauge straight pin (Microgroup) to the inlet of 2-Stop Pharmed BPT Tubing 0.25 mm (Cole-Parmer) used in the IPC 8 peristaltic pump (Ismatec). The outlet of the peristaltic pump tubing was connected to falcon tubes as collecting reservoirs. After dexamethasone treatment, to further differentiate epithelial cells, the air-liquid interface was established by carefully removing the medium from the top channel and adjusting the feeding reservoirs to a lower level in the farm so that the height of the FM in the reservoirs is always lower than the chip height. Air-liquid interface was kept between A549 cells and HUVEC for additional 5 days adding FM to the feeding reservoirs. Then, cyclic strain was started at 5% stretch (-45 kilopascal (kPa) and 0.2 Hertz (Hz)) to mimic the lung breathing motion using a vacuum pump module developed by the Wyss Institute. The next day, FM was replaced by MM to starve the cells on flow for 24 h while keeping cyclic strain and air-liquid interface. After starvation, alveolus-on-a-chip system was challenged with the inflammatory molecules TNF-α and with MSC-EVs at different number of doses, EV concentration and incubation time, statically and on flow.

Barrier function (see chapter 5.1.15), cell death (see chapter 5.1.16), IL-8 secretion (see chapter 5.1.11) and VCAM-1 and ICAM-1 expression (see chapter 5.1.7) were evaluated at different time points. To assess cell death and IL-8 secretion, supernatants were centrifuged at 500 RCF for 5 min and then supernatants were stored at 4ºC or -80ºC, respectively, until further analysis.

5.1.15 Barrier function

The barrier function of the human lung alveolus models on transwell and on chip was evaluated by measuring the permeability of the dyes cascade blue hydrazide trisodium salt (Thermo Fisher Scientific) with molecular weight 596.4 Dalton and dextran texas red (Thermo Fisher Scientific) with molecular weight 3,000 Dalton.

With lights off, a solution of 50 µg/ml cascade blue and 50 µg/ml dextran in MM was prepared. The medium was carefully removed, the dye solution was added to the top chamber and MM to the bottom chamber and incubated at 37ºC and 5% CO_2 for 2 h static. Standards diluted in MM were also incubated for the same period of time.

After incubation, the bottom and top media were collected to Eppendorf tubes and the transwells or chips were carefully washed with MM. Transwells were transferred to new 24 WP and chips were reconnected in the farm to restart flow or treated with EVs and/or inflammatory cytokines and incubated at 37ºC and 5% CO_2.

Samples and standards were added to a 96 well half area black flat bottom polystyrene NBS microplate (Corning) and fluorescence was read from the top at 4.5 mm read height, for cascade blue at excitation 390 nm, emission 420 nm, gain 50 and for dextran at excitation 580 nm, emission 620 nm, gain 80.

To calculate apparent permeability, the fluorescence of the blank (MM) was subtracted to the fluorescence of each sample and standard. A linear equation was obtained from the plot of the standard curve and used to calculate the concentration of each sample. Apparent permeability was calculated using Equation 6.

$$P_{app}(cm/s) = \frac{V_r \times C_r \times (V_d + V_r)}{A \times t \times (C_d \times V_d + C_r \times V_r)}$$

Equation 6 – Apparent permeability (P_{app} in cm/s) is dependent on the volume of receiving channel effluent after time t (V_r in ml), the volume of dosing channel effluent after time t (V_d in ml), the measured concentration of tracer in the receiving channel after time t minus input concentration (C_r in µg/ml), the measured concentration of tracer in the dosing channel after time t (C_d in µg/ml), the area of porous membrane (A in cm^2) and the incubation time (t in sec).

5.1.16 Cell death

Cell death was assessed by LDH release using the Cytotox 96 non-radioactive cytotoxicity assay (Promega). Standards were prepared from stock solution provided by the kit in the same medium as the samples.

Samples were centrifuged at 500 RCF for 5 min and supernatants were transferred to new tubes and stored at 4ºC until LDH was measured (in the same day). Samples and standards, in duplicate or triplicate, were added to a 96 well half area black with clear flat bottom polystyrene NBS microplate (Corning). The substrate solution (at equal volume of samples or standard) was added and incubated for 30 min, light protected. Then, stop solution (at equal volume of samples or standard) was added and absorbance read at 490 nm.

To calculate LDH concentration of the samples, the absorbance of the blank was subtracted to all samples and standards, the standard curve was plotted and its linear equation was determined from which the concentration of the samples was calculated.

5.1.17 MSC-EV labelling

EV samples were thawed on ice or at 4ºC and stained with PKH67 Green Fluorescent Cell Linker Kit (Sigma-Aldrich) following manufacturer guidelines. Open-Top Thinwall Polyallomer Tubes for Ultracentrifugation of 5 ml were washed with 70% ethanol and RNase-Free PBS. The appropriate EV volume was added to diluent C in the UC tube. Then PKH67 was diluted 6:1,000 in diluent C and mixed with the EV solution continuously for 30 sec by gentle pipetting and incubated for 5 min light protected. Quenching was performed with 10% BSA RNase-Free PBS and incubated for 1 min. Additional RNase-Free PBS was added and UC tubes were ultracentrifuged at 29,000 rpm (about 100,000 g) for 30 min at 4ºC using the rotor SW55Ti. The supernatant was carefully aspirated and the EV pellet resuspended in RNase-Free PBS by gentle pipetting.

5.1.18 Cell staining on microfluidic device

Cells in the lung alveolus microfluidic device were stained with calcein AM cell-permeant dye (Thermo Fisher Scientific) following manufacturer guidelines. Briefly, calcein was diluted 1:1,000 in FM and the cells in the channels of the microfluidic device were incubated for a maximum of 20 min and then washed with FM before imaging on flow with PKH67-labeled EVs using the confocal microscope.

5.1.19 Statistical analysis

Statistical analysis was performed by One-way or Two-way ANOVA using Tukey correction for multiple comparisons as indicated in the legend of each figure. A P value lower than 0.05 was considered statistically significant, which upon correcting for multiple comparisons is denoted as *GP=0.0332, **GP=0.0021, ***GP=0.0002, ****GP<0.0001. For the statistical analysis the software GraphPad Prism 7, version 7.03 from GraphPad Software was used.

6 Results and Discussion

In this chapter, it will be described the characterization results of EV populations isolated from different BM MSC-EV donors and the development of 2D potency assays (monocytic and endothelial potency assays) and more complex 3D models on transwells and on microfluidic devices to evaluate the immunomodulatory properties of MSC-EVs from different donors.

6.1 MSC-EV characterization

BM MSCs from different donors were cultured in StemPro MSC xeno- and serum-free medium and EVs were isolated by differential centrifugation and two steps of UC. BM MSC-EVs were characterized by nanoparticle tracking analysis and MicroBCA. MSC-EVs were also characterized by cryo transmission electron microscopy, a type of transmission electron microscopy in which the samples are quickly frozen to cryogenic temperatures to avoid sample degradation.

StemPro MSC serum-free medium was used for MSC culture and EV isolation to avoid contamination with EVs from the FBS, which have been found to overlap in the size of cell culture EVs and, therefore, are isolated together (Szatanek *et al.*, 2015). To overcome EV contamination from FBS, the FBS can be EV depleted by UC for at least 16 h at 100,000 RCF or higher speed (Shelke *et al.*, 2014; Szatanek *et al.*, 2015) or in alternative serum-free medium can be used. Herein, the use of serum-free culture medium was selected. In a study comparing FBS containing medium with several xeno- and serum-free media, the EVs isolated from human umbilical cord MSC cultured in StemPro MSC serum-free medium enhanced to a higher extent the proliferation and cardiac differentiation of human cardiac cells, promoted to a higher extent the formation of tube structures by endothelial cells and inhibited mitogen-stimulated PBMC proliferation (Bobis-Wozowicz *et al.*, 2017). These findings indicate that StemPro MSC serum-free medium is a good alternative for FBS containing medium.

BM MSC-EVs were evaluated by cryo transmission electron microscopy (Figure 6.1), which allowed the visualization of individual EVs with a size around 100 nm as well as larger EV aggregates with encapsulated EVs which typically occurs due to high speed of UC isolation method (Issman *et al.*, 2013; Linares *et al.*, 2015). It was also possible to notice that some EVs are darker and granulated while others are smoother indicating differences in morphology and content (highlighted by black arrows in Figure 6.1).

Issman and colleagues observed that EVs isolated from blood by UC at 18,000 RCF seem to be flexible and compressible and that smaller vesicles can be encapsulated by larger vesicles. Moreover, encapsulated vesicles seem to deform according to the shape and size of the larger vesicles or the presence of other smaller vesicles inside the larger vesicle (Issman *et al.*, 2013). These observations are in accordance with what was observed herein (Figure 6.1). EV encapsulation is reported to predominantly occur when EVs are isolated by UC rather than by filtration and dialysis isolation methods, excluding the possibility of been related to the cryo transmission electron microscopy technique (Issman *et al.*, 2013). Furthermore, EVs isolated by UC from THP-1 monocytic

cell line and MDA231 epithelial breast cancer cell line had heterogeneous morphologies and it was detected some granulated EVs enclosing high dispersed cargo and other smooth EVs that seem to be empty (Issman *et al.*, 2013), similarly to what was observed here (Figure 6.1). Likewise, the presence of EVs from blood plasma with different morphologies such as spherical and tubular was also reported (Arraud et al., 2014). Moreover, Linares and co-workers stated that UC leads to the encapsulation of EVs into larger aggregates that are heterogeneous in terms of size, number of EVs encapsulated and morphology (Linares et al., 2015).

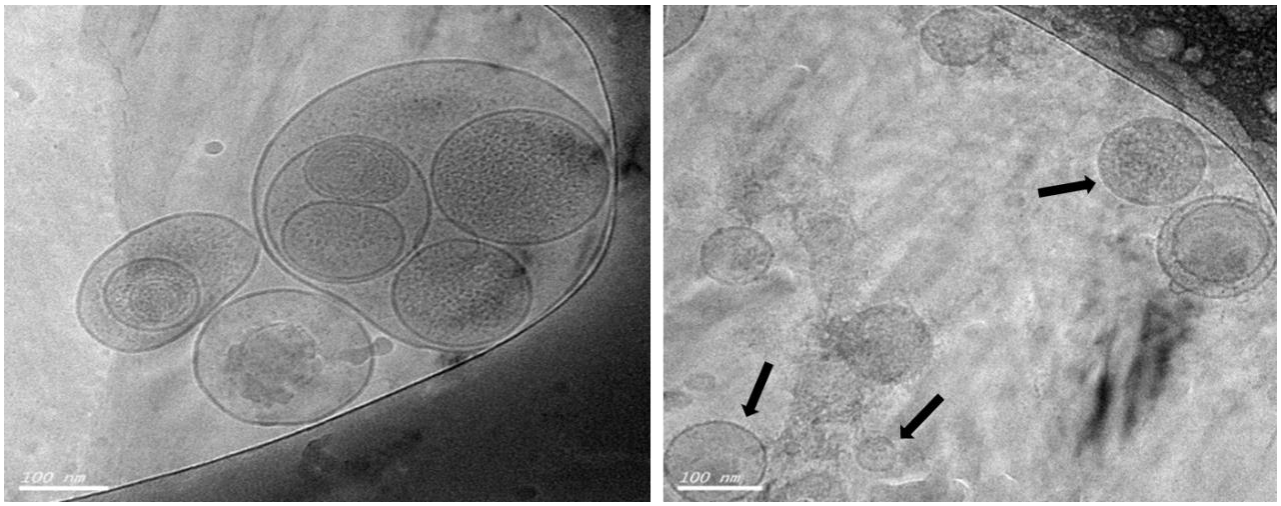

Figure 6.1 – Cryo transmission electron microscopy images of MSC-EVs isolated by ultracentrifugation showed single EVs and encapsulated EVs forming multilayered particles. EVs have heterogeneous morphology (arrows), from darker and granular to smoother resembling empty particles. Scale bar 100 nm.

EV populations from different MSC donors were characterized by MicroBCA to determine the protein content and by nanoparticle tracking analysis to determine EV concentration, mean size and size distribution. As a measure of purity and robustness of EV isolation, the PPR was calculated based on the protein and EV concentration (Table 6.1), according to Equation 5. The mean size of MSC-EVs from several MSC donors ranged from 91 to 201 nm with an average size of 146 nm, which is in accordance with the cryo transmission electron microscopy images (Figure 6.1). The size range obtained indicates the presence of exosomes and small microvesicles (exosome size range 40-120 nm and microvesicle size range 100-1,000 nm (Lee *et al.*, 2012; EL Andaloussi *et al.*, 2013)).

The EV concentration is dependent on the volume of CM from which EVs were isolated (which was different between donors and in some cases EVs from several isolations were pooled together) and on the volume in which EV pellets are resuspended (which was also different between donors). Nevertheless, EV concentration from all MSC-EV donors was in the range of 10^{11} to 10^{12} EV/ml and the average PPR was 1.9 fg protein/EV particle. Lower PPR values are indicative of higher purity of EV isolation and higher PPR values are indicative of higher protein contamination after EV isolation, as in the case of MSC-EVs from donors RB135 and 318006. Higher protein contamination could be a consequence of incomplete removal of supernatant after each UC step (and therefore lower removal of protein) and of higher dilution of the EVs after the final UC.

Table 6.1 – Characterization of MSC-EVs from different bone marrow donors by nanoparticle tracking analysis and MicroBCA in terms of mean size (in nm), EV concentration (in EV per ml) and protein to particle ratio (PPR, in fg protein per EV particle) indicating that optimized EV isolation protocol yields consistent EV populations (n = 1-6 in triplicates). Data is represented by the mean and standard error of the mean. N.a. stands for not available.

MSC donor	Mean size (nm)	EV concentration (EV/ml)	PPR (fg protein/EV particle)
RB55	171± 7	$(7 \pm 3) \times 10^{11}$	0.92 ± 0.04
RB70	185 ± 6	$(7 \pm 3) \times 10^{11}$	1.02 ± 0.05
RB81	184 ± 8	$(6 \pm 3) \times 10^{11}$	2 ± 1
RB135	201 ± 13	$(8 \pm 4) \times 10^{11}$	3.3 ± 0.4
305526	94 ± 3	$(1.13 \pm 0.02) \times 10^{12}$	n.a.
494678	100 ± 13	$(1 \pm 1) \times 10^{12}$	2.0
318006	91 ± 4	$(1.8 \pm 0.7) \times 10^{11}$	2.5
hTERT	141 ± 32	$(4 \pm 1) \times 10^{11}$	1.7

To the extent of my knowledge, purity of EV populations is not widely assessed and only a few published works refer the protein and EV concentration, the PPR or the EV particle to protein ratio. In one study, human BM MSC-EVs were isolated from protein-free culture medium by chromatography and a ratio of 5.1×10^8 EV particles per µg of protein, which corresponds to a PPR of 1.96 fg protein/EV particle was obtained (D.-K. Kim *et al.*, 2015). This PPR value is similar to the average PPR (1.9 fg protein/EV particle) of EV isolations from different donors herein obtained, indicating similar purity of EV isolation by UC compared to Kim and co-worker's results using chromatography. In another study, human BM MSCs were cultured in medium containing EV-depleted serum or in serum-reduced MSC medium supplemented with BSA and EVs were isolated by UC, resulting in a PPR of 0.13 (3×10^{11} EV particles correspondent to 40 µg of protein) (Phinney *et al.*, 2015). Phinney and co-workers obtained a much higher purity (lower PPR) than the EV samples isolated in this work, which indicates an about 10X higher protein contamination present in the samples since the EV concentration is similar. Of note, that not only the EV isolation with lower removal of supernatant is responsible for the differences but also the culture medium might influence the results.

Webber and Clayton evaluated the purity of EVs isolated by UC from several cancer cell lines cultured in medium containing EV depleted serum and stated that PPR lower than 0.03 fg protein/EV particle is considered high purity, PPR between 0.05 and 0.5 is low purity and PPR higher than 0.67 is impure (Webber and Clayton, 2013). Despite of differences in cell type and culture medium that could influence these purity classification levels, this is one of the few studies with a thorough purity analysis of EV samples proposing purity classification according to the PPR values.

Increasing one wash and UC did not result in significant increase of purity and, in fact, it resulted in loss of EV particles (data not shown), which is in accordance with Webber and Clayton who reported only a 2 fold increase in purity and loss of EV particles (Webber and Clayton, 2013), therefore, the UC protocol with 2 steps of UC was maintained.

The isolation method has significant influence on the purity of EV samples. In a study comparing UC with ultrafiltration and size-exclusion liquid chromatography, the PPR was 3 to 5 times higher (thus lower purity) when EVs from mouse neuroblastoma N2a cell line and from induced pluripotent stem cells were isolated by UC (Nordin *et al.*, 2015), which indicates that in the future other EV isolation methods that can be scaled-up and that result in higher EV purity should be considered.

The size distribution of BM MSC-EVs from the different donors was also obtained by nanoparticle tracking analysis (Figure 6.2), which accounted for the number of particles for each size interval. The size range of the different MSC-EV donors confirms the mean sizes in Table 6.1 and is in accordance with the cryo transmission electron microscopy images (Figure 6.1). The size distribution of the different MSC-EV donors also shows that most of the EV particles have lower size range within the range of 40-200 nm which is in the exosome size range (40-120 nm, EL Andaloussi *et al.*, 2013) and smaller microvesicle size range (microvesicle size range 100-1,000 nm, Lee *et al.*, 2012; EL Andaloussi *et al.*, 2013). Moreover, the size distributions indicate that the EV isolation method allowed the removal of larger microvesicles between 200-1,000 nm. EVs with size larger than 1,000 nm such as apoptotic bodies (apoptotic bodies size range 1,000-2,000 nm, Lee *et al.*, 2012; EL Andaloussi *et al.*, 2013) were not evaluated as a consequence of the settings used for nanoparticle tracking analysis, which is prepared for particles in the nanometer and not micrometer scale and, therefore, larger EV and EV aggregates as well as protein aggregates are generally considered noise (Linares *et al.*, 2015) and were eliminated from the analysis. Overall, the EV characterization methods indicate that the EV isolation protocol is optimized and yields consistent and robust EV populations among multiple donors, although even higher purities would be desirable.

In accordance with the minimal requirements to define an EV population by the ISEV, at least 3 methods should be used to characterize EV population. One is to evaluate the presence or absence of transmembrane protein (for instance, tetraspanins CD9, CD63 and CD81 characteristic of exosomes populations), cytosolic proteins (for example, TSG101), or intracellular and extracellular proteins usually by western blot, but it can also be measured by nano flow cytometry and mass spectrometry (Lötvall *et al.*, 2014). The two additional characterization methods to meet the minimal requirements to define EV populations can be imaging (for instance, cryo electron microscopy) and nanoparticle tracking analysis (Lötvall *et al.*, 2014). Herein, characterization of the EV populations was performed only with two methods, cryo electron microscopy and nanoparticle tracking analysis, thus western blot analysis is missing for a full EV characterization according to ISEV guidelines.

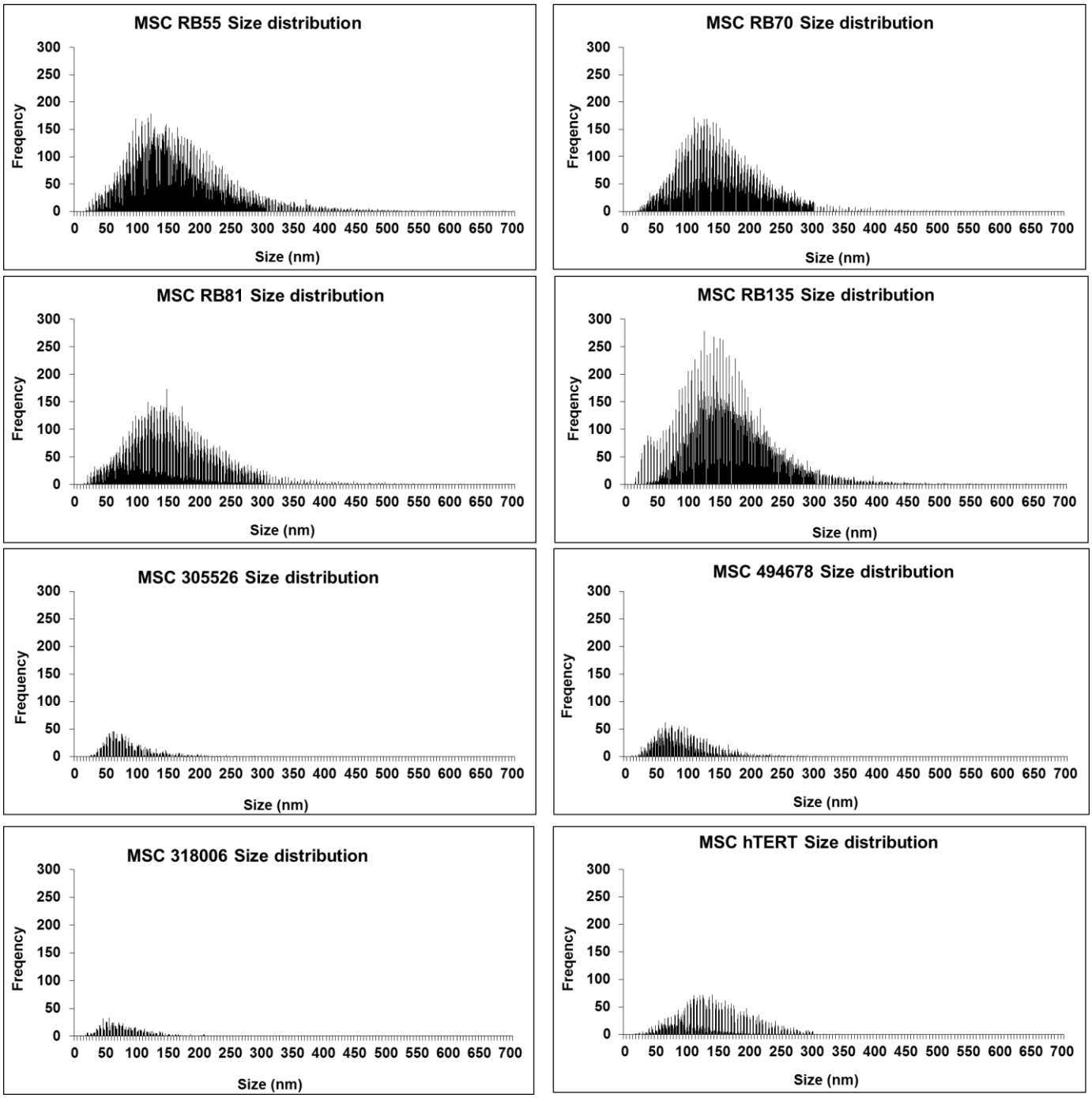

Figure 6.2 – MSC-EVs from different donors have similar size distribution graphs, which are represented by the number of particles (frequency) with size within each interval (defined as equal size intervals of 5 nm). For each biological sample, technical triplicates were measured by nanoparticle tracking analysis. The colors represent different biological samples. EV samples with higher EV concentration resulted in similar size distribution but higher frequency (n = 1-7 biological repeats in technical triplicates overlapped).

6.2 THP-1 Potency Assay

The immunomodulatory properties of MSC-EVs were evaluated using the 2D monocytic potency assay developed. To establish the potency assay with the monocytic cell line THP-1, the cells

were challenged with several LPS concentrations and the secretion of the inflammatory cytokine TNF-α was evaluated by ELISA.

THP-1 cells are a less mature cell line originally harvested from the peripheral blood of an acute monocytic leukemia patient with 1 year old. THP-1 cells are widely used to study inflammatory diseases and immunological responses and to evaluate the effect of certain drugs on immunological responses (Chanput *et al.*, 2014). THP-1 monocytic cells can be differentiated into macrophage-derived cells similar to PBMC monocyte-derived macrophages, however, the differentiation can result in a phenotypically heterogeneous macrophage population (Chanput *et al.*, 2014). PMA is considered to be the more efficient compound used for differentiation, still at least 2 days exposure to PMA followed by at least one more day without PMA is required (Chanput *et al.*, 2014). For a quicker potency assay and to avoid heterogeneous macrophage-like populations, the THP-1 potency assay developed used the cells as monocytes without promoting their differentiation into macrophages.

Additional advantages of using THP-1 cells are the high proliferation and stability of the immortalized cell line over many passages, the safety of the cell line and the cells can be stored while avoiding the donor variability of PBMCs. On the other hand, there might be differences in sensitivity and response to different stimuli of the cell line compared to healthy and primary cells and it does not fully mimic the complexity of the natural environment (Chanput *et al.*, 2014).

Upon pathogen invasion, the immune system recognizes pathogen associated molecular patterns, such as LPS from Gram negative bacteria, activating systemic inflammatory responses. Those responses include secretion of pro- and anti-inflammatory cytokines through the activation of certain transcription factors, for instance, the transcription factor NF-ΚB is involved in the regulation of IL-1β, IL-6, IL-8, TNF-α, iNOS and COX-2 and the transcription factor AP-1 is involved in the expression of IL-8 and TNF-α (Karima *et al.*, 1999; Guha and Mackman, 2001; Tripathi and Aggarwal, 2006; Chanput *et al.*, 2010; Soehnlein *et al.*, 2010).

Therefore, LPS was selected as inflammatory agent to stimulate THP-1 cells and the secretion of the pro-inflammatory cytokine TNF-α was evaluated. First, a LPS dose response was performed subjecting THP-1 cells to increasing LPS concentration of 100; 500 and 1,000 ng/ml for 24 h and the secretion of the cytokine TNF-α was quantified by ELISA. TNF-α secretion did not significantly increase at higher LPS concentrations, therefore, the lower dose of 100 ng/ml LPS was selected to avoid compromising cell viability.

In one study, THP-1 monocytes were stimulated with a dose of 1,000 ng/ml LPS and the gene expression and secretion of several cytokines and chemokines was evaluated up to 30 h. Higher concentration of secreted chemokines and cytokines was reached for the chemokine IL-8 and cytokine TNF-α. IL-8 secretion increased during the 30 h LPS stimuli, while TNF-α secretion reached the maximum secretion between 6-18 h and then was maintained constant from 18 to 30 h at an intermediate concentration (Chanput *et al.*, 2010). Herein, 10X lower LPS concentration was enough to stimulate THP-1 cells and a later time point (24 h) was selected because the aim of the potency assay is to evaluate the immunomodulatory potential of EVs which compared to LPS might need more time to exert their effect as EVs need to be uptaken by the recipient cells (THP-1 cells), deliver their cargo which will then affect gene regulation and protein secretion of THP-1 cells to cause the

biological effect on the immune response. Consequently, after optimizing the LPS dose for the THP-1 potency assay, it was used to evaluate the immunomodulatory properties of EVs released from different BM MSC donors.

When THP-1 cells were not subjected to LPS stimuli, EVs isolated from MSC donors 318006, 494678 and hTERT at a concentration of 10^9 EV/ml caused a significant increase in TNF-α release by THP-1 cells (Figure 6.3) compared to the No EV control (in which THP-1 culture medium was added instead of EVs normalizing the total volume of PBS between conditions). Therefore, these three MSC-EV donors were classified as pro-inflammatory donors. This result also shows that MSC donor-to-donor variability is reflected on their secreted EVs.

When THP-1 cells where stimulated with LPS (at 100 ng/ml), none of EV conditions at a concentration of 10^9 EV/ml isolated from seven MSC donors was able to significantly increase or decrease TNF-α secretion compared to the No EV control (Figure 6.3). Only, the positive control dexamethasone at 1 μM had an anti-inflammatory effect by reducing TNF-α secretion in about 30% compared to No EV control challenged by LPS.

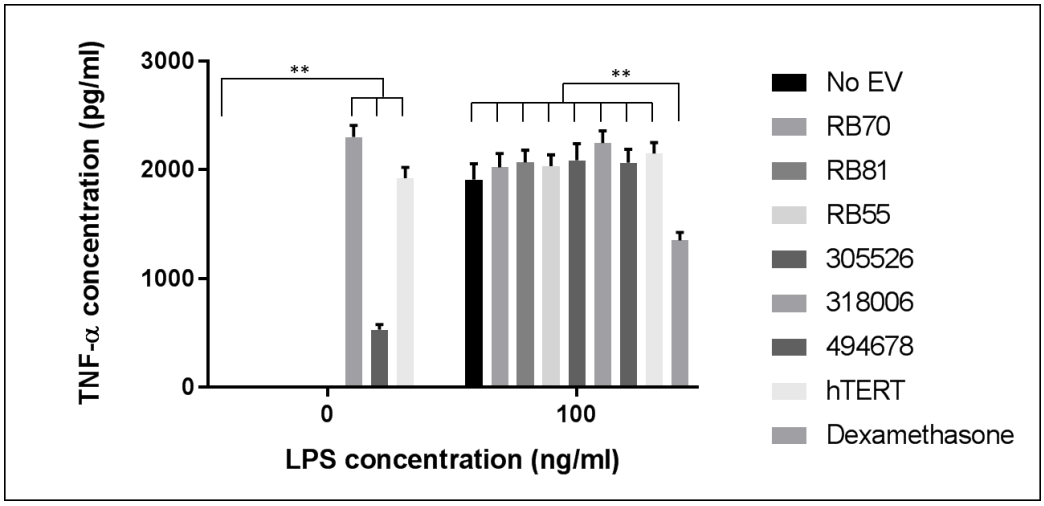

Figure 6.3 – TNF-α secretion of LPS-stimulated and unstimulated THP-1 monocytic cell line upon treatment with EVs isolated from different BM MSC donors can be used to detect pro-inflammatory MSC-EV donors. TNF-α (in pg/ml) released from THP-1 cells challenged by LPS (in ng/ml) and/or treated with MSC-EVs (at 10^9 EV/ml) from different donors was measured by ELISA. Dexamethasone at 1 μM was used as positive control. N = 3, *P value < 0.05, Two-way ANOVA with Tukey correction. Error bars represent the standard error of the mean.

To the extent of my knowledge, there are only a few studies evaluating the immunomodulatory potential of EVs or MSC-EVs using monocytic cell assays similar to the potency assay herein optimized. Moreover, most of the studies only characterized EV samples in terms of protein concentration or protein amount and no information regarding EV concentration or PPR is given in order to be able to directly compare works.

Ti and co-workers studied the potential of EVs (20 μg/ml) isolated by ultracentrifugation from UCM MSCs pre-conditioned with LPS on a THP-1 macrophage-derived cell inflammation model. THP-1 cells were differentiated by PMA and inflammation was caused by high glucose. They observed that

incubation of EVs isolated from LPS pre-conditioned MSCs resulted in a decrease of pro-inflammatory cytokines and increase in anti-inflammatory cytokines secreted by THP-1 cells compared THP-1 cells co-treated with EVs from untreated MSCs. Decreased inflammation and enhanced wound healing was also observed in a diabetic animal model after administration of 120 µg/ml EVs from LPS pre-conditioned MSCs (Ti *et al.*, 2015). Zhang and colleagues reported the immunomodulatory potential of MSC-EVs (100 ng/ml), isolated by tangential flow filtration, fractionated by high performance liquid chromatography and concentrated by filtration, on THP-1 monocytic cells resulting in increased gene expression of pro-inflammatory cytokines (such as TNF-α) and decreased gene expression of the anti-inflammatory cytokine IL-10 compared to LPS (10 ng/ml) for 24 h, indicating a pro-inflammatory effect of MSC-EVs (B. Zhang *et al.*, 2014). The differences in MSC-EV properties could be related to the culture conditions and pre-conditioning bioengineering strategies, MSC source and donor variability, MSC and EV isolation methods, EV dose and the THP-1 potency assay protocol. MSC donor-to-donor variability has been reported, however, it is not clear whether MSC-EVs would replicate that variability. Herein, we observed that MSCs from different donors, all cultured in StemPro MSC serum-free medium without stimuli or pre-conditioning, released EVs with different immunomodulatory properties indicating that MSC donor-to-donor variability is also reflected in their EVs and also that this potency assay can be used to identify and select out pro-inflammatory MSC-EV donors avoiding their use for therapeutic purposes. The detection of pro-inflammatory effect of MSC-EVs on THP-1 cells observed by Zhang and colleagues (B. Zhang *et al.*, 2014) is in accordance to what was observed here for 3 MSC-EV donors, moreover, the anti-inflammatory effect of MSC-EV donors was not observed herein for any of the donors as it was reported by Ti and co-workers (Ti *et al.*, 2015) indicating that MSC pre-conditioning, for instance with LPS, might be necessary to boost the anti-inflammatory effect of MSC-EVs on THP-1 cells.

Other examples of the use of THP-1 monocytic cells to study the effects of EVs from different cell types are the detection of pro-inflammatory effect of trophoblast-derived EVs (25-100 µg/ml) on a transwell system (Atay et al., 2011), the pro-inflammatory effect of EVs isolated from alcohol-treated hepatocytes (Momen-Heravi et al., 2015), the anti-inflammatory effect of endothelial cell-secreted EVs by pre-conditioning of THP-1 monocytes in a transwell system prior to LPS stimuli (Njock *et al.*, 2015).

Several studies showed the beneficial effect of dexamethasone and other glucocorticoids on reducing inflammation in a dose similar to the one used in this work (1 µM). Incubation of 0.01-1 µM dexamethasone for 30 min prior to LPS stimuli (10 µg/ml) of THP-1 monocytic cells for 5 h, resulted in a decrease in TNF-α secretion and the extent of the decrease was higher for 1 µM (Reddy *et al.*, 2004). In another study, THP-1 cells were treated with 0.001-1 µM dexamethasone for 1 h before 100 ng/ml LPS incubation for 20 h and 1 µM dexamethasone reduced IL-8 secretion to higher extent. Moreover, 1 µM dexamethasone also reduced IL-8, IL-6 and TNF-α secretion of PBMCs stimulated with 100 ng/ml LPS (Mogensen *et al.*, 2008). It was also reported that 1 µM dexamethasone incubated for 30 min prior to 1,000 ng/ml LPS stimuli significantly reduced TNF-α secretion from THP-1 cells (transfected with TNF-α promoter luciferase reporter constructs) after 24 h incubation (Steer *et al.*, 2000).

A typical dexamethasone dose for patients is between 0.5-16 mg per day for adults (Ho *et al.*, 2011; Cook *et al.*, 2016). If all dexamethasone would target the monocytes (5% monocytes within white blood cells, 4,000-11,000 white blood cells per mm^3 of blood, 4.5-5.5 liters of blood per average human body (Blumenreich, 1990)), then the dexamethasone dose would be about 10^{-9} mg/cell. For the potency assay herein 1 µM dexamethasone was used, which corresponds to about 8 x 10^{-11} mg/cell, which is about 13X lower than the human dose estimated, however, only a much lower dexamethasone concentration will be sensed and affect the monocytes, therefore, the difference between the dose in the clinic and the potency assay might not be too different.

6.3 HUVEC Potency Assay

The immunomodulatory properties of MSC-EVs were also evaluated using a 2D endothelial potency assay developed. The endothelial cell line HUVEC was challenged with TNF-α in co-treatment with MSC-EVs for 16 h.

MSCs secrete trophic factors (for instance VEGF, HGF, PDGF, FGF, KGF, TGF-β and angiopoietin-1) which mediate their action maintaining blood vessel integrity, enhancing endothelial cell proliferation and migration, reducing vascular permeability and edema as well as preventing interaction between endothelial cells and leukocytes (such as monocytes) (Ma *et al.*, 2014). MSC-EVs seem to promote tissue regeneration and reduce inflammation, mostly assessed by *in vivo* studies (Lai, Arslan, Lee, *et al.*, 2010; Bruno *et al.*, 2012; Cantaluppi *et al.*, 2012; Arslan *et al.*, 2013). However, there is a lack of potency assays that enable assessing each of those functions, consequently, the ability of MSC-EVs to recapitulate all those functions needs further evidence, for instance, on MSC-EV potential to prevent the interaction between endothelial cells and leukocytes, which could be assessed by a decrease in the expression of VCAM-1 and ICAM-1 adhesion molecules on endothelial cells (which are up-regulated when in an inflammatory state) or the release of chemokine IL-8 which attracts leukocytes (Soehnlein *et al.*, 2010).

TNF-α is a pro-inflammatory cytokine secreted by activated monocytes, macrophages and neutrophils (Zhou *et al.*, 2007; Soehnlein *et al.*, 2010) and, therefore, can mimic their action in an *in vitro* assay. TNF-α stimuli on HUVEC up-regulates the expression of the adhesion molecules VCAM-1, ICAM-1 and selectins, the secretion of cytokines and chemokines (such as IL-8), increases cell permeability leading to vascular leakage (edema) and is involved in coagulation responses (Friedl *et al.*, 2002; Zhou *et al.*, 2007).

To establish this potency assay the HUVEC cell line was challenged with increasing TNF-α concentration and the expression of the surface markers VCAM-1 and ICAM-1 was evaluated by immunohistochemistry (Figure 6.4 A) and by flow cytometry (Figure 6.4 B and C). For TNF-α concentration from 1 to 100 ng/ml, ICAM-1 expression is saturated both by immunohistochemistry (top panel of Figure 6.4 A) and flow cytometry (with no statistical difference between 0.1 to 100 ng/ml TNF-α, Figure 6.4 C). VCAM-1 saturation was reached for concentrations higher than 1 ng/ml TNF-α by flow cytometry (Figure 6.4 B) while by immunohistochemistry higher expression was obtained at 10 to 100 ng/ml TNF-α (Figure 6.4 A). For the HUVEC potency assay, the 10 ng/ml TNF-α was the

concentration selected as it was the minimal dose necessary to upregulate VCAM-1 and ICAM-1 expression close to saturation levels by flow cytometry analysis while minimizing negative effect on cell viability.

In one study, TNF-α-stimulated HUVEC (at 20 ng/ml) increased ICAM-1 and VCAM-1 protein level reaching a plateau between 12 to 24 h after incubation. Moreover, increased expression level of VCAM-1 and ICAM-1 was obtained at concentrations higher than 1 ng/ml after 24 h stimuli, however, while there was a small increase from 1 to 10 ng/ml TNF-α, for 100 ng/ml TNF-α a much higher increase was observed possibly indicating an exacerbation of the inflammatory reaction (Zhou *et al.*, 2007). Therefore, the choice of 16 h TNF-α at 10 ng/ml for the HUVEC potency assay is in line with Zhou and co-worker's published work.

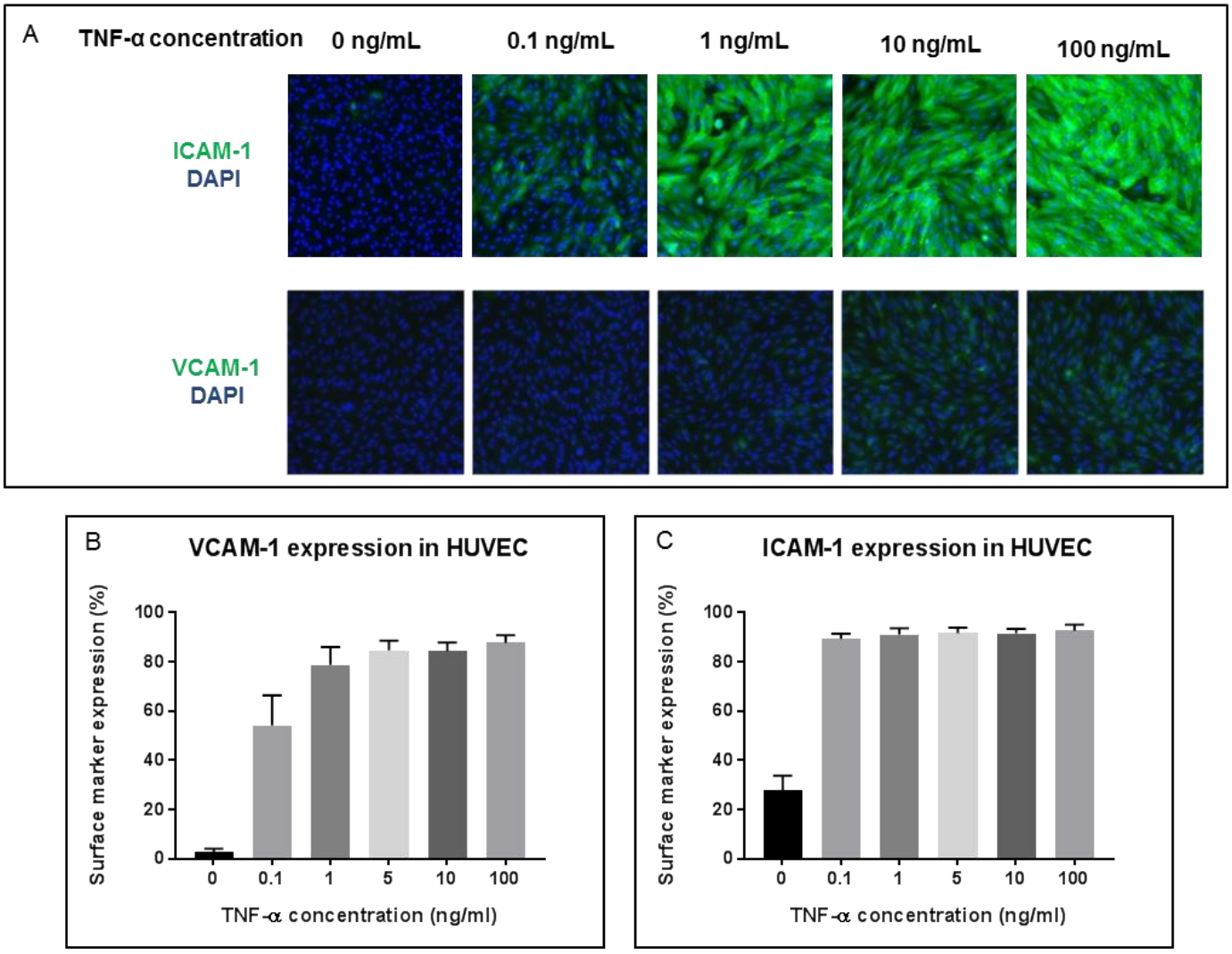

Figure 6.4 – TNF-α dose response on HUVEC after 16 h stimuli. A – Fluorescence images of increased HUVEC surface markers expression with increasing TNF-α concentration, in ng/ml, (left to right) for ICAM-1 (top) and VCAM-1 (bottom). ICAM-1 and VCAM-1 expression are stained in green and nuclei are stained in blue with DAPI. B and C – Expression (in %) of HUVEC adhesion molecules VCAM-1 (B) and ICAM-1 (C) upon TNF-α stimuli showing increased expression with increasing TNF-α concentration (in ng/ml) measured by flow cytometry. N = 3, *P value < 0.05, One-way ANOVA with Tukey correction. Error bars represent the standard error of the mean.

After optimizing the HUVEC potency assay, it was used to evaluate the immunomodulatory properties of MSC-EVs from different donors. Three MSC donors, that were not considered pro-inflammatory by the THP-1 potency assay, were selected and the effect of their EVs was evaluated. HUVEC were challenged with or without TNF-α (10 ng/ml) and co-treated with MSC-EVs (at 10^9 EV/ml) from the three donors for 16 h. The expression of the surface markers VCAM-1 and ICAM-1 was evaluated by flow cytometry and the secretion of the inflammatory chemokine IL-8 was measured by ELISA.

EVs from MSC donor RB81 and RB55 significantly reduced VCAM-1 expression upon TNF-α stimuli (Figure 6.5 A) compared to the No EV control TNF-α stimulated, in 17% and 27% respectively. Only EVs from MSC RB81 were able to significantly reduce ICAM-1 expression in about 18% (Figure 6.5 B). All MSC-EV donors were able to significantly reduce IL-8 secretion in about 7 to 11% (Figure 6.5 C). As the effect of MSC-EVs on decreasing VCAM-1 and ICAM-1 expression and IL-8 release was moderate, the MSC donors RB70, RB81 and RB55 were only considered slightly anti-inflammatory.

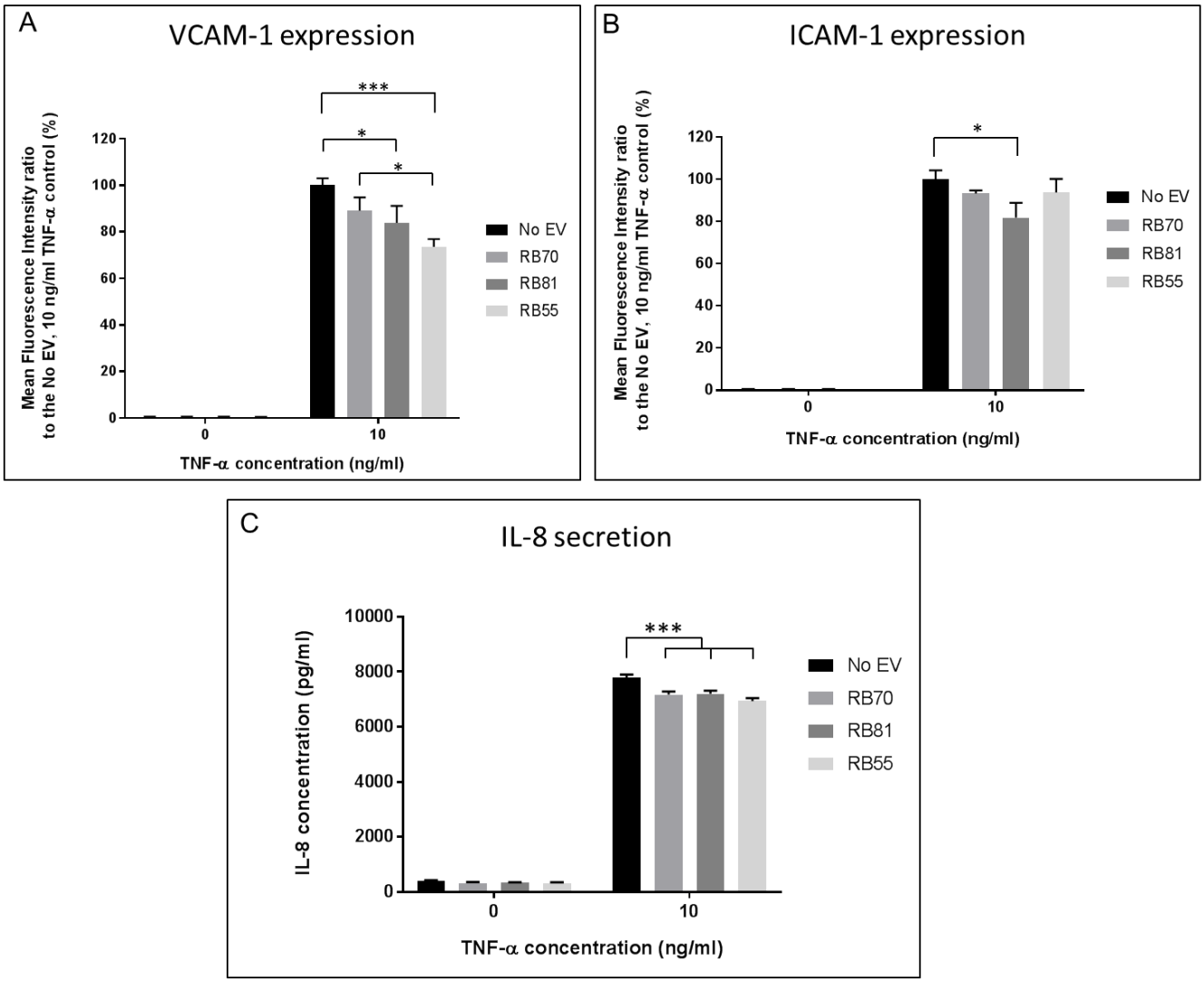

Figure 6.5 – Evaluation of the anti-inflammatory effect of different MSC-EV donors (at 10^9 EV/ml) on HUVECs challenged with TNF-α (in ng/ml) for 16 h. A – VCAM-1 expression (in %, calculated as a ratio of mean fluorescence intensity of each MSC-EV donor to the positive control No EV with 10 ng/ml TNF-α) was decreased by EVs from different MSC donors compared to the positive control set as 100% (n = 3 in technical duplicates). B – ICAM-1 expression (in %, calculated as a ratio of mean fluorescence intensity of each MSC-EV donor to the control No EV with 10 ng/ml TNF-α) was decreased only by EVs from MSC donor RB81 compared to the control set as 100% (n = 3 in technical duplicates). C – IL-8 release (in pg/ml) from TNF-α-stimulated HUVEC was reduced by EVs from all MSC donors compared to the control (n = 2 in technical triplicates). *P value < 0.05, Two-way ANOVA with Tukey correction. Error bars represent the standard error of the mean.

None of the EVs from these three donors caused upregulation of VCAM-1 and ICAM-1 or increased IL-8 secretion by HUVEC when cells where not stimulated with TNF-α, corroborating the results of THP-1 potency assay that these three donors are not pro-inflammatory. These results also show some extent of donor-to-donor variability between MSC-EV donors, but more importantly these results indicate that MSC-EVs (at 10^9 EV/ml) do not have a strong anti-inflammatory effect on TNF-α-stimulated HUVEC, which might result in inefficient treatment if tested in pre-clinical and clinical trials. Consequently, it indicates that the protocol needs further optimization or that MSC-EV bioengineering

strategies should be pursued for increased effect. Regarding the protocol, it might be possible that the EV dose (10^9 EV/ml) is not optimal, the time point evaluated (16 h) is not the most adequate to observe cell response to EVs, other outcomes rather than VCAM-1, ICAM-1 and IL-8 should be measured that could eventually be more sensitive showing other possible mechanisms of action of EVs on HUVEC or it is also possible that EVs produce enhanced action on more complex systems that integrate more than one cell type and immune cells.

To the extent of my knowledge, there are only a few studies evaluating the immunomodulatory potential of MSC-EVs using endothelial cells, however, the potency assay as herein developed was never reported. The majority of published studies evaluated the effect of MSC-EVs on endothelial cell proliferation (Bian *et al.*, 2014; Xie *et al.*, 2017), angiogenic potential by tube formation assay (Bian *et al.*, 2014; Shabbir *et al.*, 2015; McBride *et al.*, 2017; Xie *et al.*, 2017) and migration using wound healing assay by mechanical scratch (Patel *et al.*, 2017; Xie *et al.*, 2017) or using a Chemotaxicell chamber (Bian *et al.*, 2014), rather than expression of adhesion molecules VCAM-1 and ICAM-1 and secretion of chemokines as IL-8 or other cytokines. Overall, these studies reported that, compared to controls, the MSC-EVs enhanced proliferation, migration and angiogenesis and better results were observed for the higher MSC-EV doses.

EVs from other cell types such as monocytes have also been tested on endothelial cells. EVs from THP-1 monocytic cells were isolated by UC after THP-1 cell starvation to induce apoptosis. HUVEC were incubated with THP-1 monocytic-secreted EVs at a ratio of 10 EVs per cell for 24 h for ICAM-1 gene expression analysis or incubated at 1 EV per cell for 3 days for soluble ICAM-1 measured by ELISA and it was reported an increase in both ICAM-1 gene expression and soluble ICAM-1 compared to controls, indicating that THP-1 monocytic-secreted EVs after starvation have pro-inflammatory effect on endothelial cells (Hoyer *et al.*, 2012).

Plasma EVs and THP-1 monocytic cell-secreted EVs isolated by UC from cells cultured in medium containing serum were reported to contain several microRNAs, including elevated miR-150, which modulated endothelial cell function and enhanced human microvascular endothelial cell HMEC-1 migration (Zhang *et al.*, 2010). Of note that starvation with serum-free culture medium resulted in a pro-inflammatory state in THP-1 cells and consequently apoptosis (Hoyer *et al.*, 2012) which was reflected in the EV effect on activating endothelial cells, while when THP-1 cells were cultured in FBS containing medium, their EVs resulted in increased endothelial cell migration (Zhang *et al.*, 2010). It remains to be elucidated if that effect was in part due to FBS, therefore, FBS containing medium should have been EV depleted.

On the other hand, Tang and co-workers, using the Exoquick-TC isolation kit, isolated primary monocytes-secreted EVs from FBS-EV depleted culture medium after pre-conditioning with LPS, IFN-α or both and demonstrated that HUVEC incubation with EVs from LPS and LPS + IFN-α pre-conditioning increased ICAM-1 adhesion molecule, CCL-2 chemokine and IL-6 cytokine at mRNA and protein level compared to unstimulated EVs and EVs from IFN-α pre-conditioning (Tang et al., 2016). Thus, indicating that without a proper stress condition THP-1-secreted EVs do not have a pro-inflammatory action on HUVEC and upon an appropriate inflammatory stimuli the EV content of THP-1 cells will change and act as pro-inflammatory signal activating HUVECs, which are then able to

secrete cytokines and chemokines to recruit monocytes that will adhere to endothelial cells and transmigrate during the onset of the inflammation process until it is resolved (Soehnlein *et al.*, 2010).

A positive control should have been included in the HUVEC potency assay to be compared with the MSC-EV action and better understand the sensitivity and extent of HUVEC response to anti-inflammatory molecules. The glucocorticoids have been used to reduce inflammation, thus dexamethasone was tested, however, no consistent and dose dependent anti-inflammatory response was detected, which is in accordance with other published work (Dufour *et al.*, 1998). Other compounds should have been tested such as the anti-oxidants Salvianolic Acid B (Chen *et al.*, 2001) and protocatechuic aldehyde (Zhou *et al.*, 2005) or the drug curcumin (Kumar *et al.*, 1998; Kim *et al.*, 2007; Yen *et al.*, 2013).

It would also be interesting to characterize the MSC-EV content of the pro- and anti-inflammatory donors detected using the THP-1 and HUVEC potency assay to determine which molecules (nuclei acids, proteins, lipid and metabolites) are responsible for the different MSC-EV immunomodulatory effects.

6.4 EV dose study using HUVEC Potency Assay

To understand if the low anti-inflammatory effect of MSC-EVs was related to EV dose, the HUVEC potency assay was used to evaluate the effect of EV concentration on VCAM-1 and ICAM-1 expression as well as IL-8 release by HUVEC. The three MSC-EV donors that were not pro-inflammatory and were slightly anti-inflammatory were used and EV concentrations of 10^8, 10^9 and 10^{10} EV/ml were tested. Without TNF-α stimuli, EVs from the 3 MSC donors at the higher EV dose (10^{10} EV/ml) did not cause increase in VCAM-1 and ICAM-1 expression (Figure 6.6 A and B) neither IL-8 secretion (Figure 6.6 C) by HUVEC, therefore, MSC-EVs were not pro-inflammatory even at the higher dose. Upon TNF-α stimuli with 10 ng/ml, VCAM-1 and ICAM-1 expression and IL-8 release was not inversely proportional to the EV dose, meaning that VCAM-1 and ICAM-1 expression did not proportionally decrease with increasing EV concentration. Unexpectedly, EV concentration of 10^9 EV/ml was similar or worse than 10^8 EV/ml for all MSC-EV donors in terms of VCAM-1 and ICAM-1 expression as well as IL-8 secretion from TNF-α-stimulated HUVEC. Nevertheless, there was higher decrease in VCAM-1 expression and IL-8 secretion, with statistical significance, at 10^{10} EV/ml for all 3 MSC-EV donors compared to the control with 10 ng/ml TNF-α only without EVs. As for ICAM-1 expression, the decrease in expression is statistically more significant at 10^{10} EV/ml for MSC-EV donor RB70 and RB81, whereas for RB55 there is no statistical significance on ICAM-1 expression when compared to the control treated with 10 ng/ml TNF-α only. Overall, the higher EV dose (10^{10} EV/ml) resulted higher decrease in VCAM-1 and ICAM-1 expression and IL-8 secretion, therefore, the EV dose 10^{10} EV/ml or higher was used for the 3D inflammation models described in the following sub-chapters (6.5 and 6.6).

Most of the studies do not measure particle number neither purity of the samples (PPR). To compare the EV doses used with published work the 10^8 EV/ml corresponds to about 0.05-0.3 µg/ml, the 10^9 EV/ml corresponds to 0.5-3 µg/ml and 10^{10} EV/ml to 5-30 µg/ml.

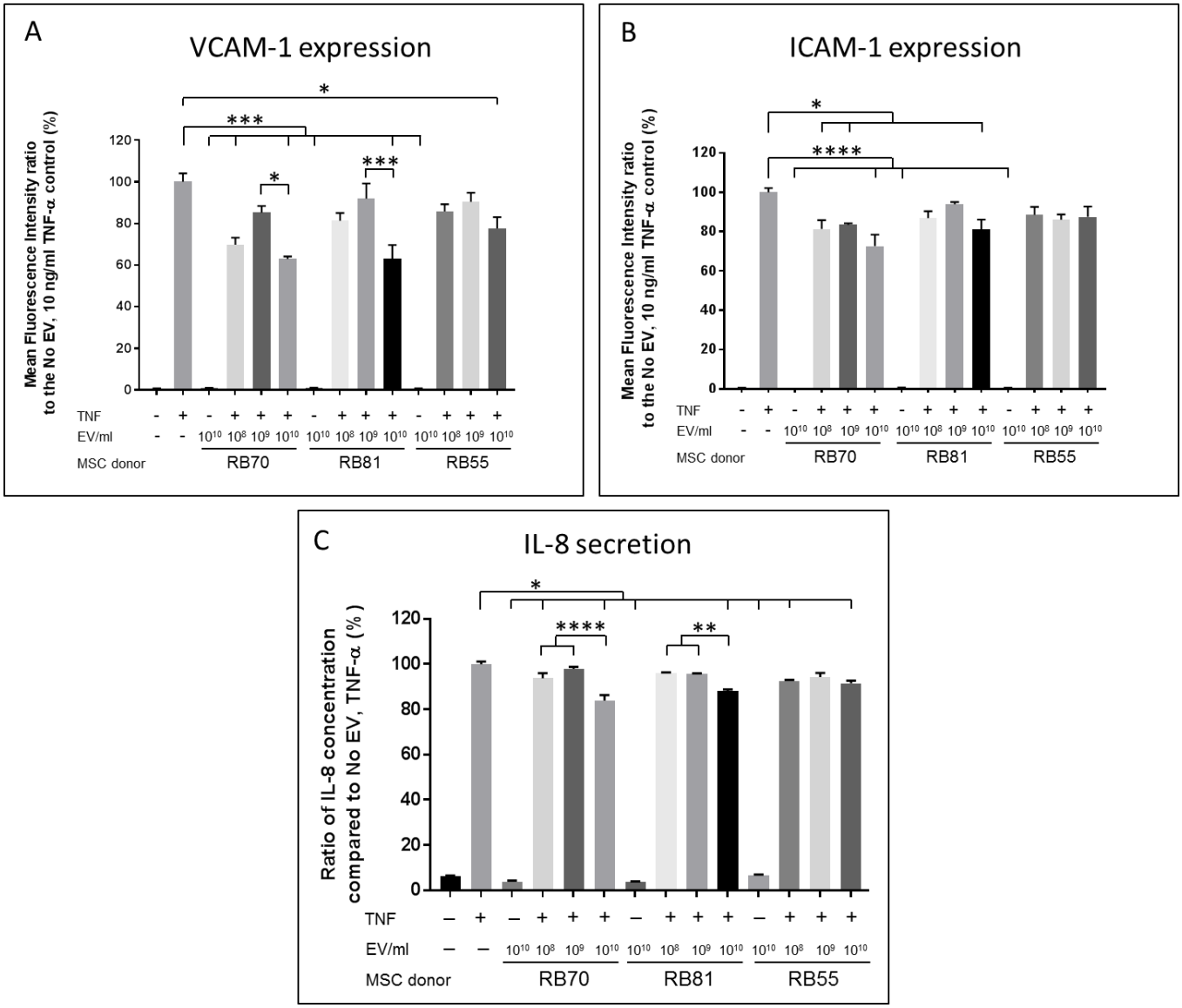

Figure 6.6 – Effect of MSC-EV dose on TNF-α-stimulated HUVECs. EVs from three BM MSC donors (RB70, RB81, RB55) were incubated at three doses (10^8, 10^9 and 10^{10} EV/ml) for 16 h. A – VCAM-1 expression (in %, calculated as a ratio of mean fluorescence intensity of each MSC-EV donor to the control No EV with 10 ng/ml TNF-α set as 100%) was decreased to higher extent at the higher EV dose for all MSC-EV donors. B – ICAM-1 expression (in %, calculated as a ratio of mean fluorescence intensity of each MSC-EV donor to the control No EV with 10 ng/ml TNF-α set as 100%) was decreased to higher extent at the higher EV dose for two of the MSC-EV donors (RB70 and RB80). C – IL-8 release (in %, calculated as a ratio of IL-8 concentration of each MSC-EV donor to the control No EV with 10 ng/ml TNF-α set as 100%) from TNF-α-stimulated HUVEC was reduced to higher extent at the higher EV dose for all MSC-EV donors. N = 2 in technical duplicates, *P value < 0.05, One-way ANOVA with Tukey correction. Error bars represent the standard error of the mean.

Xie and co-workers tested the potential of rat BM MSC-EVs at 1, 20 and 50 µg/ml and observed that the EVs enhanced HUVEC proliferation, migration by a wound healing assay and tube formation in Matrigel and higher EV dose produced better results (Xie *et al.*, 2017). In another study,

EVs isolated by UC from hypoxia-stimulated human BM MSCs cultured in medium containing EV depleted-FBS were tested at increasing EV doses (10, 40, 80 µg/ml) using a HUVEC proliferation assay, migration assay in a Chemotaxicell chamber and tube formation assay in Matrigel. It was reported increased proliferation, migration and tube formation with increased EV dose and the effect of the higher EV dose was similar to 50 ng/ml VEGF (Bian *et al.*, 2014). Shabbir and colleagues also reported increasing HUVEC angiogenic potential by a tube formation assay according to increasing EV dose (0.1, 1 and 10 µg/ml) isolated by UC from human BM MSCs cultured EV depleted-FBS medium compared to controls, after 6 h incubation (Shabbir *et al.*, 2015). The potential to reduce tumor growth by EVs isolated by UC from human umbilical cord Wharton's Jelly MSCs cultured in medium supplemented with 0.5% BSA was reported to be dose-dependent with increased EV dose (50, 100, 200 µg) resulting in improved anti-proliferative and pro-apoptotic effect (Wu *et al.*, 2013).

Although different potency assays, culture medium and differential ultracentrifugation EV isolation methods were used, the EV doses tested herein are in the range of EV-protein doses published, however, even higher doses could be tested to evaluate if higher EV number would result in higher anti-inflammatory effect. It is also not known if there is a threshold EV dose, after which the too high EV dose starts to cause inflammation and harm the cells, especially in *in vitro* assays in which there are no clearance mechanisms as in *in vivo* animal models.

Moreover, the immunosuppressive effect of MSCs and MSC-EVs by the inhibition of B cell proliferation was also reported to be dose-dependent (Budoni *et al.*, 2013) by a dilution assay, although EV concentration or protein concentration was not quantified and only the number of MSCs from which the EVs were isolated was reported.

The published studies indicate that higher EV doses result in enhanced angiogenic potential and immunomodulatory properties. However, it is not stablished for both *in vitro* and *in vivo* studies what would be the optimal EV dose, number of doses, frequency and timing. Furthermore, the studies only report the protein concentration and not the EV concentration or PPR, thus as previously mentioned the higher protein dose does not necessary mean higher number of EVs and it could mean that samples have higher protein contamination. Consequently, it is recommended to evaluate EV concentration, protein concentration and PPR as standard procedure. Of note that one limitation for testing higher MSC-EV doses is the high number of cells needed and consequent process of EV isolation, thus for scale-up other EV isolation methods (for instance, filtration and chromatography methods) might be considered.

6.5 Lung alveolus inflammation on a 3D transwell model

The potential effect of MSC-EVs was further tested on a more complex static 3D model on transwell to account for tissue-tissue interactions. The lung alveolus is an immunologically active site that is constantly subjected to toxic and infectious agents. The lung alveolus is composed of an epithelial and an endothelial cell barrier. The epithelial cell barrier is composed of alveolar epithelial cells type I, which are mainly responsible for gas exchange but are also involved on inflammatory responses to microbial agents, and type II which are responsible for healing upon injury, ion transport

and for the production of surfactants that are important for clearance of pathogens and lung defense but also for reducing the surface tension during gas exchange while keeping a thin layer of liquid to avoid cell drying (Chuquimia *et al.*, 2013). The endothelial cell barrier has an important role on gas, fluid and solute exchange (Kelly *et al.*, 1998).

To evaluate MSC-EV potential, a static lung alveolus 3D transwell inflammation model was developed. The alveolar epithelium was mimicked by the lung carcinoma epithelial A549 cell and the endothelium by HUVEC. A549 cells are type II alveolar epithelial cells (Foster *et al.*, 1998) that are able to produce surfactants (Hermanns *et al.*, 2004). The treatment of epithelial cells with the glucocorticoid dexamethasone (at 1 µM) promotes cell-cell contact and the formation of tighter junctions resulting in stronger barrier function when co-cultured with the endothelium (Hermanns *et al.*, 2004; Huh *et al.*, 2012). The lung epithelial cell line NCI H441 has been reported to form a tighter and improved barrier than A549 (Hermanns *et al.*, 2004), however, besides dexamethasone treatment the lung alveolus model developed included the establishment of an air-liquid interface. The air-liquid interface was maintained for 3 days, before starvation and inflammation challenge, to promote the production of surfactant by the epithelial cells as well as the strengthening of the intracellular junctions, decreasing permeability and improving the barrier function (Huh et al., 2010).

After dexamethasone treatment of epithelial cells and establishment of the air-liquid interface, the lung alveolus transwell model was subjected to serum and growth factor starvation and challenged with 10 ng/ml TNF-α in the endothelial chamber, similarly to the HUVEC potency assay. Endothelial cell starvation was performed overnight to avoid variability associated with FBS, to remove protective effects of FBS and growth factors and to synchronize cells to the same cell cycle phase (Shi *et al.*, 2012; S. Wang *et al.*, 2017).

No disruption was observed in the endothelial cell-cell junction VE-cadherin after 24 h with 10 ng/ml TNF-α (Figure 6.7), therefore, a dose-response study was performed.

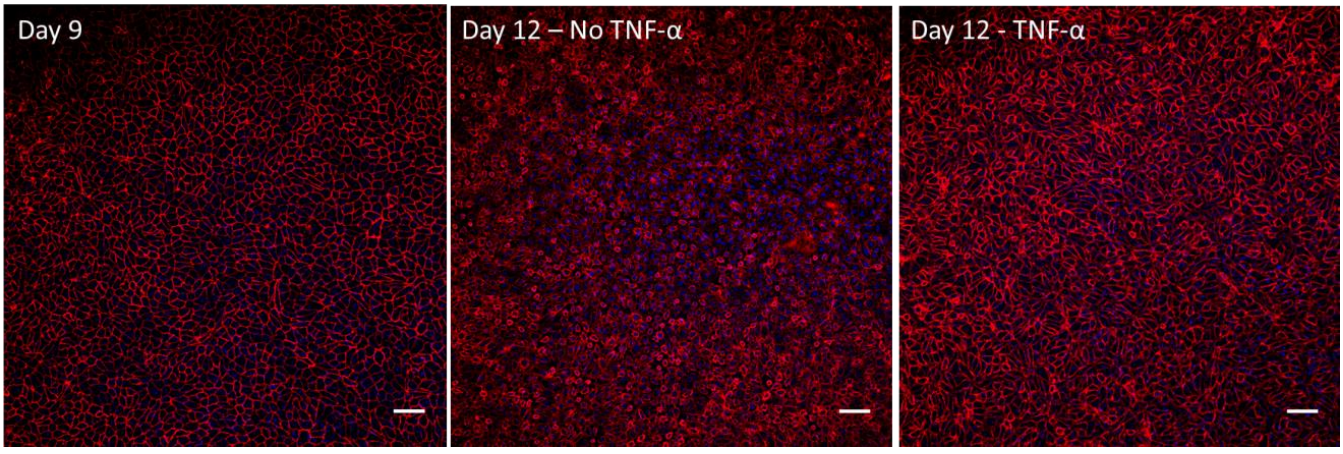

Figure 6.7 – Endothelial barrier of the lung alveolus inflammation model on transwell showed no significant disruption of HUVEC cell-cell junction VE-cadherin (red) at day 12 of culture after TNF-α incubation (10 ng/ml) for 24 h compared to control without TNF-α, by immunofluorescence microscopic analysis. Nuclei was stained with DAPI (blue). Scale bar 100 µm.

Preliminary results indicate that VCAM-1 and ICAM-1 expression of HUVEC from the lung alveolus transwell model did not greatly increase at 100 ng/ml TNF-α compared to 10 ng/ml (Figure 6.8 A and B), suggesting that expression of the HUVEC surface markers in the lung alveolus inflammation model on transwell were saturated, which is in accordance with the previous data using the HUVEC potency assay. TNF-α concentration higher than 100 ng/ml was not tested to avoid excessive damage in the barrier function and loss of surface marker expression due to cell death.

Regarding the barrier function, preliminary results indicate that the fold change in apparent permeability of cascade blue and dextran after 16 h treatment (which is given by the apparent permeability before and after treatment for each condition) did not seem to increase at 100 ng/ml TNF-α compared to 10 ng/ml (Figure 6.8 C and D), showing that a 10 fold increase in TNF-α concentration did not cause that same extent of disruption in barrier function. However, the fold change in apparent permeability of cascade blue and dextran fluorescent dyes at 16 h treatment (which is given by the apparent permeability of each condition and the control without TNF-α at the 16 h time point) seem to be higher for 100 ng/ml TNF-α than for 10 ng/ml (Figure 6.8 E and F). Although needing further confirmation, overall, these results indicate that TNF-α dose up to 100 ng/ml causes inflammation by up-regulation of endothelial adhesion molecules but does not cause great disruption in the endothelial-epithelial barrier function in the lung alveolus model on transwell.

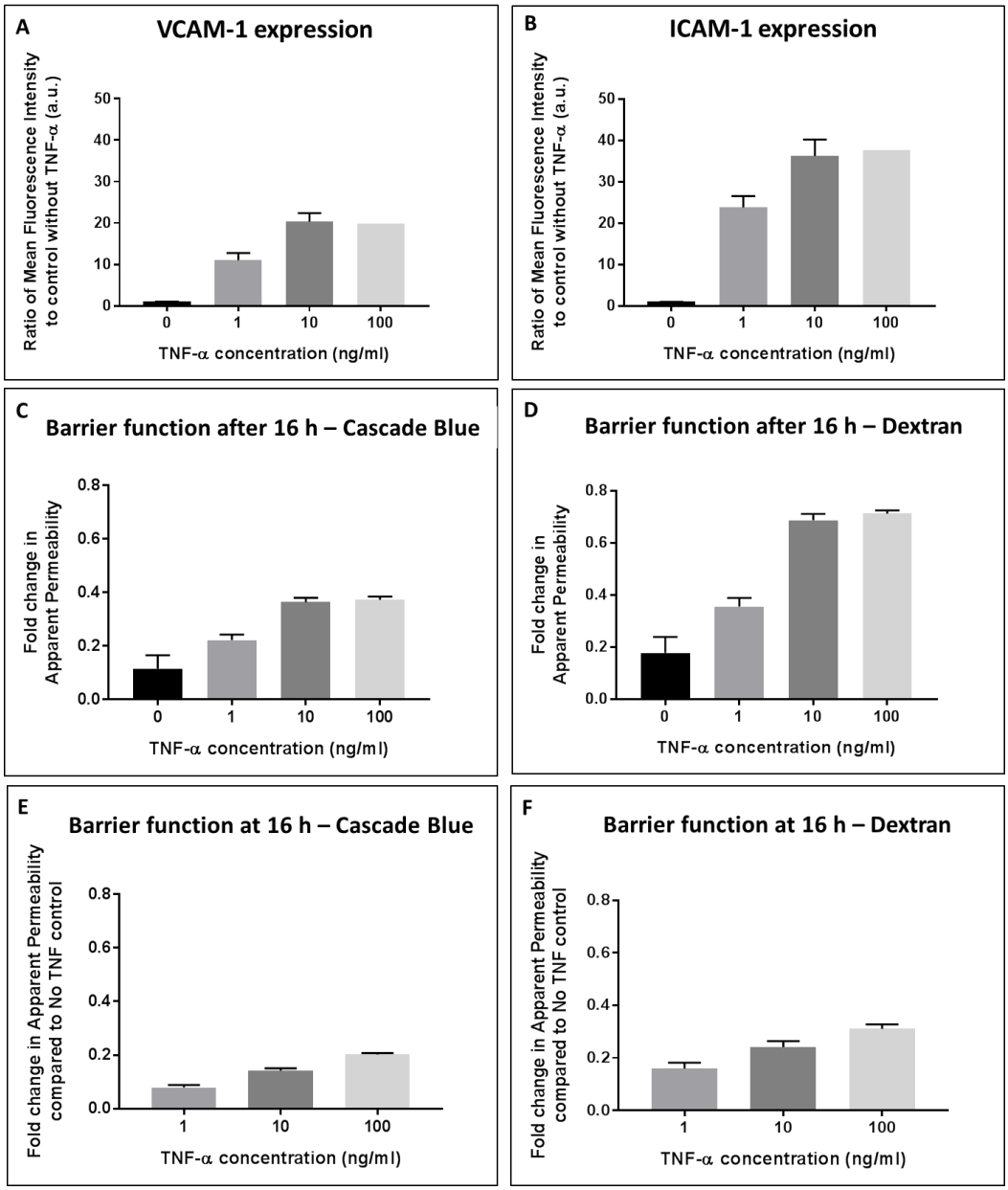

Figure 6.8 – Lung alveolus model on transwell incubated with increasing TNF-α concentration (in ng/ml) for 16 h resulted in higher inflammation and decreased barrier function. A and B – VCAM-1 and ICAM-1 expression of HUVEC from the lung alveolus transwell model increased with TNF-α dose reaching saturation at ≥10 ng/ml TNF-α. VCAM-1 (A) and ICAM-1 (B) expression was determined by the ratio of mean fluorescence intensity (in arbitrary units, a.u.) of each condition to control without TNF-α (set as ratio of 1). C and D – barrier function of the alveolus inflammation model decreased with increased TNF-α concentration reaching higher degree of permeability for TNF-α concentration ≥10 ng/ml. Barrier function was determined by the fold change in apparent permeability of cascade blue (C) and dextran (D) before and after 16 h treatment. Apparent permeability was measured after 2 h static incubation with the fluorescence dyes cascade blue and dextran. E and F – barrier function of the alveolus inflammation model at 16 h of TNF-α challenge showed decreased barrier function at higher TNF-α dose (100 ng/ml). Barrier function was calculated by the fold change in apparent permeability of cascade blue (E) and dextran (F) of each condition at 16 h to the control without TNF-α at 16 h treatment. N=1 with 1-3 technical replicates, *P value < 0.05, One-way ANOVA with Tukey correction. Error bars represent the standard error of the mean.

At the onset of inflammation and in particular in lung inflammation, cellular response is mediated not only by TNF-α but by several cytokines, for instance interleukins and interferons (Arm and Lee, 1992; Feghali and Wright, 1997). Therefore, to better mimic the inflammatory response and cause vascular leakage and decreased barrier function more than one cytokine might be necessary. Moreover, the low disruption of TNF-α on the barrier function could be explained by the higher resistance of the epithelial cell barrier compared to the endothelial cell barrier. In fact, it is described that endothelial cell barrier has lower transmonolayer electrical resistance and that TNF-α can disrupt the endothelial barrier, while the epithelial cell barrier has about 4-400X more transmonolayer electrical resistance and a combination of TNF-α and IFN-γ cytokines is necessary to disrupt the epithelial barrier (Blum *et al.*, 1997; Coyne *et al.*, 2002; Hermanns *et al.*, 2004).

TNF-α concentration from 0.2 to 15 ng/ml has been reported in patients with symptomatic pulmonary sarcoidosis and acute respiratory distress syndrome (Baughman *et al.*, 1990; Hermanns *et al.*, 2004). While for *in vitro* models 0-100 ng/ml TNF-α have been used, for instance, Ma and co-workers reported significant decrease of transmonolayer electrical resistance of colon epithelial cells after 48 h incubation with 10 ng/ml TNF-α or higher (Ma *et al.*, 2004). While Huh and colleagues mimicked the lung alveolus inflammation on a microfluidic device by challenging epithelial cells with 50 ng/ml TNF-α for 5 h which resulted in ICAM-1 upregulation of endothelial cells, adhesion of neutrophils and transmigration to the epithelial channel (Huh *et al.*, 2010) or by challenging either endothelial or epithelial cells of the lung alveolus chip with 100 ng/ml TNF-α overnight resulting in increased permeability, ICAM-1 expression by endothelial cells and thrombus formation (Jain *et al.*, 2018). IFN-γ concentration of 0.02-1 ng/ml have been reported in patients with COPD related anemia and in patients with lung cancer (Enewold *et al.*, 2009; Boutou *et al.*, 2012). While for *in vitro* models 0-100 ng/ml IFN-γ have been used for up to 72 h incubation (alone or in combination with TNF-α) resulting in increased permeability at concentrations higher than 1 ng/ml after 48 h (Blum *et al.*, 1997; Coyne *et al.*, 2002; Watson *et al.*, 2005). On the other hand, a conflicting study observed that 50 ng/ml IFN-γ improved lung epithelial barrier function and wound healing after 72 h incubation (Ahdieh, Vandenbos and Youakim, 2001).

Based on the TNF-α dose studies and on published reports, a TNF-α concentration of 50 ng/ml and an IFN-γ concentration of 10 ng/ml was selected to challenge the lung alveolus transwell model for 24 h.

To elucidate the pro- and anti-inflammatory potential of different MSC donors and their paracrine action, the effect of MSC indirect co-culture, MSC-CM and MSC-EVs was compared after 24 h incubation with 50 ng/ml TNF-α and 10 ng/ml IFN-γ using the lung alveolus model on transwell (Figure 6.9). Prior to co-treatment of the lung alveolus model: A) for the indirect MSC co-culture, the MSCs were previously cultured in full StemPro medium to be at a confluent monolayer upon inflammatory treatment with TNF-α and IFN-γ in 1% supplement in StemPro medium with the lung alveolus transwell system, B) for the MSC-CM co-treatment, the CM was collected from a T-flask cultured in 1% supplement in StemPro for 24 h after reaching confluency in full StemPro medium, then TNF-α and IFN-γ were added to the fresh CM and incubated with the alveolus transwell system, C) for MSC-EVs, the EVs were isolated from MSC-CM by UC and stored at -80ºC (for less than one week)

and then were slowly thawed on ice and added to the transwells at a final concentration of 3 x 10^{10} EV/ml in 1% supplement in StemPro with TNF-α and IFN-γ. MSC, MSC-CM and MSC-EVs as well as TNF-α and IFN-γ were added to the endothelial chamber of the lung alveolus transwells for 24 h and only 1% supplement was added to StemPro medium to avoid masking effects of full supplement addition. For the 3 MSC donors tested (RB135, RB55 and RB81), MSCs used for indirect co-culture as well as the MSCs from which CM and EVs were collected were all at passage 4 to avoid possible variation related to cell passage. MSC RB135 is another batch generated from the same donor as MSC RB70, which was out of stock. It is expected that batch to batch variability and possible differences in cell isolation process from the company RoosterBio could result in different potency of the cells as well as its CM and secreted EVs.

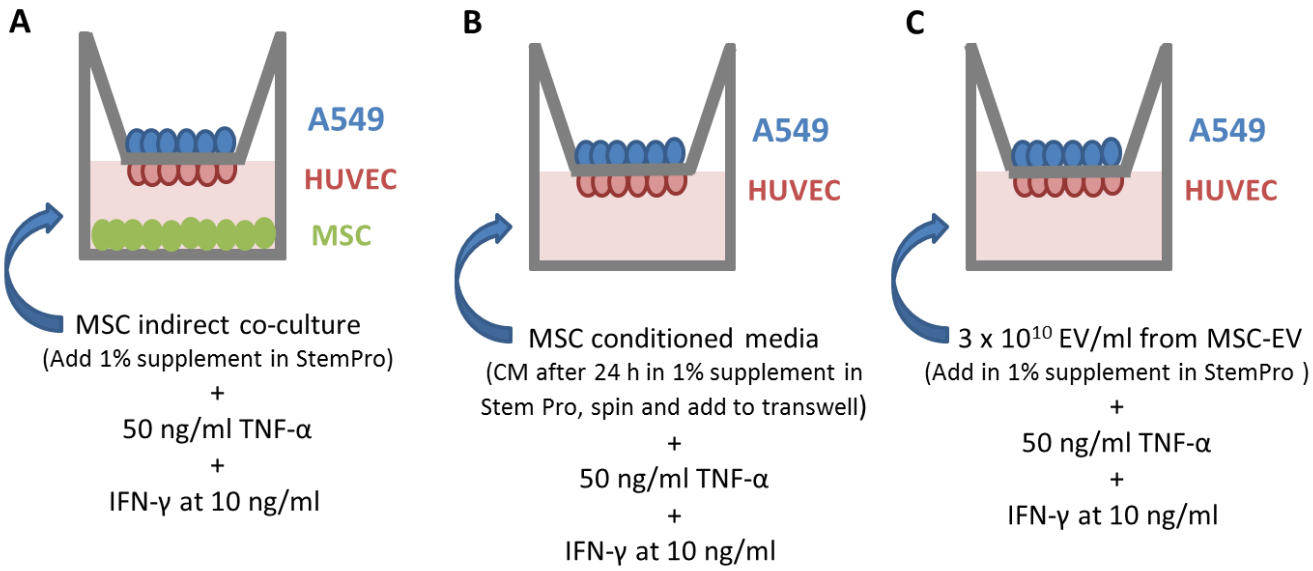

Figure 6.9 – Schematic representation of lung alveolus inflammation transwell model at air-liquid interface challenged for 24 h by the inflammatory cytokines TNF-α (at 50 ng/ml) and IFN-γ (at 10 ng/ml) and co-treated with MSC indirect co-culture (A), MSC conditioned media (CM) (B) or MSC-EVs (C). A – MSCs at passage 4 were cultured in 24 WP in full StemPro medium until confluency, and at the day of treatment the medium was changed to 1% supplement in StemPro medium with TNF-α and IFN-γ for indirect co-culture with the alveolus transwell model. B – MSCs at passage 4 were cultured in T-flasks in full StemPro medium until confluency and at the day before treatment the media was changed to 1% supplement in StemPro medium for 24 h, then the CM was collected, centrifuged and transferred to the alveolus transwell model with addition of TNF-α and IFN-γ. C – MSCs at passage 4 were cultured in T-flasks in full StemPro medium, CM was collected and the EVs were isolated from the CM by ultracentrifugation and stored at -80ºC. On the day of treatment, the alveolus transwell model was treated with 3x10^{10} EV/ml in 1% supplement in StemPro medium with TNF-α and IFN-γ.

The effects of MSC indirect co-culture, MSC-CM and MSC-EV were assessed by VCAM-1 and ICAM-1 expression of HUVEC from the lung alveolus model on transwell (Figure 6.10 A and B), LDH (Figure 6.10 C) as well as IL-8 secretion (Figure 6.10 D) and barrier function (evaluated by cascade blue and dextran apparent permeability, Figure 6.10 E and F).

Preliminary results of MSC indirect co-culture of MSC donors RB135, RB55 and RB81 seem to result in a decrease in VCAM-1 and ICAM-1 expression, with 40 to 70% reduction for VCAM-1 and 12 to 29% reduction for ICAM-1 expression compared to control challenged with TNF-α and IFN-γ only (Figure 6.10 A and B). CM from the 3 MSC donors did not seem to decrease VCAM-1 and ICAM-1 expression and in the case of VCAM-1 expression of HUVEC incubated with CM from donor RB55 and ICAM-1 expression of HUVEC incubated with CM from donor RB135, their expression seem to be even higher compared to the control challenged with TNF-α and IFN-γ only. MSC-EVs from donors RB135, RB55 and RB81 seem to be able to reduce VCAM-1 expression, in about 33, 40 and 29% respectively, compared to the control challenged with TNF-α and IFN-γ only. For MSC donor RB135, the VCAM-1 expression of HUVEC in indirect co-culture with MSCs seems to be reduce to higher extent than when HUVEC were incubated with MSC-EVs from the same donor. For the MSC donors RB55 and RB81, it seems that there was no difference between the decrease in VCAM-1 expression of HUVEC in indirect co-culture with MSCs and MSC-EV treatment. For MSC donor RB135 and RB81, ICAM-1 expression of HUVEC in indirect co-culture with MSCs seems to be reduced to higher extent than when HUVEC were incubated with MSC-EVs from the respective donors. For the MSC donor RB55, there seems to be a similar decrease in ICAM-1 expression when the lung alveolus model on transwell was indirectly co-cultured with MSCs or incubated with EVs. MSC-EVs from donors RB55 and RB81 were able to significantly reduce ICAM-1 expression, in about 13-15%, compared to control challenged with TNF-α and IFN-γ only. Flow cytometry charts of the VCAM-1 and ICAM-1 expression of HUVEC from each transwell system in Appendix 10.3.

As a positive control, the lung alveolus inflammation model on transwell was co-treated with the drug curcumin at 5 μM for the same period of time (24 h) in 1% supplement in StemPro medium. Curcumin is an anti-inflammatory drug that has been reported to reduce VCAM-1 and ICAM-1 expression and IL-8 secretion of TNF-α-activated endothelial cells (Kumar *et al.*, 1998; Kim *et al.*, 2007; Yen *et al.*, 2013). Curcumin at 5 μM was selected as it resulted in decreased VCAM-1 and ICAM-1 on HUVEC monolayer culture without causing cell death (data not shown). The treatment of the lung alveolus inflammation model on transwell with curcumin seemed to be able to reduce VCAM-1 and ICAM-1 expression in about 60% and 28%, respectively, compared to the HUVEC control challenged with TNF-α and IFN-γ only. The reduction in VCAM-1 and ICAM-1 expression by curcumin seemed to be similar to the reduction by MSC indirect co-culture of donors RB135 and RB81 with the lung alveolus model on transwell. Overall for the selected anti-inflammatory donors, MSC-EVs (at 3 x 10^{10} EV/ml) seem to be able to reduce VCAM-1 and ICAM-1 expression of activated endothelial cells to lower or similar extent as MSC indirect co-culture and the positive control curcumin, however, MSC-CM (100%) did not seem to be able to reduce inflammation.

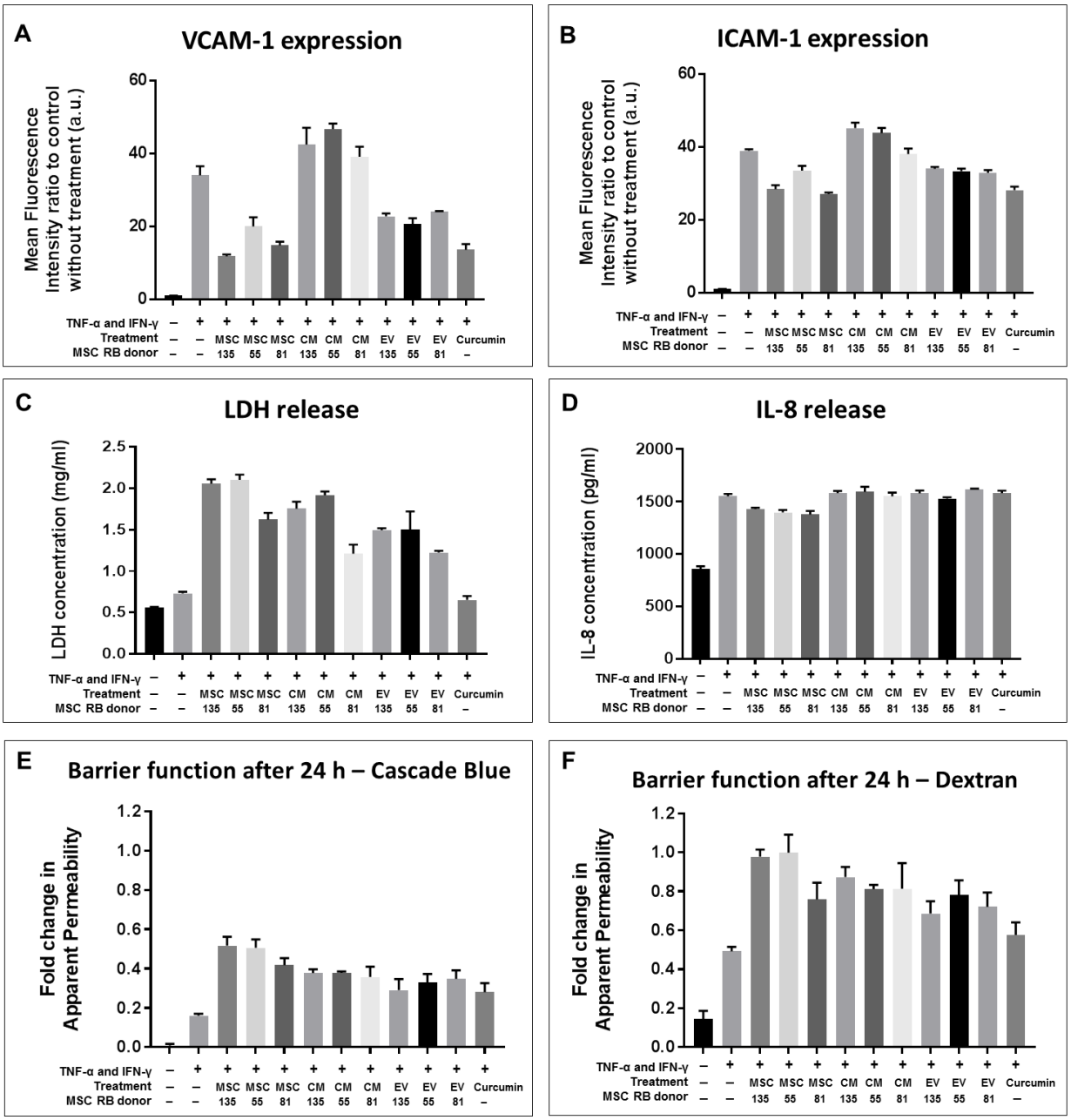

Figure 6.10 – Effect of mesenchymal stromal cell (MSC) indirect co-culture, MSC conditioned medium (CM) and MSC extracellular vesicles (EV) of donors RB135, RB55 and RB81 on lung alveolus inflammation model on transwell. TNF-α (50 ng/ml) and IFN-γ (10 ng/ml) were incubated for 24 h in 1% supplement in StemPro medium according to Figure 6.9. Curcumin (5 µM) in 1% supplement in StemPro medium was used as the positive control. A and B – VCAM-1 and ICAM-1 expression in HUVEC seemed to be reduced by MSC indirect co-culture and MSC-EVs. VCAM-1 (A) and ICAM-1 (B) expression was determined by the ratio of mean fluorescence intensity (in arbitrary units, a.u.) of each condition to the untreated control (set as 1). C – LDH release (in mg/ml) seemed to be increased for all conditions after 24 h treatment. D – Secretion of the inflammatory chemokine IL-8 (in pg/ml) seemed to be decreased only by MSC donor RB55 and RB81 in indirect co-culture with the alveolus transwell system. E and F – barrier function of the alveolus transwell model seemed to be decreased for all MSC indirect co-culture, MSC-CM and MSC-EV conditions. Barrier function was determined by the fold change in apparent permeability of cascade blue (E) and dextran (F) before and after 24 h treatment. N = 1 with technical triplicates, *P value < 0.05, One-way ANOVA with Tukey correction. Error bars represent the standard error of the mean.

Preliminary results seemed to show higher LDH release for all conditions (MSC indirect co-culture, MSC-CM and MSC-EV) for the 3 MSC donors (Figure 6.10 C). The increase in LDH release in the case of the co-culture could be explained by the addition to the lung alveolus system of another cell type (MSC) that also produced LDH when challenged by TNF-α and IFN-γ. While the increase in LDH in the case of CM and EVs could be explained by the presence of LDH already in their solutions (which has been previously seen in data not shown). Curcumin seemed to slightly reduce LDH concentration (about 10%) compared to control challenged with TNF-α and IFN-γ only. No significant number of cells were found in the supernatant compared to controls and no detachment was observed by contrast phase microscopy, indicating that TNF-α and IFN-γ are causing inflammation but not significant cell death.

Preliminary results seemed to show that the indirect co-culture with MSC donors RB55 and RB81 were the only conditions that resulted in a reduction, in about 10 to 11%, in the secretion of the inflammatory chemokine IL-8 compared to control challenged with TNF-α and IFN-γ only (Figure 6.10 D). Curcumin is reported to reduce IL-8 secretion from endothelial cells (Kim *et al.*, 2007), however, no great effect seemed to be observed for the lung alveolus model possibly indicating that MSC-indirect co-culture had higher potential on reducing the anti-inflammatory chemokine IL-8 than the anti-inflammatory drug, although confirmation of results is needed.

MSC-EVs were isolated from MSCs cultured in full StemPro and from a higher number of cells and then concentrated to 3 x 10^{10} EV/ml, while MSC-CM was collected from confluent MSCs cultured for 24 h in 1% supplement in StemPro. Therefore, the number of EVs present in the CM volume added to the alveolus transwell model is probably several orders of magnitude lower compared to the MSC-EV conditions and also the MSC-CM potential might be negatively affected by the culture in 1% supplement in StemPro. Alternatively, MSCs could be cultured in full StemPro medium and then diluted with basal StemPro medium for a final 1 % supplement for culture with the alveolus model, however, the paracrine factors and EVs in the CM would also be diluted. A dose-response study of MSC-CM could also be performed to evaluate which ratio of CM to culture medium would result in higher decrease of inflammation or MSC-CM could be filtered and concentrated previous to dilution for a final 1 % supplement in StemPro medium and after optimizing the best CM dose its anti-inflammatory potential could be compared to the optimized dose of anti-inflammatory EVs and MSC indirect co-culture. Another possibility would be to concentrate the CM and then optimize for the CM dilution/concentration in culture medium. Similarly, the number of MSCs that were in indirect co-culture was lower than the number of cells from which the EV dose of 3 x 10^{10} EV/ml was isolated, however, MSCs have the ability to continuously produce paracrine factors and EVs in response to the inflammatory challenge and in cross-talk with the lung alveolus cells, which can explain the increased ability to reduce VCAM-1 and ICAM-1 expression and IL-8 secretion.

Sun and co-workers performed a dose-response study of BM MSC-CM (0-100% CM obtained from 24 h conditioning with culture medium supplemented with 2% FBS which was filtered with 0.22 μm filter and stored at -80ºC) on neuronal and glial cells and observed that CM ratio of 30-50% resulted in higher decrease of apoptosis and inflammation (Sun *et al.*, 2013). Conforti and colleagues

evaluated BM MSC and BM MSC-EV immunomodulatory properties and observed that MSC efficiently inhibited T cell proliferation while MSC-secreted microvesicles isolated by UC had a much lower effect on T cell proliferation (and with higher variability) as well as on antibody production by B-cells (Conforti *et al.*, 2014). On the other hand, Bruno and co-workers observed comparable effect between BM MSC-EVs isolated by UC (15 µg) and BM MSC (75,000 cells) administration on the recovery from glycerol-induced acute kidney injury using a mice model, while *in vitro* MSC-EVs were able to promote proliferation and increase resistance of epithelial cells (Bruno *et al.*, 2009). Wu and colleagues reported that UC-isolated human umbilical cord Wharton's Jelly MSC-EVs (at the higher dose tested of 200 µg) produced higher anti-proliferative and pro-apoptotic effect on tumor cells *in vitro* and *in vivo* compared to MSC administration (10^7 cells) (Wu *et al.*, 2013). While, hypoxia stimulated human UCM MSC-EVs isolated by UC and administered at 100 µg (but not at lower EV-associated protein doses) were able to able to restore blood flow by promoting angiogenesis in a limb ischemic model compared to MSC administration (10^6 cells) (H.-C. Zhang *et al.*, 2012). Xing and co-workers tested the effect of rat BM MSC and MSC-CM (filtered with 0.22 µm filter) on ischemia-reperfusion kidney injury and described that cell administration resulted in kidney repair (increased angiogenic, anti-inflammatory and anti-apoptotic effect), while MSC-CM did not improve kidney repair despite of the presence of pro-angiogenic factors in the CM (Xing *et al.*, 2014). On the other hand, human embryonic MSC-CM (50 µg concentrated by a 10 kDa molecular weight cut-off ultrafiltration membrane and sterilized by 0.22 µm filter) promoted repair on a chronic kidney disease animal model, while MSC-CM derived EVs (7 µg) did not induce repair (van Koppen *et al.*, 2012). Using several animal models, MSC-EV doses in range of 0.4 to 250 µg of EV-associated protein (isolated by UC, ultrafiltration and chromatography) have been administered resulting in improved recovery and graft survival after organ transplantation (Monguió-Tortajada *et al.*, 2014; Rani *et al.*, 2015). Herein, a dose of 3 x 10^{10} EV/ml correspondent to about 10-40 µg of EV-associated protein is in the range of EV doses used for animal models, although a direct comparison cannot be performed as EV concentration per cell might be considerably different due to different number of cells that are subjected to EV action and due to EV clearance mechanisms present in the animal models.

The conflicting results on whether MSC-CM and MSC-EV have lower, similar or improved immunomodulatory and regenerative potential compared to MSC administration needs further elucidation and not only comparable doses of MSCs, MSC-CM and MSC-EVs should be tested but also to compare the best dosing condition of CM as opposed to the best dosing condition of EVs and to optimized number of cells for administration in order to predict which option would translate into an improved therapy. For therapeutic purposes, improved results could potentially be achieved by combining administration of cells with CM and/or EVs.

Preliminary results of the barrier function of the lung alveolus transwell model seemed to be decreased, as expected, when challenged with 50 ng/ml TNF-α and 10 ng/ml IFN-γ resulting in 0.16 and 0.5 fold change increase in apparent permeability of cascade blue and dextran fluorescent dyes, respectively, compared to untreated control (Figure 6.10 E) (supplemental data of the apparent permeability from each transwell system in Appendix 10.4). The apparent permeability of cascade blue fluorescent dye seemed to be increased for the MSC indirect co-culture and MSC-CM for the 3 MSC

donors compared to control challenged with TNF-α and IFN-γ only, indicating that the barrier function was weaker for those conditions compared to control (Figure 6.10 E). The apparent permeability of cascade blue for the MSC-EV conditions and the drug curcumin did not seem to be different from the control challenged with TNF-α and IFN-γ only. The apparent permeability of dextran in the alveolus model on transwell when indirectly co-cultured with MSC RB135 and RB55 or incubated with MSC-CM RB135 also seemed to be increased compared to control challenged with TNF-α and IFN-γ only, indicating weaker barrier function for those conditions (Figure 6.10 F). The apparent permeability of dextran for all the other conditions and curcumin did not seem to change considerably from the control challenged with TNF-α and IFN-γ only.

These preliminary results indicate that MSC and MSC-derived products exacerbated barrier disruption instead of promoting its recovery upon the inflammatory challenge. It is possible that MSC and MSC-derived products would promote increased permeability similarly to a scenario of inflammation in which vasodilatation occurs to increase blood flow and oxygen supply and removal of waste and dead cells and also to allow immune cells to transmigrate through the cell barrier in order to eliminate potential pathogens and faster resolve inflammation. It is also possible that MSC and MSC-derived products could promote recovery of the barrier function in a later time point, therefore, longer time points (for instance, 48 h and 72 h) could be evaluated instead of just 24 h, especially if the mechanisms of action of MSC-EVs are through nucleic acids (mRNAs and microRNAs) which might cause their effect in a later time point.

Dual effect of pro-inflammatory cytokines has also been reported. Indeed, TNF-α and IFN-γ were reported to be able to disrupt the epithelial cell barrier and increase paracellular permeability by internalization of transmembrane proteins and not through apoptotic mechanisms (Bruewer *et al.*, 2003). On the other hand, it is reported that lymphocytes and secreted cytokines such as TNF-α may up-regulate expression of tight junction-associated proteins such as zonula occludens-1 (ZO-1) in epithelial cells, accelerating tight junction assembly and promoting barrier function (X. X. Tang *et al.*, 2010). Therefore, tight junctions are considered gatekeepers that regulate paracellular flux by blocking the entrance of pathogens and other molecules or by opening and causing an exacerbation of the inflammatory response consequently followed by drainage of inflammatory cells to resolve the inflammation (Soyka *et al.*, 2012).

Moreover, increased permeability and decreased barrier function due to changes in tight junctions is associated to several inflammatory diseases such as bronchial asthma (Xiao *et al.*, 2011), chronic rhinosinusitis (Soyka *et al.*, 2012), psoriasis skin inflammation (Kirschner *et al.*, 2010) and Crohn's inflammatory intestinal disease (Schulzke *et al.*, 2009).

MSCs have been reported to up-regulate the epithelial tight junction-associated protein ZO-1 when MSCs are in direct co-culture with epithelial cells, promoting ZO-1 relocation and accelerating tight junction assembly. While, MSC-CM only slightly increased tight junction assembly (Rowart *et al.*, 2017), indicating that the mechanisms of improvement in barrier function were mainly through cell-cell direct contact, condition that was not tested herein (only MSC indirect co-culture, MSC-CM and MSC-EVs were tested).

Grupta and colleagues observed that MSC administration (750,000 cells) in mice suffering from endotoxin-induced acute lung injury improved their survival by the decrease in permeability and pulmonary edema, by the decrease in pro-inflammatory cytokines (for instance TNF-α) and by the increase in the anti-inflammatory cytokine IL-10, however, MSCs did not act on endotoxin clearance (Gupta *et al.*, 2007). MSC administration (5 or 10 x 10^6 cells) in an *ex vivo* perfused human lung model with *Escherichia coli*-induced pneumonia promoted alveolar fluid clearance, restored lung protein permeability, decreased inflammation and increased clearance of bacterial infection partially by KGF (J. W. Lee *et al.*, 2013). Moreover, MSC administration produced better results than KGF (100 ng), ampicillin (0.2 g) or normal human lung fibroblast (5 or 10 x 10^6 cells) administration alone (J. W. Lee *et al.*, 2013). MSC-EVs (30 µl equivalent to 31 $\pm$ 17 µg EV-associated protein) were also reported to reduce lung protein permeability and pulmonary edema as well as inflammation on a mice model of endotoxin-induced injury, which was in part mediated by KGF mRNA. KGF is involved in vectorial ion and fluid transport in alveolar epithelial cells type II and in anti-microbial potential of monocytes and macrophages (J. W. Lee *et al.*, 2013). Furthermore, 100 µl MSC-EVs (in proportion about 103 $\pm$ 57 µg EV-associated protein) reduced the permeability of epithelial cells challenged by 50 ng/ml mix of TNF-α, IL-1β and IFN-γ on a transwell after 24 h, effect that was similar to MSC indirect co-culture (250,000 cells) (Zhu *et al.*, 2013). Similar order of magnitude regarding MSC-EV dose (10-40 µg EV-associated protein) and MSC number of cells (20,000-100,000 cell/well at confluency) were used herein, however, reduction in permeability was not observed after 24 h. Differences might be attributed to donor variability, different cell types and culture medium as well as the more complex system including endothelial cells which are more sensitive and permeable than epithelial cells. Moreover, MSCs are known to secrete angiogenic factors such as VEGF (Hung *et al.*, 2007; Carmelo *et al.*, 2015) which increase endothelial permeability and could potentially counteract the effect of MSC-secreted factors that decrease permeability and improve barrier function such as angiopoetin-1 (Gamble *et al.*, 2000; Kim *et al.*, 2001; Pizurki *et al.*, 2003; Fang *et al.*, 2010; Amable *et al.*, 2014) and KGF (J. W. Lee *et al.*, 2013; Zhu *et al.*, 2013). Further research and deeper understanding of the balance of different cytokine and growth factor concentrations during the different stages of the inflammation process as well as of the complex mechanisms of action of MSC, MSC-CM and MSC-EV on endothelial-epithelial barrier function upon inflammation stimuli is needed in order to understand which therapeutic product (MSC, MSC-CM or MSC-EVs) has higher efficacy on reducing inflammation and increasing barrier function, to be able to control the potential and efficacy and also to determine what would be most appropriate dosing and timing for administration.

To the extent of my knowledge very few studies evaluated MSC action on a co-culture system with endothelial and epithelial cells. Most of the studies have used animal models and their findings often do not translate into clinical benefits in the human setting due to specie differences. Availability of human lungs that are rejected for transplantation and that can be used for research purposes are limiting, therefore, the use of transwell models to mimic organ level interfaces, functions and disease states such as endothelial-epithelial cell barrier of the lung alveolus in an inflammation scenario can be very useful as a screening tool and to elucidate MSC immunomodulatory and regenerative potential and its mechanisms of action. Overall, the results seemed to indicate that MSC indirect co-

culture with the lung alveolus model reduced inflammation (by decreasing VCAM-1 and ICAM-1 expression and IL-8 secretion) to higher extent than MSC-EVs and MSC-CM, however, none of the conditions was able to improve barrier function.

To improve the model, human A549 epithelial cancer cell line and HUVEC could be replaced by human organ specific primary endothelial and epithelial cells (type I and II) to better mimic the endothelial-epithelial barrier functions of the human lung alveolus and recapitulate *in vivo* pathological responses.

The co-culture of immune cells in direct contact with epithelial cells is described to improve barrier function and enhance immune cell survival (Ho *et al.*, 2006). Consequently, the lung alveolus transwell model could be further complexed by the addition of immune cells which play an important role on the resolution of inflammation and, therefore, the possible synergetic effect of immune cells on accelerating the resolution of lung alveolus inflammation by MSC direct and indirect co-culture, MSC-CM and MSC-EVs could be assessed.

6.6 Lung alveolus-on-a-chip inflammation model

The complexity of the 3D model was further increased using a microfluidic device with a top channel in which A549 epithelial cells were cultured and a bottom channel with HUVEC endothelial cells which were separated by a flexible porous membrane that enables tissue-tissue interactions. The endothelial channel was perfused with culture medium to resemble blood flow and the device was subjected to cyclic stretch to mimic breathing motion (Figure 6.11). Similarly to the lung alveolus transwell model, the epithelial cells were treated with dexamethasone and exposed to air to establish an air-liquid interface that was maintained for 5 days to promote surfactant production and improve barrier function (Huh *et al.*, 2010). Endothelial cells were seeded in all the sides of the bottom channel to mimic a blood vessel which was perfused with culture medium at laminar flow of 1.02 – 1.70 µl/min of FM and shear stress of about 0.2-0.3 dyne/cm^2, which is lower than the physiological conditions at 15 dyne/cm^2 (Huh *et al.*, 2010), therefore, endothelial cell alignment in the direction of flow and the strength of the tight junctions did not fully mimicked the *in vivo* lung alveolus. Unidirectional cyclic stretch (5% strain at -45 kPa and 0.2 Hz) mimicked the breathing motion similar to physiological levels (of about 5 to 15% strain), which also contributes to endothelial cell alignment (Birukov *et al.*, 2003; Huh *et al.*, 2010).

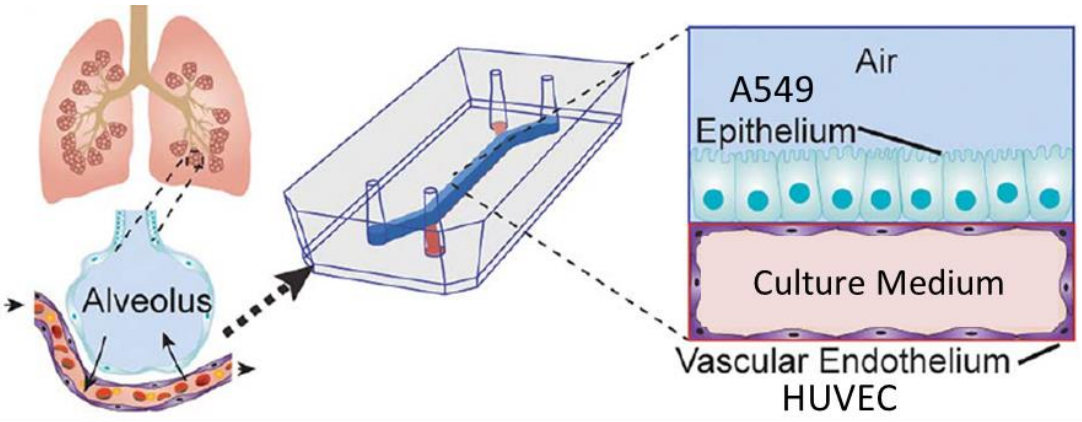

Figure 6.11 – Schematic representation of the patented microfluidic device developed at the Wyss Institute. Inspired by nature a lung alveolus-on-a-chip was designed to mimic tissue-tissue interactions that occur in the human lung between the epithelial cells in the alveoli and the endothelial cells from the blood vessel network surrounding them. The microfluidic device is a tall channel stretchable chip with a PDMS membrane between the epithelium (top channel) and the endothelium (bottom channel). The human cell lines A549 and HUVEC were cultured in the microfluidic device to model the epithelium and endothelium, respectively. To closer resemble the human lung alveolus, air-liquid interface was establish, the endothelium was perfused with continuous flow of culture medium and cyclic vacuum was applied in lateral chambers of the chip to model the breathing motion. Image adapted from Jain et al., 2018.

The lung alveolus-on-a-chip was used to model inflammation and to test the immunomodulatory properties of MSC-EVs. Similarly to the HUVEC potency assay, the lung alveolus-on-a-chip was challenged with 10 ng/ml TNF-α for 16 h. Prior to TNF-α and EV treatment, lung alveolus-on-a-chip cells were starved by flowing MM (0.5% serum without growth factors) through the endothelial chamber for 24 h. Then, alveolus-on-a-chip model was treated with TNF-α alone or TNF-α and EVs in MM on flow for 16 h, followed by a 24 h recovery period flowing medium only. For the negative control group, culture medium was flowing for the full 16 h plus 24 h (40 h total). MSC-EVs from MSC donors RB70 and RB81 were pooled and added at 10^{10} EV/ml (lower EV doses did not promote recovery from inflammation, data not shown).

A statistically significant increase in ICAM-1 expression (Figure 6.12 A), IL-8 secretion (Figure 6.12 B) as well as in apparent permeability of the fluorescent dyes cascade blue and dextran (Figure 6.12 C and D, respectively) indicates that TNF-α at 10 ng/ml flowing through the endothelial channel was able to cause inflammation in the microfluidic system when comparing the group TNF-α only (No EV, TNF-α) with the negative control group (No EV, No TNF-α). Similar results were observed after 5 h incubation with 50 ng/ml TNF-α through the epithelial channel of a lung alveolus-on-a-chip model (Huh *et al.*, 2010). Furthermore, the negative control group maintained basal ICAM-1 expression and IL-8 secretion through the 40 h (16 + 24 h) period of time indicating that unchallenged microfluidic devices on flow at air-liquid interface and subjected to cyclic strain are not under stress and inflammatory conditions, which is in accordance with Huh and co-workers published work (Huh *et al.*, 2010). Moreover the apparent permeability of the negative control decreased indicating a stronger barrier function.

The expression of the HUVEC surface marker ICAM-1 was significantly decreased in about 28% (Figure 6.12 A) when the lung alveolus-on-a-chip was co-treated with TNF-α and EVs compared to cells challenged by TNF-α only after 16 h. After 24 h recovery flowing medium only, the ICAM-1

expression of both groups decreased to similar values (no statistical significant difference between groups), however, both groups decreased to similar values (no statistical significant difference between groups) without reaching the basal levels of the negative control. Flow cytometry charts of the ICAM-1 expression of HUVEC from each microfluidic device are in Appendix 10.3.

The secretion of the chemokine IL-8 was not statistically different between alveolus-on-a-chip group co-treated with TNF-α and EVs and the group treated with TNF-α only (Figure 6.12 B), indicating that the MSC-EVs at the dose tested did not have strong enough anti-inflammatory potential to counteract the pro-inflammatory effect of TNF-α.

The group treated with TNF-α only had decreased barrier function given by a statistically significant increase in apparent permeability of cascade blue and dextran compared with the negative control group. While MSC-EVs promoted the recovery of the barrier function by decreasing the apparent permeability of cascade blue and dextran (with statistical significance for dextran only) after 16 h treatment and after 24 h recovery period when compared with the group TNF-α only. Moreover, the apparent permeability of the EV treated group was reduced to levels closer to the negative control group indicative of decreased pulmonary edema (supplemental data of the apparent permeability from each microfluidic device in Appendix 10.4).

Therefore, MSC-EVs reduced inflammation by decreasing ICAM-1 expression and improved barrier function by decreasing vascular leakage and edema. However, MSC-EVs (at 10^{10} EV/ml approximately 3-13 µg of EV-associated protein) did not fully resolve inflammation as ICAM-1 was not reduced to basal levels and EVs were not able to decrease IL-8 chemokine, indicating that endothelial inflammatory cues that attract (IL-8) and bind (ICAM-1) to immune cells such as monocytes are still active. Therefore, a stronger immunomodulatory effect of EVs is necessary by increasing MSC-EV dosing and administration regimen or testing MSC-EV bioengineering strategies to further reduce and resolve inflammation.

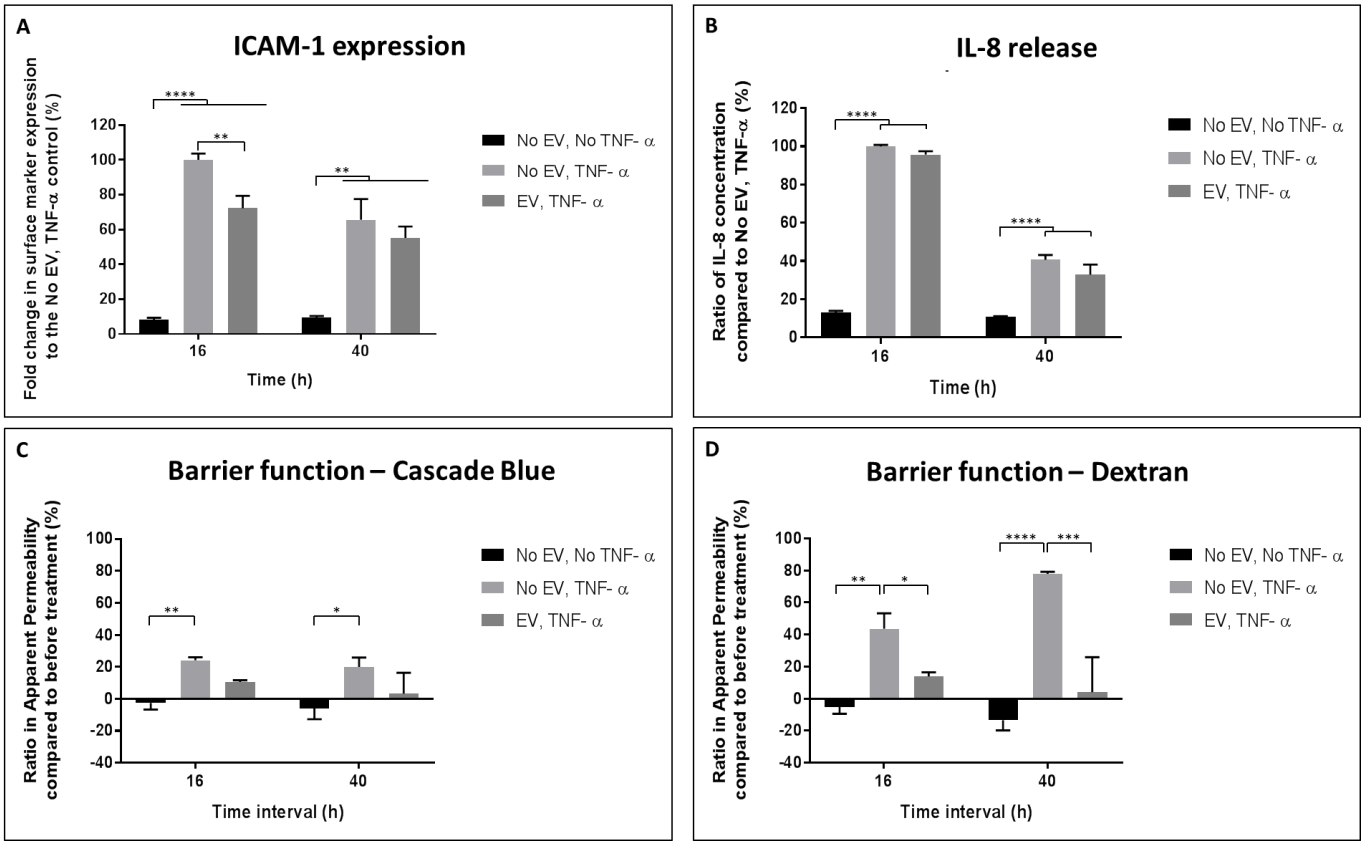

Figure 6.12 – MSC-EV action on reducing inflammation and improving barrier function of the lung alveolus-on-a-chip TNF-α-induced inflammation model. After 24 h starvation, the lung alveolus-on-a-chip models were challenged with TNF-α (10 ng/ml) and co-treated with MSC-EVs (10^{10} EV/ml from a pool of MSC donors RB70 and RB81) for 16 h on flow, followed by 24 h recovery flowing medium only. A – ICAM-1 expression of HUVEC on the alveolus-on-a-chip system was reduced by the co-treatment with MSC-EVs after 16 h challenge with TNF-α. ICAM-1 expression was determined by the ratio of mean fluorescence intensity (in %) of each condition to the control TNF-α only (No EV, with TNF-α) after 16 h treatment (which was set as 100%) (n = 3 with 2-5 total technical replicates). B – Secretion of the inflammatory chemokine IL-8 (in %) was not statistically different between the EV co-treated group and the control with TNF-α only. IL-8 release is represented by ratio of IL-8 concentration of each condition to the control TNF-α only (set as 100%) after 16 h treatment (n = 3 with 3-6 total technical replicates). C and D – barrier function of the alveolus-on-a-chip inflammation model was improved for the EV co-treated group compared to the control with TNF-α only. Barrier function was determined by the fold change in apparent permeability (in %) of cascade blue (C) and dextran (D) of each condition at 16 h and 40 h time point to before treatment (n = 3 with 2-4 total technical replicates). *P value < 0.05, Two-way ANOVA with Tukey correction. Error bars represent the standard error of the mean.

As described in the previous subchapter, MSC-EVs at similar doses have been tested in several lung injury models. BM MSC-EVs (at about 31 µg EV-associated protein isolated by UC from MSC serum-starve and supplemented with 0.5% BSA for 48 h) were reported to decrease permeability and pulmonary edema and reduce inflammation both *in vitro* and in a mice model of endotoxin-induced lung injury (Zhu *et al.*, 2013). BM MSC-EVs (30 µg EV-associated protein isolated by UC from MSCs serum-starved for 48 h) also attenuated pulmonary vascular permeability in a

hemorrhagic shock and trauma-induced lung injury mice model (Potter *et al.*, 2018). BM MSC-EVs (90 ± 48 µg EV-associated protein isolated by UC) improved survival, reduced lung inflammation and permeability and decreased bacterial growth to similar extent as MSC administration (800,000 cells) in an *Escherichia coli*-induced pneumonia mice model (Monsel *et al.*, 2015). BM MSC-EVs (83 ± 46 µg EV-associated protein isolated by UC from MSC serum-starve and supplemented with 0.5% BSA for 48 h) were also able to reduce pulmonary edema in an *ex vivo* human ischemic-reperfusion injury lung model, however, no significant reduction in inflammation was reported (Gennai *et al.*, 2015). As previously stated, it is still not clear if MSC-EVs can have similar, lower or higher potency than MSC administration. Moreover, these studies used BM MSC cell source and UC to isolate MSC-EVs, however, modifications in the protocol for EV isolation and storage, in the culture medium, MSC donor-to-donor variability and the higher MSC-EV doses used for animal models compared to the dose herein used for the microfluidic devices (despite of the differences between the systems) can influence the results and explain the differences between works.

To the extent of my knowledge this is the first study of MSC-EVs on organ-a-chip microfluidic devices and in particular of MSC-EV immunomodulatory potential in a microfluidic device mimicking the organ level functions of the human lung alveolus avoiding the use of animal models and *ex vivo* human lungs.

To evaluate the presence of MSC-EVs flowing through and attaching to the endothelial cells in the lung alveolus microfluidic device, the cells in the microfluidic device were stained with calcein AM and MSC-EVs labeled with PKH67 dye followed by imaging. Confocal microscopy was used for imaging of MSC-EVs flowing in the microfluidic device, however, due to resolution limitations, it was harder to image the smaller EVs in the size range of 90-200 nm and mostly microvesicles which have a range of 100 to 1,000 nm (examples pointed with arrows in Figure 6.13) and EV aggregates (examples surrounded by circles in Figure 6.13) were identified.

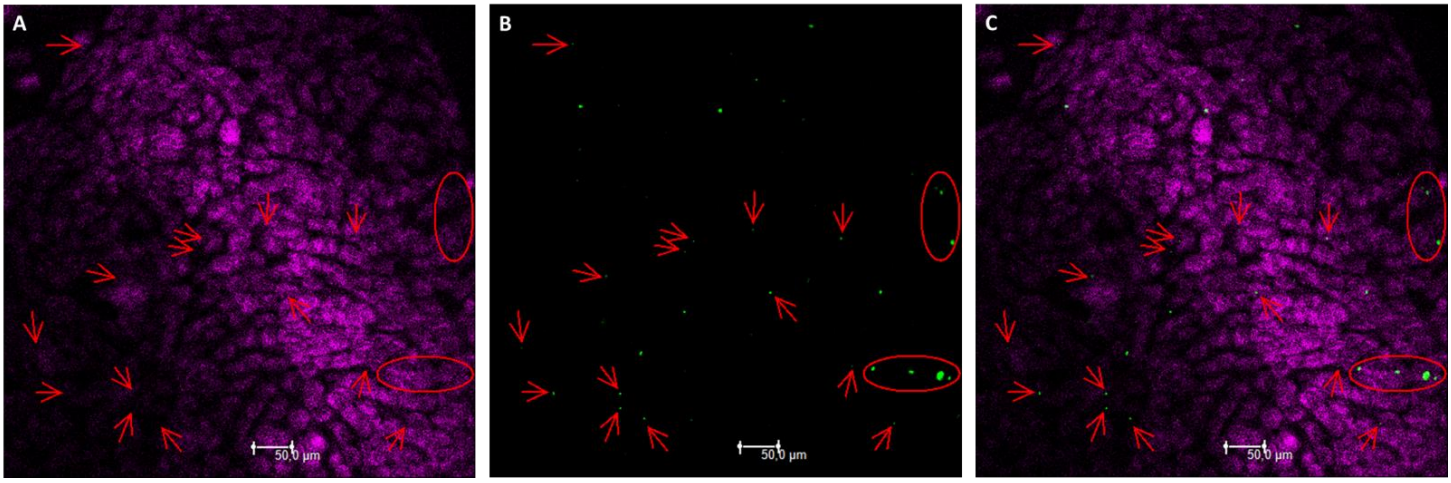

Figure 6.13 – MSC-EVs and EV aggregates attached to HUVEC on the floor of the bottom channel of the lung alveolus microfluidic device. A – HUVEC stained with calcein AM (in purple). B – MSC-EVs labelled with PKH67 (in green). C – Merge of image A and B. Arrows point to examples of larger EVs possibly microvesicles and circles surround larger size EV aggregates. Scale bar 50 µm.

The use of microfluidic devices has been reported, namely Huh and co-workers used a similar lung-alveolus model and demonstrated that this model can emulate organ-level responses to bacterial infections with *Escherichia coli*, to the inflammatory cytokine TNF-α and to toxic silica nanoparticles by observing several steps of inflammation such as endothelium activation (ICAM-1 up-regulation), secretion of inflammatory chemokines (IL-8), transmigration of circulating neutrophils through the endothelial-epithelial tissue interface and phagocytosis of bacteria. Moreover, the importance of mechanical stretch was demonstrated by observing increased nanoparticle transport with cyclic strain similar to *in vivo* conditions (Huh *et al.*, 2010).

Huh and colleagues also mimicked pulmonary edema using IL-2 (at 1,000 U/ml), a drug used to treat cancer patients which causes toxic secondary effects such as vascular leakage and fluid accumulation in the lungs. The relevance of using a model that mimics breathing motion was again demonstrated as it increased vascular leakage, exacerbating edema. Moreover, it was reported that immune cells were not required for disease progress (Huh *et al.*, 2012). Indeed, IL-2 does not promote the activation of endothelial cells as IL-2 concentrations from 0-100,000 U/ml did not up-regulate expression of the adhesion molecules VCAM-1 and ICAM-1 (data not shown), therefore, the inflammation cascade steps of endothelial activation and monocyte adhesion and transmigration were not induced, indicating that IL-2 exerts its action through mechanisms other than inflammation. Moreover, Huh and colleagues identified angiopoietin-1 as a potential therapy for pulmonary edema (Huh *et al.*, 2012). In fact, angiopoietin-1 has been reported to decrease permeability and improve barrier function (Gamble *et al.*, 2000; Kim *et al.*, 2001; Pizurki *et al.*, 2003; Fang *et al.*, 2010; Amable *et al.*, 2014), moreover angiopoietin-1 is secreted by MSCs, therefore, it would be interesting to test the effect of MSC, MSC-CM and MSC-EVs on the recovery of pulmonary edema by IL-2 induction.

Jain and co-workers cultured the microfluidic device with organ specific primary lung cells, developed a human pulmonary thrombosis model and evaluated the lung pathophysiological responses flowing whole blood through the endothelium without stimuli, with LPS endotoxin challenge and an anti-thrombotic drug. Inflammation cascade was also recapitulated by endothelial cell activation (ICAM-1 up-regulation), secretion of cytokines and chemokines (such as IL-8) and the platelet-endothelium dynamics were also mimicked (Jain *et al.*, 2018).

Similar microfluidic devices have been used to mimic lung small airway (Benam *et al.*, 2016; Benam *et al.*, 2016 (1)) and lung cancer (Hassell *et al.*, 2017) functions and development. This type of microfluidic devices recapitulating tissue-tissue interaction and barrier function can also be extended to other organs such as BM, liver, blood-brain barrier, gut, liver and other tissue-tissue interfaces. The use of microfluidic models that better mimic complex organ-level functions allows to model human pathophysiology and to advance toxicological screening and drug development in a fast and cost-effective way compared to the use of simpler *in vitro* 2D and 3D human models that fail to recapitulate, for instance, the impact of mechanical strain and reduces the need to use animal models which often fail to recapitulate human responses resulting in possible differences in response to treatments and toxicity effects.

As stated for the transwell model, to improve this model the human cell lines A549 and HUVEC could be replaced by human organ specific primary endothelial and epithelial cells to better mimic the endothelial-epithelial barrier functions of the lung alveolus and recapitulate *in vivo* pathological responses. Moreover, higher flow rate through the endothelial channel could be applied to increase shear stress and better mimic physiological conditions, thus improving endothelial cell alignment and increasing strength of the tight junctions. A mixture of TNF-α, IFN-γ and IL-1β at concentrations closer to *in vivo* lung inflammation states could be tested to better mimic pathological conditions. EV treatment could be further optimized by testing different EV doses (lower and higher than 10^{10} EV/ml from one or from different donors), different types of treatment (EV pre-treatment, co-treatment of EVs with inflammatory cytokines and/or EV treatment after inflammatory cytokines) and different treatment regimens (static and/or on flow). Bioengineered MSC-EVs could also be tested to further improve EV anti-inflammatory effect. Furthermore, more complex models can be developed by incorporating MSCs in the lung alveolus-on-a-chip model or flowing MSC-CM or combining MSC, CM or EV administration. Flow of blood (which contains several types of immune cells) through the endothelial channel or flow of monocytes only or neutrophils only could also be tested to assess EV anti-inflammatory potential and its impact on a faster resolution of inflammation as MSC-EVs are known to modulate both endothelial and immune cells possibility having a synergetic effect and also because it could be possible that immune cells may act as EV carriers delivering them to the injury sites.

Bioengineering of MSC-EVs was pursued and preliminary results are indicated in Appendix A 10.1. Moreover, to use MSC-EVs and bioengineered EVs as off-the-shelf products for therapy it is important to understand the impact of storage conditions on EV integrity and EV potential and to develop optimized storage conditions, thus a preliminary study of the impact of storage conditions is described in Appendix B 10.2.

7 Conclusions and future work

A robust MSC-EV isolation protocol by differential centrifugation and UC was optimized. EVs from different BM MSC donors were characterized by cryo electron microscopy, nanoparticle tracking analysis and MicroBCA. Cryo electron microscopy allowed the visualization of EVs and EV aggregates (due to the high speed of UC) with different morphology and content. MSC-EVs from different donors had similar size range 91-201 nm, indicating the presence of exosomes and small microvesicles. EV and protein concentration, and, consequently, the PPR were similar between different BM MSC donors indicating that the optimized EV isolation method yielded robust and consistent EV populations relatively pure.

Most of the studies do not report EV concentration or PPR and only report EV-associated protein. Higher EV-associated protein might indicate more protein contamination and not necessarily higher EV number. Therefore, a wide implementation of the parameter PPR as a measure of purity of EV populations would be quite relevant.

To evaluate the MSC-EV immunomodulatory potential, an endothelial and monocytic 2D potency assays and 3D lung alveolus inflammation model on transwell and on chip were developed.

The endothelial and monocytic potency assays intend to mimic several stages of the inflammatory process in a simpler way. The monocytic potency assay developed consisted of challenging THP-1 cells with or without LPS in co-treatment with MSC-EVs (at 10^9 EV/ml) for 24 h and consequently measure the secretion of the pro-inflammatory cytokine TNF-α. THP-1 potency assay allowed to detect and select out pro-inflammatory MSC-EV donors that increased TNF-α release in the absence of LPS. The endothelial potency assay developed comprised the challenge of HUVEC with the pro-inflammatory cytokine TNF-α in co-treatment with MSC-EVs (at 10^9 EV/ml) for 16 h, followed by evaluation of endothelial cell activation by the expression of VCAM-1 and ICAM-1 adhesion molecules and the release of IL-8 chemokine. The HUVEC potency assay allowed the detection of slightly anti-inflammatory MSC-EV donors that partly reduced VCAM-1 and ICAM-1 expression and IL-8 release, thus, higher EV dose of the anti-inflammatory MSC donors and bioengineering strategies are necessary to boost EV immunomodulatory and anti-inflammatory properties. Moreover, the 2D potency assays allowed detecting variability between MSC-EVs from different donors indicating that donor-to-donor variability of the cells of origin is replicated in their EVs. Using the HUVEC potency assay, it was determined that EV doses of 10^{10} EV/ml or higher should be used for 3D models.

The lung alveolus inflammation model on transwell consisted of a 3D system mimicking endothelial-epithelial tissue interactions at air-liquid interface allowing to evaluate not only inflammation but also the cell barrier function. A confluent MSC monolayer in indirect co-culture with the lung alveolus model exposed to the pro-inflammatory cytokines TNF-α and IFN-γ decreased inflammation to higher extent than MSC-EVs (at 3×10^{10} EV/ml) and MSC-CM, by decreasing the expression of VCAM-1 and ICAM-1 and the release of IL-8, for 3 different MSC donors considered slightly anti-inflammatory. However, none of the conditions was able to promote recovery from edema and to restore barrier function, indicating that further tests should be perform to determine optimal doses and administration regimens as well as the use of bioengineering strategies to boost MSC, MSC-CM and MSC-EV immunomodulatory potential.

The lung alveolus-on-a-chip inflammation model developed consisted of a microfluidic device composed of a flexible porous membrane that enables tissue-tissue interactions between two channels, a bottom channel with endothelial cells in all sides to resemble a blood vessel under flow with culture medium and a top channel with epithelial cells exposed to air. The microfluidic devices were subjected to unidirectional cyclic stretch to mimic breathing motion when the air-liquid interface was already established. After starvation, the lung alveolus-on-a-chip was exposed to TNF-α to cause inflammation and co-treated with MSC-EVs (at 10^{10} EV/ml) for 16 h on flow. MSC-EVs were able to partly reduce inflammation, by decreasing ICAM-1 expression but not IL-8 release, and improved barrier function by decreasing vascular leakage and edema. These results also indicated that MSC-EV anti-inflammatory potential is still sub-optimal and higher doses and different administration regimens should be tested and MSC-EV bioengineering strategies should be pursued. Therefore, it still remains to be elucidated the optimal dosing, timing of administration and frequency of EV treatment and the optimal bioenginneing strategy.

Conflicting results can be found in the literature regarding MSC, MSC-CM and MSC-EV regenerative and immunomodulatory potential, furthermore, different *in vitro* and *in vivo* models and concentration of cells, CM and EVs have been used as well as outcomes analyzed, which hinders the direct comparison between the work developed here and other published studies and makes it difficult to infer which study showed the best result to be used for comparison and positive control. Nevertheless, there is growing evidence of MSC-EV potential and the results obtained here indicate that MSC-EVs have anti-inflammatory potential, although bioengineering strategies should be pursued to further boost its immunomodulatory potential.

Moreover, the use of more complex human 3D models that mimic tissue-tissue interactions and recapitulate complex organ-level functions allow modelling human pathophysiology and evaluate different cell, CM and EV therapies as well as doses and types of administration. These models also allow toxicological screening in a fast and cost-effective way compared to the use of simpler *in vitro* 2D human models that fail to recapitulate, for instance the impact of mechanical strain, and compared to the use of animals which fail to recapitulate human responses resulting in possible opposite therapeutic responses or toxic effects.

Bioengineering of MSC-EVs should be pursued to enhance the anti-inflammatory effect of MSC-EVs as the administration of EVs at the maximum/optimal dose might still not be enough to fully resolve inflammation and also to potentially avoid the need of donor screening by conditioning all the cells to a similar state of potency. The development of MSC-EV bioengineering strategies may be focused on the modulation of EV content by targeting cells before EV production and release or the modification of already secreted EVs. The bioengineering strategy of pre-conditioning of MSCs has the advantages of being simpler, faster and straightforward, being able to target several genes, transcription factors and microRNAs while avoiding the safety concerns related to genetic modifications of the cells and transfection, which typically target only one gene. However, it is necessary to ensure that the compounds used for cell pre-conditioning do not remain in solution and do not cause toxicity when administered.

8 General considerations

Regenerative properties of MSCs and MSC-derived products have been widely studied *in vitro* and *in vivo* and it is reported that MSCs have supportive function for other cell types such as hematopoietic cells and endothelial cells, prevent apoptosis, promote proliferation and migration, are anti-fibrotic and anti-scarring, and have immunomodulatory properties and suppress inflammation.

MSCs and MSC-derived products have been tested in several pre-clinical and clinical trials for a broad range of diseases, however, expectations of using MSCs as therapies are still not met and established in the field. Mainly due to many unsolved questions regarding survival and homing capacity upon transplantation, maintenance of MSC regenerative properties after transplantation, choice of route of administration, dose of cell or cell-based product, number of doses and timing of administration according to disease onset, choice of output measurements and timing, choice of MSC cell source, lack of standardization of isolation methods, culture conditions and culture medium, donor-to-donor variability, lack of standardized and robust potency assays and 3D models to characterize MSC regenerative potential, lack of specific guidelines that characterize MSC populations, lack of knowledge of the mechanisms of action and others.

This work intended to address some of these questions by establishing a platform of potency assays to characterize several MSC properties. To evaluate MSC supportive function through cell-to-cell contact an angiogenic tube incorporation assay was developed, to assess MSC ability to survive upon transplantation an oxidative stress assays were developed, to evaluate MSC capability to promote proliferation and migration through paracrine action a wound healing assay by mechanical scratch was optimized, to assess MSC, MSC-CM and MSC-EV immunomodulatory properties a monocytic and endothelial 2D potency assays and 3D lung alveolus inflammation models on transwell and on chip were developed. Moreover, these potency assays were used to evaluate donor-to-donor variability as well as MSC-EV dose and different types and regimens of EV treatment. A summary of the achievements is present in Figure 8.1and Table 8.1.

MSCs from BM, AT and UCM were successfully isolated and characterized according to the International Society for Cellular Therapy guidelines. Determination of the most proliferative cell source was not possible as there was no matching between donors and due to reduced number of donors (3 per cell source), however, for the set of donors tested AT MSCs had higher proliferative rate than UCM and BM MSCs.

Potency assays to evaluate MSC resistance to oxidative stress as adherent and as suspension culture were developed and significant donor-to-donor variability within each cell source was detected (as only 3 donors per cell source were tested). This potency assay can be applied to select out the less resistant MSC donors, evaluate resistance of MSCs from different cell sources (as stated before to conclude what would be the best cell source for a certain therapeutic application, also higher number of donors should be tested and donor matching should be considered when possible), assess the best culture conditions and culture system that prime the cells with enhanced survival ability as well as to study the mechanisms of action that improve survival.

Although further optimization was needed for the tube incorporation assay by performing several measurements along time, MSCs did not show a strong ability to support tube formation and

angiogenesis through cell-to-cell contact. The HUVEC tube formation assay could be used to study the angiogenic potential of MSC-CM and MSC-EVs isolated from different donors or to assess if different culture conditions or pre-conditioning with certain compounds or transfection with genes of interest can potentially boost MSC or MSC-derived product's angiogenic potential by promoting faster tube formation with higher number of tubes and connections and with higher stability over time.

MSCs seem to be able to exert stronger effect on promoting migration and proliferation by the paracrine action of its CM. When tested in the optimized wound healing assay by mechanical scratch, the MSC-CM from one of the BM donors tested was able to promote HUVEC migration to similar extent as endothelial culture medium, which is composed of several angiogenic growth factors. The CM of different BM MSC donors resulted in different HUVEC remodeling rate, indicating that donor variability of the donor cell of origin is replicated in its CM. The optimized wound healing assay is a simple, quick and high-throughput method that can be widely used not only to study the angiogenic potential of MSC-CM but also of MSC-EVs isolated from different donors and cultured under different conditions and treatments.

MSCs have been reported to be able to suppress inflammation, for instance, by inhibiting proliferation of PBMCs. Further evidence is needed on whether MSC-derived products would have at least similar immunomodulatory properties (and ideally enhanced immunomodulatory properties) that would enable the development of cell-based but cell-free therapies based on MSC-CM and MSC-EVs, avoiding safety concerns associated to cell administration. Therefore, an MSC-EV isolation method was optimized and the MSC-EV immunomodulatory potential was evaluated using potency assays and 3D inflammation models developed.

The optimized MSC-EV isolation method by differential ultracentrifugation resulted in robust, consistent and relatively pure MSC-EV populations among different BM MSC donors with a size (91-201 nm) in the range of exosomes and small microvesicles. Exosomes and microvesicles have different biogenesis and is it still unknown which of these EV types or if both have regenerative properties, which in part is related to the difficulty of efficiently separate the two EV types and that is why there is now an acceptance on generally naming these mixed populations as EVs instead of differentiating in microvesicles and exosomes populations.

Herein, it is proposed that PPR, a measure of purity of EV populations, should be widely used and reported in all EV studies in order to compare works and also to evaluate if EV samples are indeed EV-enriched or have high protein contamination. Optimization of EV storage conditions is an open challenge, which is very important for the development of EV-based therapeutics and which can comprise their use as off-the-shelf products if it remains unsolved.

2D potency assays and 3D models were developed to study the immunomodulatory properties of MSCs and MSC-derived products by recapitulating several steps of the inflammatory process. The THP-1 monocytic potency assay and the HUVEC endothelial potency assay detected donor-to-donor variability between MSC-EVs from different BM MSC donors, once again indicating that variability of the cell of origin is replicated is not only in its CM but also in the secreted EVs. The optimized THP-1 potency assay is very useful as a screening tool to select out pro-inflammatory MSC-EV donors. The endothelial potency assay can be used to detect anti-inflammatory MSC-EV donors, but also showed

that further elucidation on the optimal EV dose is needed and should be one of the focuses of future work. Of note that, MSC pro- and anti-inflammatory state can change with culture conditions such as hypoxia and culture medium and by pre-conditioning with certain compounds, therefore, it is important to better understand MSC biology and to use standardized and controlled cell culture conditions as well as robust, standardized and optimized cell culture, cell and EV isolation and storage protocols.

To overcome the limitations of using animal models to predict human responses or *ex vivo* organs that have limited availability and/or simplistic 2D models that do not recapitulate organ level functions, there is a need to develop 3D models that better recapitulate relevant human organ level functions and tissue-tissue interactions, mimic human pathophysiology and responses to treatments. Therefore, two lung alveolus inflammation models were developed on transwell and on a microfluidic device. These 3D models accounted for tissue interactions of the endothelium-epithelium and mimicked the air-liquid interface of the lung alveolus. The microfluidic device further resembled the complexity of the lung alveolus by incorporating mechanical strain to mimic the physiological breathing motion and flow of culture medium to resemble blood flow through the endothelial channel.

The 3D lung alveolus inflammation models on transwell and on chip showed that MSCs and MSC-EVs have the potential to reduce inflammation and edema and improve endothelial-epithelial barrier function. However, MSC and MSC-EV immunomodulatory action was partial indicating that EV dose, frequency, timing and regimen of EV treatment are still suboptimal and also that both MSC and MSC-EV immunomodulatory properties need to be enhanced for an efficient therapy and potential full resolution of inflammation. To boost MSC and MSC-derived products anti-inflammatory and regenerative potential, bioengineering strategies should be pursued. Bioengineering MSCs and MSC-EVs might overcome the hurdles of donor-to-donor variability by conditioning all the cells to the same state and with similar and boosted immunomodulatory potential.

Most of the published bioengineering strategies involve transfection to express one gene of interest, however, transfection is time-consuming, limited to one or few genes of interest and has safety concerns associated to it. Moreover, it is known that not only one, but several genes and microRNAs are involved in enhanced therapeutic effects. Alternatively, bioengineering strategies through pre-conditioning with small molecules may up-regulate several microRNAs of interest and this strategy is simpler, faster and avoids safety concerns as long as the free residual or encapsulated compounds are not toxic when administered. TNF-α and LPS have been used for MSC pre-conditioning and improved immunomodulatory potential has been reported. Herein, several small molecules were tested and preliminary results using the HUVEC potency assay indicated that some of the bioengineered MSC-EVs seem to have improved anti-inflammatory effect. Further confirmation of the anti-inflammatory effect of bioengineered EVs needs to be performed and its potential should be evaluated using the 3D models developed and promising hits could then be tested *in vivo* using animal models. It is also important to uncover the mechanism of action, to understand if the effect is related to the encapsulation of the compounds in the EVs or by the presence/enrichment in nucleic acids (such as microRNAs evaluated by sequencing methods) or other components.

The 3D models herein developed could be further optimized by using human organ specific primary endothelial and epithelial cells type I and II, increasing the flow rate of the microfluidic device

to induce physiological shear stress levels, by better mimicking lung inflammation using pathophysiological concentration of TNF-α, IFN-γ and IL-1β. Optimization is also needed regarding CM and EV dosing and administration regimens and on defining the adequate time points to evaluate the immunomodulatory potential of MSC and MSC-derived products on the 3D lung alveolus inflammation models. Additionally, the complexity of the 3D models can be further increased by incorporation other cell types such as immune cells or by addition/flow of blood. The immunomodulatory properties of MSC, MSC-CM and MSC-EV treatment could then be studied with these improved models.

In the future, 3D models could be widely used as screening tools of cell-based and cell-free therapies and for drug testing and toxicology studies as well as to better understand organ biology and unravel mechanisms of action and human pathophysiological responses. In the future, improved 3D models are expected to reduce the number of animals sacrificed for research purposes reducing the time and costs of therapy development, however, additionally to the *in vitro* 2D and 3D data most probably the regulatory agencies FDA and EMA will always require animal testing to authorize the clinical trials in humans.

To conclude, MSCs and MSC-derived products are promising candidates for cell-based and cell-based but cell-free therapies, however, there is significant effect of donor-to-donor variability and that MSC donor variability is reflected in their CM and EVs. To ensure quality, potency and efficacy of the MSC and MSC-derived products, it is necessary to evaluate the properties of each batch with a robust platform of product characterization which includes 2D potency assays and 3D models that evaluate the different MSC regenerative properties enumerated. Therefore, in the future, after optimizing all the potency assays and 3D models under development in this work, this platform of product characterization should be widely implemented. Moreover, besides optimizing dose, boosting the potential of MSC and MSC-derived products using bioengineering strategies is needed for the development of potent MSC therapeutic products.

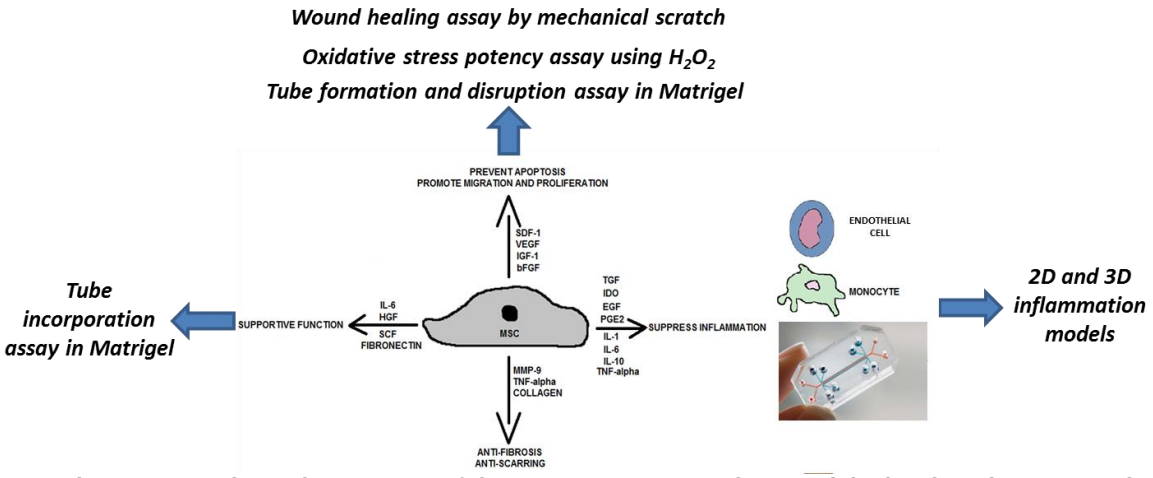

Figure 8.1 – Schematic summary of the potency assays and 3D models developed to assess the different MSC regenerative properties.

Table 8.1 – Summary of the potency assay and 3D models developed, main results obtained and further optimization needed.

Potency assay/Model	Main results	Future work
Oxidative stress as adherent culture	High variability on cell death within each MSC cell source. No detection of MSC cell source with higher resistance to oxidative stress	Cell death analysis by pooling both dead cells in suspension with the adherent cells after cell detachment
Oxidative stress as suspension culture	Quicker and more accurate protocol compared with oxidative stress as adherent culture. Closer resembles a scenario of cell infusion. MSCs are more sensitive in suspension, thus incubation should be with lower H_2O_2 moles per cell	Optimize the number H_2O_2 moles per cell (1-5 x 10^{-11} mol H_2O_2/cell). Test different donors, cell sources, culture conditions, culture systems, bioengineering strategies
Tube formation	Early passage HUVEC can be seeded at 31,250-78,125 cell/cm^2 in Matrigel and incubated with MSC-CM or MSC-EV to assess their angiogenic potential	Test MSC-CM and MSC-EV from different donors, cell sources, culture conditions, culture systems, doses, bioengineering strategies
Tube incorporation	Low supportive function by cell contact and angiogenic potential when co-culturing HUVEC and MSC in Matrigel at a ratio of 1:4 in endothelial medium. MSC donor variability detected	Optimize protocol by evaluating several time points, HUVEC:MSC ratios, time of MSC addition to the co-culture, culture medium
Tube disruption with DMSO	Early passage HUVEC can be seeded at 31,250-78,125 cell/cm^2 in Matrigel, after tube formation in endothelial medium, tube disruption is caused by 10-15% DMSO and tube remodeling is evaluated within about 1 h by incubating with MSC-CM or MSC-EV to assess their angiogenic potential. Time to remodel might be short to evaluate remodeling	Optimize DMSO concentration (10-15%). Evaluate MSC-CM and MSC-EV angiogenic potential to promote remodeling by measuring the number of tubes and branch points and the time needed to remodel
Wound healing by mechanical scratch	MSC-CM was able to promote HUVEC migration after mechanical scratch in a HUVEC monolayer. MSC donor variability detected in MSC-CM from different donors	Test MSC-CM and MSC-EV from different donors, cell sources, culture conditions, culture systems, doses, bioengineering strategies
Monocytic assay	Immunomodulatory potential of MSC-EVs from different BM MSC donors was evaluated, variability was observed in their EVs and it was possible to select out pro-inflammatory MSC-EV donors	Test MSC-EV from different donors, cell sources, culture conditions, culture systems, doses, bioengineering strategies
Endothelial assay	Immunomodulatory potential of MSC-EVs from different BM MSC donors and EV dose were evaluated. Only slightly anti-inflammatory EV donors were detected. There is a need to boost effect by bioengineering strategies	Test MSC-EV from different donors, cell sources, culture conditions, culture systems, doses, bioengineering strategies
Lung alveolus inflammation on transwell model	Immunomodulatory potential of MSC indirect co-culture, MSC-CM and MSC-EVs from 3 BM MSC donors was evaluated. MSC indirect co-culture promoted higher decrease in inflammation, but not full resolution of inflammation neither barrier function recovery. MSC-CM did not decrease inflammation. MSC-EVs reduced inflammation, but to similar or with lower extent than MSC indirect co-culture	Test MSCs in direct or indirect co-culture, MSC-CM and MSC-EV from different donors, cell sources, culture conditions, culture systems, doses, bioengineering strategies. Optimize model using organ specific primary cells, pathophysiological cytokine concentration, administration regimens
Lung alveolus-on-a-chip inflammation model	Immunomodulatory potential of MSC-EVs from 3 BM MSC donors considered slightly anti-inflammatory partially reduced inflammation and partially promoted the recovery of the barrier function and edema. There is a need to boost the immunomodulatory potential by bioengineering strategies, besides increasing dose	Test MSCs in co-culture, MSC-CM and MSC-EV from different donors, cell sources, culture conditions, culture systems, doses, bioengineering strategies. Optimize model using organ specific primary cells, physiological shear stress and strain, pathophysiological cytokine concentration, administration regimens

9 References

Adler, K. B. *et al.* (1994) 'Interactions between respiratory epithelial cells and cytokines: relationships to lung inflammation', *Ann N Y Acad Sci*, 725, pp. 128–145. Available at: http://www.ncbi.nlm.nih.gov/entrez/query.fcgi?cmd=Retrieve&db=PubMed&dopt=Citation&list_uids=8030984.

Afzal, M. R. *et al.* (2010) 'Preconditioning promotes survival and angiomyogenic potential of mesenchymal stem cells in the infarcted heart via NF-kappaB signaling.', *Antioxidants & redox signaling*, 12(6), pp. 693–702. doi: 10.1089/ars.2009.2755.

Agarwal, A. *et al.* (2013) 'Microfluidic heart on a chip for higher throughput pharmacological studies', 13(18), pp. 3599–3608. doi: 10.1039/c3lc50350j.

Ahdieh, M., Vandenbos, T. and Youakim, A. (2001) 'Lung epithelial barrier function and wound healing are decreased by IL-4 and IL-13 and enhanced by IFN-gamma.', *American journal of physiology. Cell physiology*, 281(6), pp. C2029–C2038.

Aird, W. C. (2012) 'Endothelial cell heterogeneity', *Cold Spring Harbor Perspectives in Medicine*, 2(1). doi: 10.1101/cshperspect.a006429.

Akiyama, K. *et al.* (2012) 'Mesenchymal-stem-cell-induced immunoregulation involves FAS-ligand-/FAS-mediated T cell apoptosis', *Cell Stem Cell*, 10(5), pp. 544–555. doi: 10.1016/j.stem.2012.03.007.

Akyurekli, C. *et al.* (2015) 'A Systematic Review of Preclinical Studies on the Therapeutic Potential of Mesenchymal Stromal Cell-Derived Microvesicles', *Stem Cell Reviews and Reports*, 11(1), pp. 150–160. doi: 10.1007/s12015-014-9545-9.

Al-Khaldi, A. *et al.* (2003) 'Postnatal bone marrow stromal cells elicit a potent VEGF-dependent neoangiogenic response in vivo', *Gene Therapy*, 10(8), pp. 621–629. doi: 10.1038/sj.gt.3301934.

Alberts, B. *et al.* (2002) '24. The adaptive immune system', *Molecular Biology of the Cell*, pp. 1–2.

Aliotta, J. M. *et al.* (2016) 'Exosomes induce and reverse monocrotaline-induced pulmonary hypertension in mice', *Cardiovascular Research*, 110(3), pp. 319–330. doi: 10.1093/cvr/cvw054.

Almahariq, M. *et al.* (2013) 'A Novel EPAC-Specific Inhibitor Suppresses Pancreatic Cancer Cell Migration and Invasion', *Molecular Pharmacology*, 83(1), pp. 122–128. doi: 10.1124/mol.112.080689.

Amable, P. R. *et al.* (2014) 'Protein synthesis and secretion in human mesenchymal cells derived from bone marrow, adipose tissue and Wharton's jelly.', *Stem cell research & therapy*, 5(2), p. 53. doi: 10.1186/scrt442.

EL Andaloussi, S. *et al.* (2013) 'Extracellular vesicles: biology and emerging therapeutic opportunities', *Nature Reviews Drug Discovery*, 12(5), pp. 347–357. doi: 10.1038/nrd3978.

Andrade, P. Z. *et al.* (2010) 'Systematic delineation of optimal cytokine concentrations to expand hematopoietic stem/progenitor cells in co-culture with mesenchymal stem cells', *Molecular BioSystems*. doi: 10.1039/b922637k.

in 't Anker, P. S. *et al.* (2004) 'Isolation of Mesenchymal Stem Cells of Fetal or Maternal Origin from Human Placenta', *Stem Cells*, 22(7), pp. 1338–1345. doi: 10.1634/stemcells.2004-0058.

Arm, J. P. and Lee, T. H. (1992) 'The Pathobiology of Bronchial Asthma', *Advances in Immunology*, 51(C), pp. 323–382. doi: 10.1016/S0065-2776(08)60491-5.

Armstrong, L. and Millar, a B. (1997) 'Relative production of tumour necrosis factor alpha and interleukin 10 in adult respiratory distress syndrome.', *Thorax*, 52(5), pp. 442–6. doi: 10.1136/thx.52.5.442.

Arnaoutova, I. *et al.* (2009) 'The endothelial cell tube formation assay on basement membrane turns 20: State of the science and the art', *Angiogenesis*, pp. 267–274. doi: 10.1007/s10456-009-9146-4.

Arraud, N. *et al.* (2014) 'Extracellular vesicles from blood plasma: Determination of their morphology, size, phenotype and concentration', *Journal of Thrombosis and Haemostasis*, 12(5), pp. 614–627. doi: 10.1111/jth.12554.

Arslan, F. *et al.* (2013) 'Mesenchymal stem cell-derived exosomes increase ATP levels, decrease oxidative stress and activate PI3K/Akt pathway to enhance myocardial viability and prevent adverse remodeling after myocardial ischemia/reperfusion injury', *Stem Cell Research*, 10(3), pp. 301–312. doi: 10.1016/j.scr.2013.01.002.

Arutyunyan, I. *et al.* (2016) 'Role of VEGF-A in angiogenesis promoted by umbilical cord-derived mesenchymal stromal/stem cells: In vitro study', *Stem Cell Research and Therapy*, 7(1). doi: 10.1186/s13287-016-0305-4.

Assmus, B. *et al.* (2010) 'Clinical outcome 2 years after intracoronary administration of bone marrow-derived progenitor cells in acute myocardial infarction', *Circulation: Heart Failure*, 3(1), pp. 89–96. doi: 10.1161/CIRCHEARTFAILURE.108.843243.

Atay, S. *et al.* (2011) 'Trophoblast-derived exosomes mediate monocyte recruitment and differentiation', *American Journal of Reproductive Immunology*, 65(1), pp. 65–77. doi: 10.1111/j.1600-0897.2010.00880.x.

Atoui, R. and Chiu, R. C. J. (2012) 'Concise Review: Immunomodulatory Properties of Mesenchymal Stem Cells in Cellular Transplantation: Update, Controversies, and Unknowns', *STEM CELLS Translational Medicine*, 1(3), pp. 200–205. doi: 10.5966/sctm.2011-0012.

Atoui, R., Shum-Tim, D. and Chiu, R. C. J. (2008) 'Myocardial Regenerative Therapy: Immunologic Basis for the Potential "Universal Donor Cells"', *Annals of Thoracic Surgery*, pp. 327–334. doi: 10.1016/j.athoracsur.2008.03.038.

Audet, J. *et al.* (2002) 'Common and distinct features of cytokine effects on hematopoietic stem and progenitor cells revealed by dose-response surface analysis', *Biotechnology and Bioengineering*. doi: 10.1002/bit.10399.

Baglio, S. R. *et al.* (2015) 'Human bone marrow-and adiposemesenchymal stem cells secrete exosomes enriched in distinctive miRNA and tRNA species', *Stem Cell Research and Therapy*, 6(1). doi: 10.1186/s13287-015-0116-z.

Baluna, R. and Vitetta, E. S. (1997) 'Vascular leak syndrome: A side effect of immunotherapy', *Immunopharmacology*, pp. 117–132. doi: 10.1016/S0162-3109(97)00041-6.

Bang, C., Fiedler, J. and Thum, T. (2012) 'Cardiovascular Importance of the MicroRNA-23/27/24 Family', *Microcirculation*, pp. 208–214. doi: 10.1111/j.1549-8719.2011.00153.x.

Bao, B. *et al.* (2012) 'Curcumin analogue CDF inhibits pancreatic tumor growth by switching on suppressor microRNAs and attenuating EZH2 expression', *Cancer Research*, 72(1), pp. 335–345. doi: 10.1158/0008-5472.CAN-11-2182.

Baraniak, P. R. and McDevitt, T. C. (2010) 'Stem cell paracrine actions and tissue regeneration', *Regenerative Medicine*, 5(1), pp. 121–143. doi: 10.2217/rme.09.74.

Barnes, P. J. (2008) 'Immunology of asthma and chronic obstructive pulmonary disease', *Nature Reviews Immunology*, pp. 183–192. doi: 10.1038/nri2254.

Barnes, P. J., Shapiro, S. D. and Pauwels, R. A. (2003) 'Chronic obstructive pulmonary disease: Molecular and cellular mechanisms', *European Respiratory Journal*, pp. 672–688. doi: 10.1183/09031936.03.00040703.

Barry, F. P. *et al.* (1999) 'The monoclonal antibody SH-2, raised against human mesenchymal stem cells, recognizes an epitope on endoglin (CD105)', *Biochemical and Biophysical Research Communications*, 265(1), pp. 134–139. doi: 10.1006/bbrc.1999.1620.

Bartosh, T. J. *et al.* (2010) 'Aggregation of human mesenchymal stromal cells (MSCs) into 3D spheroids enhances their antiin fl ammatory properties', *Proceedings of the National Academy of Sciences of the United States of America*, 107(31), pp. 13724–13729. doi: 10.1073/pnas.1008117107/-/DCSupplemental.www.pnas.org/cgi/doi/10.1073/pnas.1008117107.

Bassaneze, V. *et al.* (2010) 'Shear Stress Induces Nitric Oxide–Mediated Vascular Endothelial Growth Factor Production in Human Adipose Tissue Mesenchymal Stem Cells', *Stem Cells and Development*, 19(3), pp. 371–378. doi: 10.1089/scd.2009.0195.

Baughman, R. P. *et al.* (1990) 'Release of tumor necrosis factor by alveolar macrophages of patients with sarcoidosis.', *The Journal of laboratory and clinical medicine*, 115(1), pp. 36–42. Available at: http://www.ncbi.nlm.nih.gov/pubmed/2299255.

Beaglehole, R. and Bonita, R. (2008) 'Global public health: a scorecard', *The Lancet*, 372(9654), pp. 1988–1996. doi: 10.1016/S0140-6736(08)61558-5.

Beeres, S. L. M. A. *et al.* (2008) 'Cell therapy for ischaemic heart disease', *Heart*, pp. 1214–1226. doi: 10.1136/hrt.2008.149476.

Bei, Y. *et al.* (2016) 'miR-382 targeting PTEN-Akt axis promotes liver regeneration.', *Oncotarget*, 7(2), pp. 1584–97. doi: 10.18632/oncotarget.6444.

Bellagamba, B. C. *et al.* (2016) 'Human mesenchymal stem cells are resistant to cytotoxic and genotoxic effects of cisplatin in vitro', *Genetics and Molecular Biology*, 39(1), pp. 129–134. doi: 10.1590/1678-4685-GMB-2015-0057.

Benam, K. H. *et al.* (2016) 'Matched-Comparative Modeling of Normal and Diseased Human Airway Responses Using a Microengineered Breathing Lung Chip', *Cell Systems*, 3(5), p. 456–466.e4. doi: 10.1016/j.cels.2016.10.003.

Benam, K. H. *et al.* (2016) 'SL Small airway-on-a-chip enables analysis of human lung inflammation and drug responses in vitro', *Nat Meth*, 13(2), pp. 151–157. doi: 10.1038/nmeth.3697.

Bertolo, A. *et al.* (2017) 'Increased motility of mesenchymal stem cells is correlated with inhibition of stimulated peripheral blood mononuclear cells in vitro', *Journal of Stem Cells and Regenerative Medicine*, 13(2), pp. P62–P74.

Betteridge, D. J. (2000) 'What is oxidative stress?', *Metabolism*, 49(2), pp. 3–8. doi: 10.1016/S0026-0495(00)80077-3.

Bezerra, M. A. *et al.* (2008) 'Response surface methodology (RSM) as a tool for optimization in analytical chemistry', *Talanta*, pp. 965–977. doi: 10.1016/j.talanta.2008.05.019.

Bhatia, S. N. and Ingber, D. E. (2014) 'Microfluidic organs-on-chips', *Nature Biotechnology*, pp. 760–772. doi: 10.1038/nbt.2989.

Bian, S. *et al.* (2014) 'Extracellular vesicles derived from human bone marrow mesenchymal stem cells promote angiogenesis in a rat myocardial infarction model.', *Journal of molecular medicine (Berlin, Germany)*, 92(4), pp. 387–397. doi: 10.1007/s00109-013-1110-5.

Bianco, P., Robey, P. G. and Simmons, P. J. (2008) 'Mesenchymal Stem Cells: Revisiting History, Concepts, and Assays', *Cell Stem Cell*, 2(4), pp. 313–319. doi: 10.1016/j.stem.2008.03.002.

Bieback, K. *et al.* (2004) 'Critical parameters for the isolation of mesenchymal stem cells from umbilical cord blood.', *Stem cells (Dayton, Ohio)*, 22, pp. 625–34. doi: 10.1634/stemcells.22-4-625.

Birukov, K. G. *et al.* (2003) 'Magnitude-dependent regulation of pulmonary endothelial cell barrier function by cyclic stretch', *American Journal of Physiology-Lung Cellular and Molecular Physiology*, 285(4), pp. L785–L797. doi: 10.1152/ajplung.00336.2002.

Le Blanc, K. *et al.* (2003) 'HLA expression and immunologic properties of differentiated and undifferentiated mesenchymal stem cells', *Experimental Hematology*, 31(10), pp. 890–896. doi: 10.1016/S0301-472X(03)00110-3.

Le Blanc, K. *et al.* (2008) 'Mesenchymal stem cells for treatment of steroid-resistant, severe, acute graft-versus-host disease: a phase II study', *Lancet*, 371(9624), pp. 1579–1586. doi: 10.1016/s0140-6736(08)60690-x.

Block, G. J. *et al.* (2009) 'Multipotent stromal cells are activated to reduce apoptosis in part by upregulation and secretion of stanniocalcin-1.', *Stem cells (Dayton, Ohio)*, 27(3), pp. 670–681. doi: 10.1002/stem.20080742.Multipotent.

Blum, M. S. *et al.* (1997) 'Cytoskeletal rearrangement mediates human microvascular endothelial tight junction modulation by cytokines.', *The American journal of physiology*, 273(1 Pt 2), pp. H286-94. doi: 10.1152/ajpheart.1997.273.1.H286.

Blumenreich, M. (1990) 'The white blood cell and differential count', *Clinical Methods: The History, Physical and Laboratory Examinations, 3rd edition*, pp. 724–727. Available at: http://newmodernlabservices.com/userfiles/file/WBC DLC.pdf.

Bobis-Wozowicz, S. *et al.* (2017) 'Diverse impact of xeno-free conditions on biological and regenerative properties of hUC-MSCs and their extracellular vesicles', *Journal of Molecular Medicine*, 95(2), pp. 205–220. doi: 10.1007/s00109-016-1471-7.

Bobrie, A. *et al.* (2011) 'Exosome Secretion: Molecular Mechanisms and Roles in Immune Responses', *Traffic*, pp. 1659–1668. doi: 10.1111/j.1600-0854.2011.01225.x.

Böing, A. N. *et al.* (2014) 'Single-step isolation of extracellular vesicles by size-exclusion chromatography', *Journal of Extracellular Vesicles*, 3(1). doi: 10.3402/jev.v3.23430.

Booth, R. and Kim, H. (2012) 'Characterization of a microfluidic in vitro model of the blood-brain barrier (μBBB)', *Lab on a Chip*, 12(10), p. 1784. doi: 10.1039/c2lc40094d.

Bortner, C. D. and Cidlowski, J. A. (2007) 'Cell shrinkage and monovalent cation fluxes: Role in apoptosis', *Archives of Biochemistry and Biophysics*, pp. 176–188. doi: 10.1016/j.abb.2007.01.020.

Boutou, a K. *et al.* (2012) 'Levels of inflammatory mediators in chronic obstructive pulmonary disease patients with anemia of chronic disease: a case-control study.', *QJM : monthly journal of the Association of Physicians*, 105(7), pp. 657–63. doi: 10.1093/qjmed/hcs024.

Brandau, S. *et al.* (2010) 'Tissue-resident mesenchymal stem cells attract peripheral blood neutrophils and enhance their inflammatory activity in response to microbial challenge', *Journal of Leukocyte Biology*, 88(5), pp. 1005–1015. doi: 10.1189/jlb.0410207.

Brandau, S. *et al.* (2014) 'Mesenchymal stem cells augment the anti-bacterial activity of neutrophil granulocytes', *PLoS ONE*, 9(9). doi: 10.1371/journal.pone.0106903.

Brandl, A. *et al.* (2011) 'Oxidative stress induces senescence in human mesenchymal stem cells', *Experimental Cell Research*, 317(11), pp. 1541–1547. doi: 10.1016/j.yexcr.2011.02.015.

Broadwell, R. D., Salcman, M. and Kaplan, R. S. (1982) 'Morphologic effect of dimethyl sulfoxide on the blood-brain barrier.', *Science (New York, N.Y.)*, 217(4555), pp. 164–166. doi: 10.1126/science.7089551.

Brown, M. A. *et al.* (2007) 'The use of mild trypsinization conditions in the detachment of endothelial cells to promote subsequent endothelialization on synthetic surfaces', *Biomaterials*, 28(27), pp. 3928–3935. doi: 10.1016/j.biomaterials.2007.05.009.

Bruewer, M. *et al.* (2003) 'Proinflammatory Cytokines Disrupt Epithelial Barrier Function by Apoptosis-Independent Mechanisms', *The Journal of Immunology*, 171(11), pp. 6164–6172. doi: 10.4049/jimmunol.171.11.6164.

Bruno, S. *et al.* (2009) 'Mesenchymal Stem Cell-Derived Microvesicles Protect Against Acute Tubular Injury', *J Am Soc Nephrol*, 20, pp. 1053–1067. doi: 10.1681/ASN.2008070798.

Bruno, S. *et al.* (2012) 'Microvesicles derived from mesenchymal stem cells enhance survival in a lethal model of acute kidney injury', *PLoS ONE*, 7(3). doi: 10.1371/journal.pone.0033115.

Budoni, M. *et al.* (2013) 'The immunosuppressive effect of mesenchymal stromal cells on B lymphocytes is mediated by membrane vesicles', *Cell Transplantation*, 22(2), pp. 369–379. doi: 10.3727/096368911X582769.

Burova, E. *et al.* (2013) 'Sublethal oxidative stress induces the premature senescence of human mesenchymal stem cells derived from endometrium', *Oxidative Medicine and Cellular Longevity*. doi: 10.1155/2013/474931.

Burrow, K. L., Hoyland, J. A. and Richardson, S. M. (2017) 'Human Adipose-Derived Stem Cells Exhibit Enhanced Proliferative Capacity and Retain Multipotency Longer than Donor-Matched Bone Marrow Mesenchymal Stem Cells during Expansion In Vitro', *Stem Cells International*, 2017. doi: 10.1155/2017/2541275.

van Buul, G. M. *et al.* (2012) 'Mesenchymal stem cells secrete factors that inhibit inflammatory processes in short-term osteoarthritic synovium and cartilage explant culture', *Osteoarthritis and Cartilage*, 20(10), pp. 1186–1196. doi: 10.1016/j.joca.2012.06.003.

Cabrita, G. J. M. *et al.* (2003) 'Hematopoietic stem cells: From the bone to the bioreactor', *Trends in Biotechnology*, pp. 233–240. doi: 10.1016/S0167-7799(03)00076-3.

Calió, M. L. *et al.* (2014) 'Transplantation of bone marrow mesenchymal stem cells decreases oxidative stress, apoptosis, and hippocampal damage in brain of a spontaneous stroke model.', *Free radical biology & medicine*, 70, pp. 141–54. doi: 10.1016/j.freeradbiomed.2014.01.024.

Camussi, G. *et al.* (2010) 'Exosomes/microvesicles as a mechanism of cell-to-cell communication', *Kidney International*, pp. 838–848. doi: 10.1038/ki.2010.278.

Cantaluppi, V. *et al.* (2012) 'Microvesicles derived from endothelial progenitor cells protect the kidney from ischemia-reperfusion injury by microRNA-dependent reprogramming of resident renal cells', *Kidney International*, 82(4), pp. 412–427. doi: 10.1038/ki.2012.105.

Caplan, A. (1991) 'Mesenchymal stem cells.', *Journal of orthopaedic research : official publication of the Orthopaedic Research Society*, 9(5), pp. 641–50. doi: 10.1002/jor.1100090504.

Carmelo, J. G. *et al.* (2015) 'A xeno-free microcarrier-based stirred culture system for the scalable expansion of human mesenchymal stem/stromal cells isolated from bone marrow and adipose tissue', *Biotechnology Journal*, 10(8), pp. 1235–1247. doi: 10.1002/biot.201400586.

Carraro, A. *et al.* (2008) 'In vitro analysis of a hepatic device with intrinsic microvascular-based channels', *Biomedical Microdevices*, 10(6), pp. 795–805. doi: 10.1007/s10544-008-9194-3.

Castilho, Á. F. *et al.* (2012) 'Heme oxygenase-1 protects retinal endothelial cells against high glucose- and oxidative/nitrosative stress-induced toxicity', *PLoS ONE*, 7(8). doi: 10.1371/journal.pone.0042428.

de Castro, L. L. *et al.* (2017) 'Human adipose tissue mesenchymal stromal cells and their extracellular vesicles act differentially on lung mechanics and inflammation in experimental allergic asthma', *Stem Cell Research & Therapy*, 8(1), p. 151. doi: 10.1186/s13287-017-0600-8.

Celli, B. R. *et al.* (2004) 'Standards for the diagnosis and treatment of patients with COPD: A summary of the ATS/ERS position paper', *European Respiratory Journal*, pp. 932–946. doi: 10.1183/09031936.04.00014304.

Chambers, D. C. *et al.* (2014) 'A phase 1b study of placenta-derived mesenchymal stromal cells in patients with idiopathic pulmonary fibrosis', *Respirology*, 19(7), pp. 1013–1018. doi: 10.1111/resp.12343.

Chang, C.-P. *et al.* (2013) 'Hypoxic preconditioning enhances the therapeutic potential of the secretome from cultured human mesenchymal stem cells in experimental traumatic brain injury.', *Clinical science (London, England : 1979)*, 124(3), pp. 165–76. doi: 10.1042/CS20120226.

Chang, Q. *et al.* (2013) 'The IL-6/JAK/Stat3 Feed-Forward Loop Drives Tumorigenesis and Metastasis', *Neoplasia*, 15(7), pp. 848-IN45. doi:

10.1593/neo.13706.
Chang, T.-C., Hsu, M.-F. and Wu, K. K. (2015) 'High Glucose Induces Bone Marrow-Derived Mesenchymal Stem Cell Senescence by Upregulating Autophagy', *PLOS ONE*, 10(5), p. e0126537. doi: 10.1371/journal.pone.0126537.
Chang, Y. S. *et al.* (2014) 'Mesenchymal Stem Cells for Bronchopulmonary Dysplasia: Phase 1 Dose-Escalation Clinical Trial', *The Journal of Pediatrics*, 164(5), p. 966–972.e6. doi: 10.1016/j.jpeds.2013.12.011.
Chanput, W. *et al.* (2010) 'Transcription profiles of LPS-stimulated THP-1 monocytes and macrophages: a tool to study inflammation modulating effects of food-derived compounds', *Food & Function*, 1(3), p. 254. doi: 10.1039/c0fo00113a.
Chanput, W., Mes, J. J. and Wichers, H. J. (2014) 'THP-1 cell line: An in vitro cell model for immune modulation approach', *International Immunopharmacology*, pp. 37–45. doi: 10.1016/j.intimp.2014.08.002.
Che, N. *et al.* (2012) 'Umbilical cord mesenchymal stem cells suppress B-cell proliferation and differentiation', *Cellular Immunology*, 274(1–2), pp. 46–53. doi: 10.1016/j.cellimm.2012.02.004.
Chen, J. *et al.* (2003) 'Intravenous administration of human bone marrow stromal cells induces angiogenesis in the ischemic boundary zone after stroke in rats', *Circulation Research*, 92(6), pp. 692–699. doi: 10.1161/01.RES.0000063425.51108.8D.
Chen, L. *et al.* (2008) 'Paracrine factors of mesenchymal stem cells recruit macrophages and endothelial lineage cells and enhance wound healing', *PLoS ONE*, 3(4). doi: 10.1371/journal.pone.0001886.
Chen, S. *et al.* (2004) 'Effect on left ventricular function of intracoronary transplantation of autologous bone marrow mesenchymal stem cell in patients with acute myocardial infarction', *The American Journal of Cardiology*, 94(1), pp. 92–95. doi: 10.1016/j.amjcard.2004.03.034.
Chen, W. and Frangogiannis, N. G. (2013) 'Fibroblasts in post-infarction inflammation and cardiac repair', *Biochimica et Biophysica Acta - Molecular Cell Research*, pp. 945–953. doi: 10.1016/j.bbamcr.2012.08.023.
Chen, X. D. *et al.* (2007) 'Extracellular matrix made by bone marrow cells facilitates expansion of marrow-derived mesenchymal progenitor cells and prevents their differentiation into osteoblasts', *Journal of Bone and Mineral Research*, 22(12), pp. 1943–1956. doi: 10.1359/jbmr.070725.
Chen, Y.-X. *et al.* (2017) 'Novel Akt activator SC-79 is a potential treatment for alcoholinduced osteonecrosis of the femoral head', *Oncotarget*, 8(19). doi: 10.18632/oncotarget.16075.
Chen, Y. H. *et al.* (2001) 'Salvianolic acid B attenuates VCAM-1 and ICAM-1 expression in TNF-alpha-treated human aortic endothelial cells.', *Journal of cellular biochemistry*, 82(3), pp. 512–521. doi: 10.1002/jcb.1176 [pii].
Cheng, W. *et al.* (2006) 'Metabolic monitoring of the electrically stimulated single heart cell within a microfluidic platform', *Lab on a Chip*, 6(11), p. 1424. doi: 10.1039/b608202e.
Chepurny, O. G. *et al.* (2009) 'Enhanced rap1 activation and insulin secretagogue properties of an acetoxymethyl ester of an Epac-selective cyclic AMP analog in rat INS-1 cells: Studies with 8-pCPT-2'-O-Me-cAMP-AM', *Journal of Biological Chemistry*, 284(16), pp. 10728–10736. doi: 10.1074/jbc.M900166200.
Childs, B. G. *et al.* (2015) 'Cellular senescence in aging and age-related disease: From mechanisms to therapy', *Nature Medicine*, pp. 1424–1435. doi: 10.1038/nm.4000.
Chiossone, L. *et al.* (2016) 'Mesenchymal Stromal Cells Induce Peculiar Alternatively Activated Macrophages Capable of Dampening Both Innate and Adaptive Immune Responses', *Stem Cells*, 34(7), pp. 1909–1921. doi: 10.1002/stem.2369.
Chivet, M. *et al.* (2012) 'Emerging role of neuronal exosomes in the central nervous system', *Frontiers in Physiology*, 3 MAY. doi: 10.3389/fphys.2012.00145.
Cho, D. I. *et al.* (2014) 'Mesenchymal stem cells reciprocally regulate the M1/M2 balance in mouse bone marrow-derived macrophages', *Experimental and Molecular Medicine*, 46(1). doi: 10.1038/emm.2013.135.
Choi, D. *et al.* (2009) 'Ischemic heart diseases: current treatments and future.', *Journal of controlled release : official journal of the Controlled Release Society*, 140(3), pp. 194–202. doi: 10.1016/j.jconrel.2009.06.016.
Choi, M., Ban, T. and Rhim, T. (2014) 'Therapeutic use of stem cell transplantation for cell replacement or cytoprotective effect of microvesicle released from mesenchymal stem cell.', *Molecules and cells*, 37(2), pp. 133–9. doi: 10.14348/molcells.2014.2317.
Chuquimia, O. D. *et al.* (2013) 'Alveolar epithelial cells are critical in protection of the respiratory tract by secretion of factors able to modulate the activity of pulmonary macrophages and directly control bacterial growth', *Infection and Immunity*, 81(1), pp. 381–389. doi: 10.1128/IAI.00950-12.
Cohn, J. N., Ferrari, R. and Sharpe, N. (2000) 'Cardiac remodeling-concepts and clinical implications: A consensus paper from an International Forum on Cardiac Remodeling', *Journal of the American College of Cardiology*, 35(3), pp. 569–582. doi: 10.1016/S0735-1097(99)00630-0.
Collino, F. *et al.* (2015) 'AKI Recovery Induced by Mesenchymal Stromal Cell-Derived Extracellular Vesicles Carrying MicroRNAs', *Journal of the American Society of Nephrology*, 26(10), pp. 2349–2360. doi: 10.1681/ASN.2014070710.
Colucci, W. S. (1997) 'Molecular and cellular mechanisms of myocardial failure.', *The American journal of cardiology*, 80(11A), p. 15L–25L. doi: 10.1016/S0002-9149(97)00845-X.
Conant, E. F., Fox, K. R. and Miller, W. T. (1989) 'Pulmonary edema as a complication of interleukin-2 therapy', *American Journal of Roentgenology*, 152(4), pp. 749–752. doi: 10.2214/ajr.152.4.749.
Del Conde, I. *et al.* (2005) 'Tissue-factor-bearing microvesicles arise from lipid rafts and fuse with activated platelets to initiate coagulation', *Blood*, 106(5), pp. 1604–1611. doi: 10.1182/blood-2004-03-1095.
Conforti, A. *et al.* (2014) 'Microvescicles Derived from Mesenchymal Stromal Cells Are Not as Effective as Their Cellular Counterpart in the Ability to Modulate Immune Responses In Vitro', *Stem Cells and Development*, 23(21), pp. 2591–2599. doi: 10.1089/scd.2014.0091.
Conley, B. A. *et al.* (2004) 'Endoglin controls cell migration and composition of focal adhesions: Function of the cytosolic domain', *Journal of Biological Chemistry*, 279(26), pp. 27440–27449. doi: 10.1074/jbc.M312561200.

Cook, A. M. *et al.* (2016) 'Dexamethasone co-medication in cancer patients undergoing chemotherapy causes substantial immunomodulatory effects with implications for chemo-immunotherapy strategies', *OncoImmunology*, 5(3). doi: 10.1080/2162402X.2015.1066062.

Corcione, A. *et al.* (2006) 'Human mesenchymal stem cells modulate B-cell functions', *Blood*, 107(1), pp. 367–372. doi: 10.1182/blood-2005-07-2657.

Coyne, C. B. *et al.* (2002) 'Regulation of airway tight junctions by proinflammatory cytokines.', *Molecular biology of the cell*, 13(9), pp. 3218–34. doi: 10.1091/mbc.E02-03-0134.

Crisostomo, P. R. *et al.* (2008) 'Human mesenchymal stem cells stimulated by TNF- , LPS, or hypoxia produce growth factors by an NF B- but not JNK-dependent mechanism', *AJP: Cell Physiology*, 294(3), pp. C675–C682. doi: 10.1152/ajpcell.00437.2007.

Croitoru-Lamoury, J. *et al.* (2007) 'Human mesenchymal stem cells constitutively express chemokines and chemokine receptors that can be upregulated by cytokines, IFN-beta, and Copaxone', *J Interferon Cytokine Res*, 27(1), pp. 53–64. doi: 10.1089/jir.2007.0037.

Cruz, F. F. *et al.* (2015) 'Systemic Administration of Human Bone Marrow-Derived Mesenchymal Stromal Cell Extracellular Vesicles Ameliorates Aspergillus Hyphal Extract-Induced Allergic Airway Inflammation in Immunocompetent Mice.', *Stem cells translational medicine*, 4(11), pp. 1302–16. doi: 10.5966/sctm.2014-0280.

Cui, X. *et al.* (2010) 'Transplantation of Mesenchymal Stem Cells Preconditioned with Diazoxide, a Mitochondrial ATP-Sensitive Potassium Channel Opener, Promotes Repair of Myocardial Infarction in Rats', *The Tohoku Journal of Experimental Medicine*, 220(2), pp. 139–147. doi: 10.1620/tjem.220.139.

Cummings, B. S. and Schnellmann, R. G. (2002) 'Cisplatin-induced renal cell apoptosis: caspase 3-dependent and -independent pathways.', *The Journal of pharmacology and experimental therapeutics*, 302(1), pp. 8–17. doi: 10.1124/jpet.302.1.8.

Cummings, B. S., Wills, L. P. and Schnellmann, R. G. (2004) 'Measurement of Cell Death in Mammalian Cells', *Curr Protoc Phamacol*, 1(Lemasters 1999), pp. 1–30. doi: 10.1002/0471141755.ph1208s25.Measurement.

D., G. *et al.* (2013) 'Intramyocardial transplantation of mesenchymal stromal cells for chronic myocardial ischemia and decreased left ventricular function: Results of the MESAMI phase I clinical trial', *Circulation*, 128(22 SUPPL. 1), pp. 258–265. doi: 10.1016/j.ijcard.2016.02.016.

D.R., P. *et al.* (2018) 'Mesenchymal stem cell-derived extracellular vesicles attenuate pulmonary vascular permeability and lung injury induced by hemorrhagic shock and trauma', *Journal of Trauma and Acute Care Surgery*, 84(2), pp. 245–256. doi: 10.1097/TA.0000000000001744.

Dai, S. *et al.* (2008) 'Phase I clinical trial of autologous ascites-derived exosomes combined with GM-CSF for colorectal cancer', *Molecular Therapy*, 16(4), pp. 782–790. doi: 10.1038/mt.2008.1.

Dallaire, F. *et al.* (2001) 'Microbiological and inflammatory factors associated with the development of pneumococcal pneumonia.', *The Journal of infectious diseases*, 184(3), pp. 292–300. doi: 10.1086/322021.

Danieli, P. *et al.* (2015) 'Conditioned Medium From Human Amniotic Mesenchymal Stromal Cells Limits Infarct Size and Enhances Angiogenesis', *STEM CELLS Translational Medicine*, 4(5), pp. 448–458. doi: 10.5966/sctm.2014-0253.

Davies, L. C. *et al.* (2013) 'Tissue-resident macrophages', *Nature Immunology*, pp. 986–995. doi: 10.1038/ni.2705.

Denu, R. A. and Hematti, P. (2016) 'Effects of Oxidative Stress on Mesenchymal Stem Cell Biology', *Oxidative Medicine and Cellular Longevity*. doi: 10.1155/2016/2989076.

Djouad, F. *et al.* (2007) 'Mesenchymal Stem Cells Inhibit the Differentiation of Dendritic Cells Through an Interleukin-6-Dependent Mechanism', *Stem Cells*, 25(8), pp. 2025–2032. doi: 10.1634/stemcells.2006-0548.

Dominici, M. *et al.* (2006) 'Minimal criteria for defining multipotent mesenchymal stromal cells. The International Society for Cellular Therapy position statement', *Cytotherapy*, 8(4), pp. 315–317. doi: 10.1080/14653240600855905.

Douville, N. J. *et al.* (2010) 'Fabrication of two-layered channel system with embedded electrodes to measure resistance across epithelial and endothelial barriers', *Analytical Chemistry*, 82(6), pp. 2505–2511. doi: 10.1021/ac9029345.

Duffy, G. P. *et al.* (2009) 'Bone marrow-derived mesenchymal stem cells promote angiogenic processes in a time- and dose-dependent manner in vitro.', *Tissue engineering. Part A*, 15(9), pp. 2459–70. doi: 10.1089/ten.TEA.2008.0341.

Duffy, M. M. *et al.* (2011) 'Mesenchymal stem cell inhibition of T-helper 17 cell- differentiation is triggered by cell-cell contact and mediated by prostaglandin E2 via the EP4 receptor', *European Journal of Immunology*, 41(10), pp. 2840–2851. doi: 10.1002/eji.201141499.

Dufour, A. *et al.* (1998) 'Modulation of ICAM-1, VCAM-1 and HLA-DR by cytokines and steroids on HUVECs and human brain endothelial cells', *Journal of the Neurological Sciences*, 157(2), pp. 117–121. doi: 10.1016/S0022-510X(98)00059-8.

EAGLE, H. (1955) 'Nutrition needs of mammalian cells in tissue culture.', *Science (New York, N.Y.)*, 122(3168), pp. 501–14. doi: 10.1002/9780470114735.hawley00624.

Edwards, S. S. *et al.* (2014) 'Functional analysis reveals angiogenic potential of human mesenchymal stem cells from Wharton's jelly in dermal regeneration', *Angiogenesis*, 17(4), pp. 851–866. doi: 10.1007/s10456-014-9432-7.

Eirin, A. *et al.* (2014) 'MicroRNA and mRNA cargo of extracellular vesicles from porcine adipose tissue-derived mesenchymal stem cells', *Gene*, 551(1), pp. 55–64. doi: 10.1016/j.gene.2014.08.041.

Ejtehadifar, M. *et al.* (2015) 'The effect of hypoxia on mesenchymal stem cell biology', *Advanced Pharmaceutical Bulletin*, pp. 141–149. doi: 10.15171/apb.2015.021.

Eklund, S. E. *et al.* (2009) 'Metabolic discrimination of select list agents by monitoring cellular responses in a multianalyte microphysiometer', *Sensors*, 9(3), pp. 2117–2133. doi: 10.3390/s90302117.

El-Badawy, A. *et al.* (2016) 'Adipose stem cells display higher regenerative capacities and more adaptable electro-kinetic properties compared to bone marrow-derived mesenchymal stromal cells', *Scientific Reports*, 6. doi: 10.1038/srep37801.

Elnakish, M. T. *et al.* (2012) 'Mesenchymal stem cells for cardiac regeneration: Translation to bedside reality', *Stem Cells International*. doi:

10.1155/2012/646038.
Enewold, L. *et al.* (2009) 'Serum concentrations of cytokines and lung cancer survival in African Americans and Caucasians', *Cancer Epidemiology Biomarkers and Prevention*, 18(1), pp. 215–222. doi: 10.1158/1055-9965.EPI-08-0705.
Erbs, S. *et al.* (2007) 'Restoration of microvascular function in the infarct-related artery by intracoronary transplantation of bone marrow progenitor cells in patients with acute myocardial infarction: The Doppler substudy of the Reinfusion of Enriched Progenitor Cells and Infa', *Circulation*, 116(4), pp. 366–374. doi: 10.1161/CIRCULATIONAHA.106.671545.
Ertaş, G. *et al.* (2012) 'Comparative analysis of apoptotic resistance of mesenchymal stem cells isolated from human bone marrow and adipose tissue.', *TheScientificWorldJournal*, 2012, p. 105698. doi: 10.1100/2012/105698.
Esch, M. B. *et al.* (2012) 'On chip porous polymer membranes for integration of gastrointestinal tract epithelium with microfluidic "body-on-a-chip" devices', *Biomedical Microdevices*, 14(5), pp. 895–906. doi: 10.1007/s10544-012-9669-0.
Escudier, B. *et al.* (2005) 'Vaccination of metastatic melanoma patients with autologous dendritic cell (DC) derived-exosomes: results of thefirst phase I clinical trial.', *Journal of translational medicine*, 3(1), p. 10. doi: 10.1186/1479-5876-3-10.
Estrada, J. C. *et al.* (2012) 'Culture of human mesenchymal stem cells at low oxygen tension improves growth and genetic stability by activating glycolysis', *Cell Death and Differentiation*, 19(5), pp. 743–755. doi: 10.1038/cdd.2011.172.
Fadok, V. A. *et al.* (1998) 'Macrophages that have ingested apoptotic cells in vitro inhibit proinflammatory cytokine production through autocrine/paracrine mechanisms involving TGF-??, PGE2, and PAF', *Journal of Clinical Investigation*, 101(4), pp. 890–898. doi: 10.1172/JCI1112.
Fang, S. *et al.* (2016) 'Umbilical Cord-Derived Mesenchymal Stem Cell-Derived Exosomal MicroRNAs Suppress Myofibroblast Differentiation by Inhibiting the Transforming Growth Factor-β/SMAD2 Pathway During Wound Healing', *STEM CELLS Translational Medicine*, 5(10), pp. 1425–1439. doi: 10.5966/sctm.2015-0367.
Fang, W. H. *et al.* (2016) 'Mesenchymal Stem Cells Loaded with p5, Derived from CDK5 Activator p35, Inhibit Calcium-Induced CDK5 Activation in Endothelial Cells', *Stem Cells International*, 2016. doi: 10.1155/2016/2165462.
Fang, X. *et al.* (2010) 'Allogeneic human mesenchymal stem cells restore epithelial protein permeability in cultured human alveolar type II cells by secretion of angiopoietin-1', *Journal of Biological Chemistry*, 285(34), pp. 26211–26222. doi: 10.1074/jbc.M110.119917.
Favaro, E. *et al.* (2016) 'Human mesenchymal stem cells and derived extracellular vesicles induce regulatory dendritic cells in type 1 diabetic patients', *Diabetologia*, 59(2), pp. 325–333. doi: 10.1007/s00125-015-3808-0.
Feghali, C. a and Wright, T. M. (1997) 'Cytokines in acute and chronic inflammation.', *Frontiers in bioscience : a journal and virtual library*, 2, pp. d12–d26. doi: 10.2741/A171.
Feng, Y. *et al.* (2014) 'Ischemic preconditioning potentiates the protective effect of stem cells through secretion of exosomes by targeting Mecp2 via miR-22', *PLoS ONE*, 9(2). doi: 10.1371/journal.pone.0088685.
Ferlini, C. *et al.* (1996) 'Probing chromatin structure in the early phases of apoptosis', *Cell Proliferation*, 29(7), pp. 427–436. doi: 10.1111/j.1365-2184.1996.tb00985.x.
Figueroa-González, G. and Pérez-Plasencia, C. (2017) 'Strategies for the evaluation of DNA damage and repair mechanisms in cancer', *Oncology Letters*, pp. 3982–3988. doi: 10.3892/ol.2017.6002.
Folch, a *et al.* (1999) 'Molding of deep polydimethylsiloxane microstructures for microfluidics and biological applications.', *Journal of biomechanical engineering*, 121(1), pp. 28–34. doi: 10.1115/1.2798038.
Forbes, S. J. and Rosenthal, N. (2014) 'Preparing the ground for tissue regeneration: From mechanism to therapy', *Nature Medicine*, pp. 857–869. doi: 10.1038/nm.3653.
Foster, K. A. *et al.* (1998) 'Characterization of the A549 cell line as a type II pulmonary epithelial cell model for drug metabolism.', *Experimental cell research*, 243(2), pp. 359–66. doi: 10.1006/excr.1998.4172.
Frantz, S., Bauersachs, J. and Ertl, G. (2009) 'Post-infarct remodelling: Contribution of wound healing and inflammation', *Cardiovascular Research*, pp. 474–481. doi: 10.1093/cvr/cvn292.
Fraund, S. *et al.* (1999) 'Ten year survival after heart transplantation: Palliative procedure or successful long term treatment?', *Heart*, 82(1), pp. 47–51. doi: 10.1136/hrt.82.1.47.
Friedl, J. *et al.* (2002) 'Induction of permeability across endothelial cell monolayers by tumor necrosis factor (TNF) occurs via a tissue factor-dependent mechanism: relationship between the procoagulant and permeability effects of TNF.', *Blood*, 100(4), pp. 1334–1339.
Friis, T. *et al.* (2011) 'Mesenchymal stromal cell derived endothelial progenitor treatment in patients with refractory angina.', *Scandinavian cardiovascular journal : SCJ*, 45(3), pp. 161–168. doi: 10.3109/14017431.2011.569571.
Galiè, N. *et al.* (2015) '2015 ESC/ERS Guidelines for the diagnosis and treatment of pulmonary hypertension', *European Heart Journal*, 37(1), pp. 67–119. doi: 10.1093/eurheartj/ehv317.
Gamble, J. R. *et al.* (2000) 'Angiopoietin-1 is an antipermeability and anti-inflammatory agent in vitro and targets cell junctions', *Circulation Research*, 87(7), pp. 603–607. doi: 10.1161/01.RES.87.7.603.
Gandia, C. *et al.* (2008) 'Human Dental Pulp Stem Cells Improve Left Ventricular Function, Induce Angiogenesis, and Reduce Infarct Size in Rats with Acute Myocardial Infarction', *Stem Cells*, 26(3), pp. 638–645. doi: 10.1634/stemcells.2007-0484.
Gao, F. *et al.* (2016) 'Mesenchymal stem cells and immunomodulation: current status and future prospects.', *Cell death & disease*, 7, p. e2062. doi: 10.1038/cddis.2015.327.
García-Contreras, M. *et al.* (2014) 'Therapeutic potential of human Adipose-Derived Stem Cells (ADSCs) from cancer patients: A pilot study', *PLoS ONE*, 9(11). doi: 10.1371/journal.pone.0113288.
Garcia, O. *et al.* (2012) 'Cell-based therapies for lung disease', *British Medical Bulletin*, pp. 147–161. doi: 10.1093/bmb/ldr051.

Gatti, S. *et al.* (2011) 'Microvesicles derived from human adult mesenchymal stem cells protect against ischaemia-reperfusion-induced acute and chronic kidney injury.', *Nephrology, dialysis, transplantation : official publication of the European Dialysis and Transplant Association - European Renal Association*, 26(5), pp. 1474–83. doi: 10.1093/ndt/gfr015.

GBD 2015 Disease and Injury Incidence and Prevalence Collaborators (2016) 'Global, regional, and national incidence, prevalence, and years lived with disability for 310 diseases and injuries, 1990-2015: a systematic analysis for the Global Burden of Disease Study 2015', *Lancet*, 388(10053), pp. 1545–602. doi: 10.1016/S0140-6736(15)60692-4.Global.

Geng, Y. *et al.* (2014) 'Mesenchymal stem cells ameliorate rhabdomyolysis-induced acute kidney injury via the activation of M2 macrophages', *Stem Cell Research and Therapy*, 5(3). doi: 10.1186/scrt469.

Gennai, S. *et al.* (2015) 'Microvesicles Derived from Human Mesenchymal Stem Cells Restore Alveolar Fluid Clearance in Human Lungs Rejected for Transplantation', *American Journal of Transplantation*, 15(9), pp. 2404–2412. doi: 10.1111/ajt.13271.

Gerke, A. K. and Hunninghake, G. (2008) 'The Immunology of Sarcoidosis', *Clinics in Chest Medicine*, pp. 379–390. doi: 10.1016/j.ccm.2008.03.014.

Ggandison, L., Nolan, G. P. and Pfaff, D. W. (1994) 'Activation of the transcription factor NF-KB in GH3 pituitary cells', *Molecular and Cellular Endocrinology*, 106(1–2), pp. 9–15. doi: 10.1016/0303-7207(94)90180-5.

Gieseke, F. *et al.* (2010) 'Human multipotent mesenchymal stromal cells use galectin-1 to inhibit immune effector cells', *Blood*, 116(19), pp. 3770–3779. doi: 10.1182/blood-2010-02-270777.

Gille, J. J. P. and Joenje, H. (1992) 'Cell culture models for oxidative stress: superoxide and hydrogen peroxide versus normobaric hyperoxia', *Mutation Research DNAging*, 275(3–6), pp. 405–414. doi: 10.1016/0921-8734(92)90043-O.

Gimona, M. *et al.* (2017) 'Manufacturing of human extracellular vesicle-based therapeutics for clinical use', *International Journal of Molecular Sciences*, 18(6). doi: 10.3390/ijms18061190.

Glagov, S. *et al.* (1987) 'Compensatory enlargement of human atherosclerotic coronary arteries.', *The New England journal of medicine*, 316(22), pp. 1371–5. doi: 10.1056/NEJM198705283162204.

Glaser, D. E. *et al.* (2016) 'Multifactorial optimizations for directing endothelial fate from stem cells', *PLoS ONE*. doi: 10.1371/journal.pone.0166663.

Gnecchi, M. *et al.* (2005) 'Paracrine action accounts for marked protection of ischemic heart by Akt-modified mesenchymal stem cells [2]', *Nature Medicine*, pp. 367–368. doi: 10.1038/nm0405-367.

Gnecchi, M. *et al.* (2006) 'Evidence supporting paracrine hypothesis for Akt- modified mesenchymal stem cell-mediated cardiac protection and functional improvement', *ResearchGate*, 20, pp. 661–669. doi: 10.1096/fj.05-5211com.

Gnecchi, M. *et al.* (2016) 'Paracrine Mechanisms of Mesenchymal Stem Cells in Tissue Repair', in *Methods in molecular biology (Clifton, N.J.)*, pp. 123–146. doi: 10.1007/978-1-4939-3584-0_7.

Golia, E. *et al.* (2014) 'Inflammation and cardiovascular disease: From pathogenesis to therapeutic target', *Current Atherosclerosis Reports*. doi: 10.1007/s11883-014-0435-z.

Gong, M. *et al.* (2017) 'Mesenchymal stem cells release exosomes that transfer miRNAs to endothelial cells and promote angiogenesis', *Oncotarget*, 8(28). doi: 10.18632/oncotarget.16778.

Goodwin, M. *et al.* (2011) 'Bone marrow-derived mesenchymal stromal cells inhibit Th2-mediated allergic airways inflammation in mice', *Stem Cells*, 29(7), pp. 1137–1148. doi: 10.1002/stem.656.

Grandoch, M., Roscioni, S. S. and Schmidt, M. (2010) 'The role of Epac proteins, novel cAMP mediators, in the regulation of immune, lung and neuronal function', *British Journal of Pharmacology*, pp. 265–284. doi: 10.1111/j.1476-5381.2009.00458.x.

Griep, L. M. *et al.* (2013) 'BBB on CHIP: Microfluidic platform to mechanically and biochemically modulate blood-brain barrier function', *Biomedical Microdevices*, 15(1), pp. 145–150. doi: 10.1007/s10544-012-9699-7.

Gronthos, S. and Simmons, P. J. (1995) 'The growth factor requirements of STRO-1-positive human bone marrow stromal precursors under serum-deprived conditions in vitro.', *Blood*, 85(4), pp. 929–40. doi: papers://82E9EA27-E255-4A82-9E40-6DAC45A310F4/Paper/p85.

Grosberg, A. *et al.* (2011) 'Ensembles of engineered cardiac tissues for physiological and pharmacological study: Heart on a chip', *Lab on a Chip*, 11(24), p. 4165. doi: 10.1039/c1lc20557a.

Grosberg, A. *et al.* (2012) 'Muscle on a chip: In vitro contractility assays for smooth and striated muscle', *Journal of Pharmacological and Toxicological Methods*, 65(3), pp. 126–135. doi: 10.1016/j.vascn.2012.04.001.

Gross, J. C. *et al.* (2012) 'Active Wnt proteins are secreted on exosomes', *Nature Cell Biology*, 14(10), pp. 1036–1045. doi: 10.1038/ncb2574.

Gruber, H. E. *et al.* (2012) 'Human adipose-derived mesenchymal stem cells: serial passaging, doubling time and cell senescence.', *Biotechnic & histochemistry : official publication of the Biological Stain Commission*, 87(4), pp. 303–11. doi: 10.3109/10520295.2011.649785.

Gruber, R. *et al.* (2005) 'Bone Marrow Stromal Cells Can Provide a Local Environment That Favors Migration and Formation of Tubular Structures of Endothelial Cells', *Tissue Eng*, 11(5), pp. 896–903. doi: 10.1089/ten.2005.11.896.

Guha, M. and Mackman, N. (2001) 'LPS induction of gene expression in human monocytes', *Cellular Signalling*, pp. 85–94. doi: 10.1016/S0898-6568(00)00149-2.

Guo, J. *et al.* (2007) 'Anti-inflammation role for mesenchymal stem cells transplantation in myocardial infarction.', *Inflammation*, 30(3–4), pp. 97–104. doi: 10.1007/s10753-007-9025-3.

Guo, J. *et al.* (2011) 'Xenogeneic immunosuppression of human umbilical cord mesenchymal stem cells in a major histocompatibility complex-mismatched allogeneic acute graft-versus-host disease murine model', *European Journal of Haematology*, 87(3), pp. 235–243. doi: 10.1111/j.1600-0609.2011.01635.x.

Guo, J. *et al.* (2014) 'Insulin-Like Growth Factor 1 Treatment of MSCs Attenuates Inflammation and Cardiac Dysfunction Following MI', *Inflammation*, 37(6), pp. 2156–2163. doi: 10.1007/s10753-014-9949-3.

Gupta, N. *et al.* (2007) 'Intrapulmonary delivery of bone marrow-derived mesenchymal stem cells improves survival and attenuates endotoxin-induced acute lung injury in mice', *J Immunol*, 179(3), pp. 1855–1863. doi: 179/3/1855 [pii].

György, B. *et al.* (2015) 'Therapeutic Applications of Extracellular Vesicles: Clinical Promise and Open Questions', *Annual Review of Pharmacology and Toxicology*, 55(1), pp. 439–464. doi: 10.1146/annurev-pharmtox-010814-124630.

Haider, H. K. *et al.* (2008) 'IGF-1-overexpressing mesenchymal stem cells accelerate bone marrow stem cell mobilization via paracrine activation of SDF-1α/CXCR4 signaling to promote myocardial repair', *Circulation Research*, 103(11), pp. 1300–1308. doi: 10.1161/CIRCRESAHA.108.186742.

Han, B. *et al.* (2013) 'Trichostatin a stabilizes the expression of pluripotent genes in human mesenchymal stem cells during ex vivo expansion', *PLoS ONE*, 8(11). doi: 10.1371/journal.pone.0081781.

Hanson, M. A. *et al.* (2013) 'Coronary Artery Disease', *Primary Care - Clinics in Office Practice*, pp. 1–16. doi: 10.1016/j.pop.2012.12.001.

Hansson, G. K. (2005) 'Inflammation, Atherosclerosis, and Coronary Artery Disease', *New England Journal of Medicine*, 352(16), pp. 1685–1695. doi: 10.1056/NEJMra043430.

Hare, J. M. *et al.* (2009) 'A Randomized, Double-Blind, Placebo-Controlled, Dose-Escalation Study of Intravenous Adult Human Mesenchymal Stem Cells (Prochymal) After Acute Myocardial Infarction', *Journal of the American College of Cardiology*, 54(24), pp. 2277–2286. doi: 10.1016/j.jacc.2009.06.055.

Hare, J. M. *et al.* (2012) 'Comparison of allogeneic vs autologous bone marrow-derived mesenchymal stem cells delivered by transendocardial injection in patients with ischemic cardiomyopathy: The POSEIDON randomized trial', *JAMA - Journal of the American Medical Association*, 308(22), pp. 2369–2379. doi: 10.1001/jama.2012.25321.

Harrison, C. *et al.* (2012) 'JAK Inhibition with Ruxolitinib versus Best Available Therapy for Myelofibrosis', *New England Journal of Medicine*, 366(9), pp. 787–798. doi: 10.1056/NEJMoa1110556.

Harting, M. T. *et al.* (2018) 'Inflammation-Stimulated Mesenchymal Stromal Cell-Derived Extracellular Vesicles Attenuate Inflammation', *Stem Cells*, 36(1), pp. 79–90. doi: 10.1002/stem.2730.

Hartung, T. and Corsini, E. (2013) 'Immunotoxicology: challenges in the 21st century and in vitro opportunities.', *Altex*, 30(4), pp. 411–26. doi: 10.14573/altex.2013.4.411.

Hassell, B. A. *et al.* (2017) 'Human Organ Chip Models Recapitulate Orthotopic Lung Cancer Growth, Therapeutic Responses, and Tumor Dormancy In Vitro', *Cell Reports*, 21(2), pp. 508–516. doi: 10.1016/j.celrep.2017.09.043.

Hatzistergos, K. E. *et al.* (2010) 'Bone marrow mesenchymal stem cells stimulate cardiac stem cell proliferation and differentiation', *Circulation Research*, 107(7), pp. 913–922. doi: 10.1161/CIRCRESAHA.110.222703.

Heidemann, S. M. *et al.* (2017) 'Pathophysiology and Management of Acute Respiratory Distress Syndrome in Children', *Pediatric Clinics of North America*, pp. 1017–1037. doi: 10.1016/j.pcl.2017.06.004.

Heo, S. C. *et al.* (2011) 'Tumor necrosis factor-α-activated human adipose tissue-derived mesenchymal stem cells accelerate cutaneous wound healing through paracrine mechanisms.', *The Journal of investigative dermatology*, 131(7), pp. 1559–1567. doi: 10.1038/jid.2011.64.

Hermanns, M. I. *et al.* (2004) 'Lung epithelial cell lines in coculture with human pulmonary microvascular endothelial cells: development of an alveolo-capillary barrier in vitro.', *Laboratory investigation; a journal of technical methods and pathology*, 84(6), pp. 736–752. doi: 10.1038/labinvest.3700081.

Herrmann, J. L. *et al.* (2010) 'Preconditioning mesenchymal stem cells with transforming growth factor-alpha improves mesenchymal stem cell-mediated cardioprotection.', *Shock (Augusta, Ga.)*, 33(1), pp. 24–30. doi: 10.1097/SHK.0b013e3181b7d137.

Higashiyama, R. *et al.* (2007) 'Bone marrow-derived cells express matrix metalloproteinases and contribute to regression of liver fibrosis in mice', *Hepatology*, 45(1), pp. 213–222. doi: 10.1002/hep.21477.

Hill, A. F. *et al.* (2013) 'ISEV position paper: extracellular vesicle RNA analysis and bioinformatics', *Journal of Extracellular Vesicles*, 2(1), p. 22859. doi: 10.3402/jev.v2i0.22859.

Ho, C. M. *et al.* (2011) 'Dexamethasone prevents postoperative nausea and vomiting: Benefit versus risk', *Acta Anaesthesiologica Taiwanica*, pp. 100–104. doi: 10.1016/j.aat.2011.06.002.

Ho, E. *et al.* (2013) 'Biological markers of oxidative stress: Applications to cardiovascular research and practice', *Redox Biology*, 1(1), pp. 483–491. doi: 10.1016/j.redox.2013.07.006.

Ho, L. S. *et al.* (2006) 'Establishment of a mouse primary co-culture of endometrial epithelial cells and peripheral blood leukocytes: Effect on epithelial barrier function and leukocyte survival', *Cell Biology International*, 30(12), pp. 977–982. doi: 10.1016/j.cellbi.2006.07.004.

Hoffman, J. I. E. and Kaplan, S. (2002) 'The incidence of congenital heart disease', *Journal of the American College of Cardiology*, pp. 1890–1900. doi: 10.1016/S0735-1097(02)01886-7.

Hoffman, M. D. and Benoit, D. S. W. (2015) 'Agonism of Wnt-β-catenin signalling promotes mesenchymal stem cell (MSC) expansion', *Journal of Tissue Engineering and Regenerative Medicine*, 9(11), pp. E13–E26. doi: 10.1002/term.1736.

Hong, B. S. *et al.* (2009) 'Colorectal cancer cell-derived microvesicles are enriched in cell cycle-related mRNAs that promote proliferation of endothelial cells', *BMC Genomics*, 10. doi: 10.1186/1471-2164-10-556.

Hornakova, T. *et al.* (2011) 'Oncogenic JAK1 and JAK2-activating mutations resistant to ATP-competitive inhibitors', *Haematologica*, 96(6), pp. 845–853. doi: 10.3324/haematol.2010.036350.

Hosokawa, J. *et al.* (2013) 'Role of Calcium Ionophore A23187- Induced Activation of IkappaB Kinase 2 in Mast Cells', *Int Arch Allergy Immunol*,

161(2), pp. 37–43. doi: 10.1159/000350357.
Hoyer, F. F. *et al.* (2012) 'Monocytic microparticles promote atherogenesis by modulating inflammatory cells in mice', *Journal of Cellular and Molecular Medicine*, 16(11), pp. 2777–2788. doi: 10.1111/j.1582-4934.2012.01595.x.
Hsu, C. *et al.* (2010) 'Regulation of exosome secretion by Rab35 and its GTPase-activating proteins TBC1D10A-C', *Journal of Cell Biology*, 189(2), pp. 223–232. doi: 10.1083/jcb.200911018.
Hsu, P.-J. *et al.* (2015) 'Assessment of the Immunomodulatory Properties of Human Mesenchymal Stem Cells (MSCs).', *Journal of visualized experiments : JoVE*, p. 2015. doi: 10.3791/53265.
Hu, C. *et al.* (2008) 'Introduction of hIGF-1 gene into bone marrow stromal cells and its effects on the cell's biological behaviors', *Cell Transplantation*, 17(9), pp. 1067–1081. doi: 10.3727/096368908786991506.
Huh, D. *et al.* (2010) 'Reconstituting organ-level lung functions on a chip', *Science*, 328(5986), pp. 1662–1668. doi: 10.1126/science.1188302.
Huh, D. *et al.* (2012) 'A human disease model of drug toxicity-induced pulmonary edema in a lung-on-a-chip microdevice', *Science Translational Medicine*, 4(159). doi: 10.1126/scitranslmed.3004249.
Hung, S.-C. *et al.* (2007) 'Angiogenic Effects of Human Multipotent Stromal Cell Conditioned Medium Activate the PI3K-Akt Pathway in Hypoxic Endothelial Cells to Inhibit Apoptosis, Increase Survival, and Stimulate Angiogenesis', *STEM CELLS*, 25(9), pp. 2363–2370. doi: 10.1634/stemcells.2006-0686.
Hunt, M. M. *et al.* (2014) 'Factorial Experimental Design for the Culture of Human Embryonic Stem Cells as Aggregates in Stirred Suspension Bioreactors Reveals the Potential for Interaction Effects Between Bioprocess Parameters', *Tissue Engineering Part C: Methods*. doi: 10.1089/ten.tec.2013.0040.
Ibrahim, A. G. E., Cheng, K. and Marbán, E. (2014) 'Exosomes as critical agents of cardiac regeneration triggered by cell therapy', *Stem Cell Reports*, 2(5), pp. 606–619. doi: 10.1016/j.stemcr.2014.04.006.
Ingber, D. E. (2003) 'Mechanobiology and diseases of mechanotransduction', *Annals of Medicine*, pp. 564–577. doi: 10.1080/07853890310016333.
Ishizuka, T., Hinata, T. and Watanabe, Y. (2011) 'Superoxide induced by a high-glucose concentration attenuates production of angiogenic growth factors in hypoxic mouse mesenchymal stem cells', *Journal of Endocrinology*, 208(2), pp. 147–159. doi: 10.1677/JOE-10-0305.
Issman, L. *et al.* (2013) 'Cryogenic transmission electron microscopy nanostructural study of shed microparticles', *PLoS ONE*, 8(12). doi: 10.1371/journal.pone.0083680.
Jaeschke, H. *et al.* (1996) 'Mechanisms of inflammatory liver injury: Adhesion molecules and cytotoxicity of neutrophils', *Toxicology and Applied Pharmacology*, pp. 213–226. doi: 10.1006/taap.1996.0160.
Jain, A. *et al.* (2018) 'Primary Human Lung Alveolus-on-a-chip Model of Intravascular Thrombosis for Assessment of Therapeutics', *Clinical Pharmacology and Therapeutics*, 103(2), pp. 332–340. doi: 10.1002/cpt.742.
Jakobsen, R. B. *et al.* (2014) 'Analysis of the effects of five factors relevant to in vitro chondrogenesis of human mesenchymal stem cells using factorial design and high throughput mRNA-profiling', *PLOS ONE*. doi: 10.1371/journal.pone.0096615.
Jalili-Firoozinezhad, S. *et al.* (2018) 'Modeling radiation injury-induced cell death and countermeasure drug responses in a human Gut-on-a-Chip article', *Cell Death and Disease*, 9(2). doi: 10.1038/s41419-018-0304-8.
Janeczek Portalska, K. *et al.* (2012) 'Endothelial Differentiation of Mesenchymal Stromal Cells', *PLoS ONE*, 7(10). doi: 10.1371/journal.pone.0046842.
Jang, K.-J. *et al.* (2013) 'Human kidney proximal tubule-on-a-chip for drug transport and nephrotoxicity assessment', *Integrative Biology*, 5(9), p. 1119. doi: 10.1039/c3ib40049b.
Jang, K.-J. and Suh, K.-Y. (2010) 'A multi-layer microfluidic device for efficient culture and analysis of renal tubular cells', *Lab on a Chip*, 10(1), pp. 36–42. doi: 10.1039/B907515A.
Jeffery, P. K. (2001) 'Remodeling in asthma and chronic obstructive lung disease', *Am.J.Respir.Crit Care Med.*, 164(1073–449X (Print)), pp. S28–S38. doi: 10.1164/rccm2106061.
Jeong, S. G. and Cho, G. W. (2015) 'Trichostatin a modulates intracellular reactive oxygen species through SOD2 and FOXO1 in human bone marrow-mesenchymal stem cells', *Cell Biochemistry and Function*, 33(1), pp. 37–43. doi: 10.1002/cbf.3084.
Jeppesen, D. K. *et al.* (2014) 'Comparative analysis of discrete exosome fractions obtained by differential centrifugation', *Journal of Extracellular Vesicles*, 3(1). doi: 10.3402/jev.v3.25011.
Ji, Y. R. *et al.* (2012) 'Mesenchymal stem cells support proliferation and terminal differentiation of B cells.', *Cellular physiology and biochemistry : international journal of experimental cellular physiology, biochemistry, and pharmacology*, 30(6), pp. 1526–37. doi: 10.1159/000343340.
Jiang, X.-X. *et al.* (2005) 'Human mesenchymal stem cells inhibit differentiation and function of monocyte-derived dendritic cells.', *Blood*, 105(10), pp. 4120–6. doi: 10.1182/blood-2004-02-0586.
Jin, H. J. *et al.* (2009) 'Down-regulation of CD105 is associated with multi-lineage differentiation in human umbilical cord blood-derived mesenchymal stem cells', *Biochem Biophys Res Commun*, 381(4), pp. 676–681. doi: S0006-291X(09)00396-9 [pii]\n10.1016/j.bbrc.2009.02.118.
Jo, H. *et al.* (2012) 'Small molecule-induced cytosolic activation of protein kinase Akt rescues ischemia-elicited neuronal death', *Proceedings of the National Academy of Sciences*, 109(26), pp. 10581–10586. doi: 10.1073/pnas.1202810109.
Joo, S. *et al.* (2014) 'Myogenic-induced mesenchymal stem cells are capable of modulating the immune response by regulatory T cells.', *Journal of tissue engineering*, 5(0), p. 2041731414524758. doi: 10.1177/2041731414524758.
Jung, Y., Bauer, G. and Nolta, J. A. (2012) 'Concise review: Induced pluripotent stem cell-derived mesenchymal stem cells: Progress toward safe clinical products', *Stem Cells*, pp. 42–47. doi: 10.1002/stem.727.

Kane, B. J. *et al.* (2006) 'Liver-specific functional studies in a microfluidic array of primary mammalian hepatocytes', *Analytical Chemistry*, 78(13), pp. 4291–4298. doi: 10.1021/ac051856v.

Kane, R. S. *et al.* (1999) 'Patterning proteins and cells using soft lithography', *Biomaterials*, pp. 2363–2376. doi: 10.1016/S0142-9612(99)00165-9.

Kang, S.-G. *et al.* (2010) 'Isolation and Perivascular Localization of Mesenchymal Stem Cells From Mouse Brain', *Neurosurgery*, 67(3), pp. 711–720. doi: 10.1227/01.NEU.0000377859.06219.78.

Karahuseyinoglu, S. *et al.* (2007) 'Biology of stem cells in human umbilical cord stroma: in situ and in vitro surveys.', *Stem cells (Dayton, Ohio)*, 25(2), pp. 319–331. doi: 10.1634/stemcells.2006-0286.

Karantalis, V. *et al.* (2014) 'Autologous mesenchymal stem cells produce concordant improvements in regional function, tissue perfusion and fibrotic burden when administered to patients undergoing coronary artery bypass grafting - The prometheus trial', *Circulation Research*. doi: 10.1161/CIRCRESAHA.114.303180.

Karantalis, V. and Hare, J. M. (2015) 'Use of mesenchymal stem cells for therapy of cardiac disease', *Circulation Research*, pp. 1413–1430. doi: 10.1161/CIRCRESAHA.116.303614.

Karima, R. *et al.* (1999) 'The molecular pathogenesis of endotoxic shock and organ failure', *Molecular Medicine Today*, pp. 123–132. doi: 10.1016/S1357-4310(98)01430-0.

Kariyawasam, H. H. and Robinson, D. S. (2007) 'The role of eosinophils in airway tissue remodelling in asthma', *Current Opinion in Immunology*, pp. 681–686. doi: 10.1016/j.coi.2007.07.021.

Kasper, G. *et al.* (2009) 'Insights into mesenchymal stem cell aging: Involvement of antioxidant defense and actin cytoskeleton', *Stem Cells*, 27(6), pp. 1288–1297. doi: 10.1002/stem.49.

Katritsis, D. G. *et al.* (2005) 'Transcoronary transplantation of autologous mesenchymal stem cells and endothelial progenitors into infarcted human myocardium', *Catheterization and Cardiovascular Interventions*, 65(3), pp. 321–329. doi: 10.1002/ccd.20406.

Kay, A. G. *et al.* (2017) 'Mesenchymal Stem Cell-Conditioned Medium Reduces Disease Severity and Immune Responses in Inflammatory Arthritis', *Scientific Reports*, 7(1). doi: 10.1038/s41598-017-18144-w.

Keats, E. C. *et al.* (2014) 'Switch from canonical to noncanonical Wnt signaling mediates high glucose-induced adipogenesis', *Stem Cells*, 32(6), pp. 1649–1660. doi: 10.1002/stem.1659.

Kehat, I. and Molkentin, J. D. (2010) 'Molecular pathways underlying cardiac remodeling during pathophysiological stimulation', *Circulation*, 122(25), pp. 2727–2735. doi: 10.1161/CIRCULATIONAHA.110.942268.

Kelly, J. J. *et al.* (1998) 'Pulmonary microvascular and macrovascular endothelial cells: differential regulation of Ca2+ and permeability', *The American journal of physiology*, 274(5 Pt 1), pp. L810-9. Available at: papers://d8e9569c-3053-4f4e-bfb0-c8b1b3194e73/Paper/p4874.

Kern, S. *et al.* (2006) 'Comparative analysis of mesenchymal stem cells from bone marrow, umbilical cord blood, or adipose tissue.', *Stem cells (Dayton, Ohio)*, 24(5), pp. 1294–301. doi: 10.1634/stemcells.2005-0342.

Khair, O. A. *et al.* (1994) 'Effect of Haemophilus influenzae endotoxin on the synthesis of IL-6, IL-8, TNF-alpha and expression of ICAM-1 in cultured human bronchial epithelial cells.', *The European respiratory journal : official journal of the European Society for Clinical Respiratory Physiology*, 7(12), pp. 2109–16. doi: 10.1183/09031936.94.07122109.

Khanal, G. *et al.* (2011) 'Ischemia/reperfusion injury of primary porcine cardiomyocytes in a low-shear microfluidic culture and analysis device', *The Analyst*, 136(17), p. 3519. doi: 10.1039/c0an00845a.

Kilroy, G. E. *et al.* (2007) 'Cytokine profile of human adipose-derived stem cells: Expression of angiogenic, hematopoietic, and pro-inflammatory factors', *Journal of Cellular Physiology*, 212(3), pp. 702–709. doi: 10.1002/jcp.21068.

Kim, D.-K. *et al.* (2015) 'Chromatographically isolated CD63+CD81+ extracellular vesicles from mesenchymal stromal cells rescue cognitive impairments after TBI.', *Proceedings of the National Academy of Sciences of the United States of America*, (30), p. 1522297113-. doi: 10.1073/pnas.1522297113.

Kim, H. J. *et al.* (2012) 'Human gut-on-a-chip inhabited by microbial flora that experiences intestinal peristalsis-like motions and flow', *Lab on a Chip*, 12(12), p. 2165. doi: 10.1039/c2lc40074j.

Kim, H. J. and Ingber, D. E. (2013) 'Gut-on-a-Chip microenvironment induces human intestinal cells to undergo villus differentiation', *Integrative Biology*, 5(9), p. 1130. doi: 10.1039/c3ib40126j.

Kim, I. *et al.* (2001) 'Angiopoietin-1 reduces VEGF-stimulated leukocyte adhesion to endothelial cells by reducing ICAM-1, VCAM-1, and E-selectin expression', *Circulation Research*, 89(6), pp. 477–479. doi: 10.1161/hh1801.097034.

Kim, J.-A. *et al.* (2015) 'Regulation of mesenchymal stromal cells through fine tuning of canonical Wnt signaling', *Stem Cell Research*, 14(3), pp. 356–368. doi: 10.1016/j.scr.2015.02.007.

Kim, J. and Hematti, P. (2009) 'Mesenchymal stem cell-educated macrophages: A novel type of alternatively activated macrophages', *Experimental Hematology*, 37(12), pp. 1445–1453. doi: 10.1016/j.exphem.2009.09.004.

Kim, K. M. *et al.* (2012) 'MiR-182 is a negative regulator of osteoblast proliferation, differentiation, and skeletogenesis through targeting FoxO1', *Journal of Bone and Mineral Research*, 27(8), pp. 1669–1679. doi: 10.1002/jbmr.1604.

Kim, M. R. *et al.* (2009) 'Thromboxane a(2) induces differentiation of human mesenchymal stem cells to smooth muscle-like cells.', *Stem cells*, 27(1), pp. 191–199. doi: 10.1634/stemcells.2008-0363.

Kim, S. *et al.* (2016) 'Interstitial flow regulates the angiogenic response and phenotype of endothelial cells in a 3D culture model', *Lab Chip*, 16(21), pp. 4189–4199. doi: 10.1039/C6LC00910G.

Kim, Y. S. *et al.* (2007) 'Curcumin attenuates inflammatory responses of TNF-α-stimulated human endothelial cells', *Journal of Cardiovascular Pharmacology*, 50(1), pp. 41–49. doi: 10.1097/FJC.0b013e31805559b9.

Kim, Y. S. (2009) 'TNF-alpha enhances engraftment of mesenchymal stem cells into infarcted myocardium', *Frontiers in Bioscience*, Volume(14), p. 2845. doi: 10.2741/3417.

Kim, Y. S. *et al.* (2017) 'Adipose stem cell-derived nanovesicles inhibit emphysema primarily via an FGF2-dependent pathway', *Experimental and Molecular Medicine*, 49(1). doi: 10.1038/emm.2016.127.

Kinnaird, T. *et al.* (2004) 'Marrow-Derived Stromal Cells Express Genes Encoding a Broad Spectrum of Arteriogenic Cytokines and Promote In Vitro and In Vivo Arteriogenesis Through Paracrine Mechanisms', *Circulation Research*, 94(5), pp. 678–685. doi: 10.1161/01.RES.0000118601.37875.AC.

Kirschner, N. *et al.* (2010) 'Tight junctions form a barrier in human epidermis', *European Journal of Cell Biology*, 89(11), pp. 839–842. doi: 10.1016/j.ejcb.2010.07.010.

Ko, E., Lee, K. Y. and Hwang, D. S. (2012) 'Human Umbilical Cord Blood–Derived Mesenchymal Stem Cells Undergo Cellular Senescence in Response to Oxidative Stress', *Stem Cells and Development*, 21(11), pp. 1877–1886. doi: 10.1089/scd.2011.0284.

Koch, R. E. and Hill, G. E. (2017) 'An assessment of techniques to manipulate oxidative stress in animals', *Functional Ecology*, pp. 9–21. doi: 10.1111/1365-2435.12664.

Koizumi, K. *et al.* (2003) 'Anti-angiogenic effects of dimethyl sulfoxide on endothelial cells.', *Biological & pharmaceutical bulletin*, 26(9), pp. 1295–1298. doi: 10.1248/bpb.26.1295.

Kolaczkowska, E. and Kubes, P. (2013) 'Neutrophil recruitment and function in health and inflammation', *Nature Reviews Immunology*, pp. 159–175. doi: 10.1038/nri3399.

Konar, D. *et al.* (2016) 'Lung-On-A-Chip Technologies for Disease Modeling and Drug Development', *Biomedical Engineering and Computational Biology*, 2016(Suppl. 1), pp. 17–27. doi: 10.4137/BECB.S34252.

Kooistra, M. R. H. *et al.* (2005) 'Epac1 regulates integrity of endothelial cell junctions through VE-cadherin', *FEBS Letters*, 579(22), pp. 4966–4972. doi: 10.1016/j.febslet.2005.07.080.

Kopen, G. C., Prockop, D. J. and Phinney, D. G. (1999) 'Marrow stromal cells migrate throughout forebrain and cerebellum, and they differentiate into astrocytes after injection into neonatal mouse brains', *Proceedings of the National Academy of Sciences*, 96(19), pp. 10711–10716. doi: 10.1073/pnas.96.19.10711.

van Koppen, A. *et al.* (2012) 'Human Embryonic Mesenchymal Stem Cell-Derived Conditioned Medium Rescues Kidney Function in Rats with Established Chronic Kidney Disease', *PLoS ONE*, 7(6), p. e38746. doi: 10.1371/journal.pone.0038746.

Kordelas, L. *et al.* (2014) 'MSC-derived exosomes: A novel tool to treat therapy-refractory graft-versus-host disease', *Leukemia*, pp. 970–973. doi: 10.1038/leu.2014.41.

Kotmakçı, M. (2017) 'Exosome Isolation: Is There an Optimal Method with Regard to Diagnosis or Treatment?', in Erel Akbaba, G. and Wang, J. (eds) *Novel Implications of Exosomes in Diagnosis and Treatment of Cancer and Infectious Diseases*. Rijeka: InTech, p. Ch. 8. doi: 10.5772/intechopen.69407.

Krampera, M. *et al.* (2006) 'Role for interferon-gamma in the immunomodulatory activity of human bone marrow mesenchymal stem cells', *Stem Cells*, 24(2), pp. 386–398. doi: 10.1634/stemcells.2005-0008.

Kreimer, S. *et al.* (2015) 'Mass-spectrometry-based molecular characterization of extracellular vesicles: Lipidomics and proteomics', *Journal of Proteome Research*, 14(6), pp. 2367–2384. doi: 10.1021/pr501279t.

Krenning, G., Zeisberg, E. M. and Kalluri, R. (2010) 'The origin of fibroblasts and mechanism of cardiac fibrosis', *Journal of Cellular Physiology*, pp. 631–637. doi: 10.1002/jcp.22322.

Kumar, A. *et al.* (1998) 'Curcumin (Diferuloylmethane) inhibition of tumor necrosis factor (TNF)-mediated adhesion of monocytes to endothelial cells by suppression of cell surface expression of adhesion molecules and of nuclear factor-kappaB activation.', *Biochemical pharmacology*, 55(6), pp. 775–83.

Kuroki, Y., Takahashi, M. and Nishitani, C. (2007) 'Pulmonary collectins in innate immunity of the lung', *Cellular Microbiology*, pp. 1871–1879. doi: 10.1111/j.1462-5822.2007.00953.x.

Kusuma, G. D. *et al.* (2017) 'Reduced aldehyde dehydrogenase expression in preeclamptic decidual mesenchymal stem/stromal cells is restored by aldehyde dehydrogenase agonists', *Scientific Reports*, 7. doi: 10.1038/srep42397.

Labarthe, D. R. (2011) 'Cardiovascular diseases: a global public health challenge', *Epidemiology and prevention of cardiovascular diseases: a global challenge*, pp. 3–15.

Lai, R. C., Arslan, F., Tan, S. S., *et al.* (2010) 'Derivation and characterization of human fetal MSCs: An alternative cell source for large-scale production of cardioprotective microparticles', *Journal of Molecular and Cellular Cardiology*, 48(6), pp. 1215–1224. doi: 10.1016/j.yjmcc.2009.12.021.

Lai, R. C., Arslan, F., Lee, M. M., *et al.* (2010) 'Exosome secreted by MSC reduces myocardial ischemia/reperfusion injury', *Stem Cell Research*, 4(3), pp. 214–222. doi: 10.1016/j.scr.2009.12.003.

Lai, Y. C. *et al.* (2017) 'Inflammation-related microRNA expression level in the bovine milk is affected by mastitis', *PLoS ONE*, 12(5). doi: 10.1371/journal.pone.0177182.

Lama, V. N. *et al.* (2007) 'Evidence for tissue-resident mesenchymal stem cells in human adult lung from studies of transplanted allografts', *Journal of Clinical Investigation*, 117(4), pp. 989–996. doi: 10.1172/JCI29713.

Lee, C. *et al.* (2012) 'Exosomes mediate the cytoprotective action of mesenchymal stromal cells on hypoxia-induced pulmonary hypertension', *Circulation*, 126(22), pp. 2601–2611. doi: 10.1161/CIRCULATIONAHA.112.114173.

Lee, J.-K. *et al.* (2013) 'Exosomes Derived from Mesenchymal Stem Cells Suppress Angiogenesis by Down-Regulating VEGF Expression in

Breast Cancer Cells', *PLoS ONE*, 8(12), p. e84256. doi: 10.1371/journal.pone.0084256.
Lee, J.-W. *et al.* (2014) 'A Randomized, Open-Label, Multicenter Trial for the Safety and Efficacy of Adult Mesenchymal Stem Cells after Acute Myocardial Infarction', *Journal of Korean Medical Science*, 29(1), p. 23. doi: 10.3346/jkms.2014.29.1.23.
Lee, J. W. *et al.* (2013) 'Therapeutic effects of human mesenchymal stem cells in ex vivo human lungs injured with live bacteria', *American Journal of Respiratory and Critical Care Medicine*, 187(7), pp. 751–760. doi: 10.1164/rccm.201206-0990OC.
Lee, K. C. *et al.* (2015) 'Allo-transplantation of mesenchymal stem cells attenuates hepatic injury through IL1Ra dependent macrophage switch in a mouse model of liver disease', *Journal of Hepatology*, 63(6), pp. 1405–1412. doi: 10.1016/j.jhep.2015.07.035.
Lee, K. H. *et al.* (2009) 'Epigenetic silencing of microRNA miR-107 regulates cyclin-dependent kinase 6 expression in pancreatic cancer', *Pancreatology*, 9(3), pp. 293–301. doi: 10.1159/000186051.
Lee, M. J. *et al.* (2010) 'Proteomic analysis of tumor necrosis factor-alpha-induced secretome of human adipose tissue-derived mesenchymal stem cells.', *Journal of proteome research*, 9(4), pp. 1754–1762. doi: 10.1021/pr900898n.
Lee, P. J., Hung, P. J. and Lee, L. P. (2007) 'An artificial liver sinusoid with a microfluidic endothelial-like barrier for primary hepatocyte culture', *Biotechnology and Bioengineering*, 97(5), pp. 1340–1346. doi: 10.1002/bit.21360.
Lee, S. *et al.* (2014) 'The market trend analysis and prospects of scaffolds for stem cells', *Biomaterials Research*, 18(1). doi: 10.1186/2055-7124-18-11.
Lee, Y., El Andaloussi, S. and Wood, M. J. A. (2012) 'Exosomes and microvesicles: Extracellular vesicles for genetic information transfer and gene therapy', *Human Molecular Genetics*, 21(R1). doi: 10.1093/hmg/dds317.
Lemasters, J. J. *et al.* (1987) 'Blebbing, free Ca2+ and mitochondrial membrane potential preceding cell death in hepatocytes.', *Nature*, pp. 78–81. doi: 10.1038/325078a0.
Lemasters, J. J. *et al.* (1999) 'Mitochondrial dysfunction in the pathogenesis of necrotic and apoptotic cell death', *Journal of Bioenergetics and Biomembranes*, pp. 305–319. doi: 10.1023/A:1005419617371.
Li, C. *et al.* (2015) 'Comparative analysis of human mesenchymal stem cells from bone marrow and adipose tissue under xeno-free conditions for cell therapy', *Stem Cell Research & Therapy*, 6(1), p. 55. doi: 10.1186/s13287-015-0066-5.
Li, S. *et al.* (2013) 'Intracellular ATP Concentration Contributes to the Cytotoxic and Cytoprotective Effects of Adenosine', *PLoS ONE*, 8(10). doi: 10.1371/journal.pone.0076731.
Li, T. *et al.* (2013) 'Exosomes Derived from Human Umbilical Cord Mesenchymal Stem Cells Alleviate Liver Fibrosis', *Stem Cells and Development*, 22(6), pp. 845–854. doi: 10.1089/scd.2012.0395.
Li, X. *et al.* (2016) 'Exosome Derived From Human Umbilical Cord Mesenchymal Stem Cell Mediates MiR-181c Attenuating Burn-induced Excessive Inflammation', *EBioMedicine*, 8, pp. 72–82. doi: 10.1016/j.ebiom.2016.04.030.
Liang, X. *et al.* (2016) 'Exosomes secreted by mesenchymal stem cells promote endothelial cell angiogenesis by transferring miR-125a', *Journal of Cell Science*, 129(11), pp. 2182–2189. doi: 10.1242/jcs.170373.
Libby, P. (2006) 'Inflammation and cardiovascular disease mechanisms.', *The American journal of clinical nutrition*, 83(2), p. 456S–460S.
Licht, R. *et al.* (1999) 'An assay for the quantitative measurement of in vitro phagocytosis of early apoptotic thymocytes by murine resident peritoneal macrophages', *Journal of Immunological Methods*, 223(2), pp. 237–248. doi: 10.1016/S0022-1759(98)00212-9.
Lieberthal, W., Triaca, V. and Levine, J. (1996) 'Mechanisms of death induced by cisplatin in proximal tubular epithelial cells: apoptosis vs. necrosis.', *The American journal of physiology*, 270, pp. F700–F708.
Lin, H. *et al.* (2011) 'Implications of the immunoregulatory functions of mesenchymal stem cells in the treatment of human liver diseases', *Cellular and Molecular Immunology*, pp. 19–22. doi: 10.1038/cmi.2010.57.
Lin, L. and Du, L. (2017) 'The role of secreted factors in stem cells-mediated immune regulation', *Cellular Immunology*. doi: 10.1016/j.cellimm.2017.07.010.
Lin, R. Z. *et al.* (2012) 'Equal modulation of endothelial cell function by four distinct tissue-specific mesenchymal stem cells', *Angiogenesis*, 15(3), pp. 443–455. doi: 10.1007/s10456-012-9272-2.
Linares, R. *et al.* (2015) 'High-speed centrifugation induces aggregation of extracellular vesicles', *Journal of Extracellular Vesicles*. doi: 10.3402/jev.v4.29509.
Linke, A. *et al.* (2005) 'Stem cells in the dog heart are self-renewing, clonogenic, and multipotent and regenerate infarcted myocardium, improving cardiac function', *Proceedings of the National Academy of Sciences*, 102(25), pp. 8966–8971. doi: 10.1073/pnas.0502678102.
Liu, J. L. *et al.* (2012) 'MicroRNA 16 enhances differentiation of human bone marrow mesenchymal stem cells in a cardiac niche toward myogenic phenotypes in vitro', *Life Sciences*, 90(25–26), pp. 1020–1026. doi: 10.1016/j.lfs.2012.05.011.
Liu, M.-C. *et al.* (2013) 'Electrofluidic pressure sensor embedded microfluidic device: a study of endothelial cells under hydrostatic pressure and shear stress combinations', *Lab on a Chip*, 13(9), p. 1743. doi: 10.1039/c3lc41414k.
Liu, R. *et al.* (2016) 'Comparison of the Biological Characteristics of Mesenchymal Stem Cells Derived from Bone Marrow and Skin', *Stem Cells International*, 2016. doi: 10.1155/2016/3658798.
Liu, X. *et al.* (1996) 'Induction of apoptotic program in cell-free extracts: Requirement for dATP and cytochrome c', *Cell*, 86(1), pp. 147–157. doi: 10.1016/S0092-8674(00)80085-9.
Liu, X. *et al.* (2011) 'SDF-1/CXCR4 axis modulates bone marrow mesenchymal stem cell apoptosis, migration and cytokine secretion', *Protein & Cell*, 2(10), pp. 845–854. doi: 10.1007/s13238-011-1097-z.
Liu, Y. *et al.* (2010) 'Therapeutic potential of human umbilical cord mesenchymal stem cells in the treatment of rheumatoid arthritis', *Arthritis Res Ther*, 12(6), p. R210. doi: 10.1186/ar3187.

Liu, Y. *et al.* (2014) 'MSCs inhibit bone marrow-derived DC maturation and function through the release of TSG-6', *Biochemical and Biophysical Research Communications*, 450(4), pp. 1409–1415. doi: 10.1016/j.bbrc.2014.07.001.

Loffredo, F. S. *et al.* (2011) 'Bone marrow-derived cell therapy stimulates endogenous cardiomyocyte progenitors and promotes cardiac repair', *Cell Stem Cell*, 8(4), pp. 389–398. doi: 10.1016/j.stem.2011.02.002.

Lőrincz, Á. M. *et al.* (2014) 'Effect of storage on physical and functional properties of extracellular vesicles derived from neutrophilic granulocytes', *Journal of Extracellular Vesicles*, 3(1), p. 25465. doi: 10.3402/jev.v3.25465.

Lötvall, J. *et al.* (2014) 'Minimal experimental requirements for definition of extracellular vesicles and their functions: A position statement from the International Society for Extracellular Vesicles', *Journal of Extracellular Vesicles*. doi: 10.3402/jev.v3.26913.

Lou, G. *et al.* (2017) 'MiR-122 modification enhances the therapeutic efficacy of adipose tissue-derived mesenchymal stem cells against liver fibrosis', *Journal of Cellular and Molecular Medicine*, 21(11), pp. 2963–2973. doi: 10.1111/jcmm.13208.

Lu, Z. *et al.* (2017) 'Priming Adipose Stem Cells with Tumor Necrosis Factor-Alpha Preconditioning Potentiates Their Exosome Efficacy for Bone Regeneration', *Tissue Engineering Part A*, p. ten.tea.2016.0548. doi: 10.1089/ten.tea.2016.0548.

De Luca, A. *et al.* (2013) 'Comparative Analysis of Mesenchymal Stromal Cells Biological Properties', *ISRN Stem Cells*, 2013(674671), pp. 1–9. doi: 10.1155/2013/674671.

Lund, T. C., Tolar, J. and Orchard, P. J. (2008) 'Granulocyte colony-stimulating factor mobilized CFU-F can be found in the peripheral blood but have limited expansion potential', *Haematologica*, 93(6), pp. 908–912. doi: 10.3324/haematol.12384.

Luz-Crawford, P. *et al.* (2016) 'Mesenchymal Stem Cell-Derived Interleukin 1 Receptor Antagonist Promotes Macrophage Polarization and Inhibits B Cell Differentiation', *Stem Cells*, 34(2), pp. 483–492. doi: 10.1002/stem.2254.

Ma, S. *et al.* (2014) 'Immunobiology of mesenchymal stem cells', *Cell Death and Differentiation*, pp. 216–225. doi: 10.1038/cdd.2013.158.

Ma, T. Y. *et al.* (2004) 'TNF-alpha-induced increase in intestinal epithelial tight junction permeability requires NF-kappa B activation.', *American journal of physiology. Gastrointestinal and liver physiology*, 286(3), pp. G367–G376. doi: 10.1152/ajpgi.00173.2003.

Mack, M. *et al.* (2000) 'Transfer of the chemokine receptor CCR5 between cells by membrane-derived microparticles: a mechanism for cellular human immunodeficiency virus 1 infection', *Nat Med*, 6(7), pp. 769–775. doi: 10.1038/77498.

MacNee, W. (2001) 'Oxidative stress and lung inflammation in airways disease', *European Journal of Pharmacology*, pp. 195–207. doi: 10.1016/S0014-2999(01)01320-6.

Mammoto, T., Mammoto, A. and Ingber, D. E. (2013) 'Mechanobiology and Developmental Control', *Annual Review of Cell and Developmental Biology*, 29(1), pp. 27–61. doi: 10.1146/annurev-cellbio-101512-122340.

Marijon, E. *et al.* (2012) 'Rheumatic heart disease.', *Lancet*, 379(9819), pp. 953–64. doi: 10.1016/S0140-6736(11)61171-9.

MARINA MORIGI,* BARBARA IMBERTI,* CARLA ZOJA,* DANIELA CORNA,* SUSANNA TOMASONI,* MAURO ABBATE,* DANIELA ROTTOLI,* STEFANIA ANGIOLETTI,* ARIELA BENIGNI, N. P. and MALCOLM ALISON, and G. R. (2004) 'Mesenchymal Stem Cells Are Renotropic, Helping to Repair the Kidney and Improve Function in Acute Renal Failure', *Journal of the American Society of Nephrology*, 15(7), pp. 1794–1804. doi: 10.1097/01.ASN.0000128974.07460.34.

Marinho, P. A., Chailangkarn, T. and Muotri, A. R. (2015) 'Systematic optimization of human pluripotent stem cells media using Design of Experiments', *Scientific Reports*. doi: 10.1038/srep09834.

Mark, P. *et al.* (2013) 'Human mesenchymal stem cells display reduced expression of CD105 after culture in serum-free medium', *Stem Cells International*. doi: 10.1155/2013/698076.

Mathers, C. D. and Loncar, D. (2006) 'Projections of global mortality and burden of disease from 2002 to 2030', *PLoS Medicine*, 3(11), pp. 2011–2030. doi: 10.1371/journal.pmed.0030442.

McBride, J. D. *et al.* (2017) 'Bone marrow mesenchymal stem cell-derived CD63+ exosomes transport Wnt3a exteriorly and enhance dermal fibroblast proliferation, migration and angiogenesis in vitro', *Stem Cells and Development*, p. scd.2017.0087. doi: 10.1089/scd.2017.0087.

van der Meer, A. D. *et al.* (2013) 'Three-dimensional co-cultures of human endothelial cells and embryonic stem cell-derived pericytes inside a microfluidic device', *Lab on a Chip*, 13(18), p. 3562. doi: 10.1039/c3lc50435b.

Mendicino, M. *et al.* (2014) 'MSC-based product characterization for clinical trials: An FDA perspective', *Cell Stem Cell*, pp. 141–145. doi: 10.1016/j.stem.2014.01.013.

Mertens, J. J. *et al.* (1995) 'Reactive oxygen species and DNA damage in 2-bromo-(glutathion-S-yl) hydroquinone-mediated cytotoxicity', *Arch Biochem Biophys*, 320(1), pp. 51–58. doi: S0003986185713410 [pii].

Meyer, G. P. *et al.* (2009) 'Intracoronary bone marrow cell transfer after myocardial infarction: 5-year follow-up from the randomized-controlled BOOST trial', *European Heart Journal*, 30(24), pp. 2978–2984. doi: 10.1093/eurheartj/ehp374.

Mias, C. *et al.* (2008) 'Ex Vivo Pretreatment with Melatonin Improves Survival, Proangiogenic/Mitogenic Activity, and Efficiency of Mesenchymal Stem Cells Injected into Ischemic Kidney', *Stem Cells*, 26(7), pp. 1749–1757. doi: 10.1634/stemcells.2007-1000.

Michiels, C., Toussaint, O. and Remacle, J. (1990) 'Comparative study of oxygen toxicity in human fibroblasts and endothelial cells', *J Cell Physiol*, 144(2), pp. 295–302. Available at: http://www.ncbi.nlm.nih.gov/entrez/query.fcgi?cmd=Retrieve&db=PubMed&dopt=Citation&list_uids=2380255.

Miettinen, J. A. *et al.* (2012) 'The effect of bone marrow microenvironment on the functional properties of the therapeutic bone marrow-derived cells in patients with acute myocardial infarction.', *Journal of translational medicine*, 10, p. 66. doi: 10.1186/1479-5876-10-66.

Mimeault, M., Hauke, R. and Batra, S. K. (2007) 'Stem cells: a revolution in therapeutics-recent advances in stem cell biology and their therapeutic applications in regenerative medicine and cancer therapies', *Clin Pharmacol Ther*, 82(3), pp. 252–264. doi: 10.1038/sj.clpt.6100301.

Mindaye, S. T. *et al.* (2013) 'Global proteomic signature of undifferentiated human bone marrow stromal cells: Evidence for donor-to-donor proteome heterogeneity', *Stem Cell Research*, 11(2), pp. 793–805. doi: 10.1016/j.scr.2013.05.006.

Miyahara, Y. *et al.* (2006) 'Monolayered mesenchymal stem cells repair scarred myocardium after myocardial infarction', *Nature Medicine*, 12(4), pp. 459–465. doi: 10.1038/nm1391.

Mizuno, K. *et al.* (1993) 'Hepatocyte growth factor stimulates growth of hematopoietic progenitor cells', *Biochem Biophys Res Commun*, 194(1), pp. 178–186. Available at: http://www.ncbi.nlm.nih.gov/entrez/query.fcgi?cmd=Retrieve&db=PubMed&dopt=Citation&list_uids=8392836.

Mogensen, T. H. *et al.* (2008) 'Mechanisms of dexamethasone-mediated inhibition of toll-like receptor signaling induced by Neisseria meningitidis and Streptococcus pneumoniae', *Infection and Immunity*, 76(1), pp. 189–197. doi: 10.1128/IAI.00856-07.

Mohyeddin-Bonab, M. *et al.* (2007) 'Autologous In Vitro expanded mesenchymal stem cell therapy for human old myocardial infarction', *Archives of Iranian Medicine*, 10(4), pp. 467–473. doi: 009 [pii]\r07104/AIM.009.

Momen-Heravi, F. *et al.* (2015) 'Exosomes derived from alcohol-treated hepatocytes horizontally transfer liver specific miRNA-122 and sensitize monocytes to LPS', *Scientific Reports*, 5. doi: 10.1038/srep09991.

Monguió-Tortajada, M., Lauzurica, R. and Borràs, F. E. (2014) 'Tolerance in organ transplantation: From conventional immunosuppression to extracellular vesicles', *Frontiers in Immunology*, 5(AUG). doi: 10.3389/fimmu.2014.00416.

Monsel, A. *et al.* (2015) 'Therapeutic Effects of Human Mesenchymal Stem Cell–derived Microvesicles in Severe Pneumonia in Mice', *American Journal of Respiratory and Critical Care Medicine*, 192(3), pp. 324–336. doi: 10.1164/rccm.201410-1765OC.

Moore, S. A. *et al.* (1992) 'Expression and regulation of human alveolar macrophage-derived interleukin-1 receptor antagonist.', *American journal of respiratory cell and molecular biology*, 6(6), pp. 569–575. doi: 10.1165/ajrcmb/6.6.569.

Moran, J. H. and Schnellmann, R. G. (1996) 'A rapid beta-NADH-linked fluorescence assay for lactate dehydrogenase in cellular death.', *Journal of Pharmacological and Toxicological Methods*, 36(1), pp. 41–4. Available at: http://www.ncbi.nlm.nih.gov/pubmed/8872918.

Moreira, J. B. N. *et al.* (2015) 'A small molecule activator of AKT does not reduce ischemic injury of the rat heart.', *Journal of translational medicine*, 13, p. 76. doi: 10.1186/s12967-015-0444-x.

Morrison, T. J. *et al.* (2017) 'Mesenchymal stromal cells modulate macrophages in clinically relevant lung injury models by extracellular vesicle mitochondrial transfer', *American Journal of Respiratory and Critical Care Medicine*, 196(10), pp. 1275–1286. doi: 10.1164/rccm.201701-0170OC.

Morse, M. A. *et al.* (2005) 'A phase I study of dexosome immunotherapy in patients with advanced non-small cell lung cancer', *Journal of Translational Medicine*, 3. doi: 10.1186/1479-5876-3-9.

Mulcahy, L. A., Pink, R. C. and Carter, D. R. F. (2014) 'Routes and mechanisms of extracellular vesicle uptake', *Journal of Extracellular Vesicles*. doi: 10.3402/jev.v3.24641.

Muralidharan-Chari, V. *et al.* (2009) 'ARF6-Regulated Shedding of Tumor Cell-Derived Plasma Membrane Microvesicles', *Current Biology*, 19(22), pp. 1875–1885. doi: 10.1016/j.cub.2009.09.059.

Murphy, K. C. *et al.* (2017) 'Multifactorial Experimental Design to Optimize the Anti-Inflammatory and Proangiogenic Potential of Mesenchymal Stem Cell Spheroids', *Stem Cells*. doi: 10.1002/stem.2606.

Musah, S. *et al.* (2017) 'Mature induced-pluripotent-stem-cell-derived human podocytes reconstitute kidney glomerular-capillary-wall function on a chip', *Nature Biomedical Engineering*, 1(5). doi: 10.1038/s41551-017-0069.

Nagaya, N. *et al.* (2004) 'Intravenous administration of mesenchymal stem cells improves cardiac function in rats with acute myocardial infarction through angiogenesis and myogenesis.', *American journal of physiology. Heart and circulatory physiology*, 287(6), pp. H2670-6. doi: 10.1152/ajpheart.01071.2003.

Nagaya, N. *et al.* (2005) 'Transplantation of mesenchymal stem cells improves cardiac function in a rat model of dilated cardiomyopathy', *Circulation*, 112(8), pp. 1128–1135. doi: 10.1161/CIRCULATIONAHA.104.500447.

Nahid, M. A. *et al.* (2009) 'miR-146a is critical for endotoxin-induced tolerance: Implication in innate immunity', *Journal of Biological Chemistry*, 284(50), pp. 34590–34599. doi: 10.1074/jbc.M109.056317.

Najar, M. *et al.* (2012) 'Immune-Related Antigens, Surface Molecules and Regulatory Factors in Human-Derived Mesenchymal Stromal Cells: The Expression and Impact of Inflammatory Priming', *Stem Cell Reviews and Reports*, 8(4), pp. 1188–1198. doi: 10.1007/s12015-012-9408-1.

Najimi, M. *et al.* (2007) 'Adult-derived human liver mesenchymal-like cells as a potential progenitor reservoir of hepatocytes?', *Cell Transplantation*, 16(7), pp. 717–728. doi: 10.3727/000000007783465154.

Nakajima, Y. *et al.* (1999) 'H2O2 induces apoptosis in bovine tracheal epithelial cells in vitro', *Life Sci*, 64(26), pp. 2489–2496. Available at: http://www.ncbi.nlm.nih.gov/pubmed/10403508.

Nakamura, Y. *et al.* (2015) 'Mesenchymal-stem-cell-derived exosomes accelerate skeletal muscle regeneration', *FEBS Letters*, 589(11), pp. 1257–1265. doi: 10.1016/j.febslet.2015.03.031.

Nasef, A. *et al.* (2007) 'Identification of IL-10 and TGF-β transcripts involved in the inhibition of T-lymphocyte proliferation during cell contact with human mesenchymal stem cells', *Gene Expression*, 13(4–5), pp. 217–226. doi: 10.3727/000000006780666957.

Nauta, A. J. and Fibbe, W. E. (2007) 'Immunomodulatory properties of mesenchymal stromal cells', *Blood*, pp. 3499–3506. doi: 10.1182/blood-2007-02-069716.

Nayan, M. *et al.* (2011) 'Superior Therapeutic Potential of Young Bone Marrow Mesenchymal Stem Cells by Direct Intramyocardial Delivery in Aged Recipients with Acute Myocardial Infarction: In Vitro and In Vivo Investigation', *Journal of Tissue Engineering*. doi: 10.4061/2011/741213.

Negishi, M., Sugimoto, Y. and Ichikawa, A. (1995) 'Molecular mechanisms of diverse actions of prostanoid receptors', *Biochimica et Biophysica Acta (BBA)/Lipids and Lipid Metabolism*, pp. 109–119. doi: 10.1016/0005-2760(95)00146-4.

Németh, K. *et al.* (2009) 'Bone marrow stromal cells attenuate sepsis via prostaglandin E2-dependent reprogramming of host macrophages to increase their interleukin-10 production', *Nature Medicine*, 15(1), pp. 42–49. doi: 10.1038/nm.1905.

Nguyen, T. A. *et al.* (2013) 'Microfluidic chip with integrated electrical cell-impedance sensing for monitoring single cancer cell migration in three-

dimensional matrixes', *Analytical Chemistry*, 85(22), pp. 11068–11076. doi: 10.1021/ac402761s.

Nicola, M. Di *et al.* (2002) 'Human bone marrow stromal cells suppress T-lymphocyte proliferation induced by cellular or nonspecific mitogenic stimuli', *Blood*, 99(10), pp. 3838–3843. doi: 10.1182/blood.V99.10.3838.

Nicolay, N. H. *et al.* (2016) 'Mesenchymal stem cells maintain their defining stem cell characteristics after treatment with cisplatin', *Scientific Reports*, 6. doi: 10.1038/srep20035.

Nih, L. R. *et al.* (2017) 'Engineered HA hydrogel for stem cell transplantation in the brain: Biocompatibility data using a design of experiment approach', *Data in Brief*. doi: 10.1016/j.dib.2016.11.069.

Nilsson, S. K. *et al.* (1998) 'Immunofluorescence characterization of key extracellular matrix proteins in murine bone marrow in situ', *Journal of Histochemistry and Cytochemistry*, 46(3), pp. 371–377. doi: 10.1177/002215549804600311.

Ninichuk, V. *et al.* (2006) 'Multipotent mesenchymal stem cells reduce interstitial fibrosis but do not delay progression of chronic kidney disease in collagen4A3-deficient mice', *Kidney International*, 70(1), pp. 121–129. doi: 10.1038/sj.ki.5001521.

Njock, M. S. *et al.* (2015) 'Endothelial cells suppress monocyte activation through secretion of extracellular vesicles containing antiinflammatory microRNAs', *Blood*, 125(20), pp. 3202–3212. doi: 10.1182/blood-2014-11-611046.

Noiseux, N. *et al.* (2006) 'Mesenchymal stem cells overexpressing Akt dramatically repair infarcted myocardium and improve cardiac function despite infrequent cellular fusion or differentiation', *Molecular Therapy*, 14(6), pp. 840–850. doi: 10.1016/j.ymthe.2006.05.016.

Nordin, J. Z. *et al.* (2015) 'Ultrafiltration with size-exclusion liquid chromatography for high yield isolation of extracellular vesicles preserving intact biophysical and functional properties', *Nanomedicine: Nanotechnology, Biology, and Medicine*, 11(4), pp. 879–883. doi: 10.1016/j.nano.2015.01.003.

O'Neill, A. T., Monteiro-Riviere, N. A. and Walker, G. M. (2008) 'Characterization of microfluidic human epidermal keratinocyte culture', *Cytotechnology*, 56(3), pp. 197–207. doi: 10.1007/s10616-008-9149-9.

Ohnishi, S. *et al.* (2007) 'Mesenchymal stem cells attenuate cardiac fibroblast proliferation and collagen synthesis through paracrine actions', *FEBS Letters*, 581(21), pp. 3961–3966. doi: 10.1016/j.febslet.2007.07.028.

Oikonomopoulos, A. *et al.* (2015) 'Optimization of human mesenchymal stem cell manufacturing: The effects of animal/xeno-free media', *Scientific Reports*, 5. doi: 10.1038/srep16570.

Ono, M. *et al.* (2014) 'Exosomes from bone marrow mesenchymal stem cells contain a microRNA that promotes dormancy in metastatic breast cancer cells', *Science Signaling*, 7(332). doi: 10.1126/scisignal.2005231.

Ortiz, L. A. *et al.* (2003) 'Mesenchymal stem cell engraftment in lung is enhanced in response to bleomycin exposure and ameliorates its fibrotic effects', *Proceedings of the National Academy of Sciences*, 100(14), pp. 8407–8411. doi: 10.1073/pnas.1432929100.

Ostrowski, M. *et al.* (2010) 'Rab27a and Rab27b control different steps of the exosome secretion pathway', *Nature Cell Biology*, 12(1), pp. 19–30. doi: 10.1038/ncb2000.

Ouriel, K. (2001) 'Peripheral arterial disease', *Lancet*, 358(9289), pp. 1257–1264. doi: 10.1016/S0140-6736(01)06351-6.

Oyagi, S. *et al.* (2006) 'Therapeutic effect of transplanting HGF-treated bone marrow mesenchymal cells into CCl4-injured rats', *Journal of Hepatology*, 44(4), pp. 742–748. doi: 10.1016/j.jhep.2005.10.026.

Pacini, S. and Petrini, I. (2014) 'Are MSCs angiogenic cells? New insights on human nestin-positive bone marrow-derived multipotent cells', *Frontiers in Cell and Developmental Biology*, 2. doi: 10.3389/fcell.2014.00020.

Pakravan, K. *et al.* (2017) 'MicroRNA-100 shuttled by mesenchymal stem cell-derived exosomes suppresses in vitro angiogenesis through modulating the mTOR/HIF-1α/VEGF signaling axis in breast cancer cells', *Cellular Oncology*, 40(5), pp. 457–470. doi: 10.1007/s13402-017-0335-7.

Palomo, L. *et al.* (2014) 'Considerations for applying metabolomics to the analysis of extracellular vesicles', *Frontiers in Immunology*, 5(DEC). doi: 10.3389/fimmu.2014.00651.

Panchalingam, K. M. *et al.* (2015) 'Bioprocessing strategies for the large-scale production of human mesenchymal stem cells: a review', *Stem Cell Research & Therapy*, 6(1), p. 225. doi: 10.1186/s13287-015-0228-5.

Del Papa, B. *et al.* (2013) 'Notch1 modulates mesenchymal stem cells mediated regulatory T-cell induction', *European Journal of Immunology*, 43(1), pp. 182–187. doi: 10.1002/eji.201242643.

Park, S. H. *et al.* (2012) 'Chip-Based Comparison of the Osteogenesis of Human Bone Marrow- and Adipose Tissue-Derived Mesenchymal Stem Cells under Mechanical Stimulation', *PLoS ONE*, 7(9). doi: 10.1371/journal.pone.0046689.

Pasha, Z. *et al.* (2008) 'Preconditioning enhances cell survival and differentiation of stem cells during transplantation in infarcted myocardium', *Cardiovascular Research*, 77(1), pp. 134–142. doi: 10.1093/cvr/cvm025.

Patel, D. B. *et al.* (2017) 'Impact of cell culture parameters on production and vascularization bioactivity of mesenchymal stem cell-derived extracellular vesicles', *Bioeng Transl Med*, 2(2), pp. 170–179. doi: 10.1002/btm2.10065.

Patel, S. A. *et al.* (2008) 'Immunological properties of mesenchymal stem cells and clinical implications', *Archivum Immunologiae et Therapiae Experimentalis*, pp. 1–8. doi: 10.1007/s00005-008-0001-x.

Patel, S. A. *et al.* (2010) 'Mesenchymal stem cells protect breast cancer cells through regulatory T cells: role of mesenchymal stem cell-derived TGF-beta.', *Journal of immunology (Baltimore, Md. : 1950)*, 184(10), pp. 5885–94. doi: 10.4049/jimmunol.0903143.

Patterson, K. C. and Chen, E. S. (2017) 'The pathogenesis of pulmonary sarcoidosis and implications for treatment', *Chest*. doi: 10.1016/j.chest.2017.11.030.

Peng, L. *et al.* (2008) 'Comparative Analysis of Mesenchymal Stem Cells from Bone Marrow, Cartilage, and Adipose Tissue', *Stem Cells and Development*, 17(4), pp. 761–774. doi: 10.1089/scd.2007.0217.

Phan, S. H. (2002) 'The myofibroblast in pulmonary fibrosis', in *Chest*. doi: 10.1378/chest.122.6_suppl.286S.

Phinney, D. G. *et al.* (2015) 'Mesenchymal stem cells use extracellular vesicles to outsource mitophagy and shuttle microRNAs', *Nature Communications*, 6. doi: 10.1038/ncomms9472.

Pizurki, L. *et al.* (2003) 'Angiopoietin-1 inhibits endothelial permeability, neutrophil adherence and IL-8 production', *British Journal of Pharmacology*, 139(2), pp. 329–336. doi: 10.1038/sj.bjp.0705259.

Ponte, A. L. *et al.* (2007) 'The in vitro migration capacity of human bone marrow mesenchymal stem cells: comparison of chemokine and growth factor chemotactic activities.', *Stem cells (Dayton, Ohio)*, 25(7), pp. 1737–45. doi: 10.1634/stemcells.2007-0054.

Potapova, I. A. *et al.* (2007) 'Mesenchymal Stem Cells Support Migration, Extracellular Matrix Invasion, Proliferation, and Survival of Endothelial Cells In Vitro', *Stem Cells*, 25(7), pp. 1761–1768. doi: 10.1634/stemcells.2007-0022.

Potten, C. S. and Loeffler, M. (1990) 'Stem cells: attributes, cycles, spirals, pitfalls and uncertainties. Lessons for and from the crypt', *Development*, 110(4), pp. 1001–1020. Available at: http://www.ncbi.nlm.nih.gov/pubmed/2100251.

Pountos, I. *et al.* (2007) 'Mesenchymal stem cell tissue engineering: Techniques for isolation, expansion and application', *Injury*, 38(4 SUPPL.). doi: 10.1016/S0020-1383(08)70006-8.

Price, L. C. *et al.* (2012) 'Inflammation in pulmonary arterial hypertension', *Chest*, pp. 210–221. doi: 10.1378/chest.11-0793.

Puleo, C. M. *et al.* (2009) 'Integration and application of vitrified collagen in multilayered microfluidic devices for corneal microtissue culture', *Lab on a Chip*, 9(22), p. 3221. doi: 10.1039/b908332d.

Qin, J. *et al.* (2014) 'Upregulated miR-182 increases drug resistance in cisplatin-treated HCC cell by regulating TP53INP1', *Gene*, 538(2), pp. 342–347. doi: 10.1016/j.gene.2013.12.043.

Qin, Y. *et al.* (2016) 'Bone marrow stromal/stem cell-derived extracellular vesicles regulate osteoblast activity and differentiation in vitro and promote bone regeneration in vivo', *Scientific Reports*, 6. doi: 10.1038/srep21961.

Qu, X. *et al.* (2012) 'Mesenchymal stem cells inhibit Th17 cell differentiation by IL-10 secretion', *Experimental Hematology*, 40(9), pp. 761–770. doi: 10.1016/j.exphem.2012.05.006.

Qu, Y. *et al.* (2013) 'MiR-182 and miR-203 induce mesenchymal to epithelial transition and self-sufficiency of growth signals via repressing SNAI2 in prostate cells', *International Journal of Cancer*, 133(3), pp. 544–555. doi: 10.1002/ijc.28056.

Quah, B. J. C., Warren, H. S. and Parish, C. R. (2007) 'Monitoring lymphocyte proliferation in vitro and in vivo with the intracellular fluorescent dye carboxyfluorescein diacetate succinimidyl ester', *Nature Protocols*, 2(9), pp. 2049–2056. doi: 10.1038/nprot.2007.296.

Quintanilha, L. F. *et al.* (2014) 'Canine mesenchymal stem cells show antioxidant properties against thioacetamide-induced liver injury in vitro and in vivo', *Hepatology Research*, 44(10), pp. E206–E217. doi: 10.1111/hepr.12204.

Quintás-Cardama, A. *et al.* (2010) 'Preclinical characterization of the selective JAK1/2 inhibitor INCB018424: Therapeutic implications for the treatment of myeloproliferative neoplasms', *Blood*, 115(15), pp. 3109–3117. doi: 10.1182/blood-2009-04-214957.

Radpour, R. *et al.* (2011) 'Integrated epigenetics of human breast cancer: Synoptic investigation of targeted genes, microRNAs and proteins upon demethylation treatment', *PLoS ONE*, 6(11). doi: 10.1371/journal.pone.0027355.

Raffaghello, L. *et al.* (2008) 'Human Mesenchymal Stem Cells Inhibit Neutrophil Apoptosis: A Model for Neutrophil Preservation in the Bone Marrow Niche', *Stem Cells*, 26(1), pp. 151–162. doi: 10.1634/stemcells.2007-0416.

Ramasamy, R. *et al.* (2007) 'Mesenchymal Stem Cells Inhibit Dendritic Cell Differentiation and Function by Preventing Entry Into the Cell Cycle', *Transplantation*, 83(1), pp. 71–76. doi: 10.1097/01.tp.0000244572.24780.54.

Rampersad, S. N. (2012) 'Multiple applications of alamar blue as an indicator of metabolic function and cellular health in cell viability bioassays', *Sensors (Switzerland)*, 12(9), pp. 12347–12360. doi: 10.3390/s120912347.

Ranganath, S. H. *et al.* (2012) 'Harnessing the mesenchymal stem cell secretome for the treatment of cardiovascular disease', *Cell Stem Cell*, pp. 244–258. doi: 10.1016/j.stem.2012.02.005.

Rani, S. *et al.* (2015) 'Mesenchymal Stem Cell-derived Extracellular Vesicles: Toward Cell-free Therapeutic Applications.', *Molecular therapy : the journal of the American Society of Gene Therapy*, 23(5), pp. 812–823. doi: 10.1038/mt.2015.44.

Raposo, G. (1996) 'B lymphocytes secrete antigen-presenting vesicles', *Journal of Experimental Medicine*, 183(3), pp. 1161–1172. doi: 10.1084/jem.183.3.1161.

Ratajczak, J. *et al.* (2006) 'Embryonic stem cell-derived microvesicles reprogram hematopoietic progenitors: Evidence for horizontal transfer of mRNA and protein delivery', *Leukemia*, 20(5), pp. 847–856. doi: 10.1038/sj.leu.2404132.

Ratcliffe, E. *et al.* (2013) 'Application of response surface methodology to maximize the productivity of scalable automated human embryonic stem cell manufacture', *Regenerative Medicine*. doi: 10.2217/rme.12.109.

Rau, C. S. *et al.* (2014) 'Lipopolysaccharide-induced microRNA-146a targets CARD10 and regulates angiogenesis in human umbilical vein endothelial cells', *Toxicological sciences : an official journal of the Society of Toxicology*, 140(2), pp. 315–326. doi: 10.1093/toxsci/kfu097.

Reddy, K. V. *et al.* (2004) 'Dexamethasone enhances LPS induction of tissue factor expression in human monocytic cells by increasing tissue factor mRNA stability', *J Leukoc Biol*, 76(1), pp. 145–151. doi: 10.1189/jlb.0204068.

Reers, M. *et al.* (1995) 'Mitochondrial membrane potential monitored by JC-1 dye', *Methods in Enzymology*, 260(C), pp. 406–417. doi: 10.1016/0076-6879(95)60154-6.

Rehman, J. *et al.* (2004) 'Secretion of Angiogenic and Antiapoptotic Factors by Human Adipose Stromal Cells', *Circulation*, 109(10), pp. 1292–1298. doi: 10.1161/01.CIR.0000121425.42966.F1.

Ren, G. *et al.* (2008) 'Mesenchymal Stem Cell-Mediated Immunosuppression Occurs via Concerted Action of Chemokines and Nitric Oxide', *Cell Stem Cell*, 2(2), pp. 141–150. doi: 10.1016/j.stem.2007.11.014.

Ren, G. *et al.* (2009) 'Species variation in the mechanisms of mesenchymal stem cell-mediated immunosuppression', *Stem Cells*, 27(8), pp. 1954–1962. doi: 10.1002/stem.118.

Ren, G. *et al.* (2010) 'Inflammatory cytokine-induced intercellular adhesion molecule-1 and vascular cell adhesion molecule-1 in mesenchymal stem cells are critical for immunosuppression.', *Journal of immunology (Baltimore, Md.: 1950)*, 184(5), pp. 2321–8. doi: 10.4049/jimmunol.0902023.

Ren, G. *et al.* (2012) 'CCR2-dependent recruitment of macrophages by tumor-educated mesenchymal stromal cells promotes tumor development and is mimicked by TNFα', *Cell Stem Cell*, 11(6), pp. 812–824. doi: 10.1016/j.stem.2012.08.013.

Rhodes, L. V. *et al.* (2012) 'The histone deacetylase inhibitor trichostatin A alters microRNA expression profiles in apoptosis-resistant breast cancer cells', *Oncology Reports*, 27(1), pp. 10–16. doi: 10.3892/or.2011.1488.

Richardson, J. D. *et al.* (2013) 'Optimization of the Cardiovascular Therapeutic Properties of Mesenchymal Stromal/Stem Cells-Taking the Next Step', *Stem Cell Reviews and Reports*, 9(3), pp. 281–302. doi: 10.1007/s12015-012-9366-7.

Ringdén, O. *et al.* (2006) 'Mesenchymal stem cells for treatment of therapy-resistant graft-versus-host disease', *Transplantation*, 81(10), pp. 1390–1397. doi: 10.1097/01.tp.0000214462.63943.14.

Rosa-Fernandes, L. *et al.* (2017) 'A Perspective on Extracellular Vesicles Proteomics', *Frontiers in Chemistry*, 5. doi: 10.3389/fchem.2017.00102.

Rowart, P. *et al.* (2017) 'Mesenchymal Stromal Cells Accelerate Epithelial Tight Junction Assembly via the AMP-Activated Protein Kinase Pathway, Independently of Liver Kinase B1', *Stem Cells International*, 2017. doi: 10.1155/2017/9717353.

Roy, S., Hochberg, F. H. and Jones, P. S. (2018) 'Extracellular vesicles: the growth as diagnostics and therapeutics; a survey', *Journal of Extracellular Vesicles*. Taylor & Francis, 7(1), p. 1438720. doi: 10.1080/20013078.2018.1438720.

Ryan, J. M. *et al.* (2005) 'Mesenchymal stem cells avoid allogeneic rejection', *Journal of Inflammation*. doi: 10.1186/1476-9255-2-8.

Dos Santos, F. *et al.* (2010) 'Ex vivo expansion of human mesenchymal stem cells: A more effective cell proliferation kinetics and metabolism under hypoxia', *Journal of Cellular Physiology*, 223(1), pp. 27–35. doi: 10.1002/jcp.21987.

Dos Santos, F. *et al.* (2014) 'A xenogeneic-free bioreactor system for the clinical-scale expansion of human mesenchymal stem/stromal cells', *Biotechnology and Bioengineering*, 111(6), pp. 1116–1127. doi: 10.1002/bit.25187.

Sapru, A. *et al.* (2015) 'Pathobiology of acute respiratory distress syndrome', *Pediatric Critical Care Medicine*, 16(5), pp. S6–S22. doi: 10.1097/PCC.0000000000000431.

Saraste, A. and Pulkki, K. (2000) 'Morphologic and biochemical hallmarks of apoptosis', *Cardiovascular Research*, pp. 528–537. doi: 10.1016/S0008-6363(99)00384-3.

Sarir, H. *et al.* (2008) 'Cells, mediators and Toll-like receptors in COPD', *European Journal of Pharmacology*, pp. 346–353. doi: 10.1016/j.ejphar.2008.03.009.

Savina, A. *et al.* (2005) 'Rab11 promotes docking and fusion of multivesicular bodies in a calcium-dependent manner', *Traffic*, 6(2), pp. 131–143. doi: 10.1111/j.1600-0854.2004.00257.x.

Scadding, J. G. and Hinson, K. F. W. (1967) 'Diffuse fibrosing alveolitis (diffuse interstitial fibrosis of the lungs)', *Thorax*, 22(4), p. 291. Available at: http://thorax.bmj.com/content/22/4/291.abstract.

Schellenberg, A. *et al.* (2011) 'Replicative senescence of mesenchymal stem cells causes DNA-methylation changes which correlate with repressive histone marks', *Aging*, 3(9), pp. 873–888. doi: 100391 [pii].

Schulzke, J. D. *et al.* (2009) 'Epithelial tight junctions in intestinal inflammation', *Annals of the New York Academy of Sciences*, 1165, pp. 294–300. doi: 10.1111/j.1749-6632.2009.04062.x.

Schutte, B. *et al.* (1998) 'Annexin V binding assay as a tool to measure apoptosis in differentiated neuronal cells', *Journal of Neuroscience Methods*, 86(1), pp. 63–69. doi: 10.1016/S0165-0270(98)00147-2.

Seib, F. P. *et al.* (2009) 'Matrix elasticity regulates the secretory profile of human bone marrow-derived multipotent mesenchymal stromal cells (MSCs)', *Biochemical and Biophysical Research Communications*, 389(4), pp. 663–667. doi: 10.1016/j.bbrc.2009.09.051.

Selmani, Z. *et al.* (2008) 'Human leukocyte antigen-G5 secretion by human mesenchymal stem cells is required to suppress T lymphocyte and natural killer function and to induce CD4+CD25highFOXP3+ regulatory T cells.', *Stem cells*, 26(1), pp. 212–222. doi: 10.1634/stemcells.2007-0554.

Shabbir, A. *et al.* (2015) 'Mesenchymal Stem Cell Exosomes Induce Proliferation and Migration of Normal and Chronic Wound Fibroblasts, and Enhance Angiogenesis In Vitro', *Stem Cells and Development*, 24(14), pp. 1635–1647. doi: 10.1089/scd.2014.0316.

Shao, L. *et al.* (2017) 'MiRNA-Sequence Indicates That Mesenchymal Stem Cells and Exosomes Have Similar Mechanism to Enhance Cardiac Repair', *BioMed Research International*, 2017. doi: 10.1155/2017/4150705.

Shaw, M. H. *et al.* (2008) 'NOD-like receptors (NLRs): bona fide intracellular microbial sensors', *Current Opinion in Immunology*, pp. 377–382. doi: 10.1016/j.coi.2008.06.001.

Shayan, G. *et al.* (2011) 'Murine in vitro model of the blood-brain barrier for evaluating drug transport', *European Journal of Pharmaceutical Sciences*, 42(1–2), pp. 148–155. doi: 10.1016/j.ejps.2010.11.005.

Shelke, G. V. *et al.* (2014) 'Importance of exosome depletion protocols to eliminate functional and RNA-containing extracellular vesicles from fetal bovine serum', *Journal of Extracellular Vesicles*, 3(1). doi: 10.3402/jev.v3.24783.

Shen, B. *et al.* (2016) 'CCR2 Positive Exosome Released by Mesenchymal Stem Cells Suppresses Macrophage Functions and Alleviates Ischemia/Reperfusion-Induced Renal Injury', *Stem Cells International*, 2016. doi: 10.1155/2016/1240301.

Shen, C. *et al.* (2015) 'Conditioned medium from umbilical cord mesenchymal stem cells induces migration and angiogenesis', *Molecular Medicine Reports*, 12(1), pp. 20–30. doi: 10.3892/mmr.2015.3409.

Shi, C. and Pamer, E. G. (2011) 'Monocyte recruitment during infection and inflammation', *Nature Reviews Immunology*, pp. 762–774. doi: 10.1038/nri3070.

Shi, M. *et al.* (2013) 'Glia co-culture with neurons in microfluidic platforms promotes the formation and stabilization of synaptic contacts', *Lab on a Chip*, 13(15), p. 3008. doi: 10.1039/c3lc50249j.

Shi, Y. *et al.* (2012) 'Starvation-induced activation of ATM/Chk2/p53 signaling sensitizes cancer cells to cisplatin', *BMC Cancer*, 12. doi: 10.1186/1471-2407-12-571.

Shih, D. T. *et al.* (2005) 'Isolation and Characterization of Neurogenic Mesenchymal Stem Cells in Human Scalp Tissue', *Stem Cells*, 23(7), pp. 1012–1020. doi: 10.1634/stemcells.2004-0125.

Shin, L. and Peterson, D. A. (2012) 'Impaired Therapeutic Capacity of Autologous Stem Cells in a Model of Type 2 Diabetes', *STEM CELLS Translational Medicine*, 1(2), pp. 125–135. doi: 10.5966/sctm.2012-0031.

Shin, M. *et al.* (2004) 'Endothelialized networks with a vascular geometry in microfabricated poly(dimethyl siloxane)', *Biomedical Microdevices*, 6(4), pp. 269–278. doi: 10.1023/B:BMMD.0000048559.29932.27.

Shu, J. *et al.* (2015) 'Human amnion mesenchymal cells inhibit lipopolysaccharide-induced TNF-α and IL-1β production in THP-1 cells', *Biological Research*. doi: 10.1186/s40659-015-0062-3.

Silva, G. V. *et al.* (2005) 'Mesenchymal stem cells differentiate into an endothelial phenotype, enhance vascular density, and improve heart function in a canine chronic ischemia model', *Circulation*, 111(2), pp. 150–156. doi: 10.1161/01.CIR.0000151812.86142.45.

Simonsen, J. L. *et al.* (2002) 'Telomerase expression extends the proliferative life-span and maintains the osteogenic potential of human bone marrow stromal cells', *Nature Biotechnology*, 20(6), pp. 592–596. doi: 10.1038/nbt0602-592.

Simopoulos, A. P. (2008) 'The importance of the omega-6/omega-3 fatty acid ratio in cardiovascular disease and other chronic diseases.', *Experimental biology and medicine (Maywood, N.J.)*, 233(6), pp. 674–688. doi: 10.3181/0711-MR-311.

Singh, N. P. (2000) 'A simple method for accurate estimation of apoptotic cells.', *Experimental cell research*, 256(1), pp. 328–337. doi: 10.1006/excr.2000.4810.

Skolekova, S. *et al.* (2016) 'Cisplatin-induced mesenchymal stromal cells-mediated mechanism contributing to decreased antitumor effect in breast cancer cells', *Cell Communication and Signaling*, 14(1). doi: 10.1186/s12964-016-0127-0.

Soehnlein, O. and Lindbom, L. (2010) 'Phagocyte partnership during the onset and resolution of inflammation', *Nature Reviews Immunology*, pp. 427–439. doi: 10.1038/nri2779.

Sokolova, V. *et al.* (2011) 'Characterisation of exosomes derived from human cells by nanoparticle tracking analysis and scanning electron microscopy', *Colloids and Surfaces B: Biointerfaces*, 87(1), pp. 146–150. doi: 10.1016/j.colsurfb.2011.05.013.

Song, H., Song, B.-W., *et al.* (2010) 'Modification of mesenchymal stem cells for cardiac regeneration', *Expert Opinion on Biological Therapy*, 10(3), pp. 309–319. doi: 10.1517/14712590903455997.

Song, H., Cha, M. J., *et al.* (2010) 'Reactive oxygen species inhibit adhesion of mesenchymal stem cells implanted into ischemic myocardium via interference of focal adhesion complex', *Stem Cells*, 28(3), pp. 555–563. doi: 10.1002/stem.302.

Song, Y. *et al.* (2017) 'Exosomal miR-146a Contributes to the Enhanced Therapeutic Efficacy of Interleukin-1β-Primed Mesenchymal Stem Cells Against Sepsis', *Stem Cells*, 35(5), pp. 1208–1221. doi: 10.1002/stem.2564.

Sotiropoulou, P. a, Perez, S. a, Salagianni, M., *et al.* (2006) 'Characterization of the optimal culture conditions for clinical scale production of human mesenchymal stem cells.', *Stem cells (Dayton, Ohio)*, 24(2), pp. 462–71. doi: 10.1634/stemcells.2004-0331.

Sotiropoulou, P. a, Perez, S. a, Gritzapis, A. D., *et al.* (2006) 'Interactions between human mesenchymal stem cells and natural killer cells.', *Stem cells (Dayton, Ohio)*, 24(1), pp. 74–85. doi: 10.1634/stemcells.2004-0359.

de Soure, A. M. *et al.* (2017) 'Integrated culture platform based on a human platelet lysate supplement for the isolation and scalable manufacturing of umbilical cord matrix-derived mesenchymal stem/stromal cells', *Journal of Tissue Engineering and Regenerative Medicine*, 11(5), pp. 1630–1640. doi: 10.1002/term.2200.

Soyka, M. B. *et al.* (2012) 'Defective epithelial barrier in chronic rhinosinusitis: The regulation of tight junctions by IFN-γ and IL-4', *Journal of Allergy and Clinical Immunology*, 130(5). doi: 10.1016/j.jaci.2012.05.052.

Spach, M. S. and Boineau, J. P. (1997) 'Microfibrosis produces electrical load variations due to loss of side- to-side cell connections: A major mechanism of structural heart disease arrhythmias', *PACE - Pacing and Clinical Electrophysiology*, 20(2 II), pp. 397–413. doi: 10.1111/j.1540-8159.1997.tb06199.x.

Spaggiari, G. M. *et al.* (2008) 'Mesenchymal stem cells inhibit natural killer-cell proliferation, cytotoxicity, and cytokine production: Role of indoleamine 2,3-dioxygenase and prostaglandin E2', *Blood*, 111(3), pp. 1327–1333. doi: 10.1182/blood-2007-02-074997.

Spees, J. L. *et al.* (2004) 'Internalized antigens must be removed to prepare hypoimmunogenic mesenchymal stem cells for cell and gene therapy', *Molecular Therapy*, 9(5), pp. 747–756. doi: 10.1016/j.ymthe.2004.02.012.

Squillaro, T., Peluso, G. and Galderisi, U. (2016) 'Clinical Trials With Mesenchymal Stem Cells: An Update.', *Cell transplantation*, 25(5), pp. 829–48. doi: 10.3727/096368915X689622.

Staton, C. A. *et al.* (2004) 'Current methods for assaying angiogenesis in vitro and in vivo', *International Journal of Experimental Pathology*, pp. 233–248. doi: 10.1111/j.0959-9673.2004.00396.x.

Steer, J. H. *et al.* (2000) 'Glucocorticoids suppress tumor necrosis factor-?? expression by human monocytic THP-1 cells by suppressing transactivation through adjacent NF-??b and c-Jun-activating transcription factor-2 binding sites in the promoter', *Journal of Biological Chemistry*, 275(24), pp. 18432–18440. doi: 10.1074/jbc.M906304199.

Stenderup, K. *et al.* (2003) 'Aging is associated with decreased maximal life span and accelerated senescence of bone marrow stromal cells',

Bone, 33(6), pp. 919–926. doi: 10.1016/j.bone.2003.07.005.
Stockwin, L. H. *et al.* (2000) 'Dendritic cells: immunological sentinels with a central role in health and disease.', *Immunology and cell biology*, 78(2), pp. 91–102. doi: 10.1046/j.1440-1711.2000.00888.x.
Stone, K. D., Prussin, C. and Metcalfe, D. D. (2010) 'IgE, mast cells, basophils, and eosinophils', *Journal of Allergy and Clinical Immunology*, 125(2 SUPPL. 2). doi: 10.1016/j.jaci.2009.11.017.
Subramaniam, D. *et al.* (2012) 'Curcumin induces cell death in esophageal cancer cells through modulating Notch signaling', *PLoS ONE*, 7(2). doi: 10.1371/journal.pone.0030590.
Sun, H. *et al.* (2013) 'Therapeutic potential of mesenchymal stromal cells and MSC conditioned medium in Amyotrophic Lateral Sclerosis (ALS)--in vitro evidence from primary motor neuron cultures, NSC-34 cells, astrocytes and microglia.', *PloS one*, 8(9), p. e72926. doi: 10.1371/journal.pone.0072926.
Suter, P. M. *et al.* (1992) 'High Bronchoalveolar Levels of Tumor Necrosis Factor and Its Inhibitors, Interleukin-1, Interferon, and Elastase, in Patients with Adult Respiratory Distress Syndrome after Trauma, Shock, or Sepsis', *American Review of Respiratory Disease*, 145(5), pp. 1016–1022. doi: 10.1164/ajrccm/145.5.1016.
Sutherland, E. R. and Martin, R. J. (2003) 'Airway inflammation in chronic obstructive pulmonary disease', *Journal of Allergy and Clinical Immunology*, 112(5), pp. 819–827. doi: 10.1016/S0091-6749(03)02011-6.
Suzuki, Y. *et al.* (2010) 'Diazoxide potentiates mesenchymal stem cell survival via NF- B-dependent miR-146a expression by targeting Fas', *AJP: Heart and Circulatory Physiology*, 299(4), pp. H1077–H1082. doi: 10.1152/ajpheart.00212.2010.
Szatanek, R. *et al.* (2015) 'Isolation of extracellular vesicles: Determining the correct approach (review)', *International Journal of Molecular Medicine*, pp. 11–17. doi: 10.3892/ijmm.2015.2194.
Szöke, K., BeckstrØm, K. J. and Brinchmann, J. E. (2012) 'Human adipose tissue as a source of cells with angiogenic potential', *Cell Transplantation*, 21(1), pp. 235–250. doi: 10.3727/096368911X580518.
Takahashi, S. *et al.* (2018) 'Ruxolitinib protects skin stem cells and maintains skin homeostasis in murine graft-versus-host disease', *Blood*, p. blood-2017-06-792614. doi: 10.1182/blood-2017-06-792614.
Tang, J. *et al.* (2010) 'Mesenchymal stem cells modified with stromal cell-derived factor 1 alpha improve cardiac remodeling via paracrine activation of hepatocyte growth factor in a rat model of myocardial infarction.', *Molecules and Cells*, 29(1), pp. 9–19. doi: 10.1007/s10059-010-0001-7.
Tang, N. *et al.* (2016) 'Monocyte exosomes induce adhesion molecules and cytokines via activation of NF-κB in endothelial cells', *FASEB Journal*, 30(9), pp. 3097–3106. doi: 10.1096/fj.201600368RR.
Tang, X. X. *et al.* (2010) 'Lymphocytes accelerate epithelial tight junction assembly: Role of AMP-activated protein kinase (AMPK)', *PLoS ONE*, 5(8). doi: 10.1371/journal.pone.0012343.
Tavana, H. *et al.* (2011) 'Epithelium damage and protection during reopening of occluded airways in a physiologic microfluidic pulmonary airway model', *Biomedical Microdevices*, 13(4), pp. 731–742. doi: 10.1007/s10544-011-9543-5.
Templin, C. *et al.* (2008) 'Ex vivo expanded hematopoietic progenitor cells improve cardiac function after myocardial infarction: role of beta-catenin transduction and cell dose', *J Mol Cell Cardiol*, 45(3), pp. 394–403. doi: 10.1016/j.yjmcc.2008.06.010.
Théry, C. *et al.* (2006) 'Isolation and characterization of exosomes from cell culture supernatants and biological fluids.', *Current protocols in cell biology / editorial board, Juan S. Bonifacino ... [et al.]*, Chapter 3, p. Unit 3.22. doi: 10.1002/0471143030.cb0322s30.
Thomas, H. *et al.* (2014) 'Interaction with mesenchymal stem cells provokes natural killer cells for enhanced IL-12/IL-18-induced interferon-gamma secretion', *Mediators of Inflammation*, 2014. doi: 10.1155/2014/143463.
Thomas, R. J., Hourd, P. C. and Williams, D. J. (2008) 'Application of process quality engineering techniques to improve the understanding of the in vitro processing of stem cells for therapeutic use', *Journal of Biotechnology*. doi: 10.1016/j.jbiotec.2008.06.009.
Thornberry, N. A. *et al.* (1997) 'A combinatorial approach defines specificities of members of the caspase family and granzyme B: Functional relationships established for key mediators of apoptosis', *Journal of Biological Chemistry*, 272(29), pp. 17907–17911. doi: 10.1074/jbc.272.29.17907.
Thygesen, K. *et al.* (2012) 'Third universal definition of myocardial infarction', *European Heart Journal*, 33(20), pp. 2551–2567. doi: 10.1093/eurheartj/ehs184.
Ti, D. *et al.* (2015) 'LPS-preconditioned mesenchymal stromal cells modify macrophage polarization for resolution of chronic inflammation via exosome-shuttled let-7b', *Journal of Translational Medicine*, 13(1). doi: 10.1186/s12967-015-0642-6.
Tögel, F. *et al.* (2005) 'Administered mesenchymal stem cells protect against ischemic acute renal failure through differentiation-independent mechanisms.', *American journal of physiology. Renal physiology*, 289(1), pp. F31–F42. doi: 10.1152/ajprenal.00007.2005.
Tögel, F. *et al.* (2007) 'Vasculotropic, paracrine actions of infused mesenchymal stem cells are important to the recovery from acute kidney injury.', *American journal of physiology. Renal physiology*, 292(5), pp. F1626–F1635. doi: 10.1152/ajprenal.00339.2006.
Toms, D., Deardon, R. and Ungrin, M. (2017) 'Climbing the mountain: Experimental design for the efficient optimization of stem cell bioprocessing', *Journal of Biological Engineering*. doi: 10.1186/s13036-017-0078-z.
Torella, D. *et al.* (2007) 'Growth-factor-mediated cardiac stem cell activation in myocardial regeneration', *Nature Clinical Practice Cardiovascular Medicine*, 4(SUPPL. 1). doi: 10.1038/ncpcardio0772.
Torisawa, Y. S. *et al.* (2014) 'Bone marrow-on-a-chip replicates hematopoietic niche physiology in vitro', *Nature Methods*, 11(6), pp. 663–669. doi: 10.1038/nmeth.2938.
Di Trapani, M. *et al.* (2016) 'Differential and transferable modulatory effects of mesenchymal stromal cell-derived extracellular vesicles on T, B and

NK cell functions', *Scientific Reports*, 6. doi: 10.1038/srep24120.

Tripathi, P. and Aggarwal, A. (2006) 'NF-kB transcription factor: A key player in the generation of immune response', *Current Science*, pp. 519–531.

Tsai, P.-C. *et al.* (2009) 'The therapeutic potential of human umbilical mesenchymal stem cells from Wharton's jelly in the treatment of rat liver fibrosis', *Liver Transplantation*, 15(5), pp. 484–495. doi: 10.1002/lt.21715.

Tsantoulas, C. *et al.* (2013) 'Probing functional properties of nociceptive axons using a microfluidic culture system', *PLoS ONE*, 8(11). doi: 10.1371/journal.pone.0080722.

Tsubokawa, T. *et al.* (2010) 'Impact of anti-apoptotic and anti-oxidative effects of bone marrow mesenchymal stem cells with transient overexpression of heme oxygenase-1 on myocardial ischemia.', *American journal of physiology. Heart and circulatory physiology*, 298(5), pp. H1320–H1329. doi: 10.1152/ajpheart.01330.2008.

Tsuji, K. *et al.* (2017) 'Effects of Different Cell-Detaching Methods on the Viability and Cell Surface Antigen Expression of Synovial Mesenchymal Stem Cells', *Cell Transplantation*, 26(6), pp. 1089–1102. doi: 10.3727/096368917X694831.

Tzouvelekis, A. *et al.* (2011) 'Stem cell therapy for idiopathic pulmonary fibrosis: A protocol proposal', *Journal of Translational Medicine*, 9(1). doi: 10.1186/1479-5876-9-182.

Uccelli, A., Moretta, L. and Pistoia, V. (2008) 'Mesenchymal stem cells in health and disease', *Nature Reviews Immunology*, pp. 726–736. doi: 10.1038/nri2395.

Unanue, E. R. (1984) 'Antigen-Presenting Function of the Macrophage', *Annual Review of Immunology*, 2(1), pp. 395–428. doi: 10.1146/annurev.iy.02.040184.002143.

Valadi, H. *et al.* (2007) 'Exosome-mediated transfer of mRNAs and microRNAs is a novel mechanism of genetic exchange between cells', *Nature Cell Biology*, 9(6), pp. 654–659. doi: 10.1038/ncb1596.

Vallabhaneni, K. C. *et al.* (2015) 'Extracellular vesicles from bone marrow mesenchymal stem/stromal cells transport tumor regulatory microRNA, proteins, and metabolites', *Oncotarget*, 6(7), pp. 4953–4967. doi: 10.18632/oncotarget.3211.

Vannucchi, A. M. *et al.* (2015) 'Ruxolitinib versus Standard Therapy for the Treatment of Polycythemia Vera', *New England Journal of Medicine*, 372(5), pp. 426–435. doi: 10.1056/NEJMoa1409002.

Vasandan, A. B. *et al.* (2016) 'Human Mesenchymal stem cells program macrophage plasticity by altering their metabolic status via a PGE2-dependent mechanism', *Scientific Reports*, 6(1), p. 38308. doi: 10.1038/srep38308.

Vasilevko, V. *et al.* (2002) 'CD80 (B7-1) and CD86 (B7-2) are Functionally Equivalent in the Initiation and Maintenance of CD4 $^{+}$ T-Cell Proliferation after Activation with Suboptimal Doses of PHA', *DNA and Cell Biology*, 21(3), pp. 137–149. doi: 10.1089/10445490252925404.

Viravaidya, K. and Shuler, M. L. (2004) 'Incorporation of 3T3-L1 cells to mimic bioaccumulation in a microscale cell culture analog device for toxicity studies', *Biotechnology Progress*, 20(2), pp. 590–597. doi: 10.1021/bp034238d.

Vivier, E. *et al.* (2008) 'Functions of natural killer cells', *Nature Immunology*, pp. 503–510. doi: 10.1038/ni1582.

Voyta, J. C. *et al.* (1984) 'Identification and isolation of endothelial cells based on their increased uptake of acetylated-low density lipoprotein', *Journal of Cell Biology*, 99(6), pp. 2034–2040. doi: 10.1083/jcb.99.6.2034.

Wagers, A. J. and Weissman, I. L. (2004) 'Plasticity of adult stem cells', *Cell*, pp. 639–648. doi: 10.1016/S0092-8674(04)00208-9.

Wagner, W., Saffrich, R. and Ho, A. D. (2008) 'The stromal activity of mesenchymal stromal cells', *Transfusion Medicine and Hemotherapy*, pp. 185–193. doi: 10.1159/000128956.

Wakabayashi, K. *et al.* (2010) 'Transplantation of human mesenchymal stem cells promotes functional improvement and increased expression of neurotrophic factors in a rat focal cerebral ischemia model', *Journal of Neuroscience Research*, 88(5), pp. 1017–1025. Available at: http://ovidsp.ovid.com/ovidweb.cgi?T=JS&CSC=Y&NEWS=N&PAGE=fulltext&D=med6&AN=19885863%0Ahttp://oxfordsfx.hosted.exlibrisgroup.com/oxford?sid=OVID:medline&id=pmid:19885863&id=doi:10.1002%2Fjnr.22279&issn=0360-4012&isbn=&volume=88&issue=5&spage=1017&pages=1.

Wakitani, S., Saito, T. and Caplan, A. I. (1995) 'Myogenic cells derived from rat bone marrow mesenchymal stem cells exposed to 5-azacytidine.', *Muscle & nerve*, 18(12), pp. 1417–26. doi: 10.1002/mus.880181212.

Walter, M. N. M. *et al.* (2010) 'Mesenchymal stem cell-conditioned medium accelerates skin wound healing: An in vitro study of fibroblast and keratinocyte scratch assays', *Experimental Cell Research*, 316(7), pp. 1271–1281. doi: 10.1016/j.yexcr.2010.02.026.

Wang, H.-S. *et al.* (2004) 'Mesenchymal Stem Cells in the Wharton's Jelly of the Human Umbilical Cord', *Stem Cells*, 22(7), pp. 1330–1337. doi: 10.1634/stemcells.2004-0013.

Wang, J. X. *et al.* (2015) 'MicroRNA-103/107 regulate programmed necrosis and myocardial ischemia/reperfusion injury through targeting FADD', *Circulation Research*, 117(4), pp. 352–363. doi: 10.1161/CIRCRESAHA.117.305781.

Wang, K. *et al.* (2017) 'Enhanced Cardioprotection by Human Endometrium Mesenchymal Stem Cells Driven by Exosomal MicroRNA-21', *STEM CELLS Translational Medicine*, 6(1), pp. 209–222. doi: 10.5966/sctm.2015-0386.

Wang, M. *et al.* (2007) 'STAT3 mediates bone marrow mesenchymal stem cell VEGF production', *Journal of Molecular and Cellular Cardiology*, 42(6), pp. 1009–1015. doi: 10.1016/j.yjmcc.2007.04.010.

Wang, N. *et al.* (2016) 'Curcumin protects human adipose-derived mesenchymal stem cells against oxidative stress-induced inhibition of osteogenesis', *Journal of Pharmacological Sciences*, 132(3), pp. 192–200. doi: 10.1016/j.jphs.2016.10.005.

Wang, N. *et al.* (2017) 'Mesenchymal stem cells-derived extracellular vesicles, via miR-210, improve infarcted cardiac function by promotion of angiogenesis', *Biochimica et Biophysica Acta - Molecular Basis of Disease*, 1863(8), pp. 2085–2092. doi: 10.1016/j.bbadis.2017.02.023.

Wang, Q. *et al.* (2016) 'Comparative analysis of human mesenchymal stem cells from fetal-bone marrow, adipose tissue, and Warton's jelly as

sources of cell immunomodulatory therapy', *Human Vaccines and Immunotherapeutics*, 12(1), pp. 85–96. doi: 10.1080/21645515.2015.1030549.
Wang, S. *et al.* (2017) 'Growth differentiation factor 15 promotes blood vessel growth by stimulating cell cycle progression in repair of critical-sized calvarial defect', *Scientific Reports*, 7(1). doi: 10.1038/s41598-017-09210-4.
Wang, X. *et al.* (2015) 'Exosomal MIR-223 Contributes to Mesenchymal Stem Cell-Elicited Cardioprotection in Polymicrobial Sepsis', *Scientific Reports*, 5. doi: 10.1038/srep13721.
Watanabe, S. *et al.* (2014) 'Conditioned mesenchymal stem cells produce pleiotropic gut trophic factors', *Journal of Gastroenterology*, 49(2), pp. 270–282. doi: 10.1007/s00535-013-0901-3.
Watson, C. J. *et al.* (2005) 'Interferon-gamma selectively increases epithelial permeability to large molecules by activating different populations of paracellular pores.', *Journal of cell science*, 118(Pt 22), pp. 5221–5230. doi: 10.1242/jcs.02630.
Watson, R. L. *et al.* (2015) 'Endothelial CD99 signals through soluble adenylyl cyclase and PKA to regulate leukocyte transendothelial migration', *The Journal of Experimental Medicine*, 212(7), pp. 1021–1041. doi: 10.1084/jem.20150354.
Webber, J. and Clayton, A. (2013) 'How pure are your vesicles?', *Journal of Extracellular Vesicles*, 2(1). doi: 10.3402/jev.v2i0.19861.
West, J. B. (2012) *Respiratory Physiology-The Essentials*, *Lippincott, Williams & Wilkins*. doi: 10.1159/000087456.
White, H. D. and Chew, D. P. (2008) 'Acute myocardial infarction.', *Lancet*, 372(9638), pp. 570–84. doi: 10.1016/S0140-6736(08)61237-4.
WHO (2007) 'World Health Organization. Global surveillance, prevention and control of chronic respiratory diseases: a comprehensive approach. Geneva, Switzerland', *Chronic respiratory disease*, pp. 1–146. doi: 10.1177/1479972306070070.
Widowati, W. *et al.* (2014) 'Effect of oxygen tension on proliferation and characteristics of Wharton's jelly-derived mesenchymal stem cells', *Biomarkers and Genomic Medicine*, 6(1), pp. 43–48. doi: 10.1016/j.bgm.2014.02.001.
Willerson, J. T. and Ridker, P. M. (2004) 'Inflammation as a Cardiovascular Risk Factor', *Circulation*, 109(21 suppl 1), pp. 1360–1369. doi: 10.1161/01.cir.0000129535.04194.38.
Williams, A. R. *et al.* (2011) 'Intramyocardial stem cell injection in patients with ischemic cardiomyopathy: Functional recovery and reverse remodeling', *Circulation Research*, 108(7), pp. 792–796. doi: 10.1161/CIRCRESAHA.111.242610.
Wilson, J. G. *et al.* (2015) 'Mesenchymal stem (stromal) cells for treatment of ARDS: A phase 1 clinical trial', *The Lancet Respiratory Medicine*, 3(1), p. 24. doi: 10.1016/S2213-2600(14)70291-7.
Wisel, S. *et al.* (2009) 'Pharmacological preconditioning of mesenchymal stem cells with trimetazidine (1-[2,3,4-trimethoxybenzyl]piperazine) protects hypoxic cells against oxidative stress and enhances recovery of myocardial function in infarcted heart through Bcl-2 expression.', *The Journal of pharmacology and experimental therapeutics*, 329(2), pp. 543–50. doi: 10.1124/jpet.109.150839.
Wollert, K. C. *et al.* (2004) 'Intracoronary autologous bone-marrow cell transfer after myocardial infarction: The BOOST randomised controlled clinical trial', *Lancet*, 364(9429), pp. 141–148. doi: 10.1016/S0140-6736(04)16626-9.
Wu, S. *et al.* (2013) 'Microvesicles Derived from Human Umbilical Cord Wharton's Jelly Mesenchymal Stem Cells Attenuate Bladder Tumor Cell Growth In Vitro and In Vivo', *PLoS ONE*, 8(4). doi: 10.1371/journal.pone.0061366.
Wu, Y. *et al.* (2005) 'Versican protects cells from oxidative stress-induced apoptosis', *Matrix Biol*, 24(1), pp. 3–13. doi: S0945-053X(04)00158-1 [pii]\r10.1016/j.matbio.2004.11.007.
Wu, Y. *et al.* (2007) 'Mesenchymal stem cells enhance wound healing through differentiation and angiogenesis', *Stem Cells*, 25(10), pp. 2648–2659. doi: 10.1634/stemcells.2007-0226.
Wynn, T. A., Chawla, A. and Pollard, J. W. (2013) 'Macrophage biology in development, homeostasis and disease', *Nature*, pp. 445–455. doi: 10.1038/nature12034.
Xiao, C. *et al.* (2011) 'Defective epithelial barrier function in asthma', *Journal of Allergy and Clinical Immunology*, 128(3). doi: 10.1016/j.jaci.2011.05.038.
Xie, H. *et al.* (2017) 'Extracellular Vesicle-functionalized Decalcified Bone Matrix Scaffolds with Enhanced Pro-angiogenic and Pro-bone Regeneration Activities', *Scientific Reports*, 7. doi: 10.1038/srep45622.
Xin, H. *et al.* (2013) 'MiR-133b promotes neural plasticity and functional recovery after treatment of stroke with multipotent mesenchymal stromal cells in rats via transfer of exosome-enriched extracellular particles', *Stem Cells*, 31(12), pp. 2737–2746. doi: 10.1002/stem.1409.
Xing, L. *et al.* (2014) 'Mesenchymal stem cells, not conditioned medium, contribute to kidney repair after ischemia-reperfusion injury', *Stem Cell Research and Therapy*, 5(4). doi: 10.1186/scrt489.
Xu, J.-F. *et al.* (2014) 'Altered MicroRNA Expression Profile in Exosomes during Osteogenic Differentiation of Human Bone Marrow-Derived Mesenchymal Stem Cells', *PLoS ONE*, 9(12), p. e114627. doi: 10.1371/journal.pone.0114627.
Xu, X. *et al.* (2005) 'Effects of mesenchymal stem cell transplantation on extracellular matrix after myocardial infarction in rats', *Coronary Artery Disease*, 16(4), pp. 245–255. doi: 10.1097/00019501-200506000-00006.
Yagi, H. *et al.* (2010) 'Reactive bone marrow stromal cells attenuate systemic inflammation via sTNFR1', *Molecular Therapy*, 18(10), pp. 1857–1864. doi: 10.1038/mt.2010.155.
Yang, F. *et al.* (2010) 'Genetic engineering of human stem cells for enhanced angiogenesis using biodegradable polymeric nanoparticles.', *Proceedings of the National Academy of Sciences of the United States of America*, 107(8), pp. 3317–22. doi: 10.1073/pnas.0905432106.
Yang, J. *et al.* (2010) 'Curcumin reduces the expression of Bcl-2 by upregulating miR-15a and miR-16 in MCF-7 cells', *Medical Oncology*, 27(4), pp. 1114–1118. doi: 10.1007/s12032-009-9344-3.
Yang, Z. *et al.* (2010) 'A novel approach to transplanting bone marrow stem cells to repair human myocardial infarction: Delivery via a noninfarct-relative artery', *Cardiovascular Therapeutics*, 28(6), pp. 380–385. doi: 10.1111/j.1755-5922.2009.00116.x.
Yao, Y. *et al.* (2009) 'Lipopolysaccharide preconditioning enhances the efficacy of mesenchymal stem cells transplantation in a rat model of acute

myocardial infarction', *Journal of Biomedical Science*, 16(1). doi: 10.1186/1423-0127-16-74.

Yazdanbakhsh, M., Kremsner, P. G. and Van Ree, R. (2002) 'Immunology: Allergy, parasites, and the hygiene hypothesis', *Science*, pp. 490–494. doi: 10.1126/science.296.5567.490.

Yedjou, C. G. and Tchounwou, P. B. (2012) 'In vitro assessment of oxidative stress and apoptotic mechanisms of garlic extract in the treatment of acute promyelocytic leukemia.', *Journal of cancer science & therapy*, 2012(Suppl 3), p. 6. doi: 10.4172/1948-5956.S3-006.

Yen, F. L. *et al.* (2013) 'Curcumin Nanoparticles Ameliorate ICAM-1 Expression in TNF-α-Treated Lung Epithelial Cells through p47 phox and MAPKs/AP-1 Pathways', *PLoS ONE*, 8(5). doi: 10.1371/journal.pone.0063845.

Yu, B. *et al.* (2015) 'Exosomes secreted from GATA-4 overexpressing mesenchymal stem cells serve as a reservoir of anti-apoptotic microRNAs for cardioprotection', *International Journal of Cardiology*, 182(C), pp. 349–360. doi: 10.1016/j.ijcard.2014.12.043.

Yu, H. *et al.* (2017) 'Stem cell therapy for ischemic heart diseases', *British Medical Bulletin*, pp. 135–154. doi: 10.1093/bmb/ldw059.

Yu, J. (2008) 'Inflammatory mechanisms in the lung', *Journal of Inflammation Research*, p. 1. doi: 10.2147/JIR.S4385.

Yu, J. Le *et al.* (2016) 'Epac Activation Regulates Human Mesenchymal Stem Cells Migration and Adhesion', *Stem Cells*, 34(4), pp. 948–959. doi: 10.1002/stem.2264.

Yu, P. F. *et al.* (2017) 'TNFα-activated mesenchymal stromal cells promote breast cancer metastasis by recruiting CXCR2+ neutrophils', *Oncogene*, 36(4), pp. 482–490. doi: 10.1038/onc.2016.217.

Yun, D. H. *et al.* (2009) 'Thromboxane A(2) modulates migration, proliferation, and differentiation of adipose tissue-derived mesenchymal stem cells.', *Experimental & molecular medicine*, 41(1), pp. 17–24. doi: 10.3858/emm.2009.41.1.003.

Yun, S. P. *et al.* (2014) 'Galectin-1 stimulates motility of human umbilical cord blood-derived mesenchymal stem cells by downregulation of smad2/3-dependent collagen 3/5 and upregulation of NF-κB-dependent fibronectin/laminin 5 expression', *Cell Death and Disease*, 5(2). doi: 10.1038/cddis.2014.3.

Zacharek, A. *et al.* (2007) 'Angiopoietin1/Tie2 and VEGF/Flk1 induced by MSC treatment amplifies angiogenesis and vascular stabilization after stroke', *Journal of Cerebral Blood Flow and Metabolism*, 27(10), pp. 1684–1691. doi: 10.1038/sj.jcbfm.9600475.

Von Zglinicki, T. (2002) 'Oxidative stress shortens telomeres', *Trends in Biochemical Sciences*, pp. 339–344. doi: 10.1016/S0968-0004(02)02110-2.

Zhang, B. *et al.* (2014) 'Mesenchymal Stem Cells Secrete Immunologically Active Exosomes', *Stem Cells and Development*, 23(11), pp. 1233–1244. doi: 10.1089/scd.2013.0479.

Zhang, G. *et al.* (2012) 'Cisplatin treatment leads to changes in nuclear protein and microRNA expression.', *Mutation research*, 746(1), pp. 66–77. doi: 10.1016/j.mrgentox.2012.03.004.

Zhang, H.-C. *et al.* (2012) 'Microvesicles Derived from Human Umbilical Cord Mesenchymal Stem Cells Stimulated by Hypoxia Promote Angiogenesis Both In Vitro and In Vivo', *Stem Cells and Development*, 21(18), pp. 3289–3297. doi: 10.1089/scd.2012.0095.

Zhang, J. *et al.* (1999) 'Inhibition of caspases inhibits the release of apoptotic bodies: Bcl-2 inhibits the initiation of formation of apoptotic bodies in chemotherapeutic agent-induced apoptosis', *Journal of Cell Biology*, 145(1), pp. 99–108. doi: 10.1083/jcb.145.1.99.

Zhang, W. *et al.* (2004) 'Effects of Mesenchymal Stem Cells on Differentiation, Maturation, and Function of Human Monocyte-Derived Dendritic Cells', *Stem Cells and Development*, 13(3), pp. 263–271. doi: 10.1089/154732804323099190.

Zhang, W. *et al.* (2014) 'Patient-Specific 3D Microfluidic Tissue Model for Multiple Myeloma', *Tissue Engineering Part C: Methods*, 20(8), pp. 663–670. doi: 10.1089/ten.tec.2013.0490.

Zhang, X. and Li, W. (2012) '5-Fluorouracil in combination with cisplatin alters the microRNA expression profile in the CNE nasopharyngeal carcinoma cell line', *Molecular Medicine Reports*, 6(2), pp. 303–308. doi: 10.3892/mmr.2012.917.

Zhang, Y. *et al.* (2010) 'Secreted Monocytic miR-150 Enhances Targeted Endothelial Cell Migration', *Molecular Cell*, 39(1), pp. 133–144. doi: 10.1016/j.molcel.2010.06.010.

Zhang, Y. *et al.* (2011) 'Patterning osteogenesis by inducible gene expression in microfluidic culture systems', *Integr. Biol.*, 3(1), pp. 39–47. doi: 10.1039/C0IB00053A.

Zhang, Z. *et al.* (2016) 'Pretreatment of cardiac stem cells with exosomes derived from mesenchymal stem cells enhances myocardial repair', *Journal of the American Heart Association*, 5(1). doi: 10.1161/JAHA.115.002856.

Zhang, Z. G. and Chopp, M. (2009) 'Neurorestorative therapies for stroke: underlying mechanisms and translation to the clinic', *The Lancet Neurology*, pp. 491–500. doi: 10.1016/S1474-4422(09)70061-4.

Zhao, X. *et al.* (2014) 'The toll-like receptor 3 Ligand, Poly(I:C), improves immunosuppressive function and therapeutic effect of mesenchymal stem cells on sepsis via inhibiting MiR-143', *Stem Cells*, 32(2), pp. 521–533. doi: 10.1002/stem.1543.

Zhou, N. *et al.* (2016) 'Degradation prediction model and stem cell growth of gelatin-PEG composite hydrogel', *Journal of Biomedical Materials Research - Part A*. doi: 10.1002/jbm.a.35847.

Zhou, Z. *et al.* (2005) 'Protocatechuic aldehyde suppresses TNF-alpha-induced ICAM-1 and VCAM-1 expression in human umbilical vein endothelial cells', *Eur J Pharmacol*, 513(1–2), pp. 1–8. doi: S0014-2999(05)00157-3 [pii]\r10.1016/j.ejphar.2005.01.059.

Zhou, Z., Connell, M. C. and MacEwan, D. J. (2007) 'TNFR1-induced NF-κB, but not ERK, p38MAPK or JNK activation, mediates TNF-induced ICAM-1 and VCAM-1 expression on endothelial cells', *Cellular Signalling*, 19(6), pp. 1238–1248. doi: 10.1016/j.cellsig.2006.12.013.

Zhu, Y.-G. *et al.* (2013) 'Human Mesenchymal Stem Cell Microvesicles for Treatment of E.coli Endotoxin-Induced Acute Lung Injury in Mice.', *Stem cells (Dayton, Ohio)*, 51854(1), pp. 1–17. doi: 10.1002/stem.1504.

Zhu, Y.-G. *et al.* (2014) 'Human mesenchymal stem cell microvesicles for treatment of Escherichia coli endotoxin-induced acute lung injury in mice.', *Stem cells (Dayton, Ohio)*, 32(1), pp. 116–25. doi: 10.1002/stem.1504.

Zhuo, Y. *et al.* (2010) 'Aging impairs the angiogenic response to ischemic injury and the activity of implanted cells: Combined consequences for cell therapy in older recipients', *Journal of Thoracic and Cardiovascular Surgery*, 139(5). doi: 10.1016/j.jtcvs.2009.08.052.

Zimmermann, J. A. and Mcdevitt, T. C. (2014) 'Pre-conditioning mesenchymal stromal cell spheroids for immunomodulatory paracrine factor secretion', *Cytotherapy*, 16(3), pp. 331–345. doi: 10.1016/j.jcyt.2013.09.004.

Zuk, P. A. *et al.* (2002) 'Human Adipose Tissue Is a Source of Multipotent Stem Cells', *Molecular biology of the cell*, 13(December), pp. 4279–4295. doi: 10.1091/mbc.E02.

Zuk, P. a *et al.* (2001) 'Multilineage cells from human adipose tissue: implications for cell-based therapies.', *Tissue engineering*, 7(2), pp. 211–228. doi: 10.1089/107632701300062859.

de Zwaan, C., Daemen, M. J. A. P. and Hermens, W. T. (2001) 'Mechanisms of cell death in acute myocardial infarction: pathophysiological implications for treatment.', *Netherlands heart journal : monthly journal of the Netherlands Society of Cardiology and the Netherlands Heart Foundation*, 9(1), pp. 30–44. Available at: http://www.pubmedcentral.nih.gov/articlerender.fcgi?artid=2499566&tool=pmcentrez&rendertype=abstract.

10 Appendices

10.1 Appendix A – Bioengineering EVs

Materials and Methods

Bioengineering of MSC-EVs was performed by preconditioning with small molecules using MSCs from donors RB135 and RB81 at passage 4.

As similarly described in chapter 5.1.1, MSCs were seeded at about 5,000 cell/cm^2 and incubated at 37ºC and 5% CO_2, performing medium change every 2-4 days.

When cells reached about 70% confluency, supernatant was removed and small molecules in pre-warmed full StemPro medium were added at desired concentration and incubation time (detailed in Table 10.1). After incubation at 37ºC and 5% CO_2, the cells were washed twice with PBS -/-, new pre-warmed full StemPro medium was added and cells were incubated for 2-3 days at 37ºC and 5% CO_2 followed by MSC-EV isolation as described in chapter 5.1.2.

Most of the small molecules were dissolved in DMSO Hybri-Max (Sigma-Aldrich) with exception of TNF-α that was reconstituted in water and diluted in MM (as described in chapter 5.1) and cisplatin that was dissolved in DMEM:F12. Final DMSO concentration in full StemPro medium was equal or lower than 0.1% DMSO.

Table 10.1 – Small molecules used to bioengineer MSC-EVs by preconditioning at described concentration and incubation time. Solvent and supplier is also indicated.

Small molecule	Solvent	Final concentration	Incubation time	Supplier
TNF-α	MM	10 ng/ml	24 h	Peprotech
8-pCPT-2-O-Me-cAMP-AM	DMSO	1 µM	16 h	Tocris
Curcumin	DMSO	10 µM	24 h	Tocris
Diazoxide	DMSO	20 µM	3 h	Sigma-Aldrich
Cisplatin	DMEM:F12	3 µM	24 h	Sigma-Aldrich
5-Aza-CdR	DMSO	2 µM	24 h	Sigma-Aldrich
Trichostatin A (TSA)	DMSO	0.1 µM	8 h	Sigma-Aldrich
Ruxolitinib Phosphate	DMSO	0.5 µM	1 h	Santa Cruz
Calcimycin/Calcium Ionophore	DMSO	5 µM	2 h	Sigma-Aldrich
U-46619	DMSO	5 µM	8 h	Santa Cruz
SC-79	DMSO	5 µM	24 h	Santa Cruz
Wnt Agonist	DMSO	0.5 µM	10 h	Sigma-Aldrich

Results and discussion

In order to try to improve the immunomodulatory properties of MSC-EVs, a pre-conditioning strategy was used to bioengineer MSC-EVs because it is simple and fast, avoids safety concerns related to transfection and may target several genes, transcription factors and microRNAs. Several compounds were tested aiming the possible up-regulation of several microRNAs of interest and

targeting of certain signaling pathways that could potentially improve MSC immunomodulatory and regenerative properties. Based on the literature several compounds were selected: 5-Aza-CdR, Calcimycin, 8-pCPT-2-O-Me-cAMP-AM, Cisplatin, Curcumin, Diazoxide, Ruxolitinib Phosphate, SC-79, U-46619, Wnt agonist and TSA. TNF-α was used as positive control and DMSO the negative control as most of the compounds were dissolved in DMSO. For all compounds, the final DMSO concentration was equal or less than 0.1%.

TNF-α role on inflammation (Soehnlein *et al.*, 2010) as well as tissue repair and regeneration (Forbes *et al.*, 2014) has been reported. Heo and co-workers showed that AT MSCs pre-conditioned with TNF-α (10 ng/ml for 48 h) enhanced cutaneous wound healing, angiogenesis and infiltration of immune cells through paracrine action by increasing the secretion pro-inflammatory cytokines and chemokines such as IL-6 and IL-8 important in the inflammatory response by monocytes (Heo *et al.*, 2011). Other works have shown that TNF-α pre-conditioning of MSCs improved their engraftment into the infarcted myocardium (10 ng/ml TNF-α for 24 h) (Kim, 2009), increased VEGF production (50 ng/ml TNF-α for 24 h) and increased *in vitro* migration capacity in response to growth factor and chemokine (1 ng/ml TNF-α for 24 h) (Ponte *et al.*, 2007). Moreover, EVs isolated from MSCs pre-conditioned with TNF-α (1 ng/ml TNF-α for 72 h) resulted in enhanced bone repair and regeneration (Lu *et al.*, 2017). Based on the published works, 10 ng/ml TNF-α for 24 h incubation was selected.

5-Aza-CdR or 5-aza-2'-deoxycytidine is an epigenetic factor that causes DNA demethylation and can regulate gene expression. Wakitani and co-workers used 5-Aza-CdR (0.1-10 μM for 24 h) to induce MSC differentiation into myogenic and adipocyte phenotypes (Wakitani, Saito and Caplan, 1995). Joo and colleagues used 5-Aza-CdR (0.5 and 3 μM for 24 h) to induce MSC differentiation into myogenic lineage and observed increased immunomodulatory properties by inhibiting lymphocyte proliferation and increasing induction of Treg cells (Joo *et al.*, 2014). 5-Aza-CdR has also been reported to reduce tumor growth and regulate several microRNAs such as miR-16, miR-34a, miR-182, miR-191 by incubation with 1 μM 5-Aza-CdR for 4 days (Lee *et al.*, 2009) or 0.1 μM 5-Aza-CdR for 5 days (Radpour *et al.*, 2011). Lee and co-workers identified the presence of miR-16 in MSC-EVs and miR-16 was responsible for suppressing angiogenesis by targeting VEGF in breast cancer cells (J.-K. Lee *et al.*, 2013), while another study reported that miR-16 promoted myogenesis of MSCs, while inducing cell cycle arrest in G_1 phase (Liu *et al.*, 2012). It was reported that MSC-EVs also contain miR-34a which regulates cell survival and proliferation supporting breast cancer (Vallabhaneni *et al.,* 2015). miR-182 was reported to repress osteogenesis of MSCs (K. M. Kim *et al.*, 2012) and to induce mesenchymal to epithelial transition (Qu *et al.*, 2013). MSC-EVs have been reported to contain high amounts of miR-191 which is involved in cell cycle progression and proliferation (Baglio *et al.*, 2015). Based on the published works, MSC were pre-conditioned with 2 μM 5-Aza-CdR for 24 h.

Calcimycin is a calcium ionophore and an activator of NF-ĸB (Ggandison, Nolan and Pfaff, 1994; Hosokawa *et al.*, 2013). NF-ĸB is involved in the immune response and in the regulation of pro- and anti-inflammatory secreted cytokines and chemokines by MSCs (Karima *et al.*, 1999; Guha and Mackman, 2001; Tripathi and Aggarwal, 2006; Crisostomo *et al.*, 2008; Chanput *et al.*, 2010; Soehnlein and Lindbom, 2010; Yagi *et al.*, 2010). A calcimycin concentration of 10 μM for a short time incubation has been reported for MSCs (Yun *et al.*, 2014) and a concentration of 5 μM for up to 4 h

was used for endothelial cells (W. H. Fang *et al.*, 2016). Calcium ionophore was also used to increase EV secretion from human mast cell line by incubation with 1 µM calcium ionophore for 30 min (Valadi *et al.*, 2007). Based on the published works, a concentration of 5 µM calcimycin was selected for pre-conditioning of MSCs during 2 h.

8-pCPT-2-O-Me-cAMP-AM is a cAMP analog that selectively activates the Exchange protein directly activated by cAMP, shortly Epac, and does not activate other cAMP targets such as protein kinase A and ion channels (Kooistra *et al.*, 2005). MSC treatment with 100 µM 8-pCPT-2-O-Me-cAMP-AM for 30 min activated Epac resulting in increased migration and adhesion which enhanced homing and engraftment (Yu *et al.*, 2016). In HUVEC, 8-pCPT-2-O-Me-cAMP-AM activated Epac which regulated the formation of VE-cadherin cell junction resulting in junction tightening and decreased permeability, when HUVEC were incubated with 100 µM 8-pCPT-2-O-Me-cAMP-AM for 30 min (Kooistra *et al.*, 2005). While in another study HUVEC and PBMCs were treated with 3 µM 8-pCPT-2-O-Me-cAMP-AM for 10 min to evaluate its effect on Epac and protein kinase A and to study leukocyte transmigration through the endothelial cell layer (Watson *et al.*, 2015). Moreover, cAMP activation of Epac proteins was reported in several lung and neuronal disorders and are involved in the regulation of several immune cells such as monocytes, macrophages, leukocytes and lymphocytes (Grandoch, Roscioni and Schmidt, 2010). 8-pCPT-2-O-Me-cAMP-AM was also reported to suppress pancreatic cancer cell migration and invasion, when incubated at 10 µM for 15-30 min (Almahariq *et al.*, 2013) and to promote insulin secretion in rat pancreatic beta cell line INS-1, when incubated at 1-10 µM for 30 min (Chepurny *et al.*, 2009). Herein, it was selected to pre-condition MSCs with 1 µM 8-pCPT-2-O-Me-cAMP-AM for 16 h.

Cisplatin, or Cis-diamminedichloroplatinum-II, is a chemotherapeutic drug administered in several cancer types, which hinders cell division by blocking DNA replication and transcription (Bellagamba *et al.*, 2016). MSCs have been shown to be resistant to cisplatin treatment avoiding DNA damage and apoptosis while keeping cell morphology and immunophenotype, adhesion capacity and differentiation potential when incubated with cisplatin at 0.5-50 µM for 72 h (Bellagamba *et al.*, 2016) or 0.3-10 µM for 4h up to 5 days (Nicolay *et al.*, 2016). Cisplatin plasma levels of 5 µM have been detected in patients (Nicolay *et al.*, 2016). In another study, it was shown that MSCs resisted to apoptosis induced by cisplatin but might undergo senescence, furthermore, MSC secretory profile is altered with increased pro-inflammatory IL-6 and IL-8 release and changed phosphorylation profiles of several kinases, when cisplatin was incubated at about 3 µM for 48 h (Skolekova *et al.*, 2016). In HeLa cells, cisplatin treatment (5 µM for 12 and 24 h) up-regulated the levels of miR-16 and miR-21 (G. Zhang *et al.*, 2012), while in cisplatin-treated (1 µM) hepatocellular carcinoma miR-182 was up-regulated (Qin *et al.*, 2014). In another study, a combined treatment with 5-fluorouracil and cisplatin of nasopharyngeal carcinoma cell line resulted in up-regulation of miR-204 and let-7b (Zhang and Li, 2012). Up-regulation of miR-16, miR-21 and let-7b in MSC-EVs compared to fibroblast-derived EVs was reported resulting in the recovery from hypoxia-induced pulmonary hypertension by suppressing macrophage influx, secretion of pro-inflammatory trophic factors and vascular remodeling as well as by increasing miR-204 levels in the lungs (Lee *et al.*, 2012). miR-204 is reported to be downregulated in pulmonary hypertension (Lee *et al.*, 2012) but also in vascular inflammation (Lai *et al.*, 2017),

therefore, it might be involved in lung inflammation and pulmonary edema. miR-21 is also involved in cell cycle progression and proliferation (Baglio *et al.*, 2015) and immunomodulatory properties (Song *et al.*, 2017) of MSCs. Based on the literature, a concentration of 3 µM cisplatin for 24 h was chosen.

Curcumin is an anti-inflammatory and anti-oxidant drug. Curcumin (1-100 µM for up to 16 days) has been reported to protect MSCs against oxidative stress and to prevent cell death and reverse the oxidative stress-inhibition of osteogenic differentiation through Wnt pathway (N. Wang *et al.*, 2016). In cancer cells, curcumin is involved in changes in miR-16 (J. Yang *et al.*, 2010), Notch-1 specific miR-21 (Bao *et al.*, 2012; Subramaniam *et al.*, 2012), Notch-1 specific miR-34a (Subramaniam *et al.*, 2012), miR-146a (Bao *et al.*, 2012) and the tumor suppressor let-7 family (Bao *et al.*, 2012; Subramaniam *et al.*, 2012), when cancer cells were challenged with 0.1-60 µM curcumin for 18-72 h (J. Yang *et al.*, 2010; Bao *et al.*, 2012; Subramaniam *et al.*, 2012). Curcumin also targets the transcription factor NF-KB (Bao *et al.*, 2012), which is involved in the immune response and in the regulation of pro- and anti-inflammatory secreted cytokines and chemokines by MSCs (Karima *et al.*, 1999; Guha and Mackman, 2001; Tripathi and Aggarwal, 2006; Crisostomo *et al.*, 2008; Chanput *et al.*, 2010; Soehnlein and Lindbom, 2010; Yagi *et al.*, 2010). Based on the published reports, MSCs were incubated with 10 µM curcumin for 24 h for pre-conditioning.

Diazoxide is a potassium channel activator. Pre-conditioning of MSCs with diazoxide suppressed apoptosis and induced cell survival through NF-KB and increased miR-146a (Suzuki *et al.*, 2010). Diazoxide pre-treatment of MSCs resulted in increased survival and recovery in an infarcted heart animal model and enhanced secretion of angiongenic, anti-apoptotic and anti-inflammatory cytokines (Afzal *et al.*, 2010; Cui *et al.*, 2010) . MSC were pre-conditioned with diazoxide at 200 µM for 0.5-3 h (Afzal *et al.*, 2010; Cui *et al.*, 2010; Suzuki *et al.*, 2010). miR-146a is involved in cell survival and immune response (Nahid *et al.*, 2009; Suzuki *et al.*, 2010), MSC immunomodulatory properties (Song *et al.*, 2017) and in angiogenesis of MSCs (Afzal *et al.*, 2010), endothelial cells (Rau *et al.*, 2014) and the heart (Ibrahim, Cheng and Marbán, 2014). miR-146a containing EVs from human cardiosphere-derived cells also suppressed apoptosis and promoted proliferation of cardiomyocytes (Ibrahim, Cheng and Marbán, 2014). Based on the published studies, a concentration of 20 µM diazoxide was used for MSC pre-conditioning for 3 h.

Ruxolitinib phosphate is a selective janus kinase (JAK) 1 and 2 inhibitor and a STAT3 activator. JAK-STAT signaling pathway plays a major role in the survival and proliferation of hematopoietic precursor cells (Vannucchi *et al.*, 2015). Ruxolitinib phosphate showed benefits for the treatment of myelofibrosis (Harrison *et al.*, 2012), myeloproliferative neoplasia (Vannucchi *et al.*, 2015) and skin GVHD accompanied by hair regeneration and wound healing (Takahashi *et al.*, 2018). Moreover, IL-6 pro-inflammatory cytokine activates JAK signaling pathways (Q. Chang *et al.*, 2013), while ruxolitinib phosphate has immunosuppressive effect by reducing TNF-α and IL-6 and consequently acting on JAK (Quintás-Cardama *et al.*, 2010). In a study of myeloproliferative neoplasia, it was reported an IC_{50} > 400 nM for healthy donors to ruxolitinib phosphate after 2.5 h treatment (Quintás-Cardama *et al.*, 2010) and on a cancer report a ruxolitinib phosphate concentration between 0.1-10 µM for 0.5 h was tested (Hornakova *et al.*, 2011). Based on the literature, a concentration of 0.5 µM ruxolitinib phosphate for 1 h was selected.

SC-79 is a selective Akt activator. Akt kinase has anti-apoptotic activity and mediates cell survival (Jo *et al.*, 2012). Pre-treatment with SC-79 (10-50 μM for 20-30 min) was reported to activate Akt in the cytosol which reduced neuronal excitotoxicity and prevented neuronal death in a ischemic stroke animal model, therefore, enhancing neuronal survival (Jo *et al.*, 2012). MSC treatment with SC-79 (10 μM for 3 h for Akt localization study and 14 days for osteogenic differentiation) was also reported to be a potential candidate for the treatment of alcohol-induced osteonecrosis of the femoral head (Chen *et al.*, 2017). SC-79 (at about 11 μM for 24 h) was also reported to act on hepatocyte proliferation and cell growth through Akt signaling, improving liver regeneration (Bei *et al.*, 2016). On the other hand, in an ischemic heart injury model in rat, Akt activation by SC-79 (0.1-0.9 μM for 30 min) did not have enough anti-apoptotic and pro-survival action on protecting from ischemic heart injury (Moreira *et al.*, 2015). Based on the literature, a concentration 5 μM SC-79 for 24 h was used for MSC pre-conditioning.

U-46619 is a p38 MAPK activator (Yun *et al.*, 2009) and a stable analog of Thromboxane A2 (Kim *et al.*, 2009). Thromboxane A2 is a prostanoid metabolite synthetized by platelets involved in pathophysiological responses including platelet aggregation, smooth muscle contraction, cell proliferation and migration (Yun *et al.*, 2009) and a mediator in atherosclerotic vascular diseases, MI, and bronchial asthma (Negishi, Sugimoto and Ichikawa, 1995). U-46619 was reported to increase AT MSC proliferation and migration (5 μM for 12 h) and smooth muscle-like cell differentiation (1 μM for 4 days) through ERK and p38 MAPK signaling cascades (Yun *et al.*, 2009). U-46619 (5 μM for up to 4 days) was also reported to induce AT MSC differentiation to contractile smooth muscle-like cells through CaM/ML CK- and RhoA-Rho kinase-dependent actin polymerization (Kim *et al.*, 2009). Based on the published studies, 5 μM U-46619 were incubated for 8 h for MSC pre-conditioning.

Wnt agonist is a cell-permeable pyrimidine which selectively activates Wnt signaling cascade. Wnt signaling pathway in MSCs has been reported to regulate cell fate and development by activating the proliferation under undifferentiated state or the differentiation towards specific lineages (J.-A. Kim *et al.*, 2015). Wnt induces β-catenin stabilization, enabling MSCs to exert supportive function on hematopoietic cells (J.-A. Kim *et al.*, 2015). In a study of Wnt signaling in high glucose-induced adipogenesis, Wnt agonist at 0.1-5 μM up to 7 days of differentiation was used (Keats *et al.*, 2014). In another study of the Wnt/β-catenin role on MSC proliferation, BIO an analog of Wnt agonists was used at 0.2-5 μM for 24 h (Hoffman and Benoit, 2015). Based on the published works, 10 h incubation with 0.5 μM Wnt agonist was used for MSC pre-conditioning.

TSA is a histone deacetylase. In MSCs, this epigenetic molecule suppresses the reduction of histone acetylation maintaining MSC's naive properties, when TSA was incubated for 3 days with 0-0.3 μM (Han *et al.*, 2013). In another study, TSA improved MSC resistance to oxidative stress at low doses (0.05-0.5 μM for 8 h) by increasing the level of anti-oxidant enzymes, while high doses (1-5 μM for 8 h) did not protect from oxidative stress (Jeong and Cho, 2015). In cancer cells, TSA at higher doses has been reported to reduce tumor growth by cell apoptosis and to change the expression of miR-16, miR-34a, miR-143, miR-182 and miR-191 (Lee *et al.*, 2009; Rhodes *et al.*, 2012). The role of the other microRNAs was previously described, except miR-143. miR-143 is involved in the

immunomodulatory function of MSCs (Zhao *et al.*, 2014; Song *et al.*, 2017). Based on the literature, a concentration 0.1 µM TSA for 8 h was selected for MSC pre-conditioning.

After selection of compounds and their concentration and incubation time, the MSCs were pre-conditioned and bioengineered MSC-EVs were isolated. When BM MSCs at passage 4 from donors RB81 and RB135 reached about 70% confluency, MSCs were incubated with compounds and then the T-flasks were washed, new medium was added and incubated for 3 days prior to EVs isolation from the CM. Bioengineered MSC-EVs were characterized and tested using the THP-1 and HUVEC potency assays.

Preliminary results of the mean size of the different bioengineered EVs isolated from BM MSC RB81 and RB135 (Table 10.2) seem to be similar between them and similar to the respective untreated MSC-EVs (Table 6.1), indicating that the treatment with the compounds is not causing the EV burst or considerable EV and protein aggregation. The average size of the bioengineering EVs isolated from MSC RB81 pre-conditioned with the different compounds was 212 $\pm$ 10 nm and the average PPR was 4 $\pm$ 1 fg protein/EV particle. The average size of the bioengineered EVs isolated from MSC RB135 pre-conditioned with the different compounds was 215 $\pm$ 6 nm and the average PPR was 4 $\pm$ 1 fg protein/EV particle. The higher PPR values of some bioengineered MSC-EVs is directly related to less removal of supernatant by aspiration upon each UC and lower volume in which EVs were resuspended after the 1st UC (for instance a full 1st UC run of 230 ml CM was pelleted and resuspended 10 ml RNase-Free PBS instead of the full 2nd UC run with 30 ml, will result in higher protein contamination and, therefore, higher PPR will be obtained). The EV concentration is also dependent on the volume of CM from which EVs were isolated and on the final volume in which EV pellets are resuspended. EV concentration of all bioengineered MSC-EVs from RB81 and RB135 are in the range of 10^{11} EV/ml, with exception of EVs from MSC RB81 pre-conditioned with SC-79 with a concentration of 8.0 x 10^{10} EV/ml which is explained by the double of the dilution done compared to other bioengineered EVs.

Table 10.2 – Pre-conditioning of MSCs with several small molecules to bioengineer MSC-EVs does not greatly change EV properties from BM MSC donors RB81 and RB135. Concentration and incubation time of the compounds used for MSC pre-conditioning are described. MSC-EVs were characterized by nanoparticle tracking analysis to determine EV concentration (in EV/ml) and mean size (in nm) and by MicroBCA to determine the PPR (in fg protein/EV particle). N = 1-4 in triplicates. Data is represented by the mean and standard error of the mean.

Pre-conditioning compound	Concentration and incubation time	EV concentration (x10^{11} EV/ml)		Mean size (nm)		PPR (fg protein/EV)	
		RB81	RB135	RB81	RB135	RB81	RB135
Control DMSO	0.1 % for 24 h	4 ± 2	6 ± 4	206 ± 9	222 ± 17	4 ± 1	6 ± 6
TNF-α	10 ng/ml for 24 h	5 ± 3	6 ± 5	202 ±15	225 ±7	3.3 ± 0.7	4 ± 2
5-Aza-CdR	2 µM for 24 h	3 ± 1	5 ± 2	205 ± 10	213 ± 17	5 ± 1	6 ± 6
Calcimycin	5 µM for 2 h	1.430 ± 0.006	2.28 ± 0.04	227 ± 4	213 ± 1	2.7	3.2
8-pCPT-2-O-Me-cAMP-AM	1 µM for 16 h	1.38 ± 0.02	1.73 ± 0.04	218 ± 3	211 ± 3	5.9	2.9
Cisplatin	3 µM for 24 h	3.04 ± 0.09	2.50 ± 0.06	199 ± 3	215 ± 2	3.1	2.6
Curcumin	10 µM for 24 h	4 ± 2	7 ± 4	201 ± 10	210 ± 13	4.4 ± 0.3	5 ± 3
Diazoxide	20 µM for 3 h	1.65 ± 0.07	2.12 ± 0.08	220 ± 1	213 ± 1	3.0	3.0
Ruxolitinib Phosphate	0.5 µM for 1 h	3.2 ± 0.6	4 ± 1	200 ± 5	222 ± 15	5 ± 1	5 ± 3
SC-79	5 µM for 24 h	0.8 ± 0.03	2.94 ± 0.08	222 ± 3	205 ± 5	3.6	4.4
U-46619	5 µM for 8 h	1.43 ± 0.04	2.76 ± 0.07	225 ± 2	202 ± 2	3.0	3.4
Wnt agonist	0.5 µM for 10 h	2 ± 1	1.00 ± 0.06	218 ± 2	218 ± 2	2.3	3.7
TSA	0.1 µM for 8 h	1.07 ± 0.07	1.3 ± 0.1	215 ± 3	221 ± 3	6.4	3.2

The immunomodulatory properties of the bioengineered EVs from MSC RB81 were assessed with the THP-1 and HUVEC potency assays. The EVs used for THP-1 and HUVEC potency assay from RB81 and RB135 were isolated from cells treated twice with compounds followed by one EV isolation 3 days after each treatment. EVs from the two isolations were pooled prior to EV characterization and evaluation of the immunomodulatory properties with the potency assays.

Preliminary results of the THP-1 potency assay (Figure 10.1) seem to indicate that the pre-conditioning with the compounds does not change the not pro-inflammatory properties of MSC-EVs from RB81, as none of the different bioengineered EVs caused by themselves an increase in TNF-α secretion when no LPS was added. It seems that there was no difference between the control without EVs and the bioengineered EVs for LPS-stimulated THP-1 cells and that only dexamethasone (1 µM) seem to be able to decrease TNF-α secretion compared to the control without EVs and all the bioengineered EVs.

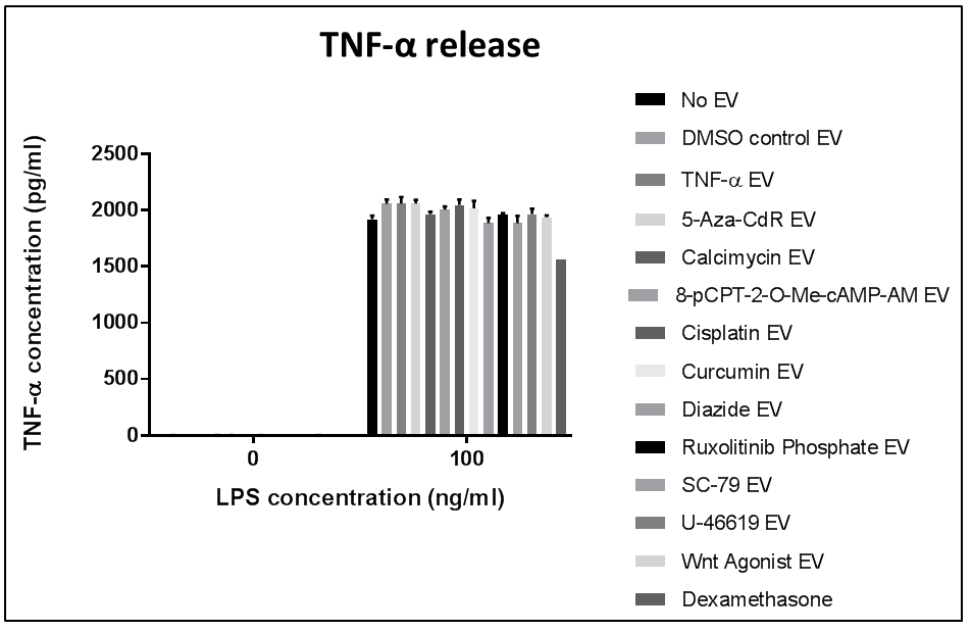

Figure 10.1 – Preliminary results of the pre-conditioning of MSC RB81 with several compounds to bioengineer MSC-EVs seem to show that bioengineered MSC-EVs do not change EV not pro-inflammatory properties when incubated with THP-1 monocytic cell line. TNF-α release (in pg/ml) by LPS-stimulated THP-1 cells when treated with MSC-EVs at 10^9 EV/ml and LPS at (0 or 100 ng/ml) for 24 h was measured by ELISA. Dexamethasone at 1 μM was used as positive control. N = 1 (in triplicates). Error bars represent the standard error of the mean.

Preliminary results of the HUVEC potency assay seem to indicate that bioengineered EVs from MSC RB81 and RB135 at 10^9 EV/ml were not pro-inflammatory for HUVEC, as IL-8 release (data not shown) and VCAM and ICAM-1 expression did not seem to increase (Figure 10.2) when EVs were added alone without TNF-α, which is in line with the THP-1 potency assay results.

It seems that none of the different bioengineered EVs from MSC donor RB81 and RB135, at 10^9 EV/ml, was able to reduce IL-8 secretion of HUVEC stimulated with 10 ng/ml TNF-α compared to the control without EV treatment and DMSO control EVs (data not shown).

Preliminary results seem to show that EVs isolated from MSC RB81 pre-conditioned with DMSO only (EV control), reduced VCAM-1 and ICAM-1 expression of TNF-α-stimulated HUVEC, in about 20 and 12% respectively, compared with the control without EV treatment (Figure 10.2 A and B). The VCAM-1 and ICAM-1 expression seem to be reduced to a higher extent when TNF-α-stimulated HUVEC were co-treated with bioengineered EVs from MSC pre-conditioned with TNF-α, 5-Aza-CdR, calcimycin, curcumin, ruxolitinib phosphate and U-46619 compared to the control without EV treatment. TNF-α, 5-Aza-CdR, calcimycin and curcumin EVs also seem to reduce to a higher extent the VCAM-1 expression of TNF-α-stimulated HUVEC when compared to DMSO EVs (Figure 10.2 A). TNF-α, calcimycin and curcumin EVs also seem to reduce to a higher extent the ICAM-1 expression of TNF-α-stimulated HUVEC when compared to DMSO EVs (Figure 10.2 B).

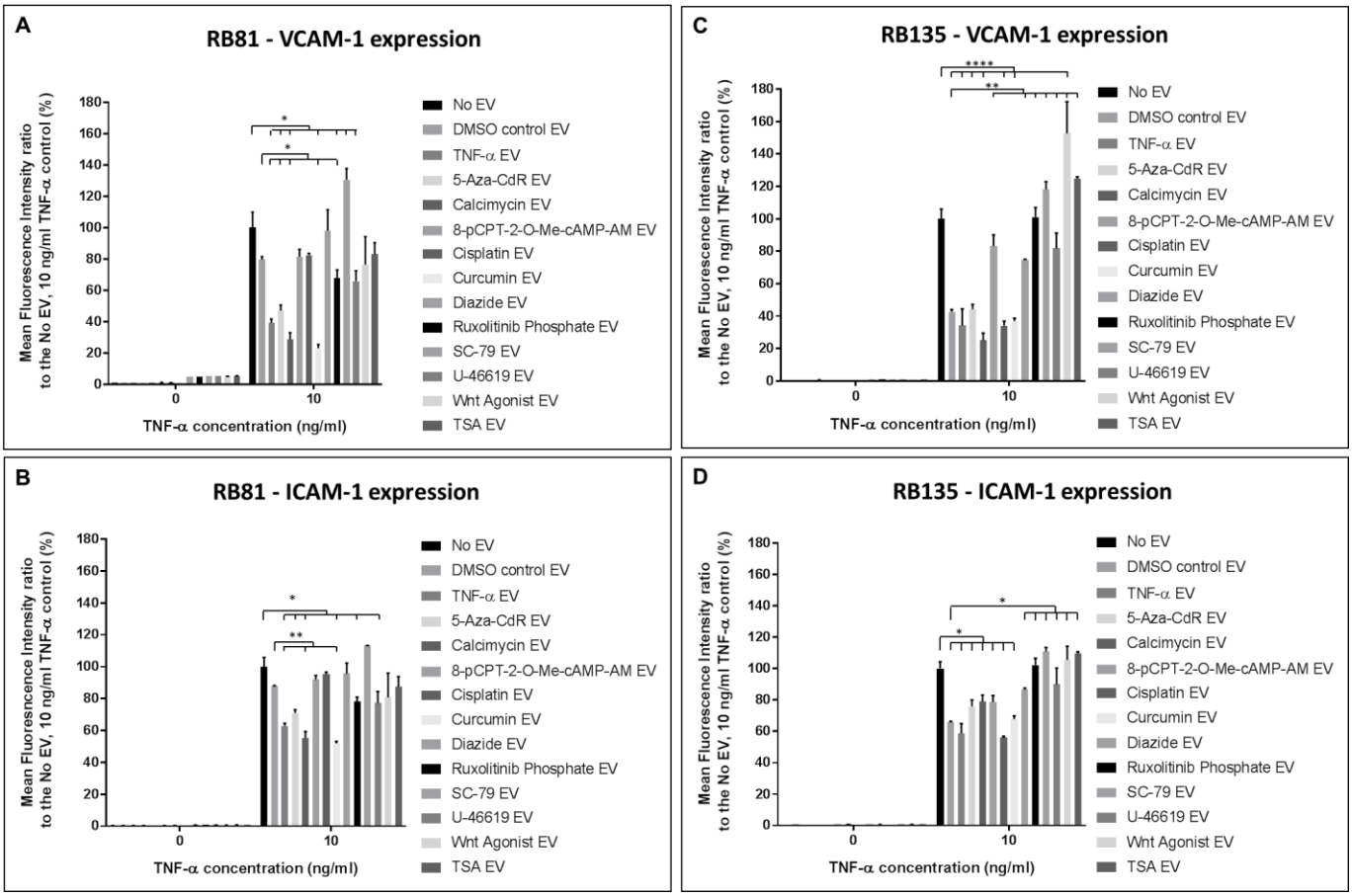

Figure 10.2 – Preliminary study of bioengineered MSC-EVs from MSC pre-conditioned with TNF-α, 5-Aza-CdR, calcimycin and curcumin seem to show their ability to reduce VCAM-1 (A – MSC RB81, C – MSC RB135) and ICAM-1 (B – MSC RB81, D – MSC RB135) expression of TNF-α-stimulated HUVEC. MSC-EVs were added at 10^9 EV/ml. No EV addition and EVs from DMSO pre-conditioning were used as controls compared to control without EV treatment. VCAM-1 and ICAM-1 expression is given by the ratio of mean fluorescence intensity (in %) of each condition to control stimulated with TNF-α and without EV treatment (which was set as 100%). N = 1 (in duplicates). Error bars represent the standard error of the mean.

Preliminary results seem to indicate that EVs isolated from MSC RB135 pre-conditioned with DMSO only (EV control) reduced VCAM-1 and ICAM-1 expression of TNF-α-stimulated HUVEC, in about 57 and 34% respectively, compared with the control without EV treatment (Figure 10.2 C and D, respectively). VCAM-1 and ICAM-1 expression seem to be also reduced when TNF-α-stimulated HUVEC were co-treated with bioengineered EVs from MSCs pre-conditioned with TNF-α, 5-Aza-CdR, calcimycin, cisplatin and curcumin, with a decrease in expression of about 56 to 75% for VCAM-1 and 21 to 44% for ICAM-1 compared to the control TNF-α without EV treatment. However, the change in VCAM-1 and ICAM-1 expression after challenge with TNF-α and EVs from MSCs pre-conditioned TNF-α, 5-Aza-CdR, calcimycin, cisplatin and curcumin does not seem to change much compared to the DMSO EV condition for MSC RB135 at 10^9 EV/ml.

Although needing further confirmation, it seems that the anti-inflammatory trend of bioengineered MSC-EVs is similar between BM MSC donors RB81 and RB135 and, overall, bioengineered EVs from MSCs pre-conditioned with TNF-α, 5-Aza-CdR, calcimycin and curcumin

seem to reduce HUVEC activation of adhesion molecules. A loss of function of the bioengineered MSC-EVs was observed when experiments were repeated indicating a loss of function with storage time as shown in Appendix B 10.2.

As previously stated: TNF-α pre-conditioning enhanced wound healing, angiogenesis and increased immunomodulatory properties by promoting infiltration of immune cells and secretion of pro-inflammatory cytokines and chemokines; 5-Aza-CdR modulated cell cycle progression and proliferation and increased MSC immunomodulatory properties; calcimycin and curcumin activated NF-ΚB which is involved in the immune response and in the regulation of MSC secretion of pro- and anti-inflammatory cytokines and chemokines. TNF-α, calcimycin and curcumin seem to have in common the activation of NF-ΚB signaling cascade. Future elucidation of the signaling cascades involved as well as analysis of the EV content, namely microRNAs, would shed a light on the mechanisms of action and possibly enabling the development of a more selective and potent small molecule that could be used to bioengineer MSC-EVs for testing in *in vitro* (2D and 3D models) and *in vivo* studies using animal models.

It is relevant to understand if the decrease in surface marker expression could be related to toxicity effect due to the presence of the compounds in the EV solution and not due to compound encapsulation, nuclei acids or other content inside the EVs. Therefore, the free compounds were tested using the HUVEC potency assay by incubating the free compounds instead of EVs. HUVEC surface marker expression and LDH release were evaluated. The concentration of the compounds used on the HUVEC potency assay was the same as the concentration used for MSC pre-conditioning (Table 10.1). The same concentration was used for an indication of toxicity as that would be the maximum concentration cells would be subjected in case they are present in the EV solution. All the compounds were incubated for 16 h as previously done, knowing that longer exposure of some compounds at the concentration used for MSC pre-conditioning could have higher toxicity in HUVEC.

Preliminary results seem to indicate that calcimycin at the concentration tested for 16 h caused cell death (observed in the microscope) and increased LDH release from HUVEC of about 1.4 and 0.7 fold increase compared to the controls without compound and without or with TNF-α stimuli, respectively (Figure 10.3 A). Due to cell detachment and death, VCAM-1 and ICAM-1 expression in the cellular debris was minimal (Figure 10.3 B and C). Future elucidation is needed on of effect calcimycin treatment in MSC and HUVEC, namely 1) a dose response on HUVEC should be performed to understand if toxicity is related to high dose and long incubation time and if lower concentration of the free compound would reduce VCAM-1 and ICAM-1 expression as calcimycin MSC-EVs, 2) MSC-EV content should be analyzed by mass spectrometry and sequencing and it should be determined if the decrease in VCAM-1 and ICAM-1 in HUVEC upon MSC-EV treatment is due to cell death by the calcimycin encapsulated inside the EVs and if it is because of protein and nuclei acid EV content.

As seem before, TNF-α treatment increased VCAM-1 and ICAM-1 expression and moderately increased LDH release from HUVEC in about 0.3 fold increase compared to untreated HUVEC.

Similar to TNF-α treatment, treatment with curcumin without or with TNF-α seems to increase LDH release compared to DMSO control without TNF-α stimuli and to TNF-α treated HUVEC,

respectively (Figure 10.3 A). VCAM-1 and ICAM-1 expression also seem to be greatly reduced on TNF-α–stimulated HUVEC (Figure 10.3 B and C) possibly indicating that curcumin at the 10 μM is causing toxicity, although to a lower extent than calcimycin. This toxicity effect seem to be related to the curcumin dose as curcumin at the 5 μM did not increase LDH and reduced VCAM-1 and ICAM-1 expression (data not shown with 2D potency assays, Figure 6.10 for 3D models).

The compounds 5-Aza-CdR, ruxolitinib phosphate and Wnt agonist seem to reduce VCAM-1 and ICAM-1 expression compared to HUVEC TNF-α–stimulated without compound and DMSO controls (Figure 10.3 B and C), and did not seem to increase LDH secretion from HUVEC indicating that these compounds are not causing toxicity and cell death.

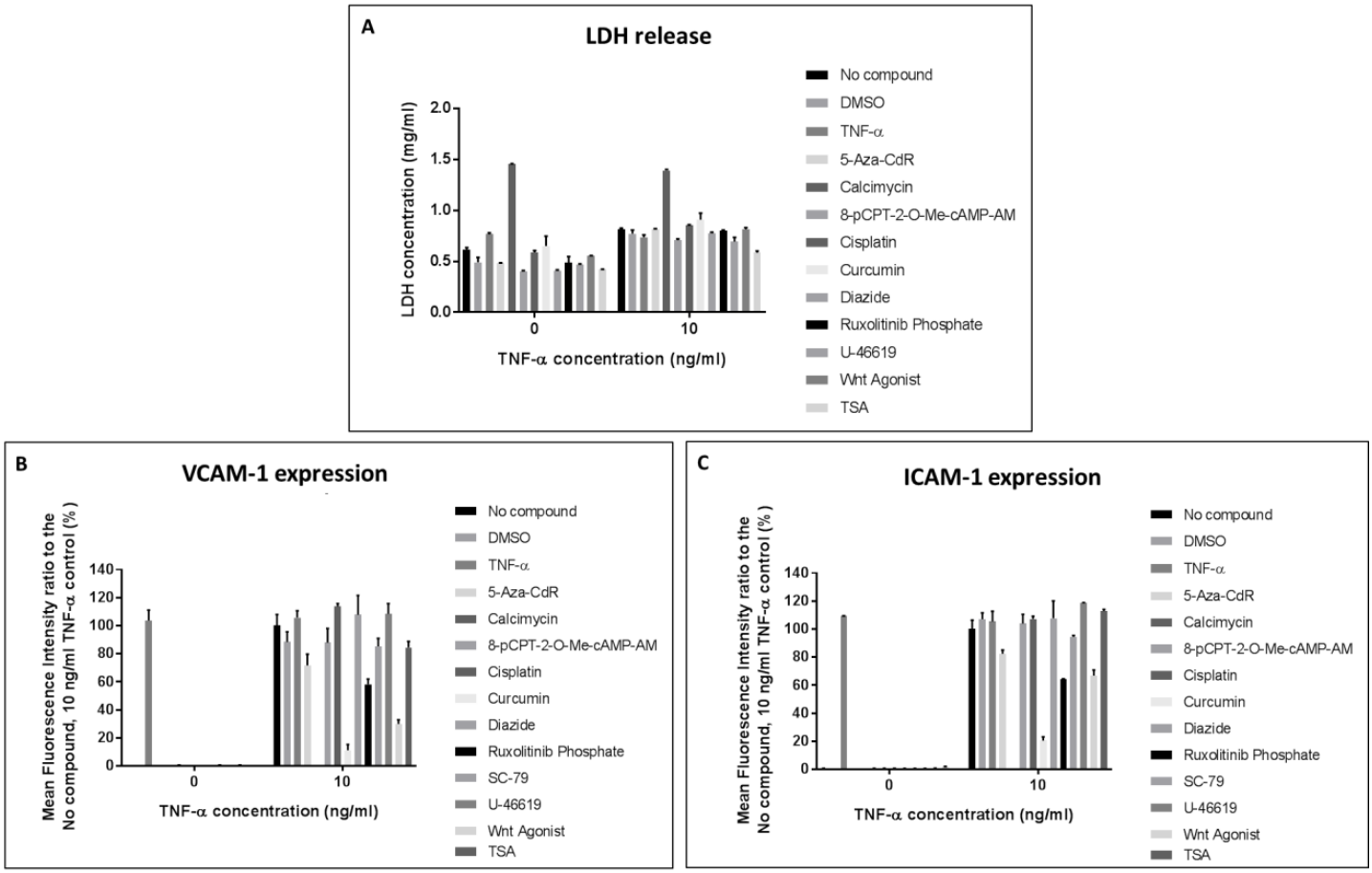

Figure 10.3 – Preliminary study of the effect of direct incubation of bioengineering compounds on HUVEC after 16 h treatment and TNF-α (in ng/ml) stimuli. The concentration of each compound is described in Table 10.1. No compound addition and DMSO were used as controls. A – LDH (in mg/ml) secretion from HUVEC after incubation with compounds showed increased release for TNF-α, calcimycin and curcumin. B and C – Compounds such as 5-Aza-CdR, Ruxolitinib phosphate and Wnt agonist were able to reduce VCAM-1 (B) and ICAM-1 (C) expression. VCAM-1 and ICAM-1 expression is given by ratio of mean fluorescence intensity (in %) of each condition to control stimulated with TNF-α and without compound treatment (which was set as 100%). N = 1 (in duplicates). Error bars represent the standard error of the mean.

In summary, preliminary results with THP-1 potency assay seem to indicate that bioengineered EVs from MSC donor RB81 were not pro-inflammatory. Preliminary results with the HUVEC potency assay with bioengineered EVs from MSC donor RB81 and RB135 seem to indicate that MSC pre-conditioning with TNF-α, 5-Aza-CdR, calcimycin and curcumin decreased VCAM-1 and ICAM-1 expression possibly through the increase of MSC immunomodulatory properties and through the NF-ΚB pathway. It remains to be elucidated if calcimycin toxic effect is also dose dependent as for curcumin, while 5-Aza-CdR did not induce LDH release. Further confirmation of the anti-inflammatory effect of bioengineered EVs needs to be performed as well as elucidation of EV content, signaling pathways targeted and mechanisms of action in future work. Moreover, the potential bioengineered MSC-EVs could be further tested using the 3D models developed to select the best bioengineered MSC-EVs that could then be evaluate using *in vivo* animal models. Moreover, it would be important to evaluate if the effect observed is due to small molecule encapsulation or to changes in the gene expression that lead to differences in content (for instance DNA, mRNA and microRNA EV content using sequencing techniques) to elucidate the mechanisms of action.

Other compounds such as IL-1β (Song *et al.*, 2017), TNF-α in combination with IFN-γ (Di Trapani *et al.*, 2016; Harting *et al.*, 2018), LPS (Ti *et al.*, 2015) and omega-3 (Simopoulos, 2008) could also be tested for MSC pre-conditioning to potentially boost immunomodulatory and regenerative properties of bioengineered MSC-EVs.

10.2 Appendix B – EV potency upon storage

An important factor to take into account when developing stem cell-based therapies as off-the-shelf products is the ability to store the product without degradation of its properties. In the case of EV products it is important to preserve not only the vesicle integrity but also its function and potency.

By nanoparticle tracking analysis, the effect of EV storage conditions after one week was evaluated by comparing storage at 4ºC with freezing at -80ºC and freezing at -80ºC in freezing containers overnight, which decrease 1ºC per minute, before transfer to -80ºC until analysis (Table 10.3). Preliminary results seem to indicate that EVs stored at 4ºC have larger mean size compared to storage at -80ºC with and without freezing containers, indicating that at 4ºC EVs tend to swell and aggregate and therefore, it is not a suitable storage condition, which is in accordance with published work (Lőrincz *et al.*, 2014). The rationale for testing EV freezing at -80ºC in freezing containers was to possibly avoid crystal formation and burst of EVs during freezing as well as EV swelling during the storage period of time and it seems to be beneficial (Table 10.3), although further testing and confirmation is needed. Moreover, it was implemented as standard procedure after EV isolation that the EVs resuspended in RNase-Free PBS are aliquoted in Eppendorf Protein Lobind to minimize EV adhesion to the tubes and then stored at -80ºC in freezing containers. Although some studies have reported that EVs can undergo freezing/thawing cycles up to 10 times (Sokolova *et al.*, 2011), there is a general consensus on avoiding freeze and thawing and once is the recommended (Szatanek *et al.*, 2015). There is still a lack of knowledge on the optimal EV storage conditions. Herein, it was decided to use freezing containers for a slow freezing as performed for cell freezing based on preliminary

results, however, other studies tested fast freezing in liquid nitrogen followed by storage at -80ºC and opposite results were reported (Issman *et al.*, 2013; Lőrincz *et al.*, 2014), thus it remains to be elucidated whether slow or fast freezing is beneficial.

The expression of the HUVEC surface markers VCAM-1 and ICAM-1 was evaluated using the potency assay developed to assess the impact of longer EV storage at -80ºC. Bioengineered EVs were stored at -80ºC and EVs were tested after one, five and eight weeks of storage. To avoid loss of function due to freezing and thawing cycles, aliquots were used only once.

Table 10.3 – Preliminary characterization by nanoparticle tracking analysis of MSC-EVs stored at different temperature (4ºC and -80ºC) and conditions (with or without freezing container overnight) seem to indicate swelling of EVs at 4ºC. The mean size (in nm) and EV concentration (in EV/ml) of EVs isolated from MSC RB135 at passage 4 was evaluated. N = 1 in triplicates. Data is represented by the mean and standard error of mean.

Condition	Mean size (nm)	EV concentration (EV/ml)
4ºC after 1 week	245 $\pm$ 2	(1.28 $\pm$ 0.03) x 10^{11}
-80ºC after 1 week	222 $\pm$ 5	(1.44 $\pm$ 0.08) x 10^{11}
-80ºC in freezing containers after one week	209.6 $\pm$ 0.4	(1.59 $\pm$ 0.04) x 10^{11}

After one week of EV storage at -80ºC, all bioengineered EVs seem to be able to reduce VCAM-1 and ICAM-1 expression (Figure 10.4). Preliminary results seem to indicate that, after about five weeks, EVs isolated from MSCs pre-conditioned with DMSO and TNF-α are still functional being able to reduce VCAM-1 and ICAM-1 expression, however, EVs isolated from MSCs pre-conditioned with to 5-Aza-CdR and calcimycin did not seem to be able to reduce their expression. The preliminary results also seem to indicate that upon eight weeks of EV storage at -80ºC, none of the bioengineered EVs was able to reduce VCAM-1 and ICAM-1 expression.

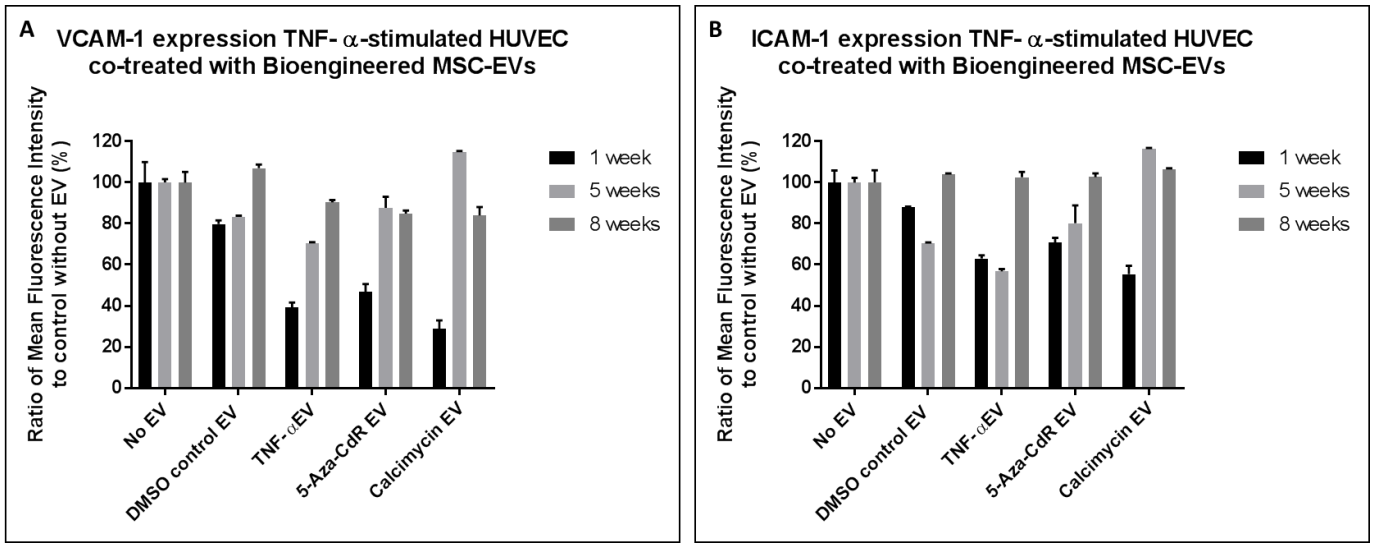

Figure 10.4 – Preliminary study of the effect of storage time at -80ºC on EV potency. Preliminary results of VCAM-1 (A) and ICAM-1 (B) expression of TNF-α stimulated HUVEC co-treated with bioengineered EVs (at 10^9 EV/ml) seem to show loss of function with time. Bioengineered MSC-EVs were isolated from donor RB81 at passage 4. No EV addition and EVs from MSC pre-conditioned with DMSO were used as controls. VCAM-1 and ICAM-1expression is giving by ratio of mean fluorescence intensity (in %) of each condition to control stimulated with TNF-α and without EV treatment (which was set as 100%). N = 1 (in duplicates). Error bars represent the standard error of the mean.

Lorincz and co-workers studied the effect of storage conditions of EVs from neutrophilic granulocytes and their results showed that EV storage at 4ºC or higher decreased EV number and anti-bacterial properties within one day, while storage at -20ºC did not affect EV number but affected EV size and the anti-bacterial action was lost after 28 days. Although not optimal, storage at -80ºC did not change EV number and size but partial loss of anti-bacterial function occurred. Moreover, snap-freezing did not did not protect EVs from loss of function and cryoprotectants such as DMSO burst the EVs (Lőrincz *et al.*, 2014). The partial loss of anti-bacterial properties after about one month is in accordance with the loss of immunomodulatory properties herein observed after about 5 weeks.

Overall, the results indicate that storage conditions greatly affect EV integrity and potency and longer storage is not recommended. Therefore, EVs should be use as fresh as possible which is already a consensus in the EV field (Szatanek *et al.*, 2015). The limited time of storage may condition or even hinder the use of EVs as an off-the-shelf product, consequently more efforts are needed on finding better storage conditions. Moreover, strict quality controls and assessment of function using potency assays will be necessary for each produced batch of MSC-EVs as cell-based but cell-free therapy.

10.3 Appendix C – Flow cytometry supplemental data

Human BM MSC characterization

The immunophenotype of three MSC donors per cell source (BM, AT and UCM) was performed by flow cytometry. The expression of the surface markers from the different donors selected was in line with that expected for MSCs, according to The International Society for Cellular Therapy (Dominici *et al.*, 2006), negative expression (≤2%) for the hematopoietic lineage markers CD14, CD19, CD34, CD45, CD80 and HLA-DR and the endothelial lineage marker CD31 and highly positive (≥95%) for CD73, CD90 and CD105 with exception of UCM donor 2 that had 91% of positive cells and UCM donor 78 with only 57% of positive cells for the surface marker CD105. All MSC donors were at passage 4 with exception of BM M79A15 that was at passage 5. The flow cytometer charts from the MSC donors BM M72A07 (Figure 10.5), BM M79A15 (Figure 10.6), BM M83A15 (Figure 10.7), AT L090403 (Figure 10.8), AT L090602 (Figure 10.9), AT L090724 (Figure 10.10), UCM 2 (Figure 10.11), UCM 38 (Figure 10.12), UCM 78 (Figure 10.13) are presented below.

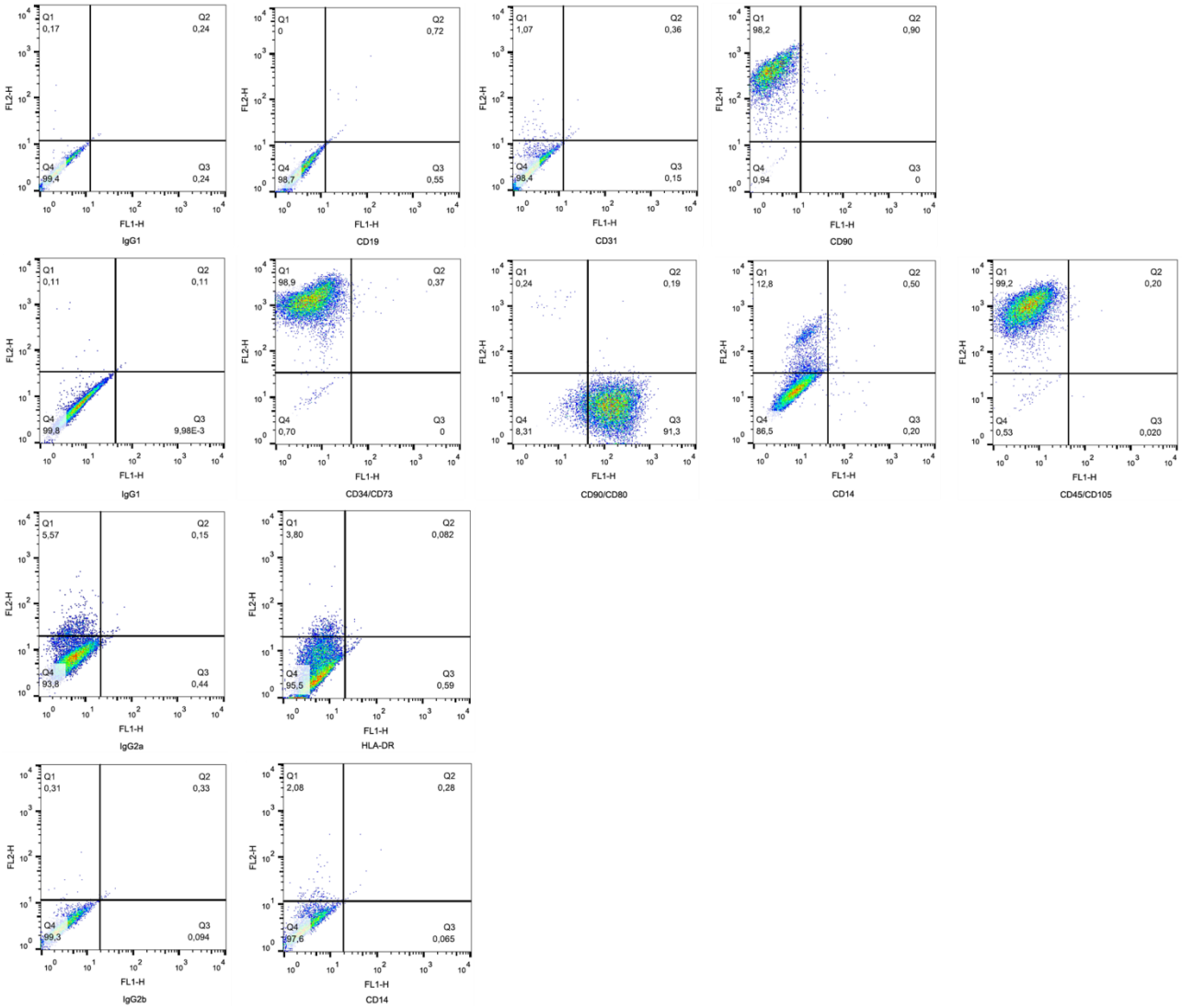

Figure 10.5 – Flow cytometry charts of BM MSC M72A07, including the surface markers CD14, CD19, CD31, CD34, CD45, CD80, HLA-DR, CD73, CD90 and CD105 and respective isotype controls.

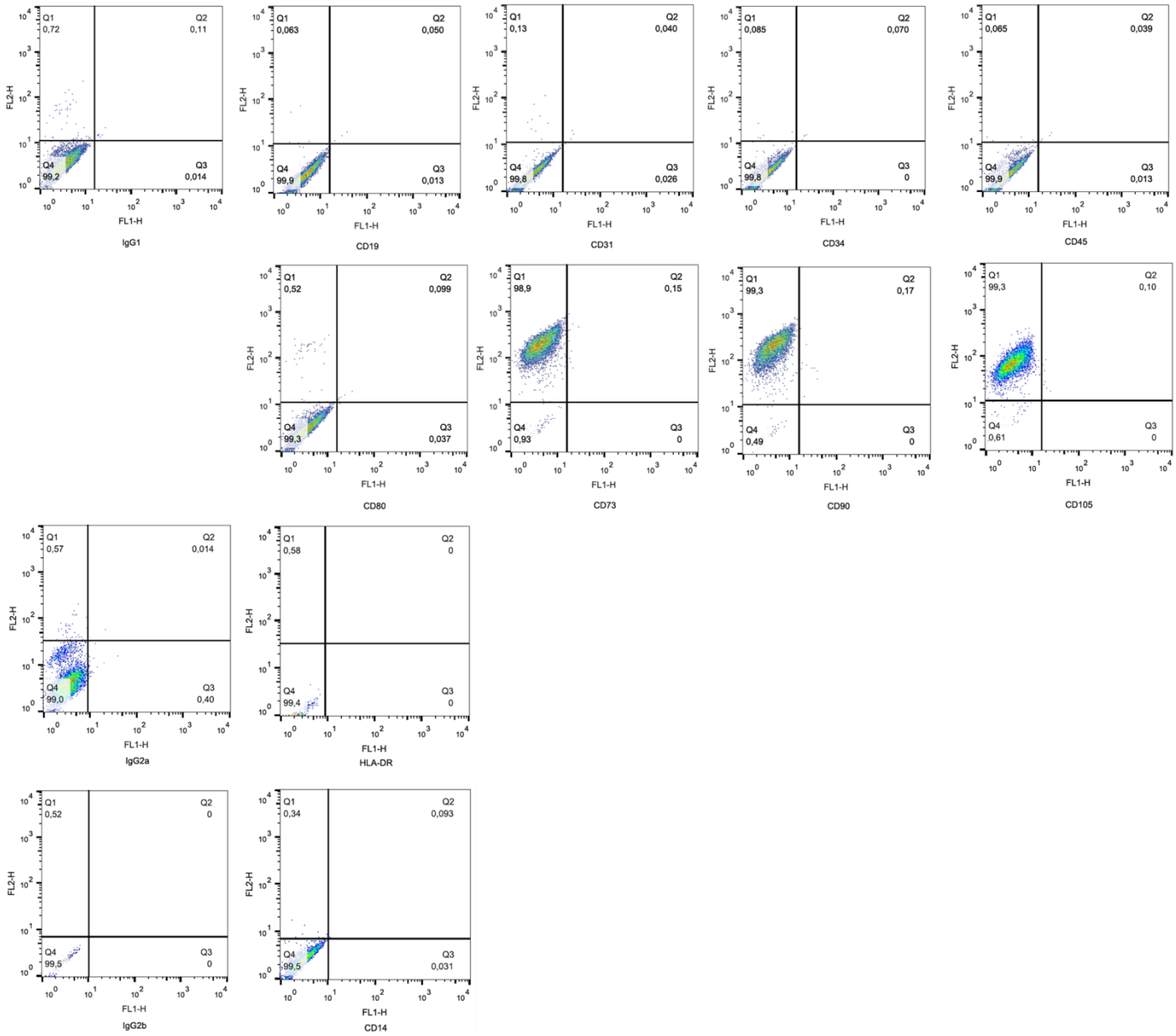

Figure 10.6 – Flow cytometry charts of BM MSC M79A15, including the surface markers CD14, CD19, CD31, CD34, CD45, CD80, HLA-DR, CD73, CD90 and CD105 and respective isotype controls.

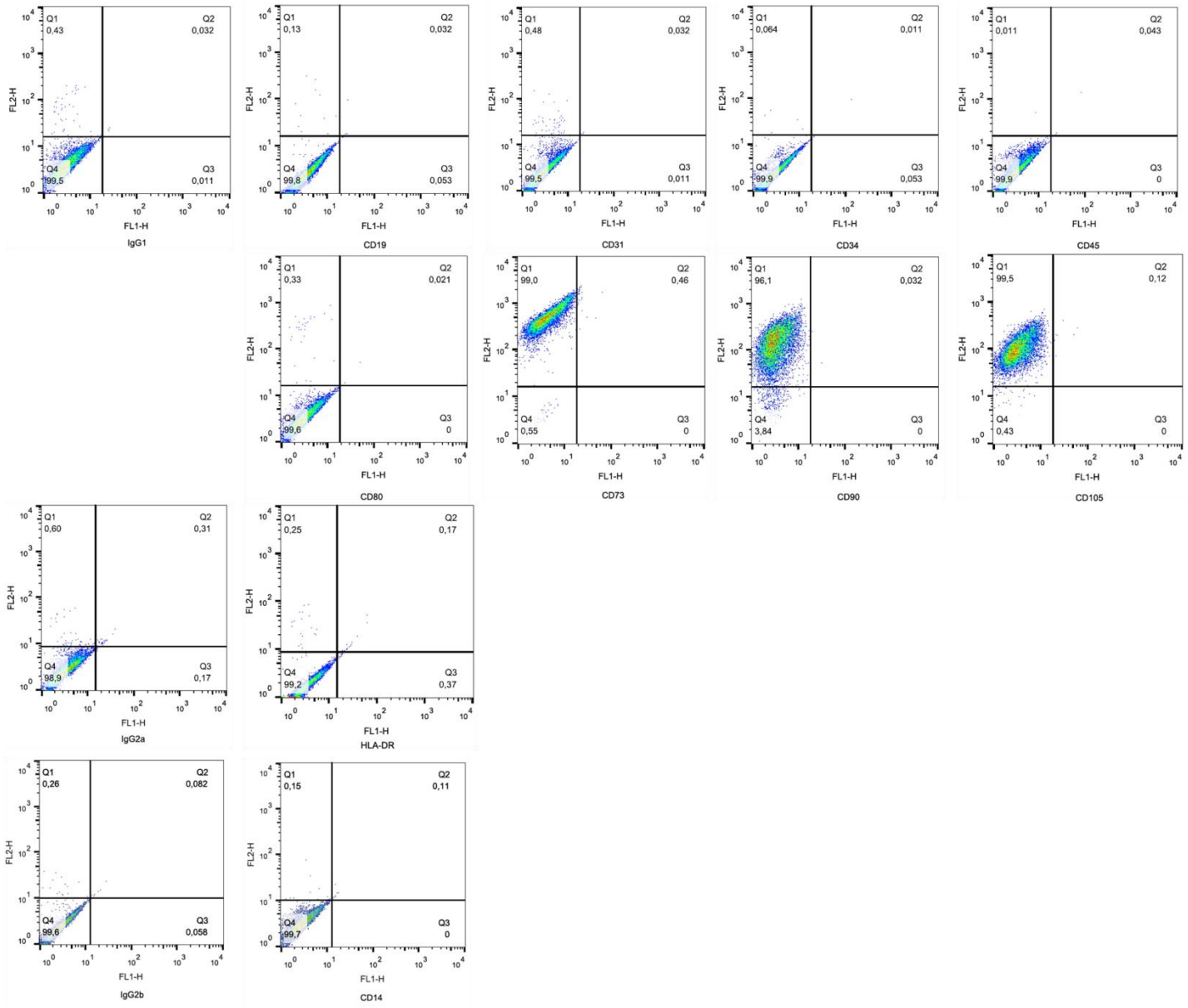

Figure 10.7 – Flow cytometry charts of BM MSC M83A15, including the surface markers CD14, CD19, CD31, CD34, CD45, CD80, HLA-DR, CD73, CD90 and CD105 and respective isotype controls.

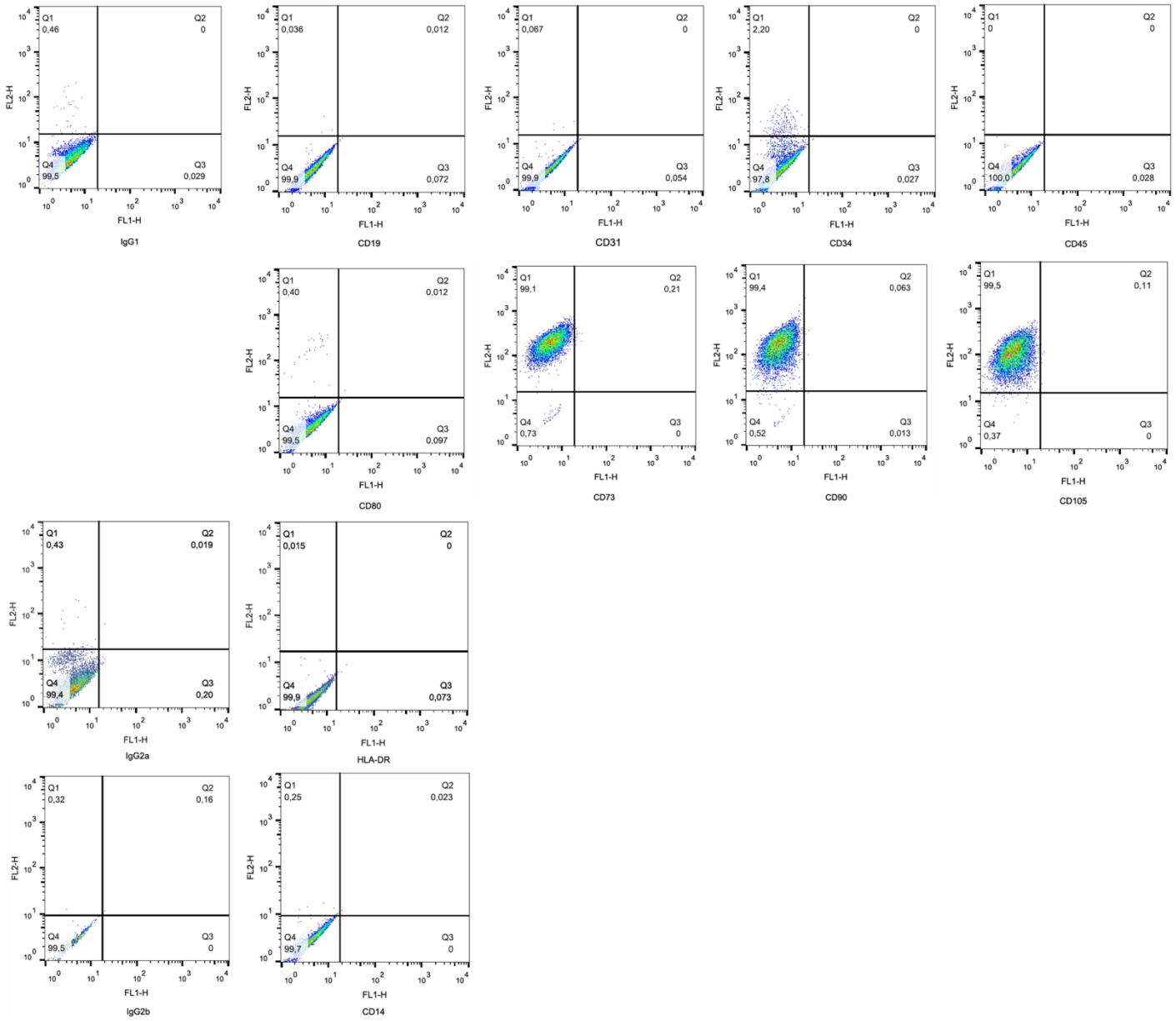

Figure 10.8 – Flow cytometry charts of AT MSC L090403, including the surface markers CD14, CD19, CD31, CD34, CD45, CD80, HLA-DR, CD73, CD90 and CD105 and respective isotype controls.

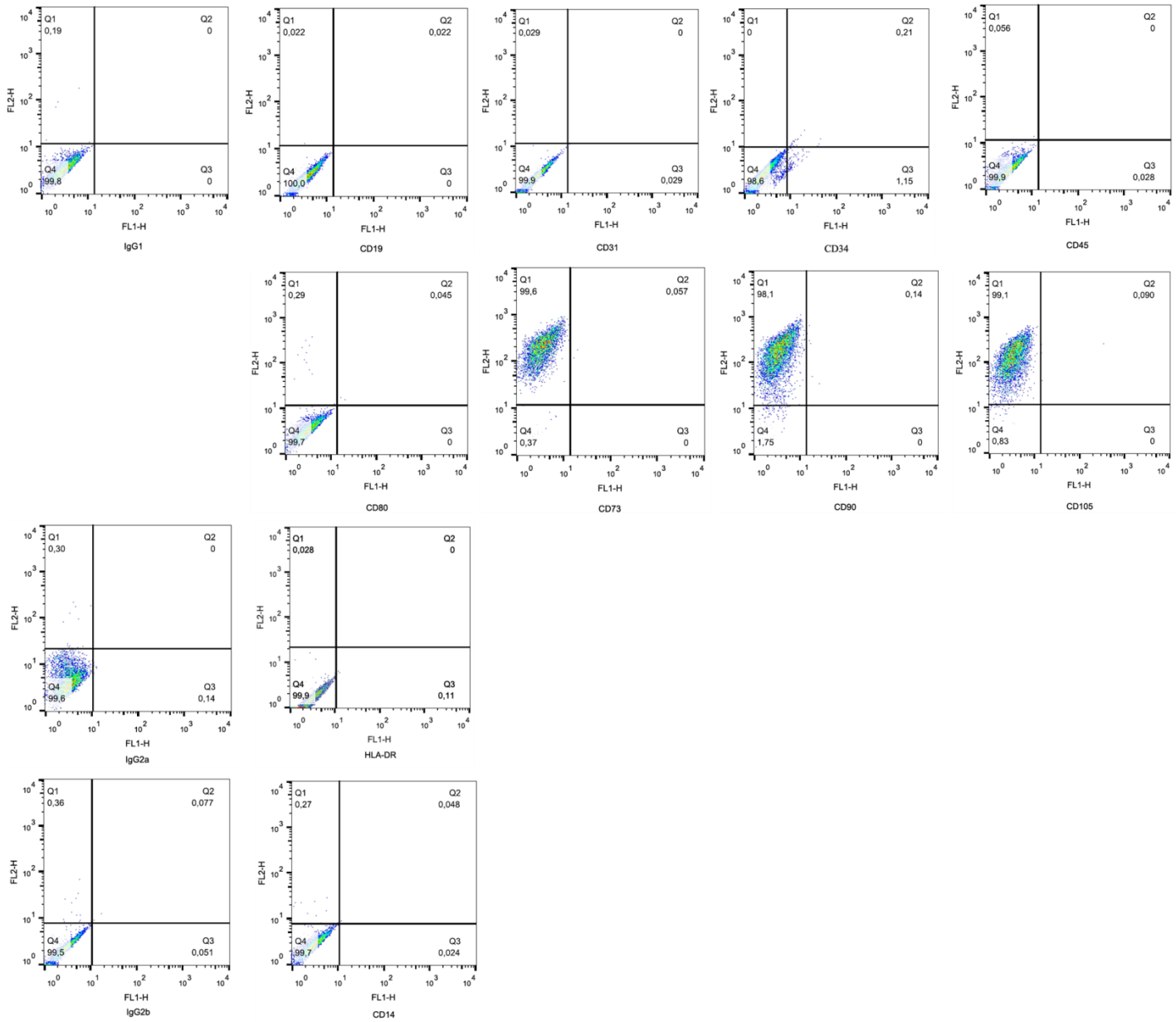

Figure 10.9 – Flow cytometry charts of AT MSC L090602, including the surface markers CD14, CD19, CD31, CD34, CD45, CD80, HLA-DR, CD73, CD90 and CD105 and respective isotype controls.

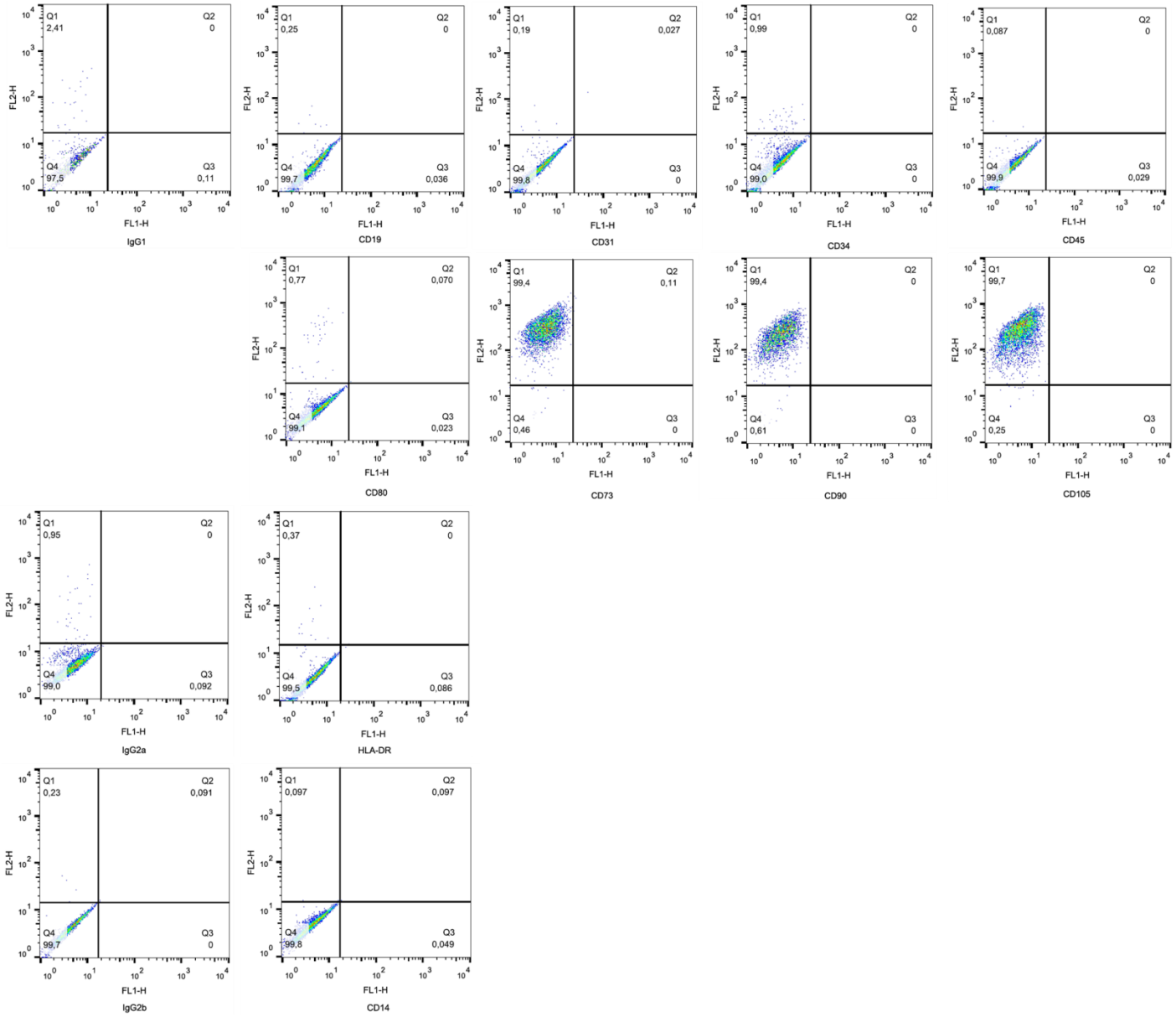

Figure 10.10 – Flow cytometry charts of AT MSC L090724, including the surface markers CD14, CD19, CD31, CD34, CD45, CD80, HLA-DR, CD73, CD90 and CD105 and respective isotype controls.

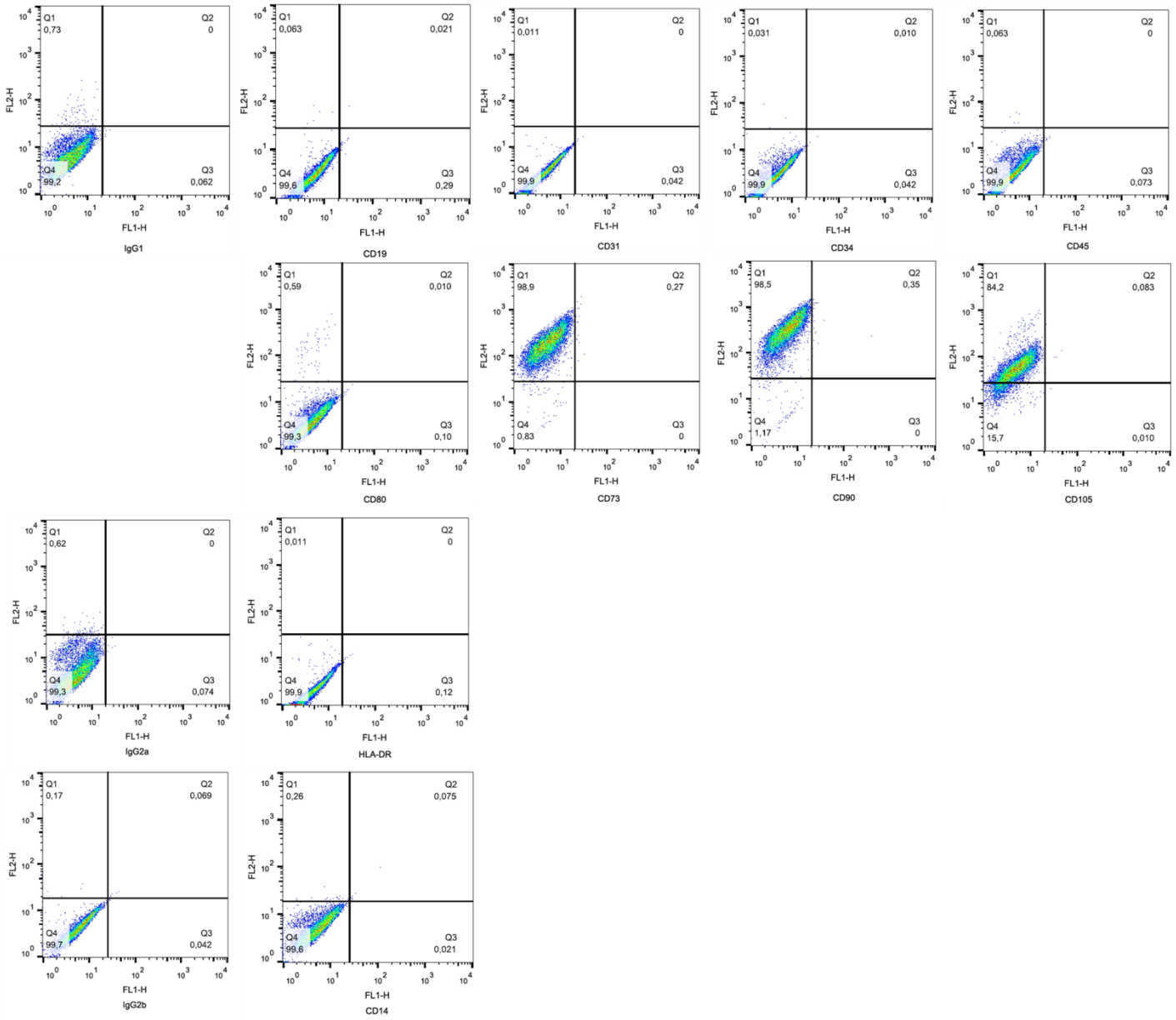

Figure 10.11 – Flow cytometry charts of UCM MSC 2, including the surface markers CD14, CD19, CD31, CD34, CD45, CD80, HLA-DR, CD73, CD90 and CD105 and respective isotype controls.

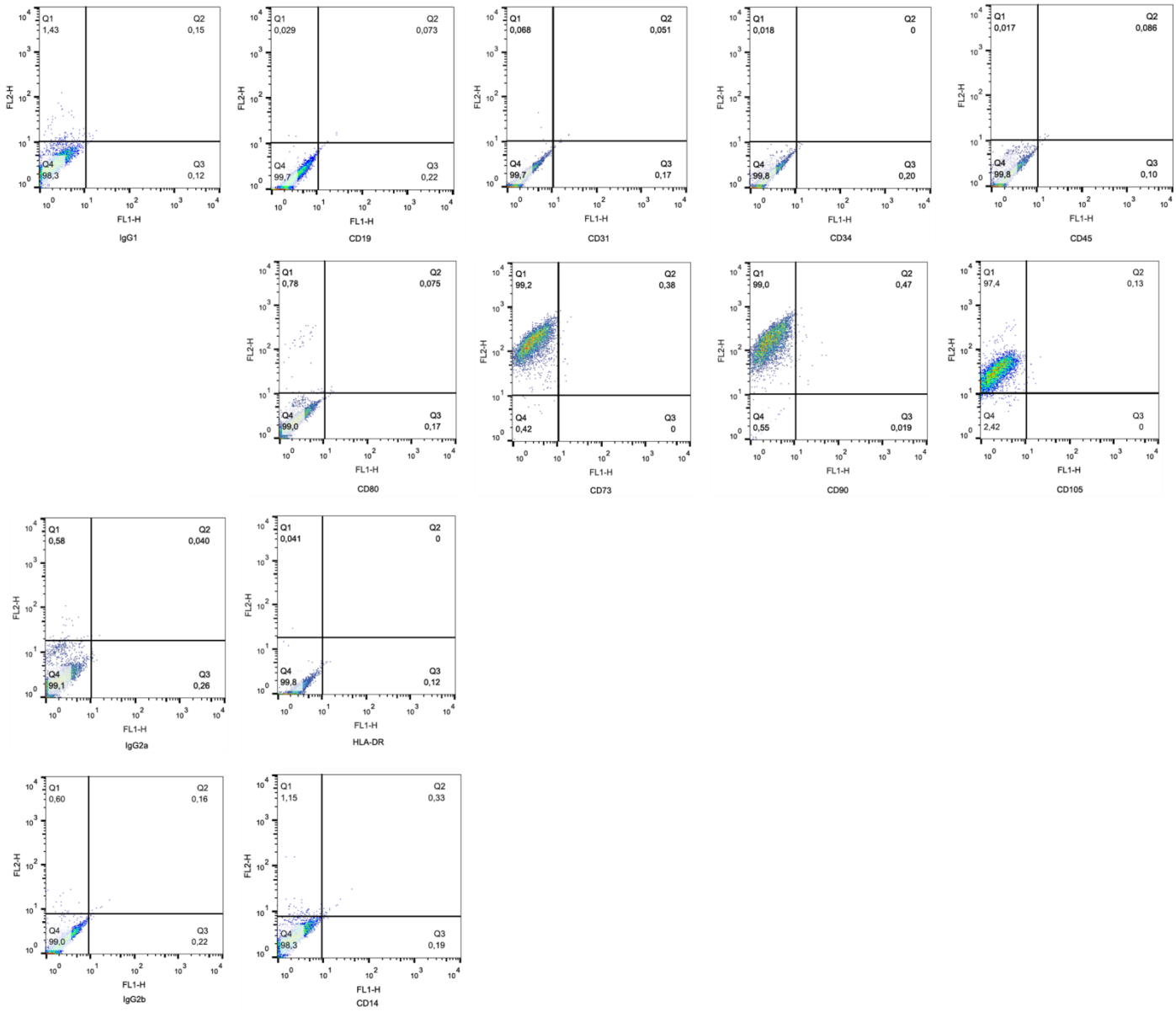

Figure 10.12 – Flow cytometry charts of UCM MSC 38, including the surface markers CD14, CD19, CD31, CD34, CD45, CD80, HLA-DR, CD73, CD90 and CD105 and respective isotype controls.

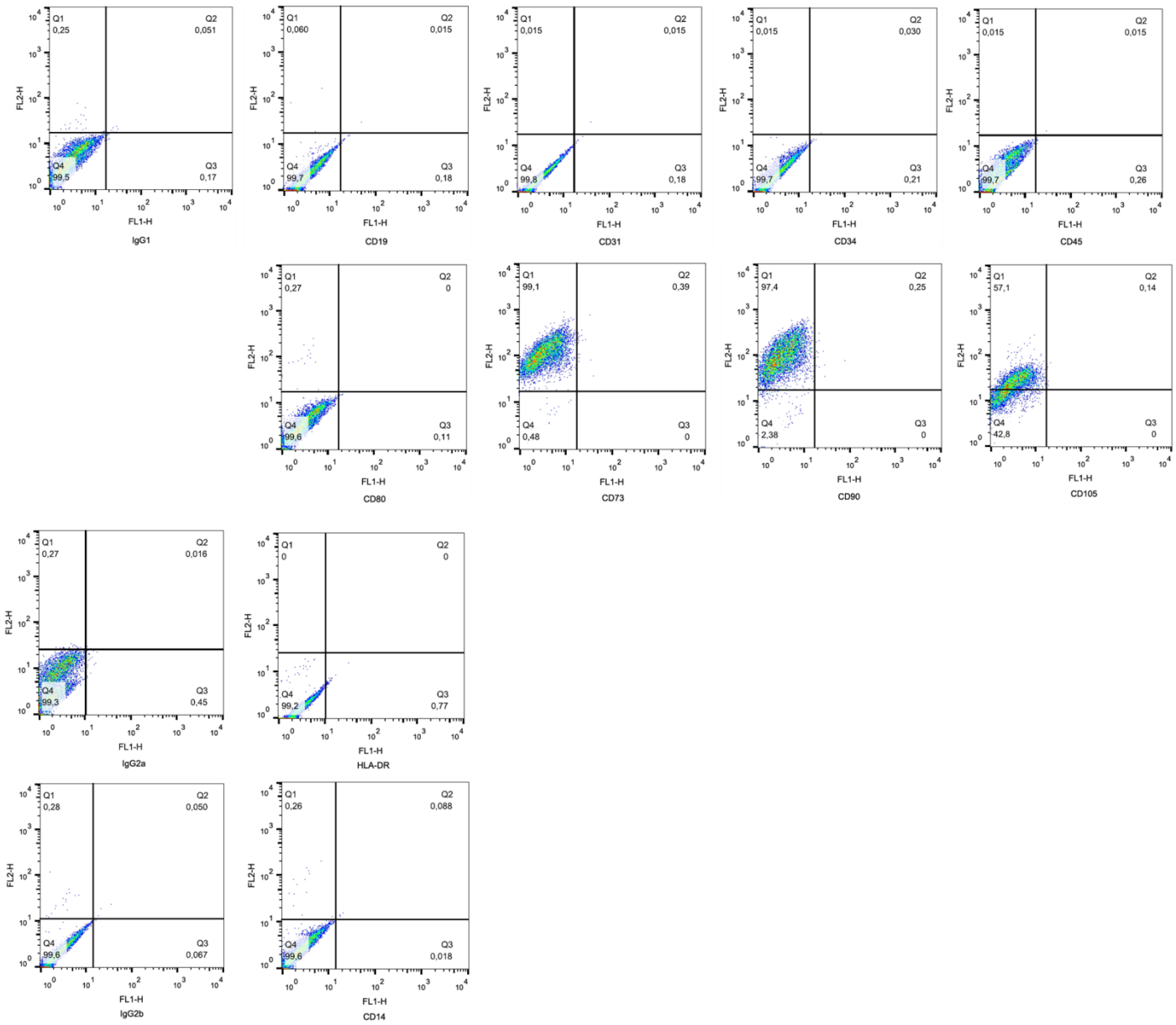

Figure 10.13 – Flow cytometry charts of UCM MSC 78, including the surface markers CD14, CD19, CD31, CD34, CD45, CD80, HLA-DR, CD73, CD90 and CD105 and respective isotype controls.

Lung alveolus inflammation model on transwell

The VCAM-1 expression of the HUVEC cultured in the undermembrane of the transwell system after 24 h treatment with TNF-α (50 ng/ml), IFN-γ (10 ng/ml) and MSC or MSC-derived products is represented in the following histograms (per donor in Figure 10.14 and per condition in Figure 10.15) obtained by flow cytometry. The indirect MSC co-culture, MSC-CM and MSC-EVs from 3 BM MSC donors RB135, RB55 and RB81 were tested (final results in chapter 6.5). The ICAM-1 expression of the HUVEC cultured in the undermembrane of the transwell system after 24 h treatment with the inflammatory cytokines and MSC indirect co-culture, MSC-CM and MSC-EVs from 3 BM MSC donors (RB135, RB55 and RB81) is also represented in the following flow cytometry histograms (per donor in Figure 10.16 and per condition in Figure 10.17) .

The MSC indirect co-culture of all the 3 MSC donors RB135, RB55 and RB81 resulted in a decrease in VCAM-1 (Figure 10.14) and ICAM-1 (Figure 10.16) expression compared to control challenged with TNF-α and IFN-γ only. MSC indirect co-culture decreased VCAM-1 and ICAM-1 to similar or higher extent then MSC-EVs from the 3 BM MSC donors. MSC-CM from the 3 BM MSC donors did not reduce VCAM-1 and ICAM-1 expression. The 3 BM MSC donors that were previously selected as not pro-inflammatory and slightly anti-inflammatory showed similar responses to inflammation on VCAM-1 (Figure 10.15) and ICAM-1 (Figure 10.17) expression of HUVEC from the lung alveolus model on transwell. Curcumin was used as postitive control, being able to reduce VCAM-1 and ICAM-1 expression compared to the group treated with TNF-α and IFN-γ only.

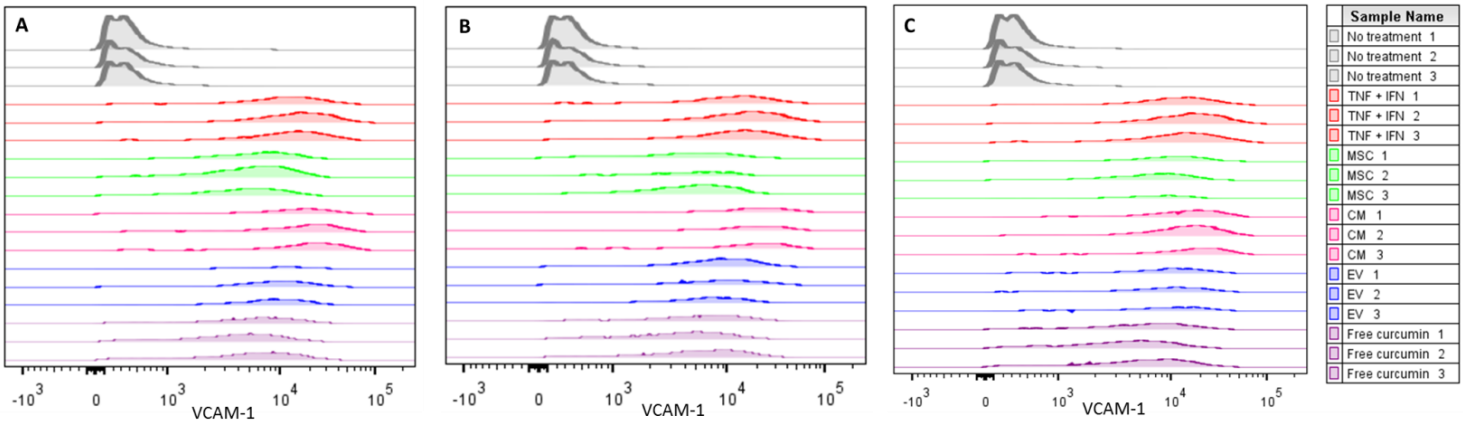

Figure 10.14 – Flow cytometry charts comparing the effect of MSC indirect co-culture (MSC), MSC-conditioned media (CM) and MSC-EVs (EV) on VCAM-1 expression of HUVEC from the lung alveolus inflammation on a 3D transwell model using three BM MSC donors RB135 (A), RB55 (B) and RB81 (C). HUVEC were detached from the undermembrane of the lung alveolus transwells after 24 h TNF-α (50 ng/ml) and IFN-γ (10 ng/ml) and MSC indirect co-culture, MSC-CM and MSC-EVs in 1% supplement StemPro (as described in chapter 6.5). The control group of transwells was not exposed to inflammatory cytokines neither MSC nor MSC-derived products. The TNF+IFN group of transwells was exposed to inflammatory cytokines only. The Free curcumin group of transwells was exposed to inflammatory cytokines and 5 µM curcumin as positive control. N =1, triplicates per condition were used.

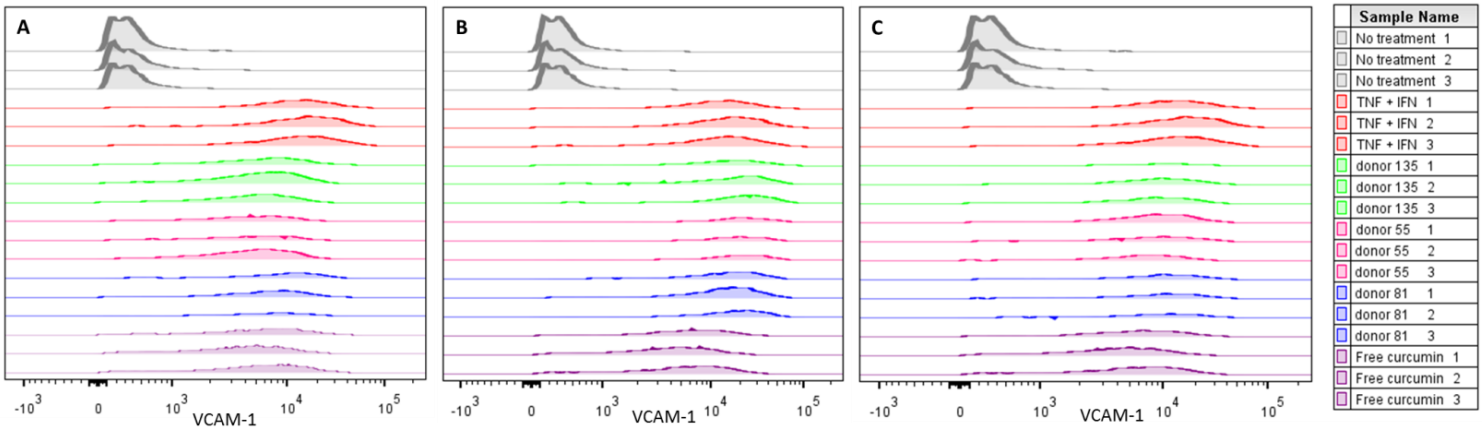

Figure 10.15 – Flow cytometry charts comparing MSC indirect co-culture (MSC) (A), CM (B) and EVs (C) from three BM MSC donors RB135, RB55 and RB81 on VCAM-1 expression of HUVEC from the lung alveolus inflammation on a 3D transwell model. HUVEC were detached from the undermembrane of the lung alveolus transwells after 24 h stimuli with TNF-α (50 ng/ml) and IFN-γ (10 ng/ml) and MSC indirect co-culture, MSC-CM and MSC-EVs in 1% supplement StemPro (as described in chapter 6.5) The control group of transwells was not exposed to inflammatory cytokines neither MSC nor MSC-derived products. The TNF+IFN group of transwells was exposed to inflammatory cytokines only. The Free curcumin group of transwells was exposed to inflammatory cytokines and 5 µM curcumin as positive control. N =1, triplicates per condition were used.

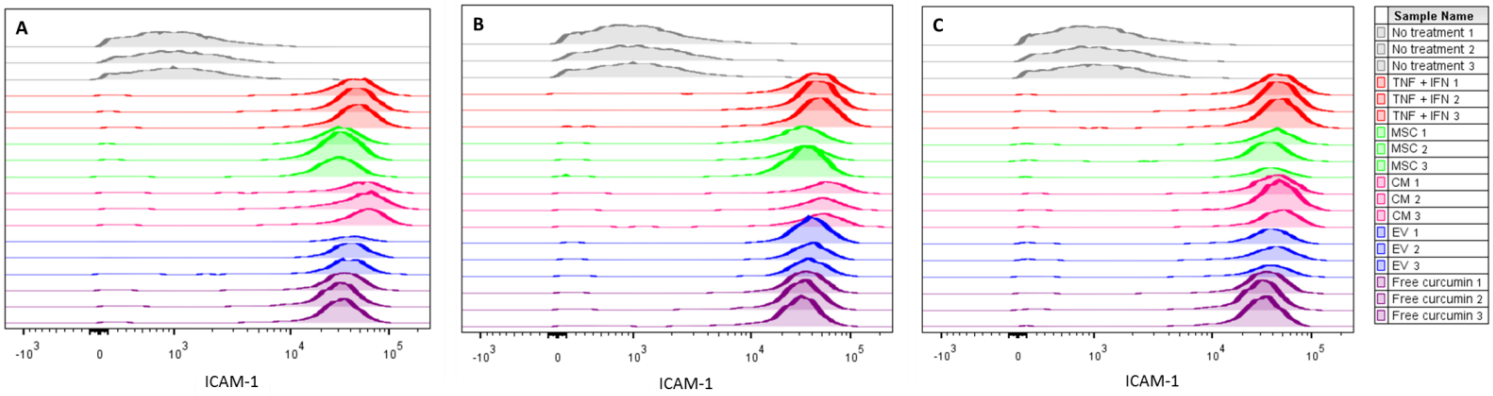

Figure 10.16 – Flow cytometry charts comparing the effect of MSC indirect co-culture (MSC), MSC-conditioned media (CM) and MSC-EVs (EV) on ICAM-1 expression of HUVEC from the lung alveolus inflammation on a 3D transwell model using three BM MSC donors RB135 (A), RB55 (B) and RB81 (C). HUVEC were detached from the undermembrane of the lung alveolus transwells after 24 h TNF-α (50 ng/ml) and IFN-γ (10 ng/ml) and MSC indirect co-culture, MSC-CM and MSC-EVs in 1% supplement StemPro (as described in chapter 6.5). The control group of transwells was not exposed to inflammatory cytokines neither MSC nor MSC-derived products. The TNF+IFN group of transwells was exposed to inflammatory cytokines only. The Free curcumin group of transwells was exposed to inflammatory cytokines and 5 µM curcumin as positive control. N =1, triplicates per condition were used.

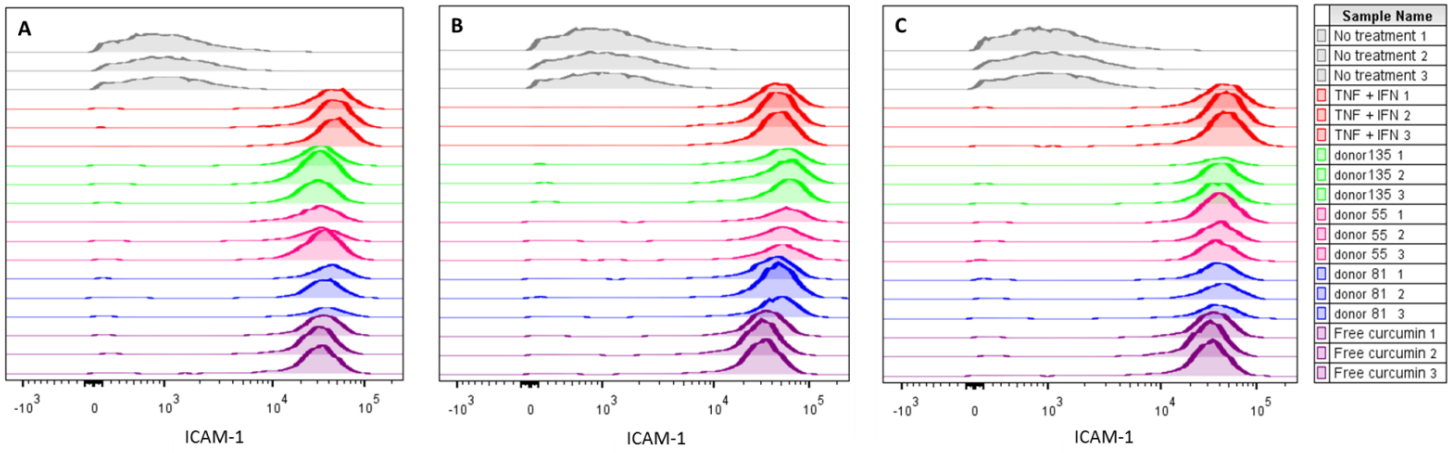

Figure 10.17 – Flow cytometry charts comparing MSC indirect co-culture (MSC) (A), CM (B) and EVs (C) from three BM MSC donors RB135, RB55 and RB81 on ICAM-1 expression of HUVEC from the lung alveolus inflammation on a 3D transwell model. HUVEC were detached from the undermembrane of the lung alveolus transwells after 24 h stimuli with TNF-α (50 ng/ml) and IFN-γ (10 ng/ml) and MSC indirect co-culture, MSC-CM and MSC-EVs in 1% supplement StemPro (as described in chapter 6.5) The control group of transwells was not exposed to inflammatory cytokines neither MSC nor MSC-derived products. The TNF+IFN group of transwells was exposed to inflammatory cytokines only. The Free curcumin group of transwells was exposed to inflammatory cytokines and 5 μM curcumin as positive control. N =1, triplicates per condition were used.

Lung alveolus-on-a-chip inflammation model

The ICAM-1 expression of the HUVEC from each microfluidic device and respective number of counts is represented in the following histograms (Figure 10.18) obtained by flow cytometry for 3 independent experiments using the lung alveolus inflammation model (final results in chapter 6.6).

TNF-α at 10 ng/ml flowing through the endothelial channel of the lung alveolus-on-a-chip was able to cause inflammation in the microfluidic system by up-regulating the expression of ICAM-1 of the TNF-α only group (TNF, No EV) compared to the negative control group (Control 16 h, also denominated No EV, No TNF-α). Additionally, as expected the negative control group maintained basal ICAM-1 expression along the 40 h period of time. ICAM-1 expression on HUVEC decreased when the alveolus-on-a-chip microfluidic devices were co-treated with TNF-α and MSC-EVs for 16 h (TNF, EV 16 h) compared to cells challenged by TNF-α only (TNF, No EV 16 h). After 24 h recovery flowing medium only, the ICAM-1 expression of both groups (TNF, No EV 24h and TNF, EV 24h) decreased to similar values, however, it did not reach the basal levels of the negative control group (Control 24 h).

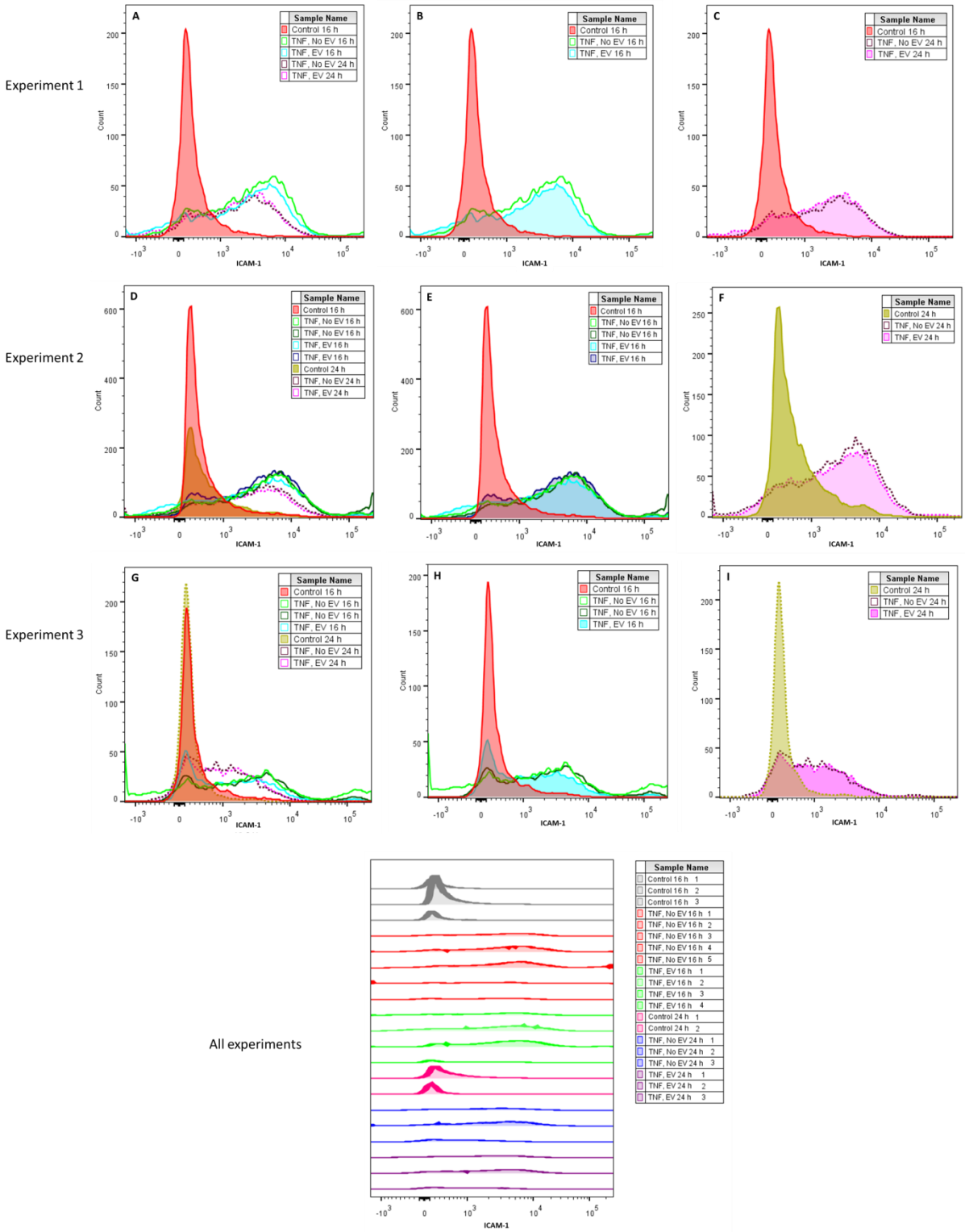

Figure 10.18 – Flow cytometry charts of 3 independent experiments (experiment 1, 2 and 3) using the lung alveolus-on-a-chip inflammation model. HUVEC were detached from the bottom channel of the lung alveolus inflammation model after 16 h TNF-α (10 ng/ml) and EV (10^{10} EV/ml from a pool of MSC donors RB70 and RB81) treatment on flow or after additional 24 h recovery flowing medium only (the two time points making a total of 40 h). The control group of chips was not exposed to TNF-α nor EVs, while the TNF, No EV group of chips was exposed to TNF-α but not EVs and the TNF, EV group of chips was exposed to both TNF-α and EVs. The expression of ICAM-1 on HUVEC (within the singlets and live cell population) was measured and plotted in the histograms. Each row corresponds to an independent experiment and the last row the devices from all experiments. The first chart of each row (A, D, G) represent all chips at both time points, the middle charts (B, E, H) the 16 h time point of exposure to TNF-α and EVs and the last charts (C, F, I) the 24 h recovery time point flowing medium only.

10.4 Appendix D – Barrier function supplemental data

Lung alveolus inflammation on a transwell model

The barrier function of the lung alveolus inflammation on a transwell model was evaluated by determining the apparent permeability (using Equation 6) of the fluorescent dyes cascade blue and dextran (Figure 10.19 A and B) before and after 24 h stimuli with the inflammatory cytokines TNF-α (50 ng/ml) and IFN-γ (10 ng/ml) in co-treatment with MSC indirect co-culture, MSC-CM and MSC-EVs in 1% supplement StemPro for each transwell system (as described in chapter 6.5). The fold change in apparent permeability for cascade blue and dextran dyes was calculated based on the apparent permeability before and after treatment (Figure 10.19 C and D) for each transwell system and the final results in which the replicates of the same condition are averaged are present in chapter 6.5.

As expected, the inflammatory cytokines TNF-α (at 50 ng/ml) and IFN-γ (at 10 ng/ml) decreased the barrier function of the lung alveolus model on transwell, which was given by an increase in apparent permeability of cascade blue (Figure 10.19 A) and dextran (Figure 10.19 B) fluorescent dyes, also observed in the fold change of apparent permeability of cascade blue (Figure 10.19 C) and dextran (Figure 10.19 D) for each transwell system. The apparent permeability of cascade blue and dextran fluorescent dyes for all the other conditions including MSC indirect co-culture, MSC-CM, MSC-EV and curcumin was similar or higher than the transwell systems incubated with inflammatory cytokines only, indicating similar or higher extent of decreased barrier function.

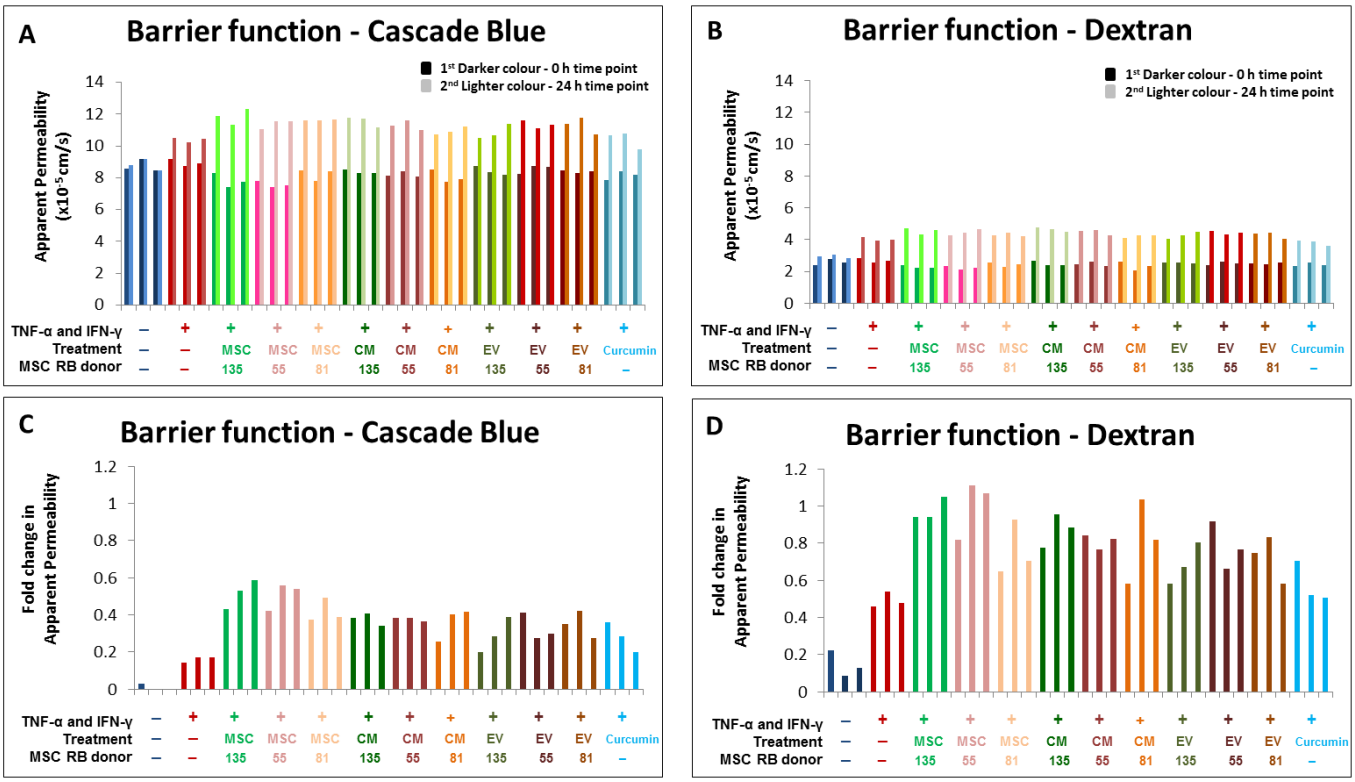

Figure 10.19 – Effect of mesenchymal stromal cell (MSC) indirect co-culture, MSC conditioned medium (CM) and MSC extracellular vesicles (EV) from donors RB135, RB55 and RB81 on the barrier function of the lung alveolus inflammation model on transwell. TNF-α at 50 ng/ml and IFN-γ at 10 ng/ml were incubated for 24 h in 1% supplement in StemPro medium according to Figure 6.9. Curcumin at 5 µM in 1% supplement in StemPro medium was used as a positive control. A and B – Apparent permeability (in cm/s x 10^{-5}) of cascade blue (A) and dextran (B) before (first column in darker color – 0 h time point) and after treatment (second column in lighter color – 24 h time point) for each lung alveolus transwell system. Apparent permeability was determined after 2 h static incubation with the two fluorescence dyes and the Equation 6 was used for the calculations. C and D – Barrier function given be the fold change in apparent permeability of cascade blue (C) and dextran (D) for each lung alveolus transwell system after 24 h treatment. N = 1.

Lung alveolus-on-a-chip inflammation model

The barrier function of the lung alveolus-on-a-chip inflammation model was evaluated by determining the apparent permeability (using Equation 6) of the fluorescent dyes cascade blue and dextran (Figure 10.20 A and B) before (0 h), after 16 h stimuli with the inflammatory cytokines TNF-α (10 ng/ml) in co-treatment with MSC-EVs (at 10^{10} EV/ml from a pool of BM MSC donors RB70 and RB81) on flow and then after 24 h recovery time flowing medium only, making a total of 40 h. The cascade blue and dextran apparent permeability values for each microfluidic device is represented in Figure 10.20 A and B. The ratio of the apparent permeability of cascade blue and dextran dyes was calculated based on the apparent permeability after 16 h (Figure 10.20 C and D) or 40 h treatment (Figure 10.20 E and F) for each microfluidic device. The final results in which the replicates of the same condition are averaged are present in chapter 6.6. The apparent permeability of cascade blue

(Figure 10.20 A) and dextran (Figure 10.20B) fluorescent dyes increased for the lung alveolus-on-a-chip group treated with TNF-α only (No EV, TNF-α) after 16 h treatment compared to before treatment (0 h time point) and that tendency was maintained after 24 h recovery flowing medium only (40 h time point). The ratio of apparent permeability of cascade blue and dextran for the microfluidic devices of the group stimulated with TNF-α only was also higher than for the control group (No EV, No TNF-α) and the group co-treated with MSC-EVs (EV, TNF-α) after 16 h treatment (Figure 10.20 C and D for cascade blue and dextran, respectively) and also after 24 h recovery (40 h time point) (E and F for cascade blue and dextran, respectively). Additionally, the ratio of apparent permeability was negative for most of the microfluidic devices from control group (No EV, No TNF-α) indicating a stronger barrier function over time. Moreover, the lower extent of increase in apparent permeability of the MSC-EV treated group was indicative of increased barrier function and decreased pulmonary edema compared to TNF-α only group (No EV, TNF-α).

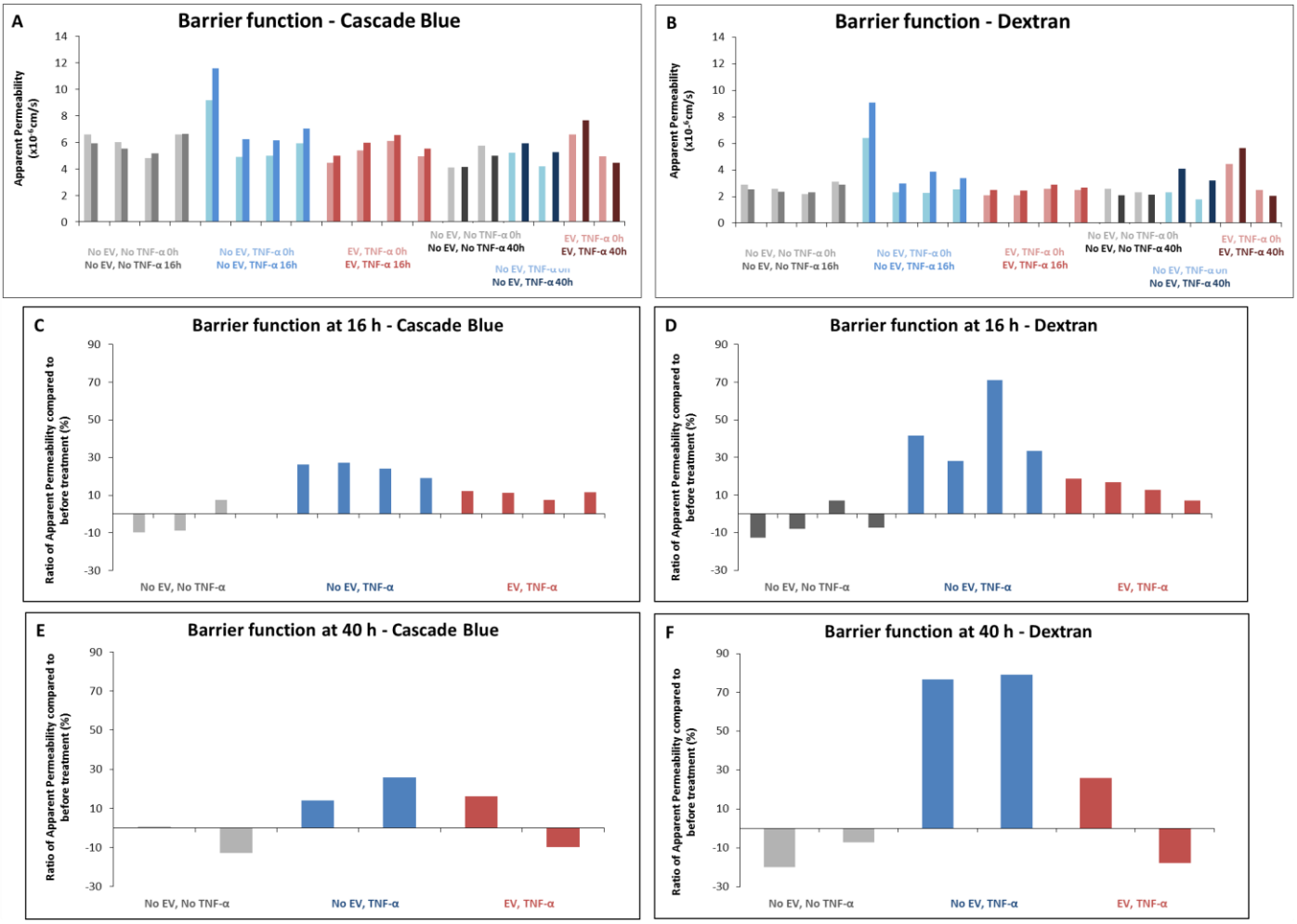

Figure 10.20 – Effect of MSC extracellular vesicles (EV) on the barrier function of lung alveolus-on-a-chip inflammation model. TNF-α at 10 ng/ml in co-treatment with MSC-EVs at 10^{10} EV/ml from a pool of BM MSC donors RB70 and RB81 were incubated for 16 h on flow, followed by 24 h recovery time flowing medium only (40 h time point). A and B – Apparent permeability (in cm/s x 10^{-5}) of cascade blue (A) and dextran (B) before (first column – 0 h time point) and after 16 h or 40 h treatment (second column – 16 or 40 h time point) for each lung alveolus-on-a-chip microfluidic device. Apparent permeability was determined after 2 h static incubation with the two fluorescence dyes and the Equation 6 was used for the calculations. C and D – Barrier function given by the ratio of apparent permeability (in %) of cascade blue (C) and dextran (D) for each microfluidic device after 16 h treatment compared to before treatment. E and F – Barrier function given by the ratio of apparent permeability (in %) of cascade blue (E) and dextran (F) for each microfluidic device after 40 h treatment (16 h treatment + 24 h recovery time) compared to before treatment. N = 3.

10.5 Appendix E – IL-8 secretion supplemental data

Lung alveolus-on-a-chip inflammation model

The IL-8 release from the lung alveolus-on-a-chip inflammation model was evaluated by measuring the IL-8 secretion on the outlet of the microfluidic devices after 16 h stimuli with the inflammatory cytokines TNF-α (10 ng/ml) in co-treatment with MSC-EVs (at 10^{10} EV/ml from a pool of BM MSC donors RB70 and RB81) on flow and then after 24 h recovery time flowing medium only

(which made a total of 40 h). The IL-8 concentration of the inlets of the different microfluidic devices was measured as control and neither the medium neither the EV solutions contained IL-8 (Figure 10.21 A, B and C). Three independent experiments were performed with one or two microfluidic devices per condition and the IL-8 concentration of the outlets after 16 h treatment and 24 h recovery period was measured by ELISA and plotted in Figure 10.21 A, B and C. The ratio of IL-8 concentration of each microfluidic device compared to the TNF-α only group after 16 h treatment (No EV, No TNF 16h, set as 100%) was calculated and plotted for each of the 3 experiments (Figure 10.21 D, E and F) and for all experiments (Figure 10.21 G). The outlet of the lung alveolus-on-a-chip control group (No EV, No TNF) after 16 h treatment and after 24 h recovery period on flow had basal IL-8 secretion. IL-8 secretion increased with TNF-α stimuli for 16 h (No EV, TNF 16 h) compared to control group. The treatment with MSC-EVs (EV, TNF 16 h) did not have a strong effect on reducing IL-8 secretion after 16 h treatment compared to TNF-α only group (No EV, TNF 16 h). After 24 h recovery period, IL-8 release was reduced in a similar extent for the TNF-α only group (No EV, TNF 24 h) and the MSC-EV group (EV, TNF 24 h), however, the IL-8 secretion was not reduced enough to reach the basal level of the control group (No EV, No TNF 24 h). The final results in which the ratio of the microfluidic devices from the same group were averaged are present in chapter 6.6.

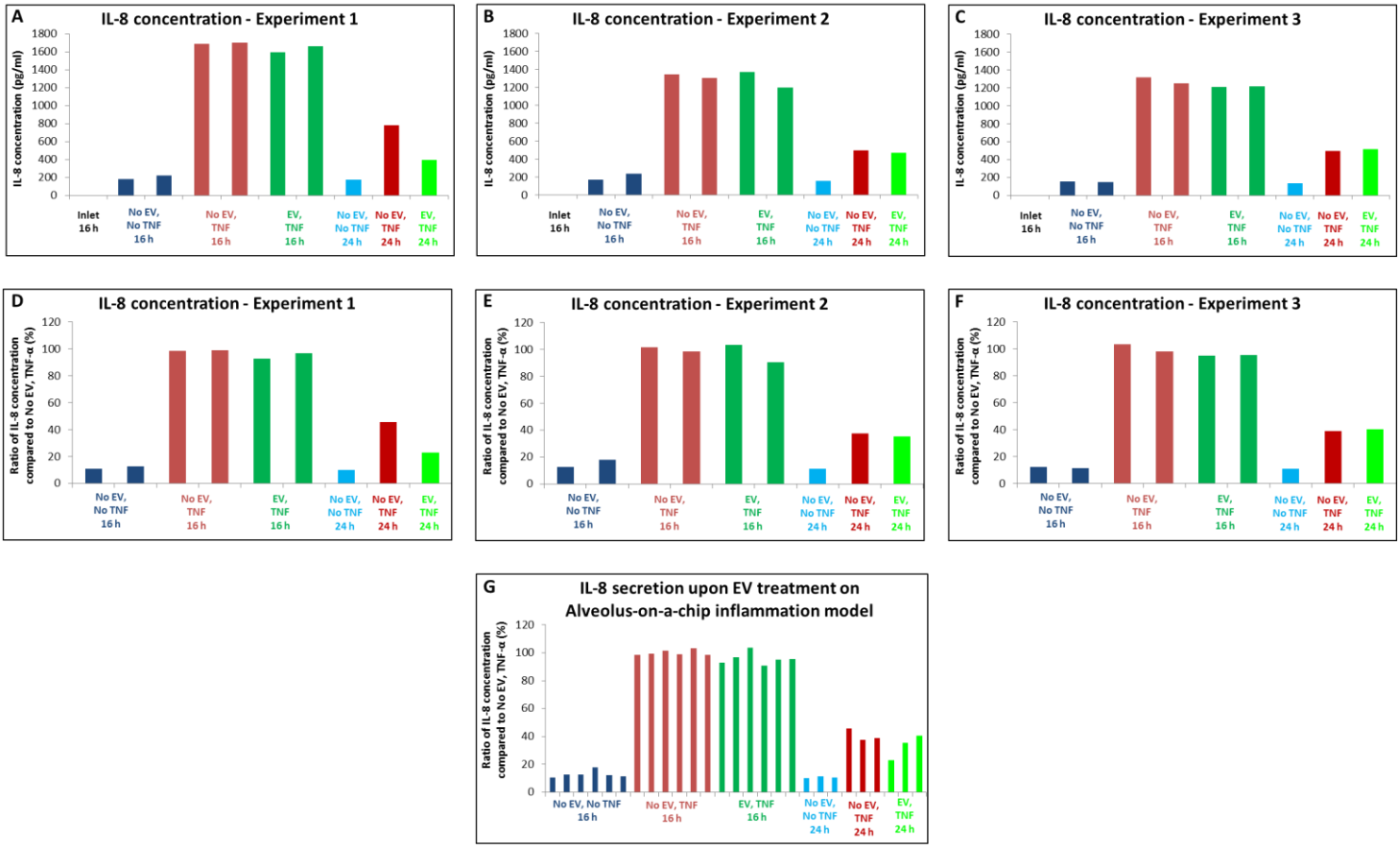

Figure 10.21 – Effect of MSC extracellular vesicles (EV) on the IL-8 secretion of the lung alveolus-on-a-chip inflammation model. TNF-α at 10 ng/ml in co-treatment with MSC-EVs at 10^{10} EV/ml from a pool of BM MSC donors RB70 and RB81 were incubated for 16 h on flow, followed by 24 h recovery time flowing medium only. A, B and C – IL-8 concentration (in pg/ml) of the inlet and outlet of the microfluidic devices from experiment 1 (A), 2 (B) and 3 (C) after 16 h treatment with TNF-α and EVs and after 24 h recovery period showing increased IL-8 release after stimuli for the TNF-α only group (No EV, TNF) and for the group co-treated with TNF-α and MSC-EVs (EV, TNF). D, E and F – Ratio of IL-8 concentration (in %) of each microfluidic device from experiment 1 (D), 2 (E) and 3 (F) compared to TNF-α only group (No EV, TNF 16 h) at 16 h time point, which was set as 100 %. G – Ratio of IL-8 concentration (in %) of each microfluidic device from all the 3 experiments. N = 3.